GEOLOGICA ULTRAIECTINA

Mededelingen van de
Faculteit Aardwetenschappen
Universiteit Utrecht

No. 223

Paleo-environmental effects of the Mid-Pleistocene Transition in the tropical Atlantic and equatorial Africa

Enno Schefuß

GEOLOGICA ULTRAIECTINA

Mededelingen van de
Faculteit Aardwetenschappen
Universiteit Utrecht

No. 223

Paleo-environmental effects of the Mid-Pleistocene Transition in the tropical Atlantic and equatorial Africa

Paleo-environmental effects of the Mid-Pleistocene Transition in the tropical Atlantic and equatorial Africa

Milieu-veranderingen in de tropische Atlantische Oceaan en equatoriaal Afrika tijdens de Midden-Pleistocene klimaatsovergang

(met een samenvatting in het Nederlands)

Umweltveränderungen im tropischen Atlantik und äquatorialen Afrika während des Mittel-Pleistozänen Klimawechsels

(mit einer Zusammenfassung in deutscher Sprache)

Proefschrift

ter verkrijging van de graad van doctor
aan de Universiteit Utrecht
op gezag van Rector Magnificus, Prof. Dr. W.H. Gispen,
ingevolge het besluit van het College voor Promoties
in het openbaar te verdedigen
op maandag 13 januari 2003 des middags te 12.45 uur

door

Enno Schefuß
geboren op 27 juli 1971 te Brühl, Duitsland

Promotor: Prof. Dr. J. W. de Leeuw
Royal Netherlands Institute for Sea Research,
Den Burg, Texel, The Netherlands

Co-promotores: Dr. J. S. Sinninghe Damsté
Department of Marine Biogeochemistry and Toxicology,
Royal Netherlands Institute for Sea Research,
Den Burg, Texel, The Netherlands

Dr. J. H. F. Jansen
Department of Marine Chemistry and Geology,
Royal Netherlands Institute for Sea Research,
Den Burg, Texel, The Netherlands

The research described in this thesis was carried out in the Department of Marine Biogeochemistry and Toxicology of the Royal Netherlands Institute for Sea Research, Landsdiep 4, 1790 AB Den Burg, Texel, The Netherlands. The investigations were supported by the Research Council for Earth and Life Sciences (ALW) with the financial support from the Netherlands Organisation for Scientific Research (NWO).

ISBN 90-5744-081-4

Für meine Eltern

Table of contents

Chapter 1

Introduction and outline

Enno Schefuß

1.1. The Mid-Pleistocene Transition

The most recent geological past, i.e., the Quaternary, covering the last 2.5 million years, is characterised by the periodic build-up of major continental ice sheets in the Northern and Southern Hemisphere. This present cold state of the Earth is the result of 55 million years of global cooling (Miller et al., 1987), which was not continuous, but occurred in a stepwise manner. While cyclic fluctuations in global climate occurred throughout the Cenozoic, the last 65 million years (Raymo and Ruddiman, 1992), a distinctive feature of the last two third of a million year are the severe and long-lasting ice ages of the Late Pleistocene. The important climate step leading to the Late Pleistocene ice ages is the Mid-Pleistocene Transition (MPT) lasting from 940 to 640 thousand years (kyrs) before present (BP) (Mudelsee and Schulz, 1997). Not only the mean global ice volume increased during the MPT, but also the main periodicity of its variations (Mudelsee and Schulz, 1997; Prell, 1982). Before the MPT, global ice-volume records are dominated by 41-kyr variations, while they varied in a sawtooth-like 100-kyr cycle with a larger amplitude afterwards (Pisias and Moore, 1981; Ruddiman et al., 1989a; Shackleton and Opdyke, 1976). Another cyclicity, which is present throughout, has a 23-kyr period.

The occurrence of all these periods has been explained by astronomical variations in the Earth's orbit, changing the incoming solar radiation (Milankovitch, 1930). The 100-kyr variations are related to the eccentricity of the Earth's elliptical orbit around the Sun. The short axis of this ellipse varies over time, changing the mean distance between Earth and Sun. The insolation changes by eccentricity variations have therefore a globally symmetrical impact and felt equally at all latitudes. The spin axis of the Earth is tilted by 23.5° from the perpendicular of the Earth's orbit today. This tilt changes from about 22 to about 24° with a period of 41 kyrs, having the highest effect on the incoming insolation at the high latitudes. The 23-kyr variations are related to the precession of the Earth's spin axis, which changes the strength of the seasonal variability. Low-latitude regions are very sensitive to these precessional changes since the differences in solar heating drive the seasonal atmospheric circulation changes, the monsoon.

For the MPT, there are no apparent astronomical reasons The orbital insolation parameters, that can be calculated back in time with high accuracy (Berger and Loutre, 1991; Laskar, 1990), varied in the same way before and after. It is therefore assumed that the cause for the MPT must be a different response of the global ice volume on orbital forcing. Thus, it has been suggested that the increase in ice volume was mainly due to the establishment of shelf-based ice sheets in high-latitude regions (Berger and Jansen, 1994). Time-series analyses of $\delta^{18}O$ records of deep-sea carbonates, which mainly reflect the global ice-volume development (Shackleton, 1987), showed that the increase in mean continental ice mass significantly preceded the establishment of the 100-kyr glacial cycle as dominant frequency (Mudelsee and Schulz, 1997). The most recent statistical examination of the ice-volume evolution indicates that a gradual increase in global ice mass lasting from 942 to 902 kyr BP

was followed by a rather abrupt onset of the 100-kyr cyclicity in ice-volume variations at 640 kyr BP (Fig. 1.1; Mudelsee and Schulz, 1997).

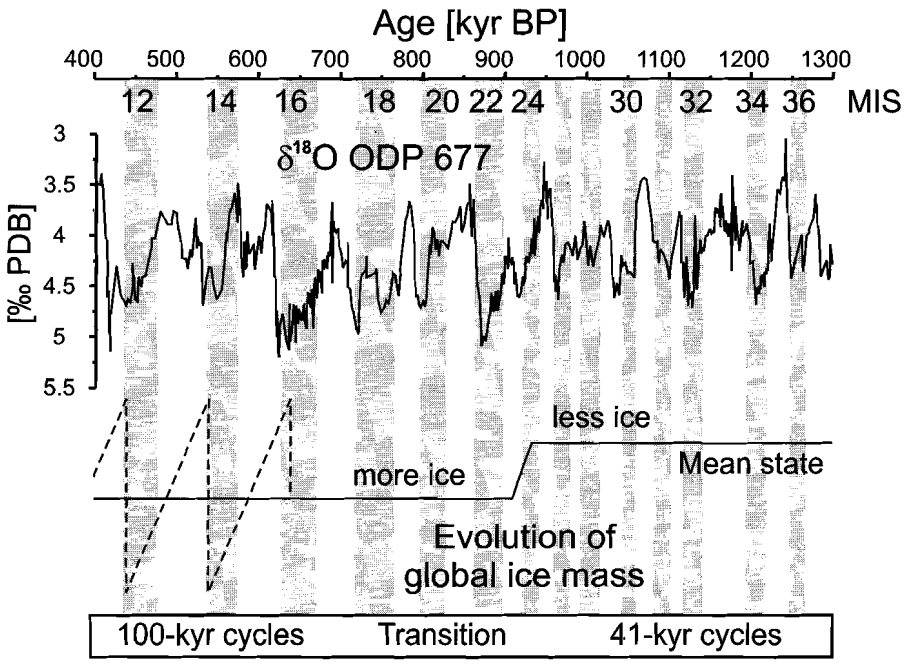

Figure 1.1: Above: The benthic $\delta^{18}O$ record of ODP Site 677 (Shackleton et al., 1990), used as ice-volume proxy for the mid-Pleistocene. Below: Schematic development of the global ice volume, based on investigation of several benthic ODP $\delta^{18}O$ records (Mudelsee and Schulz, 1997). Grey bars indicate glacial marine isotope stages (MIS). Both isotope records and the scheme are oriented towards less ice-volume conditions to the top.

A prominent feature of the MPT is the substantial perturbation of the global oceanic thermohaline circulation system (Broecker, 1991). The surface and deep currents in the sea are driven by the distribution of heat and salt in the Oceans and lead to a net northward transport of surface-water heat in the present Atlantic Ocean (Miller and Russell, 1989). North Atlantic Deep-Water (NADW), which dominates today's deep Atlantic Ocean, did the same during most of the period from 2.5 million years BP to the MPT. During the MPT, however, the NADW formation was most severely weakened, while its influence was reduced during the peak glacial times after the MPT (Raymo et al., 1997; Raymo et al., 1990). The reduced bottomwater ventilation during the MPT led to an inflow of more corrosive Antarctic Bottom Waters and decreased the carbonate accumulation rate in the deep South Atlantic (Schmieder et al., 2000). Apparently the ocean circulation system changed its operational mode during the MPT. The effect of the high-latitude ice-volume change and the breakdown of the thermohaline circulation during the MPT on the low-latitude climate are, however, largely unknown.

1.2. Research area

The South Atlantic is very sensitive to changes in the interhemispheric heat transport by surface water since it delivers immense amounts of tropical heat to the North Atlantic (Hastenrath, 1982). The region offshore the Congo River is characterised by a relatively high primary marine production (Berger, 1989) and high sedimentation rates due to the supply of erosion material by the Congo River (Jansen, 1985; Jansen et al., 1984). The long sediment cores drilled during ODP Leg 175 in the Congo deep-sea fan (Wefer et al., 1998) thus provide the possibility to construct a high-resolution record of environmental change in the tropical Atlantic and equatorial Africa during the MPT.

1.2.1. Hydrography of the Angola Basin

The Angola Basin is connected to the surface-circulation system of the tropical Atlantic via a cyclonic gyre (Fig. 1.2; Peterson and Stramma, 1991; van Bennekom and Berger, 1984). The eastward-flowing South Equatorial Counter Current (SECC) in the equatorial Atlantic feeds the warm, nutrient-poor Angola Current (AC), which flows southwards along the western African margin. At about 15°-17°S it converges with the northward-flowing cold, nutrient-rich Benguela Current (BC), is deflected to the north-west and combines with the South Atlantic Current (SAC) flowing to the equator (Fig. 1.2). At about 5°S, the low-salinity plume of the Congo (Zaire) River, the World's second largest river is superimposed on the surface circulation of the Angola Basin. The Congo plume stretches as far as 800 km offshore (van Bennekom and Berger, 1984). There is a seasonal variation in discharge, connected to the monsoonal circulation change (Eisma and van Bennekom, 1978; van Bennekom and Berger, 1984).

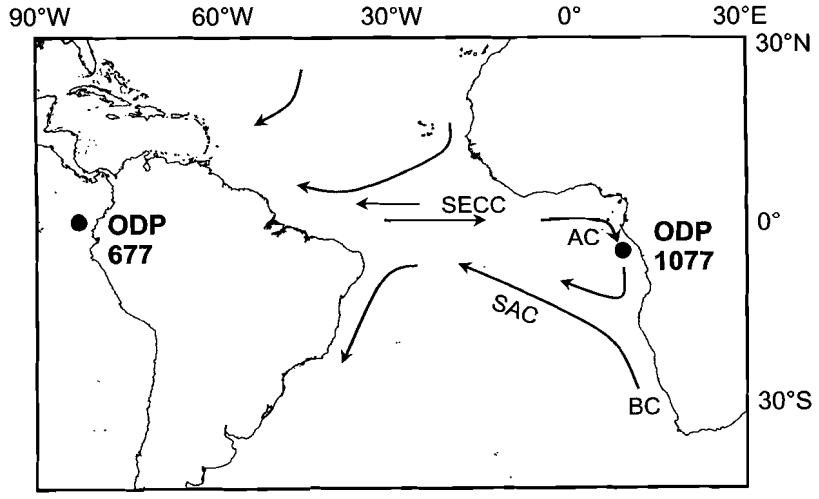

Figure 1.2: Overview map with the location of ODP Site 1077 and ODP Site 677 and the present-day surface and shallow subsurface currents in the Central Atlantic Ocean: BC = Benguela Current, SAC = South Atlantic Current, SECC = South Equatorial Counter Current, AC = Angola Current.

1.2.2. Seasonal atmospheric circulation change and effects on marine production

The SE trade winds of the Southern Hemisphere drive coastal upwelling along the African coast of the South Atlantic. But, while intense, year-round upwelling is causing high primary production, >200 $gC/m^2/yr$ off the coast of South Africa and Namibia (Berger, 1989; Shannon, 1985; Shannon and Pillar, 1986), elevated coastal productivity in the Angola Basin is restricted to two small, coastal upwelling cells north and south of the Congo River mouth (Fig. 1.3; Servain et al., 1982; Voituriez and Herbland, 1982). This shallow upwelling activity has the strongest effect on the nitrate concentrations and to a lesser extent on the phosphate concentrations, while its effect on silicate concentrations is insignificant (van Bennekom et al., 1978).

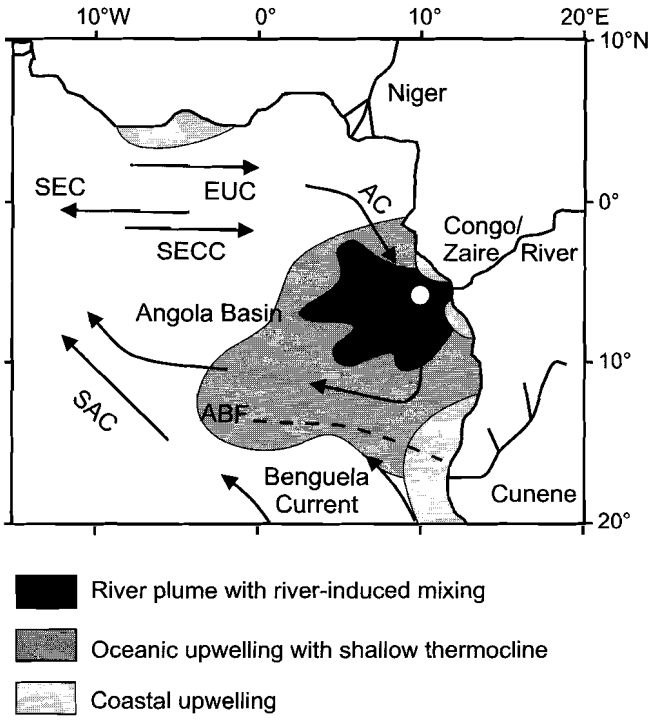

Figure 1.3: Detailed map of the Angola Basin with the major present-day currents: SAC = South Atlantic Current, SEC = South Equatorial Current, SECC = South Equatorial Counter Current, EUC = Equatorial Under Current, AC = Angola Current, ABF = Angola-Benguela Front. Shaded areas are regions of elevated productivity in the Angola Basin (after Schneider et al., 1994). Dark shading: River-induced production, medium shading: oceanic upwelling with shallow thermocline, light shading: coastal upwelling cells. Location of ODP 1077 is indicated by the white dot in the river plume.

During the austral winter (June to August), the Intertropical Convergence Zone (ITCZ) is furthest north (~20°N) causing strong zonal SE trade winds to blow over the Angola Basin (Fig. 1.4). These winds transport vast amounts of atmospheric dust from dry areas in southern Africa, i.e., the Kalahari savannah and the Namib Desert. A pronounced effect of the cyclonic gyre circulation in the Angola Basin is the shoaling of the thermo- and nutricline in the so-called Angola Dome, providing an elevated

supply of nutrients to the photic zone upon wind-driven surface-water mixing, the so-called oceanic upwelling, which leads to a high phytoplankton productivity (Fig. 1.3; Lutjeharms and Stokton, 1987; van Bennekom and Berger, 1984). In the eastern equatorial Atlantic the sea-surface temperature is at its annual minimum during the austral winter, when the surface-water productivity reaches its annual maximum (Katz and Garzoli, 1982). Offshore oceanic upwelling outside the Congo River plume induces moderate to high primary productivity of 90 to 180 gC/m^2/yr (Berger, 1989).

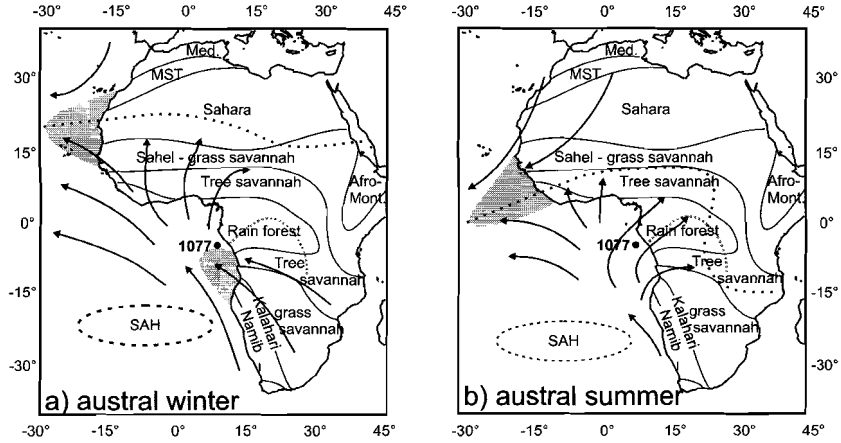

Figure 1.4: General pattern of present-day atmospheric circulation over Africa and the Southeast Atlantic Ocean in a) austral winter (June to August)) and b) austral summer (December to February). SAH, South Atlantic high-pressure system. The dotted lines indicate the Intertropical Convergence Zone (ITCZ). Dust plumes are shaded. Areas in Africa indicate vegetation zones. Med.: Mediterranean; MST: Mediterranean-Saharan transitional vegetation; Afro-Mont.: Afro-Montane vegetation zone. The grey stippled line in Equatorial Africa represents the main stream of the Congo River. The location of ODP Site 1077 is indicated.

During the austral summer (December to February) the ITCZ is in its southernmost position (5°-10°N), causing maximum monsoon conditions in southern equatorial Africa with a large influx of moist air and a high precipitation in the catchment area of the Congo River (Fig. 1.4; Hsü and Wallace, 1976). Dust transport does not occur during that season. The maximum extension of the Congo River plume is in February-March, later than the maximum river discharge in December (van Bennekom and Berger, 1984) and is associated with the highest annual sea-surface temperatures (SST) in the equatorial Atlantic (Katz and Garzoli, 1982). The outflowing Congo River water entrains subsurface waters with elevated concentrations of nitrate and phosphate to the silicate-rich river water, which causes river-induced productivity (Fig. 1.3; van Bennekom et al., 1978). About 150 to 200 km offshore the plume broadens. A marine phytoplankton bloom develops in the plume with a maximum of primary productivity found in a narrow meridional zone around 10°E (Cadée, 1978; Cadée, 1984). River-induced phytoplankton productivity off the Congo River mouth reaches values of 90 to 125 gC/m^2/yr (Berger, 1989) and is dominated by a high diatom contribution, 40 to 60 % of the total productivity (van Bennekom and Berger, 1984). Offshore, the level of primary productivity in the Congo River plume decreases due to the dilution of the river-derived nutrients with oceanic waters.

1.3. Sedimentary lipids
1.3.1. Lipid biomarkers

Of all the organic material produced in the World's ocean, only about 0.1 to 1 % is ultimately preserved in the sediments (Calvert and Pedersen, 1992). Because of the different preservation potential of organic compounds against oxic degradation during settling, burial and diagenesis, the composition of the sedimentary organic matter is highly biased from the originally produced material (Cowie and Hedges, 1994; Harvey et al., 1995). Solvent-extractable lipids comprise usually less than 5 % of the sedimentary organic matter since the predominant part consists of insoluble macromolecular material. This consists for a part of resistant biomacromolecules, such as lignin, cutan and algeanan (de Leeuw and Largeau, 1993) or is formed upon polymerisation/condensation of organic compounds from various sources (Tissot and Welte, 1984) or by natural vulcanisation, i.e., the incorporation of reduced inorganic sulphur species into organic compounds (Sinninghe Damsté and de Leeuw, 1990), leading to their preservation in sediments. Nevertheless, some biochemicals present in the sedimentary organic matter can provide highly specific information on the lipid contributions of organisms and its preservation state. Several classes of biota produce highly specific biochemicals as pigments, membrane lipids, or storage materials. These lipids can be distinguished by the structure of their carbon skeletons, the position(s) and nature of their functional groups and their stable carbon isotope composition. When this information can be retrieved from the sedimentary lipids it is often possible to relate the molecular fossils to classes of contributing organisms or even highly specific types of biota. If so, the sedimentary lipid can be called a biomarker, which can provide valuable insights in the environmental conditions during sediment deposition (de Leeuw et al., 1995). Under stable depositional conditions the varying concentration of the lipid biomarkers in the sediments can be related to the relative abundance of the contributing organisms in the ancient marine environment.

For example, 4,23,24-trimethylcholesterol (dinosterol) has been detected in many dinoflagellate algae (Nes and McKean, 1977). Consequently, the occurrence of dinosterol, and its diagenetic product dinosterane (de Leeuw and Baas, 1986), in sediments and crude oils has been related to the presence of dinoflagellates in the depositional environment (Boon et al., 1979). Another example are the di- and triunsaturated C_{37} methyl- and ethyl-alkenones, which are produced by the coccolithophorid *Emiliania huxleyi* (Volkman et al., 1980) and a few other Haptophyte algae (Volkman et al., 1995). The long-chain alkenones can furthermore be used to provide estimates for paleo sea-surface temperatures (Brassell et al., 1986a; Prahl et al., 1988). The ratio of the di- to the sum of the tri- and diunsaturated C_{37} alkenones, i.e., the U^{K}_{37}'-index, correlates with the annual mean sea-surface temperature (Müller et al., 1998). Long-chain *n*-alkanes are rather non-specific biochemicals with several origins. However, when exhibiting a strong odd- over even-number predominance in the C_{25} to C_{35} carbon number range, the occurrence of this compound class reflects the contribution of epicuticular waxes from terrestrial higher plants (Eglinton and Hamilton, 1963; Eglinton and Hamilton, 1967).

1.3.2. Stable carbon-isotope compositions

Carbon occurs in two natural stable isotopes on Earth: ^{12}C (ca. 98.9 %) and ^{13}C (ca. 1.1 %). Their relative amounts in organic material, however, vary significantly due to physical and biochemical fractionation processes. This variation is expressed as the ratio $^{13}C/^{12}C$ and compared with the ratio $^{13}C/^{12}C$ of a standard material (e.g., CO_2 produced from a carbonate belemnite of the Pee Dee formation in South Carolina: $^{12}C/^{13}C = 88.99$). The difference between these ratios is expressed in ‰ and termed:

$$\delta^{13}C_{sample} = (R_{sample}/R_{standard} - 1) \times 10^3, \text{ with } R = {}^{13}C/{}^{12}C.$$

Thus, a positive $\delta^{13}C$ of a sample indicates that it is enriched in ^{13}C relative to the standard.

The stable carbon isotope composition of organic material is determined by both the $\delta^{13}C$ of the carbon source and the physical and biochemical pathways by which it was formed from the carbon source. Mass-dependent fractionation effects occur during the diffusion of atmospheric CO_2 into plant cells. Additionally, the enzymatic preference for $^{12}CO_2$ relative to $^{13}CO_2$ during photosynthetic carbon fixation results in organic matter that is approximately 20 to 25 ‰ depleted in ^{13}C relative to the $\delta^{13}C$ value of the CO_2 from which it was formed. Heterotrophy, selective preservation and diagenetic alteration can, however, strongly affect the stable carbon isotope composition of bulk organic matter. The $\delta^{13}C$ values of biomarkers, in contrast, remain largely unaffected (Freeman et al., 1990; Grice et al., 1998; Hayes, 1993). Measurement of the ^{13}C content of lipid biomarkers therefore enables the recognition of biosynthetic pathways and other processes involving fractionation effects (Freeman et al., 1990; Hayes, 1993; Hayes et al., 1990) and can provide important insights into paleoenvironmental conditions under which photosynthetic carbon fixation occurred (Farquhar et al., 1989; O'Leary, 1981). The stable carbon isotope composition of leaf-wax lipids of different terrestrial vegetation types (C_3, C_4, CAM), for instance, depends on the carbon-fixation pathway utilised during photosynthesis (Collister et al., 1994; Rieley et al., 1993), enabling the recognition of large-scale vegetation changes from their $\delta^{13}C$ values in sediments.

1.4. Scope and framework of this thesis

The investigations presented in this thesis were conducted to study the effects of the MPT on the sea-surface conditions and the marine and terrestrial ecosystems of the tropical Atlantic and in equatorial Africa. This examination has been performed by organic geochemical investigations of sediments deposited in the Angola Basin. For a proper interpretation of the lipid parameters and their $\delta^{13}C$ values, we conducted calibrations of the lipid biomarker proxies in modern surface sediments and recent atmospheric dust materials. In this way, the significance and applicability of the lipid biomarker parameters in the investigated depositional setting were tested. Using these lipid proxies, the response and impact of the tropics on the enlarged global ice volume and its lower-frequency variations was examined. We studied how the high-latitude climate changes manifest themselves in the low-latitudes. The deviation of some climate proxies from a cyclic behaviour in the course of the MPT allows the recognition of dominant forcing factors for paleoenvironmental changes. This sheds new lights on the significance of the low-latitude climatic conditions and their (paleo)-environmental effects.

This thesis is divided in three parts: **Part I** consists of this introduction (**Chapter 1**) and an introductory **Chapter 2** that gives an overview of the lipid geochemistry of sediments drilled during ODP Leg 175 in the eastern South Atlantic. Using shipboard samples from six cores of ODP Leg 175, an attempt is made to characterise the different depositional settings by their biomarker geochemistry. Specific assemblages of terrigenous and marine biomarker compounds are distinguished and an initial environmental interpretation is given. Based on these findings, it was decided to investigate one of the sites located in the Congo River fan in greater detail, since these cores exhibit the largest downcore variations in lipid biomarker contents of all examined sites. We, therefore, expected to find the strongest signals of environmental changes in the sediments deposited offshore the Congo River and focused on ODP Site 1077 (Fig. 1.5).

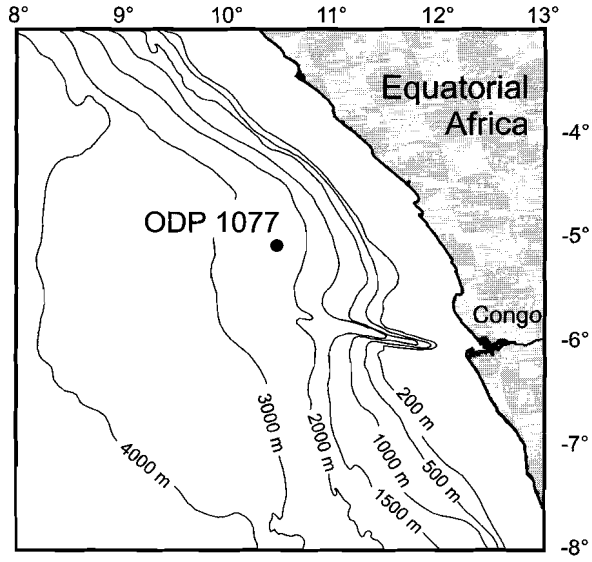

Figure 1.5: The location of ODP Site 1077 (10°26.2'E, 5°10.8'S) on the northern lobe of the Congo deep-sea fan at 2382 m water depth.

Part II contains the examinations on the modern lipid biomarker distributions. For a proper interpretation of variations in the past, an accurate understanding of the present significance of organic geochemical parameters in the research area is needed.

Atmospheric dust samples collected along a transect off the West African coast reveal changes in the distributions of terrigenous lipids and their stable carbon isotopic compositions (**Chapter 3**). The organic solvent extracts consist mainly of lipids derived from the epicuticular wax coating of terrestrial higher plants. The backward trajectories for each sampling day and location, calculated using a global atmospheric circulation model, show that the dust transport mainly took place in the low-level trade-wind layer, except in the equatorial region, where long-range transport in the mid-troposphere may have occurred. The stable carbon isotopic composition of the leaf-wax biomarkers reveals the contribution of C_4 plant-derived lipids in the aerosols. These lipids were picked up along the dust transport pathways and reflect mainly the contemporary vegetation type on the adjacent continent (Fig. 1.4). Wind

abrasion of wax particles from leaf surfaces, therefore, is presumably the dominant process of terrigenous lipid contribution to dust.

In **Chapter 4** the bulk and molecular organic geochemical parameters in a set of twenty-nine surface sediments from the eastern South Atlantic were examined. A principal component analysis identified the groups of geochemical parameters with a similar spatial distribution. The five main processes controlling the modern distributions of lipid biomarkers and bulk organic geochemical parameters are wind-driven deep upwelling, shallow coastal upwelling, river transport of terrigenous material, eolian transport of plant waxes from dry continental areas, and marine productivity related to river-induced productivity or oceanic upwelling off the Congo. The lipid distributions adequately reflect phytoplankton-specific production (Fig. 1.3), transport and preservation processes in the eastern South Atlantic, thus providing a strong base for paleoenvironmental reconstructions based on the fossil record.

In **Part III** of the thesis the paleoenvironmental changes during the MPT in the tropical eastern Atlantic and in Equatorial Africa are investigated in detail with lipid geochemical parameters from ODP Site 1077 (10°26.2'E, 5°10.8'S, 2382 m water depth). The drill site is located on the northern lobe of the Congo deep-sea fan, which is cut by a 200-700 m deep canyon, about 275 km off the mouth of the Congo River (Fig. 1.5; Wefer et al., 1998). The continuous 205.1 m long, hemipelagic sedimentary section is composed of greenish grey diatom-rich, diatom-bearing, nannofossil-bearing, and nannofossil-rich clay (Wefer et al., 1998).

In **Chapter 5** the tropical mid-Pleistocene sea-surface temperature (SST) record, based on the unsaturation pattern of long-chain alkenones, is compared with the temporal evolution of orbital variance, global ice volume and Atlantic deepwater ventilation. The increase of the 100-kyr period power in the SST variations coincided with the onset of 100-kyr periodicity in the ice-volume changes. However, in both the obliquity and eccentricity cycle, tropical SST significantly led over high-latitude ice-volume changes. This tropical lead is most likely an early response of wind-driven upwelling and heat advection, controlled by the surface thermal gradient of the South Atlantic, on orbital-driven insolation changes. The long-term evolution of the tropical SST, however, appears to be influenced primarily by the strength of NADW formation, ventilating the deep Atlantic. All glacials in the MPT are characterised by severe reductions of NADW formation, causing decreased surface-water heat export from the tropics to higher latitudes and, successively, a long-term heat accumulation in the tropical Atlantic Ocean (Fig. 1.2). The growth of enlarged ice sheets during the MPT thus strengthened the role of the thermohaline circulation in the climatic coupling between high- and low latitudes.

The location of ODP Site 1077 receives its modern dust input by the Southern Hemisphere trade winds with the austral winter dust plume originating from the dry areas of southern Africa (Fig. 1.4). In **Chapter 6** the accumulation rates and stable carbon isotope compositions of terrestrial plant-wax *n*-alkanes in sediments of ODP Site 1077 are examined. The leaf-wax accumulation in the mid-Pleistocene was significantly increased when the global ice volume had grown to a larger volume. Compression and intensification of the atmospheric Hadley cell by the steeper thermal gradient in the South Atlantic strengthened the zonal trade-wind vector and shifted the belt of zonal trade winds northwards after the increase of the ice-volume. The large-scale vegetation changes in southern Africa, however, recorded as C_3/C_4 plant variations in the stable carbon isotope compositions of the *n*-alkanes, do not resemble the development of the global ice-volume and inferred parallel pCO_2 variations. Instead, a strong correlation can be detected between the C_3/C_4 plant variations and

the tropical SST changes from ODP Site 1077. The SST maxima are in phase with C_4 plant minima in the long-term and in the eccentricity and obliquity cycle. This rules out a direct forcing by air temperatures, as elevated growing season temperatures should lead to more C_4 plants. In line with recent climate models, African aridity is a direct function of low-latitude sea-surface temperatures, controlling the tropical atmospheric precipitation-evaporation balance. Only in the precession cycle, the maximum monsoonal influx of moisture during the austral summer corresponds with the maximum austral winter upwelling, leading to coinciding SST and C_4 plant minima.

In **Chapter 7** we examine the environmental changes during the mid-Pleistocene in the tropical Atlantic in relation to the enlarged ice volume and its changing frequency behaviour using the majority of the investigated lipid biomarkers and bulk geochemical parameters. The accumulation of lipids derived from river-induced production and wind-driven oceanic upwelling was enhanced during the contemporary maximum of trade-wind zonality and river runoff in the precessional cycle. Precessional forcing of river-related and total marine productivity was dominant before the MPT. The ice-volume growth suppressed the precessional variability in monsoonal trade-wind zonality and river runoff, and thus decreased the low-latitude influence on the tropical phytoplankton ecosystem. In turn, the contributions of wind-transported plant waxes and lipids produced during wind-driven upwelling were strongly enhanced after the growth of the global ice volume and responded to the onset of the 100-kyr variability in trade-wind strength and zonality. Generally, the MPT caused a shift from a primary low-latitude forcing in the tropical Atlantic to a stronger ice-volume forcing, manifesting itself as a suppression of the river-influence and as stronger and more zonal trade winds.

Chapter 2

Marine and terrigenous lipids in South-East Atlantic sediments (Leg 175) as paleoenvironmental indicators: initial results

Enno Schefuß, Gerard J. M. Versteegh, J. H. Fred Jansen, Jaap S. Sinninghe Damsté

Published in *Proceedings of the Ocean Drilling Program, Scientific Results Vol. 175* (Editors: Wefer, G., Berger, W.H., Richter, C. et al.), College Station, Texas, p. 1-34, [Online at: http://www-odp.tamu.edu/publications/175_SR/chap_10/chap_10.htm].

Abstract

Lipid compositions of sediments recovered during Ocean Drilling Program (ODP) Leg 175 in the eastern South Atlantic reflect a variety of oceanographic and climatological environments. Most of the identified lipids can be ascribed to marine sources, notably haptophytes, eustigmatophytes, dinoflagellates, archaea, and diatoms. Elevated concentrations of cholesterol suggest zooplankton herbivory, characteristic for sites influenced by upwelling. At these sites, sulphurised highly branched isoprenoids from diatoms are also present in high amounts. Sterols, sterol ethers, hopanoids, and mid-chain hydroxy fatty acids could also be detected. Terrigenous lipids are *n*-alkanes, fatty acids, *n*-alcohols, and triterpenoid compounds like taraxerol and β-amyrine. *n*-Alkanes, fatty acids and *n*-alcohols are derived from leaf waxes of higher land plants and transported to the sea by airborne dust or fresh water. Triterpenoid compounds are most probably derived from mangroves and solely transported by rivers. Lipid compositions below the Congo low-salinity plume are strongly influenced by terrigenous material from the Congo River. Elevated organic carbon contents and predominantly marine lipid distributions at the Angola margin may indicate a highly productive plankton population, probably sustained by the Angola Dome. Sedimentary lipids in the Walvis Basin contain an upwelling signal, likely transported by the Benguela Current. Sedimentary lipids off Lüderitz Bay and in the southern Cape Basin are dominated by plankton lipids in high to intermediate amounts, reflecting persistent and seasonal upwelling, respectively.

2.1. Introduction

The eastern South Atlantic plays an important role in the global heat transport system (Berger and Wefer, 1996). It contains one of the largest upwelling systems world-wide and receives clastic and organic material from the second-largest river in the World. The oceanographic environments include: a tropical region strongly affected by river discharge, a tropical oceanic region, and a region influenced by coastal upwelling. It should thus be possible to distinguish all these depositional settings by specific assemblages of terrigenous and marine components. Lipid biomarker compositions provide information on different types of terrigenous lipid sources and a detailed view on marine plankton groups contributing to the sedimentary organic matter. Furthermore, the biomarkers in marine sediments can supply information on early diagenetic reactions in the sediments, and paleoceanographic conditions (Brassell, 1993).

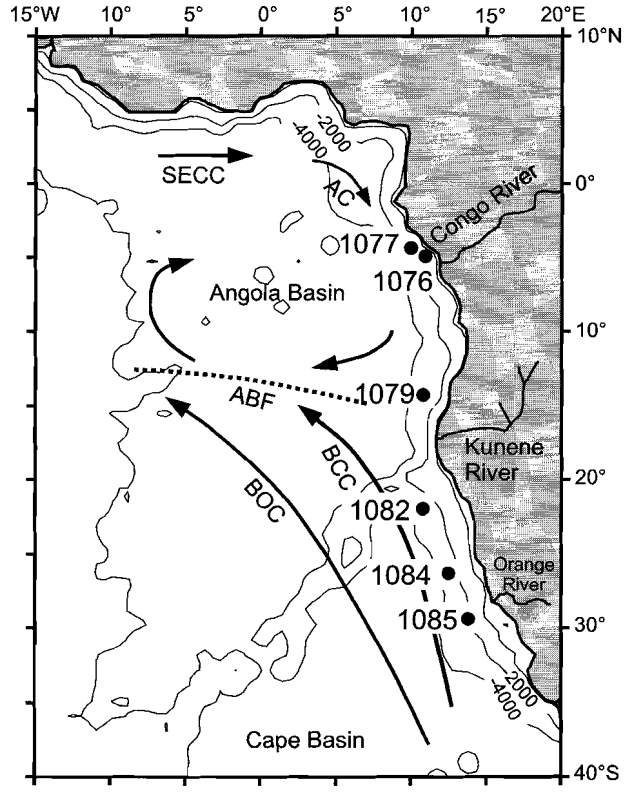

Figure 2.1: Site locations and generalised surface hydrography (after Wefer et al., 1998). SECC = South Equatorial Counter Current, AC = Angola Current, ABF = Angola-Benguela Front, BCC = Benguela Coastal Current, BOC = Benguela Oceanic Current.

For these purposes, a detailed molecular organic geochemical overview study was performed on 2-3 samples each from ODP Sites 1076, 1077, 1079, 1082, 1084, and 1085 in the Southeast Atlantic Ocean (Fig. 2.1). The study is intended to be solely inventory; samples were chosen randomly from different sediment depths in each core

(Table 2.1). Therefore, only restricted paleoceanographic interpretations can be drawn from the results. The concentrations of single compounds and lipid classes are used to compare the different oceanographic environments with respect to terrigenous, phytoplanktonic, and zooplanktonic lipids. An attempt is made to give an overview for each site about the lipid biomarkers present and their potential use as paleoceanographic indicators. Earlier organic geochemical investigations of sediments from this particular ocean area (e.g., Boon, 1978) provided valuable background information.

2.1.1. Oceanographic setting

In the present-day eastern South Atlantic, the South Equatorial Countercurrent in the north feeds the warm southward-flowing waters of the Angola Current (AC, Fig. 2.1). At about 15°-17°S, these waters converge with the cold northward-flowing Benguela Coastal Current and are deflected to the northwest. A sharp frontal zone, the Angola-Benguela Front (ABF), is established and extends to a distance of up to 1000 km off the coast (Meeuwis and Lutjeharms, 1990). The ABF effectively forms a barrier for surface-ocean transport, as does the Walvis Ridge for deep water.

The cyclonic gyre in the Angola Basin is overlain by the low-salinity plume of the Congo River at about 5°S. Sites 1076 and 1077 are located below the Congo plume. Riverine input, coastal upwelling and incursions of open ocean waters influence this environment. Site 1076 is the shallowest location and should record the strongest interaction of river discharge and coastal upwelling. Site 1077 is at larger water depth and presumably more influenced by open-ocean conditions.

In the eastern Angola Basin the cyclonic circulation causes shoaling of the thermocline and supply of nutrients to the photic zone. Site 1079 is located on the Angola margin and is neither directly influenced by rivers nor situated under a coastal upwelling cell (Lutjeharms and Stokton, 1987). Productivity benefits from seasonal supply of nutrients from the Angola Dome.

In the south, the Benguela Current is fed by the South Atlantic Current and the Agulhas Current. At about 30°S, the Benguela Current splits into the Benguela Oceanic Current, the main current in northwestern direction, and the Benguela Coastal Current, flowing as a sluggish, wide current along the continental margin. These currents are driven by the predominantly southerly and southeasterly winds (Shannon, 1985). Off the coast of South Africa and Namibia, these winds drive coastal upwelling of cold, nutrient-rich South Atlantic Central Water (Shannon, 1985). Productivity reaches high values of over 180 $gC/m^2/yr$ (Berger, 1989). Site 1082 is located in the Walvis Basin, outside recent upwelling activity. Since filaments of cold, nutrient-rich waters extend up to 600 km offshore (Lutjeharms and Stokton, 1987) where they mix with low-productivity waters sustaining intermediate productivity, Site 1082 most probably records an upwelling signal transported by filaments and eddies. Site 1084 is situated close to the upwelling cell in Lüderitz Bay. At this site, persistent upwelling of South Atlantic Central Water (Shannon, 1985) causes high productivity and high rates of sedimentary accumulation of phytoplankton biomass (Brown et al., 1991). Site 1085 is located in the southern part of the Cape Basin, near the continent. Besides seasonal upwelling activity, this site may also record terrigenous supply from the Orange River.

2.2. Material and Methods

2.2.1. Samples

The samples investigated were taken during the expedition onboard the JOIDES RESOLUTION and kept frozen until analyses. Because the sampling was already done onboard, no detailed sampling strategy was applied. Sample information is given in Table 2.1.

Table 2.1: Samples analysed in this study, locations, water depths, depths below sea floor (in meters composite depth), organic carbon contents, and approximate ages.

Core, section, interval (cm)	Location (Longitude, Latitude)	Water depth (m)	Depth (mcd)	TOC (%)	Age (Ma)
175-1076A 4H 2, 75-77	11°6.1'E,	1402	30.51	3.06	0.15
7H 2, 75-77	5°4.1'S		61.16	1.74	0.25
15H 2, 75-77			142.08	1.90	1.0
175-1077A 9H 2, 75-77	10°26.2'E,	2394	79.13	1.83	0.7
13H 2, 75-77	5°10.8'S		118.47	1.15	0.9
175-1079A 2H 4, 46-49	13°18.5'E,	749	10.26	2.50	0.1
13H 4, 46-49	11°55.8'S		117.65	2.97	0.7
175-1082A 6H 1, 105-108	11°49.2'E,	1280	51.86	10.69	0.65
53X 3, 27-30	21°5.6'S		503.63	8.50	5.0
175-1084A 12H 6, 140-143	13°1.7'E,	1990	120.72	12.82	0.7
25X 3, 20-23	25°30.8'S		242.6	11.61	1.4
51X 3, 20-23			493.00	5.12	3.2
175-1085A 11X 3, 20-23	13°59.4'E,	1713	102.4	8.10	2.2
50X 3, 20-23	29°22.5'S		489.56	7.32	10

Note: All data, except TOC data, from Wefer et al. (1998).

2.2.2. Extraction and fractionation of soluble organic matter

Sediment samples were lyophilised and finely ground in an agate mortar, and subsequently extracted ultrasonically using 40 mL of methanol (MeOH) (3x), 40 mL of dichloromethane (DCM):MeOH (1:1, v/v) (3x), and 40 mL of DCM (3x), each for 5 min. For each sample, the extracts were combined and concentrated with a rotary evaporator at 35°C. Salts were removed by washing with double-distilled H_2O in a separatory funnel and extraction of the lipids with DCM (3x). For total lipid analysis known aliquots of the extracts with an added amount of standard (2,3-dimethyl-5-1',1'-d_2-hexadecyl-thiophene) were methylated with diazomethane after drying with anhydrous Na_2SO_4. Before silylation with bis(trimethyl-silyl)trifluoro-acetamide in pyridine (1 hr at 60°C), very polar compounds were removed on a silica-gel column eluted with ethyl acetate. Before fractionation, extracts were mixed with known amounts of thiophene and chroman standards and separated on a column (4 cm) packed with activated Al_2O_3. Apolar fractions were collected by elution with four

column volumes of hexane:DCM (9:1, v/v) and polar fractions by stripping the columns with MeOH:DCM (1:1, v/v).

One sample, 175-1084A-12H-6, 140-143 cm, was further separated by thin-layer chromatography (TLC). The plate was developed with di-isopropylether/acetic acid (96:4, v/v) to 75 % of the height of the plate and redeveloped with petroleum ether 40-60/ether/acetic acid (89:10:1, v/v; Skipski et al., 1965). Eight fractions were scraped off the TLC plate and ultrasonically extracted using hexane (3x) for the TLC fractions 1 and 2 and ethyl acetate (3x) for other fractions. Fractions were cleaned on a small column filled with non-activated alumina by elution with hexane/DCM (9:1, v/v) and subsequently methylated and silylated before analyses. The polar fraction of Sample 175-1084A-12H-6, 140-143 cm was desulphurised with Raney nickel (Sinninghe Damsté et al., 1988) followed by hydrogenation.

2.2.3. Instrumental analyses

Gas chromatography (GC) was performed on a Hewlett Packard 5890 series II chromatograph equipped with an on-column injector and fitted with a fused-silica capillary column (25 m x 0.32 mm) coated with CP Sil 5 (film thickness 0.12 μm). helium was used as carrier gas, and the oven was programmed from 70°C to 130°C at 20°C/min, followed by 4°C/min to 320°C (10 min holding time). Effluents were detected using flame ionisation (FID). GC-mass spectrometry (GC-MS) was performed using the same type of gas chromatograph and the conditions described above. The chromatographic column was directly inserted into the electron impact ion source of a VG Autospec Ultima mass spectrometer operated with an ionisation energy of 70 eV and scanned over a mass range of *m/z* 50-800 with a cycle time of 1.8 s. Compound identifications are based on comparison of relative GC retention times and mass spectra with those in the literature. Quantification of long-chain alkenones, alkyldiols and biphytanediols was performed by integration of their peaks and those of internal standards in FID chromatograms. Data were acquired and integrated using Atlas analytical software. Other biomarkers were quantified using characteristic fragment ions in mass chromatograms. Resulting abundance values were converted to concentrations by compound-specific correction factors determined in samples, in which these compounds could be identified in FID traces. The relative precision of the entire analytical procedure, based on duplicate sediment extractions, was between 10 % and 15 %. Concentrations are calculated in μg/g TOC. Total organic carbon (TOC) contents were measured after decalcification of samples on a Carlo Erba NA-1500 Elemental Analyser using flash combustion at 1050°C. Standard deviations of duplicate measurements were better than 0.3 %.

2.3. Results and Discussion

Figure 2.2 shows chromatograms of two total lipid fractions (Samples 175-1077A-9H-2, 75-77 cm, and 175-1084A-12H-6, 140-143 cm), with compounds listed in Tables 2.2 and 2.3. A wide variety of biomarkers from both terrestrial plants and marine sources such as algae, (cyano)bacteria, and archaea occurs in the samples. These will be discussed according to compound classes.

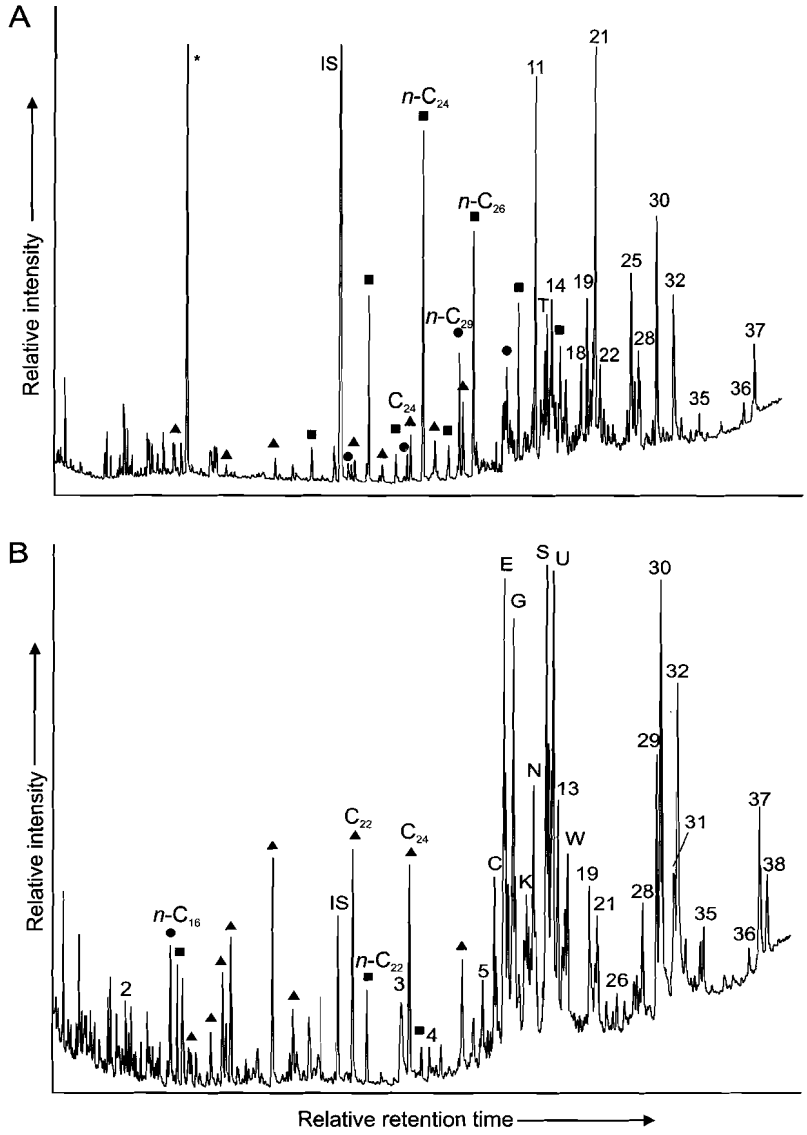

Figure 2.2: Total ion current (TIC) chromatogram of total lipid fraction of A) Sample 175-1077A-9H-2, 75-77 cm, and B) Sample 175-1084A-12H-6, 140-143 cm. Numbers indicate compounds listed in Table 2.2, letters indicate sterols listed in Table 2.3; triangles = fatty acids; dots = *n*-alkanes; squares = *n*-alcohols; IS = internal standard; * = contamination.

Table 2.2: Compounds identified in selected samples from Leg 175.

Number	Compound	Structure
1	*Iso*-loliolide	
2	Loliolide	XI
3	Perylene	XIV
4	C_{27} steradiene	
5	C_{27} sterene	
6	Hop-17(21)-ene	
7	*Neo*-hop-13(18)-ene	
8	Fern-9(11)-ene	
9	12-hydroxy-hexacosanoic acid	
10	17β,21β(H)-*homo*-hopane	
11	Taraxer-14-en-3β-ol (taraxerol)	II
12	Olean-12-en-3β-ol (β-amyrin)	III
13	12-hydroxy-octacosanoic acid	VIII
14	4α,23,24-trimethylcholest-22-en-3β-ol (dinosterol)	IXd
15	Octacosane-1,14-diol	
16	Friedelan-3-one	IV
17	4α,23,24-trimethyl-5α-cholestan-3β-ol (dinostanol)	
18	Hopan-22-ol (diplopterol)	
19	Glyceroldipentadecylether	
20	*n*-Triacontan-1-ol-x-one; x = 13, 15	VII
21	Triacosane-1,x-diol; x = 13, 14, 15	VI
22	*n*-Untriacontan-1-ol-x-one; x = 13, 15	
23	Untriacontane-1,x-diol; x = 13, 14, 15	
24	*n*-Dotriacontan-1-ol-x-one; x = 13, 15	
25	Dotriacontane-1,15-diol	
26	17β,21β(H)-*homo*-hopan-31-ol	
27	17β,21β(H)-*dihomo*-hopanoic acid	
28	17β,21β(H)-*dihomo*-hopan-32-ol	XIII
29	$C_{37:3}$ methyl ketone	
30	$C_{37:2}$ methyl ketone	V
31	$C_{38:3}$ methyl + ethyl ketones	
32	$C_{38:2}$ methyl + ethyl ketones	
33	$C_{38:3}$ alkene-3-ol	
34	*Trihomo*-hopan-32,33-diol	
35	$C_{39:2}$ ethyl ketone	
36	C_{40} dicyclic biphytanediol	XIIb
37	C_{40} tricyclic biphytanediol	XIIa
38	*Pentakishomo*-hopane-keto-diol	

2.3.1. Terrigenous lipids

n-Alkanes

n-Alkanes in the studied sediments range in carbon number from 18 to 35, with C_{25}-C_{33} *n*-alkanes as the most dominant homologues (Fig. 2.3). A strong odd-over-even carbon number predominance (carbon preference index, $CPI_{25\text{-}33}$ = 3-10; Table 2.4) was observed in all samples, indicating a predominantly terrigenous origin of the *n*-alkanes. These distributions resemble those of *n*-alkanes from leaf waxes of higher plants (Eglinton and Hamilton, 1967; Kolattukudy, 1976) and in eolian dust samples (Gagosian et al., 1987; Gagosian et al., 1981; Simoneit et al., 1977), supporting a terrigenous origin.

Concentrations of *n*-alkanes in sediments from Sites 1076 and 1077 are much higher than in sediments from the southern sites (see Table 2.4). These differences can probably be related to the different oceanographic and climatologic settings for both regions. The northern sites (1076, 1077, and to a minor extent also 1079) receive river

input of terrigenous organic matter, while the terrigenous compounds in the southern sites are mainly transported via the wind and diluted by a high production of marine lipids due to the upwelling activity. The variations in concentrations of leaf-wax components at the southern sites possibly result from changes in the strength and direction of the trade winds, influencing the strength of marine upwelling and, therefore, the relative dilution of terrigenous by marine lipids.

At the northern sites (Sites 1076, 1077, and 1079) the *n*-alkane distributions maximise at *n*-nonacosane (*n*-C_{29}; structure I, see Fig. 2.4 for structures). In samples from Sites 1082, 1084, and 1085, *n*-untriacontane (*n*-C_{31}) is most abundant. The chain-length distributions of the *n*-alkanes could thus reflect different sources of the terrigenous compounds in both regions. The average chain length (ACL) of the C_{25}-C_{33} *n*-alkanes changes from about 29.6 in the northern sediments to about 30.4 at the southern sites (Table 2.4). It has been suggested that plants produce longer-chain compounds in warmer climates (Poynter et al., 1989). The observed shift in our limited data set contradicts this interpretation. At present, vegetation in southern Africa consists predominantly of savannah-type grasslands, whereas in the more northern, tropical parts lowland rainforest and Afromontane forest dominate. Therefore, an influence of vegetation type on chainlength of terrigenous leaf lipids seems more likely. Leaf lipids derived from grasslands may on average have longer chain lengths than leaf lipids from rainforest plants (Cranwell, 1973). Obviously, the limited number of samples in this study prevents any further conclusions on this subject, which will be addressed in future research.

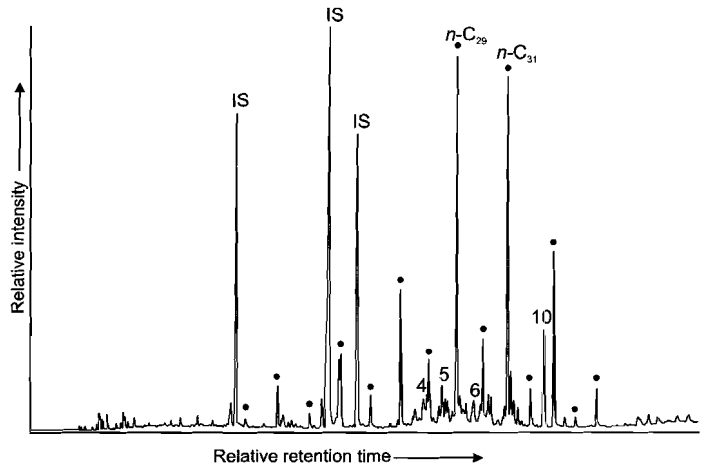

Figure 2.3: TIC chromatogram of the apolar fraction of Sample 175-1076A-15-2, 75-77 cm. Numbers refer to compounds listed in Table 2.2. *n*-Alkanes are indicated by black dots. IS = internal standard.

Fatty acids and *n*-alcohols

Fatty acids in the sediments range in carbon number from C_{16} to C_{30} with only small amounts of C_{16} to C_{18} fatty acids. *n*-Alcohols occur in the carbon number range of C_{20} to C_{30}. The highest concentrations of fatty acids and *n*-alcohols occur in the sediments close to the Congo River, where also the largest variation could be detected (Table 2.4). The lowest concentrations of both compound classes are present in the sediments from the Walvis Basin (Site 1082). Even-carbon-numbered long-chain

compounds dominate the distributions of both compound groups. The dominance of the long-chain compounds, together with the observed strong even-over-odd carbon-number predominance (for both classes, $CPI_{22\text{-}28}$ = 5-11), indicate a terrigenous origin for fatty acids and *n*-alcohols. Series of long-chain fatty acids and *n*-alcohols with a strong even-carbon-number predominance are characteristic constituents of surface waxes of higher plants (Kolattukudy, 1976). Therefore, the biological source of these compounds is closely related to that of the leaf-wax-derived *n*-alkanes. Similar to the *n*-alkanes, the high concentrations of fatty acids and wax alcohols in the Congo plume sediments suggest a predominant fluvial supply, while the smaller amounts at other sites are more readily explained to be derived from dust (Gagosian et al., 1987; Gagosian et al., 1981; Simoneit et al., 1977). An algal origin of the long-chain fatty acids, however, cannot be completely excluded (Volkman et al., 1998). Marine microalgae are not a major source of long-chain *n*-alcohols but may contain minor amounts of these compounds (for a review see Volkman et al., 1998). However, the strong covariance of the concentrations of fatty acids and *n*-alcohols with the concentrations of *n*-alkanes, together with their high CPI values indicate that autochthonous sources of fatty acids and *n*-alcohols are of minor importance. Higher-plant leaf-waxes are the main source.

Pentacyclic triterpenoids

Two pentacyclic triterpenoid alcohols were detected in samples from Sites 1076, 1077, and 1079 (see Fig. 2.2). They were identified as taraxerol (taraxer-14-en-3β-ol, II, Fig. 2.4) and β-amyrine (olean-12-en-3β-ol, III, Fig. 2.4) by comparison with mass spectra published by Killops and Frewin (1994) and relative retention times. The largest quantities were found in sediments located below the Congo River plume (Sites 1076 and 1077), and a smaller amount in sediments from the Angola margin (Site 1079). In samples from the Congo, the triterpenoid concentrations varied strongly, and they were below the detection limit in samples from the southern Sites 1082, 1084, and 1085. Another triterpenoid compound present in trace amounts in samples from Sites 1076, 1077, and 1079 is friedelan-3-one (IV, Fig. 2.4), a triterpenoid ketone.

All three pentacyclic triterpenoids (II - IV, Fig. 2.4) are widespread in higher plants (Beaton et al., 1955) and therefore represent a terrigenous source. Their occurrence has been reported in several marine sediments (Brassell and Eglinton, 1983; Volkman et al., 1987). β-Amyrine has been isolated from several species of mangroves, including some species of *Rhizophora* (Ghosh et al., 1985). In *Rhizophora mangle*, it was found to be a major component of the epicuticular wax of the leaves, while taraxerol was largely bound in the cutin fraction of the leaves (Frewin et al., 1993; Killops and Frewin, 1994). Another mangrove species, *Avicennia germinans*, contains smaller amounts of β-amyrine and taraxerol (Killops and Frewin, 1994). At present, the dominant mangrove species in the Congo area is *Rhizophora racemosa* (Moguedet, 1980). We suggest therefore, that this species, or its predecessor, is the major source of β-amyrine and taraxerol in the sediments. The strong variation in triterpenoid content between the samples could, thus, give an indication of the proximity and the extent of mangrove vegetation in the Congo area. Interestingly, none of the pentacyclic triterpenoid compounds could be detected in sediments from sites south of the Angola-Benguela Front (ABF). This is in agreement with the present restriction of mangrove swamps to humid, tropical environments north of the ABF. Furthermore, it strongly favours the hypothesis of fluvial rather than atmospheric

transport of mangrove lipids. The northward-flowing Benguela Coastal Current could limit southward transport of lipids at the ABF.

2.3.2. Marine lipids

Long-chain alkenones

All sediment samples contain C_{37} and C_{38}, and to a lesser extent C_{39}, di-, and tri-unsaturated methyl and ethyl ketones (V, Fig. 2.2; de Leeuw et al., 1980). The highest concentrations of these compounds were found in samples from Site 1084 (up to 1400 μg/g TOC), but the highest variability was detected in samples from Site 1076, where the maximum concentration was slightly smaller. Concentrations of alkenones in sediments from other sites are much smaller in range and absolute amount. These lipids are exclusively biosynthesised by haptophyte algae like *Emiliania huxleyi* and *Gephyrocapsa spp.* (Marlowe et al., 1984; Volkman et al., 1995; Volkman et al., 1980) and were detected in numerous marine sediments (Brassell et al., 1986a), including the South Atlantic. Changes in coccolithophorid assemblages seem not to have affected alkenone production (Müller et al., 1997). Sedimentary alkenone concentrations have also been used as an indicator for marine primary production (Hinrichs et al., 1999; Schubert et al., 1998; Villanueva et al., 1998). The U^{K}_{37}' index, the ratio of the diunsaturated to the sum of the di- and triunsaturated C_{37} alkenones, is extensively used in paleoceanography as a temperature proxy. It has been shown that the U^{K}_{37}' index is strongly correlated to sea-surface temperature (Brassell, 1993). The calculated sea-surface temperature estimates using the temperature calibration for the South Atlantic by Müller et al. (1998) are given in Table 2.4. The lowest sea-surface temperature is reconstructed for samples from below the upwelling activity. This suggests upwelling of cold South Atlantic Central Water as the main cause. Highest temperatures and largest temperature variability were detected for samples from Site 1082 in the Walvis Basin. Because of our limited data set, we regard any suggestion on the cause of this large range of temperatures as highly speculative. Alkenone concentrations are generally elevated during times of lower sea-surface temperatures (Table 2.4). This observation indicates that haptophyte algae are strongly dependent on upwelling events, which decrease sea-surface temperature and increase nutrient concentrations.

Alkyl diols and -keto-ols

Long-chain saturated C_{28}-C_{32} alkyl diols (VI, Fig. 2.4) were detected in all samples. The highest concentrations were found in samples from Sites 1076 and 1077, off the mouth of the Congo River (Table 2.4). Samples from Sites 1082 and 1085 contain only small amounts of these compounds (cf. Fig. 2.2), whereas samples from Sites 1079 and 1084 have intermediate quantities. Highest variability in alkyl diol content was also detected in samples from Site 1076. The major source are probably microalgae of the class *Eustigmatophyceae* (Volkman et al., 1999; Volkman et al., 1992). The high concentrations of alkyl diols in sediments underlying the Congo River plume may point to a contribution by freshwater eustigmatophyte algae in the low-salinity waters (Volkman et al., 1999), although marine eustigmatophytes of the genus *Nannochloropsis* are also known to contain alkyl diols (Volkman et al., 1992). Alkyl diols have been reported to occur in sediments from various areas (de Leeuw et al., 1981; Versteegh et al., 1997). Remarkably, samples from the Congo area predominantly contain the C_{30} homologue, while the C_{28} compound is the dominant alkyl diol in sediments from the southern upwelling region. A similar change was

detected for the isomeric composition of the diols. 1,15-Isomers dominate diol distributions from sites north of the ABF, while sediments south of it contain smaller amounts of the 1,15- but more of 1,14-diols. The same change in isomer composition was reported from surface sediments and from the oxygen isotope stage 5/6 transition in this area (Versteegh et al., 2000). The differences are most likely to be explained by different algal communities living under contrasting temperature and nutrient conditions.

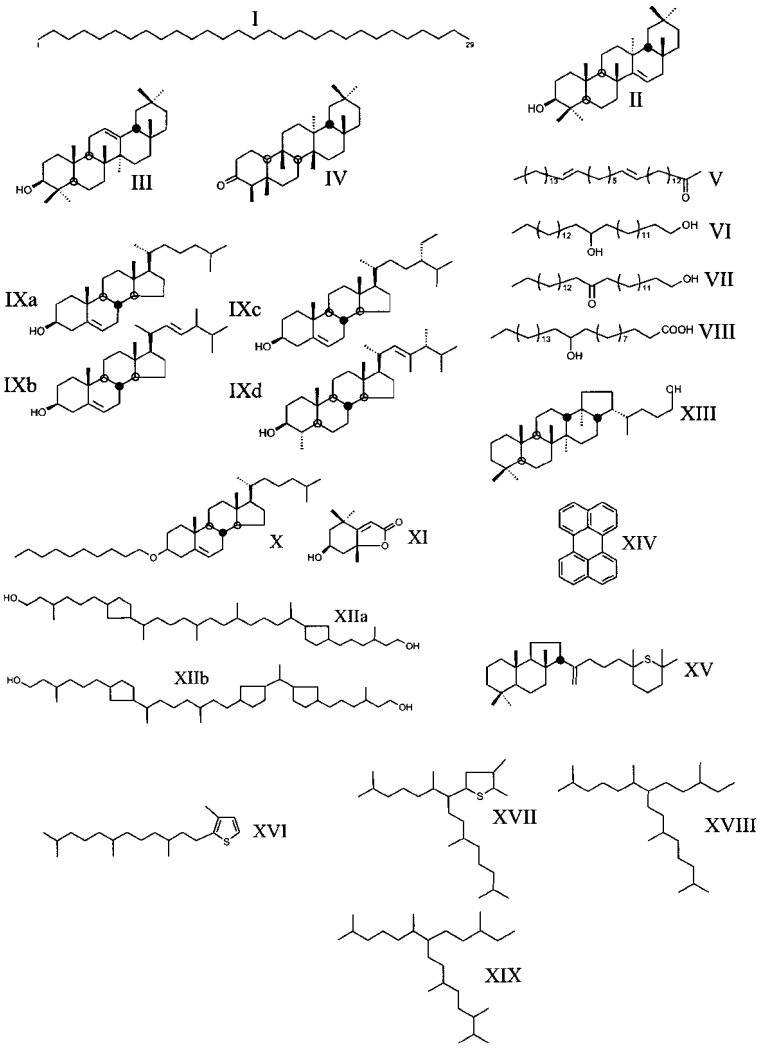

Figure 2.4: Compound structures of identified biomarker lipids.

C_{30} and C_{32} alkyl keto-ols (VII, Fig. 2.4) are present in all samples. Their amounts do not exceed trace levels, except in sediments from Site 1079 on the Angola margin. In these sediments, the C_{30} and C_{32} alkyl keto-ols are major components. By comparison of chain length and isomer distributions of diols and keto-ols, Versteegh

et al. (1997) concluded that both compound classes are diagenetically independent. Therefore, the high amounts of keto-ols in Angola margin sediments seem to reflect a specific planktonic source of a yet unidentified nature.

Mid-chain hydroxy fatty acids

In sediments from Site 1084, C_{26} and C_{28} mid-chain hydroxy fatty acids are present in relatively large amounts. At Site 1082 they occur in trace amounts, whereas they could not be detected at other sites. Both compounds are dominated by the 12-hydroxy-isomer. The C_{28} 12-hydroxy fatty acid (VIII, Fig. 2.4) has already been detected in organic matter-rich sediments, like Mediterranean sapropels (ten Haven et al., 1987b), sediments from the Oman margin (ten Haven and Rullkötter, 1991), the Arabian Sea (Prahl et al., 2000; Versteegh et al., 1997), and K/T boundary sediments (Yamamoto et al., 1996). Their phytoplanktonic origin was indicated by occurrence in sediment trap samples from high productive Arabian Sea waters (Prahl et al., 2000). Mid-chain hydroxy fatty acids have been reported from the genus *Nannochloropsis* (Gelin et al., 1997) but only homologues $\geq C_{30}$. Therefore, organisms different from the *Nannochloropsis* investigated must have been the source of the detected compounds in the investigated South Atlantic sediments. Because these compounds could only be identified in sediments from Sites 1082 and 1084, which are potentially influenced by upwelling, an origin from planktonic organisms living at high nutrient availability seems likely.

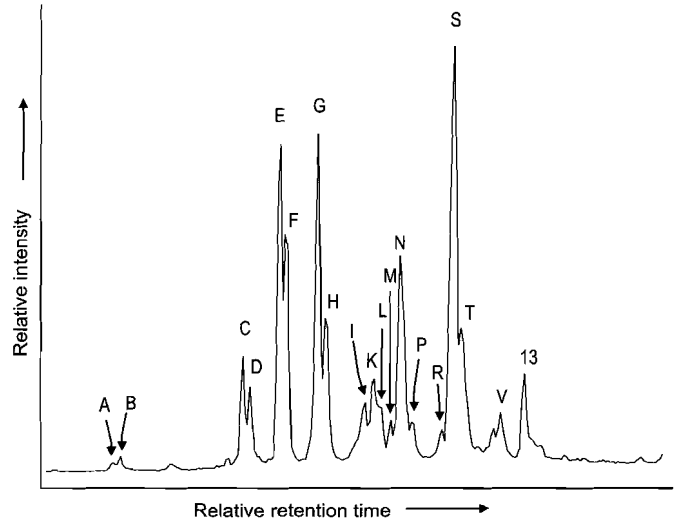

Figure 2.5: Partial TIC chromatogram of the TLC 5 fraction of Sample 175-1084A-12-6, 140-143 cm. Letters refer to steroids listed in Table 2.3.

Steroids

A range of C_{26}-C_{30} sterols was detected. An overview of compounds identified in the TLC 5 fraction of Sample 175-1084A-12H-6, 140-143 cm (Fig. 2.5), is given in Table 2.3. The sterol distribution is dominated by only few components: cholesta-5-en-3β-ol (cholesterol, IXa, Fig. 2.4), 24-methylcholesta-5,22-dien-3β-ol (IXb, Fig. 2.4), 24-ethylcholest-5-en-3β-ol (IXc, Fig. 2.4), and 4α,23,24-trimethylcholest-22-en-3β-ol (dinosterol, IXd, Fig. 2.4). All other detected sterols contribute only minor to

trace amounts. The sterol content is highest in sediments from drill sites under upwelling cells (Sites 1084 and 1085), where phytoplankton primary production is high. Sediments from the Congo (Sites 1076 and 1077) and the Walvis Basin (Site 1082) contain minor quantities of sterols, and only trace amounts were detected in samples from the Angola margin (Site 1079). A conclusive interpretation of sterol distributions is complicated by the multiple sources of most sterols (Volkman, 1986).

Cholesta-5-en-3β-ol (cholesterol) in marine sediments is derived from a variety of planktonic organisms, including haptophyte algae (Volkman, 1986). Zooplankton was found to be a major source of cholesterol in the Peru upwelling system through dietary alteration of phytosterols (Volkman et al., 1987). Therefore, the intermediate to high abundance of cholesterol in the samples from Site 1084 probably indicates extensive grazing of primary marine biomass by zooplankton.

Table 2.3: Steroids identified in selected samples.

Peak number	Compound
A	24-*nor*-cholesta-5,22-diene-3β-ol
B	24-*nor*-5α-cholest-22-ene-3β-ol
C	Cholesta-5,22-diene-3β-ol
D	5α-cholest-22-ene-3β-ol
E	Cholest-5-ene-3β-ol (IXa)
F	5α-cholestan-3β-ol
G	24-methylcholesta-5,22-diene-3β-ol
H	24-methyl-5α-cholest-22-ene-3β-ol
I	24-methylcholesta-5,24(28)-dien-3β-ol
K	24-methylcholest-5-ene-3β-ol
L	24-methyl-5α-cholestan-3β-ol
M	23,24-dimethylcholest-5,22-diene-3β-ol (IXb)
N	23,24-dimethyl-5α-cholest-22-ene-3β-ol
O	4,24-dimethyl-5α-cholest-22-ene-3β-ol
P	24-ethylcholesta-5,22-diene-3β-ol
Q	24-ethyl-5α-cholest-22-ene-3β-ol
R	23,24-dimethylcholest-5-ene-3β-ol
S	24-ethylcholest-5-ene-3β-ol (IXc)
T	24-ethyl-5α-cholestan-3β-ol
U	4α,23,24-trimethylcholest-22-ene-3β-ol (IXd)
V	24-ethyl-5α-cholest-24-ene-3β-ol
W	4α,23,24-trimethyl-5α-cholestan-3β-ol
X	4α-methyl-24-ethylcholestan-3β-ol

The occurrence of the C_{28} sterol 24-methylcholesta-5,22-dien-3β-ol in sediments is often ascribed to a lipid contribution from diatoms. However, it was also detected in cultures of dinoflagellates (Goad and Goodwin, 1972; Teshima et al., 1980) and haptophytes (Volkman et al., 1998) and detected in the water column after massive blooms of *Emiliania huxleyi* (Conte et al., 1995). Its occurrence in sediment samples from Sites 1082, 1084, and 1085, all characterised by a substantial long-chain alkenone content (i.e., 80-1400 μg/g TOC, Table 2.4), thus can not be used to specifically indicate remnants of diatom biomass. More likely, a combined contribution of haptophytes and diatoms was responsible for the relatively high content of 24-methylcholesta-5,22-dien-3β-ol.

Another C_{28} sterol proposed as a marker compound for diatoms is 24-methylcholesta-5,24(28)-dien-3β-ol because of its elevated concentrations in some centric diatom species (Volkman et al., 1998), although it also occurs in marine

dinoflagellates (Nichols et al., 1984). It was only detected in minor amounts in samples from Site 1084 and was below the detection limit in all other samples. Specific diatom occurrence from sterol distributions is therefore only indicated at the site of the most substantial upwelling intensity.

Another major sterol, 24-ethylcholest-5-en-3β-ol, together with its stanol analogue (24-ethyl-5α-cholestan-3β-ol) is present in smaller amounts. Both are commonly associated with terrestrial higher plants, in which they are the dominant sterols (Huang and Meinschen, 1976). In environmental settings, where terrigenous material is scarce, the main contributors likely are microalgae like diatoms and xantophyceae (Volkman et al., 1998). The source of these compounds in samples containing high concentrations of long-chain *n*-alkanes may have been terrestrial higher plant detritus, as in the samples from the Congo area. In samples from upwelling sites, which contain minor or negligible amounts of other terrigenous lipids, marine phytoplankton sources seem more likely.

The occurrence of 4α,23,24-trimethylcholest-22-en-3β-ol (dinosterol), accompanied by a range of other 4-methyl sterols, is ascribed to dinoflagellates. Dinosterol is almost uniquely produced by dinoflagellates (Boon et al., 1979; Robinson et al., 1984), with minor quantities occurring in diatoms (Volkman et al., 1993). High concentrations of dinosterol were found in samples from Sites 1076, 1079, and 1084, with the highest variability in the Congo Fan sediments. Dinoflagellates, therefore, are considered to have contributed significantly to the marine extractable lipids in the Congo plume and in the upwelling cells, although the detection as a major lipid does not necessarily imply that dinoflagellates were dominant constituents of the phytoplankton community in these environments. Other, less abundant sterols are less specific and may be derived from a variety of algal sources (Volkman, 1986).

In the apolar fractions of samples from the upwelling Sites 1084 and 1085, and to a lesser extent also in samples from Sites 1079 and 1082, series of sterenes, steradienes, and steratrienes are present. The most abundant compounds are C_{27} and C_{28} homologues. They are diagenetic transformation products of sterols. Their formation proceeds via microbiologically mediated reduction and/or dehydration of sterols (de Leeuw and Baas, 1986; Gagosian and Farrington, 1978).

Sterol ethers

In samples from Sites 1084 and 1085 relatively large amounts of sterol ethers are present; they occur in minor amounts at Site 1079. They commonly consist of C_{27} and C_{28}, Δ^5 and $\Delta^{5,22}$ steroid moieties, ether bound to a nonyl or decyl moiety (structure X shows the C_{27} Δ^5 decyl ether, Fig. 2.4). These compounds have been identified by comparison with reported mass spectra (Schouten et al., 2000a). Their distributions show distinct differences from the sterol distributions. Steroid moieties larger than C_{28}, or stanol analogs, could not be detected. A diagenetic origin of sterol ethers from alkylation of the sterols therefore seems unlikely. The occurrence of sterol ethers has earlier been reported for Walvis Bay diatomaceous ooze (Boon and de Leeuw, 1979), and from sediments from the Miocene Monterey formation and the Arabian Sea (Schouten et al., 2000a). All these settings, including the samples under consideration, are known to receive a large amount of organic matter from diatoms, from which these compounds could be derived. It is assumed that the sterol ethers either represent primary biosynthetic products or are derived from zooplankton feeding on specific source organisms. Copepods are known to convert algal sterols to steryl chlorin esters (Talbot et al., 1999). In that case, algal sterols were converted with equal efficiency to

steryl esters, resulting in the same ratio for sterols and steryl esters. We suggest that the formation of sterol ethers could take place by a similar mechanism during herbivory, although no sterol ether-producing organism has yet been identified.

Loliolide and *iso*-loliolide

An omnipresent compound pair in all investigated samples is loliolide (XI, Fig. 2.4) and its isomer, *iso*-loliolide. They are the dominant lipids in the TLC 8 fraction of Sample 175-1084A-12H-6, 140-143 cm. Highest concentrations in samples from Site 1084 are followed by slightly lower contents in samples from Sites 1076 and 1079. At Site 1076 the highest variability was detected. Loliolide and *iso*-loliolide are known as end products of anaerobic degradation of fucoxanthin (Klok et al., 1984; Repeta, 1989). Fucoxanthin is the major carotenoid in diatoms and haptophytes. Loliolide and *iso*-loliolide were earlier reported from sediments receiving abundant marine phytoplankton biomass, like the Mediterranean sapropels (ten Haven et al., 1987a), the Namibian margin (Klok et al., 1984), and the Peruvian shelf (Repeta, 1989). The elevated concentrations of loliolide and *iso*-loliolide in the sediments from Sites 1076, 1079, and 1084 therefore indicate a large carotenoid contribution from diatoms and/or haptophyte algae at these sites. Furthermore, it is concluded that anaerobic degradation of carotenoids to loliolides has taken place in the sediments.

Biphytane diols

Two C_{40} cyclic biphytanediols were detected in the TLC 5 fraction of Sample 175-1084A-12H-6, 140-143 cm. By comparison with published mass spectra, they were identified as the C_{40} dicyclic (XIIa, Fig. 2.4; Schouten et al., 1998) and C_{40} tricyclic biphytanediol (XIIb, Fig. 2.4, Sinninghe Damsté, personal communication, 2000). Investigations of all samples showed that those lipids are present in highest concentrations and with the largest variation in samples from Site 1084. Although these compounds have not yet been identified in organisms, they were encountered in various sediments from, for example the Indian Ocean, Arabian Sea, Angola Basin, Walvis Bay, and Madeira Abyssal Plain (Schouten et al., 1998; Schouten et al., 2000a). From the structural similarities with sedimentary C_{40} ether-bound biphytanes, it was proposed that biphytane diols are biosynthesised by archaea (Hoefs et al., 1997; Schouten et al., 1998). The presence of intact archaeal tetraether lipids was proven for Sample 175-1084A-25X-3, 20-23 cm, by High Performance Liquid Chromatography (Hopmans et al., 2000). Their high abundance in water-column samples of the Black Sea and the Cariaco Basin and in surface sediments from the Indian Ocean (Hoefs et al., 1997) suggests that they are already produced in the water column. The carbon skeleton structure of the sedimentary $C_{40:3}$ biphytane diol (and ether-bound biphytane) differs from that of thermophilic archaea (Schouten et al., 1998). Therefore, it is assumed that these compounds derive from non-thermophilic archaea (Hoefs et al., 1997). Possibly, the pelagic archaea are associated with low-oxygen conditions (Hoefs et al., 1997).

Hopanoids

Small amounts of hop-17(21)-ene and *neo*-hop-13(18)-ene were detected in all samples. These compounds are present in slightly elevated concentrations in samples from Sites 1082, 1084, and 1085, influenced by upwelling. For *neo*-hopenes a direct biological origin was suggested (Sinninghe Damsté et al., unpublished data), but hop-17(21)-ene is likely to be derived from diploptene by isomerisation during early diagenesis.

Extended hopanoids identified in the sediments are 17β,21β(H)-*homo*-hopane, 17β,21β(H)-*homo*-hopan-31-ol, 17β,21β(H)-*dihomo*-hopan-32-ol (XIII, Fig. 2.4), a C_{33} hopane-diol, and a C_{35} hopane-keto-diol. The latter two compounds were tentatively identified by their mass spectra (Fig. 2.6). They are present in all investigated samples but occur in highest amounts in samples from the Congo Fan (Sites 1076 and 1077). Common precursors of hopanoid compounds are bacteriohopanepolyols (Rohmer et al., 1989). Hopanoids are exclusively biosynthesised by prokaryotes as membrane rigidifiers and can be considered the bacterial counterparts of steroids in cell membranes of algae (Rohmer et al., 1989). Recently, it has been inferred that extended hopanoids in sediments are predominantly derived from cyanobacteria and much less from heterotrophic bacteria or bacterial reworking (Schoell et al., 1994; Summons et al., 1999). Sediments located under the Congo plume are therefore considered to receive a larger cyanobacterial contribution than the other sediments investigated.

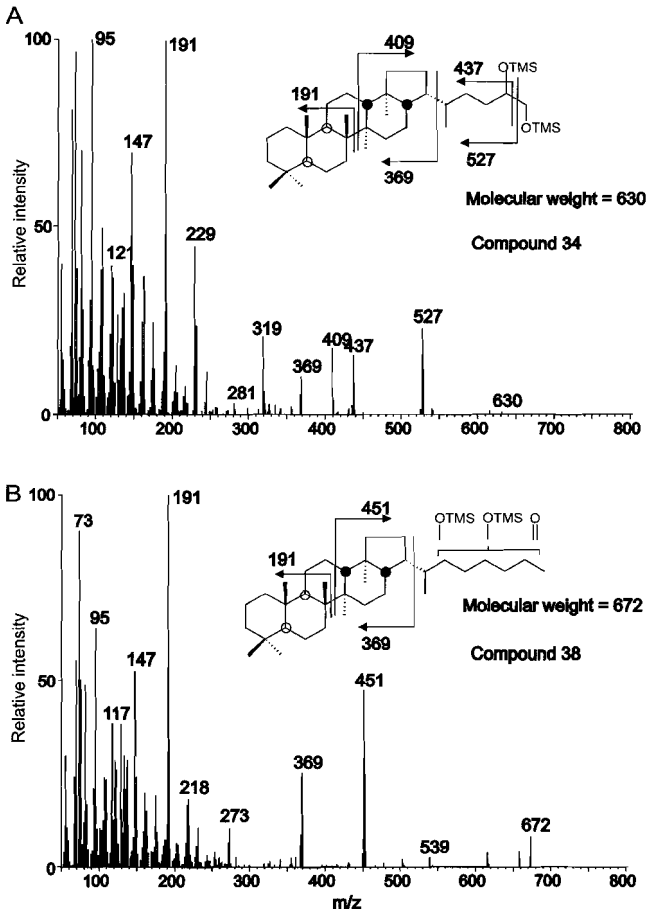

Figure 2.6: A) Mass spectrum of compound 34 tentatively identified as *trihomo*-hopane-32,33-diol (as TMS ether). B) Mass spectrum of compound 38 tentatively identified as *pentakishomo*-hopane-keto-diol (as TMS ether). Both compounds are present in the TLC 6 fraction of Sample 175-1084A-12-6, 140-143 cm.

Wax esters

Wax esters identified in the TLC 1 fraction of Sample 175-1084A-12H-6, 140-143 cm, range from C_{32} to C_{40} and have exclusively saturated fatty acid and alcohol moieties. The fatty acid moieties range from C_{14} to C_{24} and the alcohol moieties from C_{16} to C_{24}. For both counterparts, the C_{16}, C_{18}, and C_{20} homologues are quantitatively the most important ones. Wax esters are minor components of the total extractable organic matter and they could only be detected in the TLC fraction. Besides their occurrence in leaf waxes of higher plants (Kolattukudy, 1976), wax esters were reported to occur in pelagic marine animals, especially copepods. Copepods contain relatively large amounts of wax esters as energy reserves (Sargent et al., 1976). The storage of wax esters in copepods is connected to intermittent food supply with periods of starvation. The occurrence of wax esters in sediments from Site 1084 thus could be potentially indicative of zooplankton lipids at upwelling-influenced sites.

Perylene

In the TLC 2 fraction of Sample 175-1084A-12H-6, 140-143 cm, perylene (XIV, Fig. 2.4) was identified as a major compound. It is the only detected polycyclic aromatic hydrocarbon in all samples. It was earlier identified in Namibian shelf sediments (Wakeham et al., 1979). Perylene was reported to be most abundant in anoxic diatomaceous sediments (Louda and Baker, 1984). Although the actual precursor compound is still unknown, in-situ diagenetic formation of perylene under anoxic conditions is commonly assumed (Silliman et al., 1999). The conclusion that diatoms are the most likely source of a precursor compound (Venkatesan, 1988) fits well with our finding of perylene in sediments below the Lüderitz upwelling cell. Besides suggesting an origin from diatom lipids, the occurrence of perylene is related to a large abundance of labile organic matter, leading to strong oxygen consumption in the sediments.

Organic sulphur compounds

Two tricyclic triterpenoid thianes were detected in minor amounts in the apolar fractions of samples from Site 1084. By comparison with reported mass spectra (Werne et al., 2000), they were identified as monounsaturated malabaricane thianes (XV, Fig. 2.4).

A sulphur compound present in trace amounts in sediments from Sites 1084 and 1082 was identified as a C_{20} isoprenoid thiophene, 3-methyl-2-(3,7,11-trimethyldodecyl)-thiophene (XVI, Fig. 2.4). Its occurrence in sediments from Walvis Bay was reported earlier (Brassell et al., 1986b; ten Haven et al., 1990). Sulphur incorporation into phytol-derived phytadienes leads to the formation of isoprenoid thiophenes (Brassell et al., 1986b). Source organisms of phytol are chlorophyll producing photoautotrophic algae.

Several isomers of highly branched isoprenoid (HBI) thiolanes were detected in sediments from Site 1084 and, in much lower amounts, from Site 1082. They were identified as C_{25} monounsaturated and saturated HBI thiolanes (XVII, Fig. 2.4) by comparison with published mass spectra (Kohnen et al., 1990). These compounds derive from the reaction of inorganic sulphur species with specific double bonds of the precursor HBI polyenes during early diagenesis (Kohnen et al., 1990). Precursor compounds of the HBI thiolanes are HBI polyenes biosynthesised by specific diatom species, like *Rhizosolenia setigera* and *Haslea sp.* (Belt et al., 1996; Sinninghe Damsté et al., 1999; Volkman et al., 1994). Desulphurisation of the polar fraction of Sample 175-1084A-12H-6, 140-143 cm, released C_{25} (XVIII, Fig. 2.4) and C_{26} HBI

(XIX, Fig. 2.4) compounds (Fig. 2.7) in quantities similar to those of the long-chain alkenones. The C_{26} HBI compound most probably originates from the same diatom species as the C_{25} HBI (Rospondek et al., 1997). The presence of these compounds in samples from Site 1084 therefore indicates an important contribution of diatom lipid material to sediments deposited in upwelling-influenced environments. Rapid sulphur incorporation into alkenes may account for the absence of unsulphurised HBI compounds in samples from Site 1084 (Kohnen et al., 1990; Werne et al., 2000).

This rapid formation of organosulphur compounds is in line with the high rate of sulphate reduction in the uppermost meters of sediment at Sites 1082 and 1084 (Wefer et al., 1998), suggesting a high abundance of labile organic matter and low-oxygen conditions at these locations. In other sediments, organic sulphur compounds were not detected. The formation of organic sulphur compounds at other locations could possibly be inhibited by a higher availability of reactive iron.

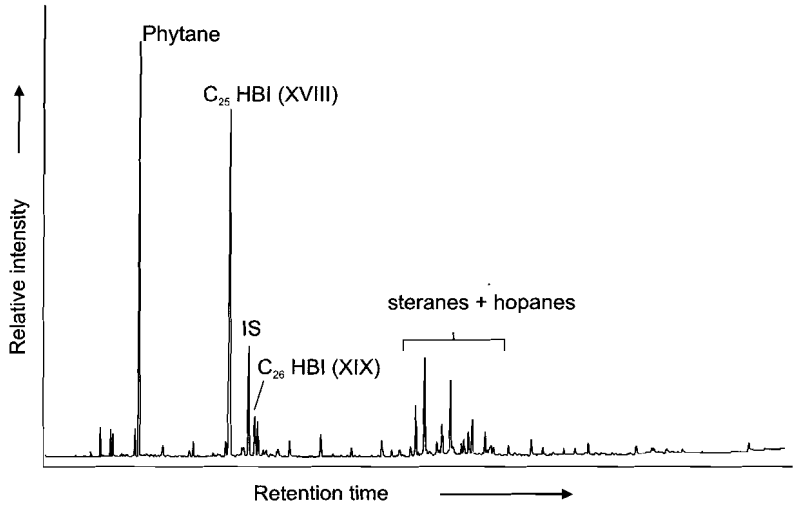

Figure 2.7: TIC chromatogram of the apolar fraction of the desulphurised and hydrogenated polar fraction of Sample 175-1084A-12-6, 140-143 cm. IS = internal standard.

2.3.3. Site summaries

The majority of biomarker lipids in sediment samples drilled during Leg 175 in the eastern South Atlantic is of marine, autochthonous origin. Terrigenous lipids, detected in minor but varying amounts, were transported into the marine environment via dust or fresh water. Their contribution to the sedimentary lipid material could be used as a measure of the relative importance of terrigenous vs. marine organic matter deposition in each setting. Because of the limited sample number of this study, and their different ages, paleoceanographic interpretations are restricted. The study is solely intended to provide an inventory and underline the potential of detailed biomarker analyses for paleoceanographic purposes. Figure 2.8 shows the concentrations of selected biomarkers and compound classes to illustrate the lipid composition at each site, as summarised below.

Site 1076 is the shallow-water drill site in the lower Congo Basin. The sediments contain the highest amounts of terrigenous lipids of all investigated samples (Table

2.4; Fig. 2.8). The concentrations of *n*-alkanes, derived from leaf waxes of higher plants, and taraxerol, most probably derived from mangroves, show strong variations between the samples (Fig. 2.8). This suggests a dependence of the concentrations of terrigenous lipids on fluctuations in river discharge, similar to the late Quaternary (Jansen, 1990; Jansen et al., 1984; Schneider et al., 1997; van der Gaast and Jansen, 1984). Long-chain alkenone concentrations in samples from Site 1076 display a strong variability with elevated concentrations when sea-surface temperatures were low (Table 2.4). This is in agreement with the results from the late Quaternary of stronger coastal upwelling during cold times with low river discharge (Jansen and van Iperen, 1991). On average, samples from Site 1076 contain the highest concentrations of alkyl diols and intermediate amounts of dinosterol and loliolide. These compounds also exhibit strong variability in concentrations, suggesting that the production of eustigmatophytes, dinoflagellates, and diatoms co-varied with river discharge of nutrients or coastal upwelling. The presence of large amounts of eustigmatophyte-derived lipids may indicate a significant contribution by eustigmatophyte algae from brackish waters. Cholesterol is present in trace amounts and biphytanediols are absent. Zooplankton herbivory and pelagic archaea are therefore suggested to have been of minor importance.

Site 1077 is the intermediate-depth drill site on the Congo Fan. Samples from this location have the lowest organic carbon content of all investigated sediments. The content of terrigenous lipids, *n*-alkanes and taraxerol is lower than in the sediments from Site 1076 but still elevated compared to the more southern sites (Table 2.4). On average, concentrations of alkenones, loliolide, alkyl diols, and dinosterol are lower than at Site 1076 (Table 2.4). Slightly higher concentrations were detected for biphytanediols and cholesterol (Table 2.4). This suggests that haptophyte algae, diatoms, eustigmatophytes, and dinoflagellates on average were less important as primary producers. In contrast, archaea generally contributed slightly higher amounts to the lipid material (Fig. 2.8). This change agrees, despite the limited sample numbers, with a zonation of plankton groups depending on the proximity to the river mouth (Ufkes et al., 1998; van Iperen et al., 1987). The influence of fluviatile nutrients (on diatoms) and river-induced upwelling (on haptophytes) thus would be much smaller at Site 1077 than at Site 1076.

Samples from **Site 1079** on the Angola margin contain intermediate concentrations of alkenones, loliolide, dinosterol, cholesterol, and alkyl diols. Terrigenous lipids (e.g., *n*-alkanes and taraxerol) are present in low but significant amounts in both samples (Table 2.4). A direct supply of river-transported terrigenous lipid material seems unlikely because of the absence of rivers draining into this area. However, alongshore transport from the Kunene River might carry terrigenous lipids to this site. The composition of marine lipids, with alkenones, loliolide, and dinosterol as the major components is, except for the high content of alkyl keto-ols, not significantly different from the lipid composition of sediments in the Congo area. The elevated sedimentary organic carbon contents of these samples therefore probably result from a similar plankton community, with haptophyte algae, diatoms, dinoflagellates, and unidentified, keto-ol producing microalgae as main lipid producers. Supply of nutrients from subsurface waters, likely involving the Angola Dome nearby, may sustain high productivity.

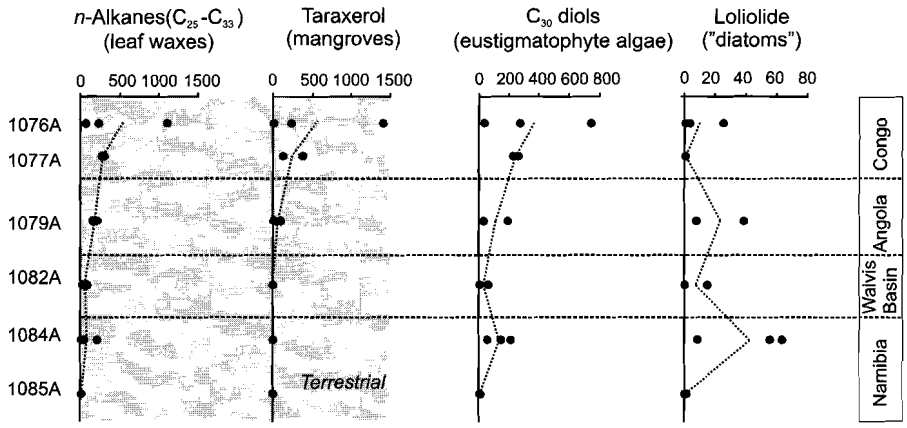

Figure 2.8: Quantified lipid biomarker concentrations (in µg/g TOC). Average concentrations of each site are connected by stippled line.

Table 2.4: Concentrations of quantified biomarker lipids (in µg/g TOC) and compound indices.

Core section, interval (cm)	C_{25}-C_{33} *n*-alkanes	CPI $alk_{27\text{-}31}$[a]	ACL 25-33[b]	C_{20}-C_{30} fatty acids	C_{20}-C_{30} *n*-alcohols	C_{37} alkenones	U^K_{37}'[c]	Temp.[d] (°C)
175-1076A-								
4H-2, 75-77	64	6.0	29.5	29	59	90	0.79	22.5
7H-2, 75-77	230	3.8	29.6	40	81	230	0.93	26.9
15H-2, 75-77	1100	10.4	29.6	550	1100	1300	0.73	20.8
175-1077A-								
9H-2, 75-77	280	7.0	29.7	330	720	350	0.86	24.6
13H-2, 75-77	300	4.2	29.6	960	780	230	0.89	25.7
175-1079A-								
2H-4, 46-49	210	7.4	29.9	47	94	490	0.78	22.2
13H-4, 46-49	150	6.0	30.4	150	310	370	0.85	24.4
175-1082A-								
6H-1, 105-108	90	8.4	31.0	39	78	960	0.58	16.4
53X-3, 27-30	18	5.6	30.3	7.5	15	80	0.95	27.4
175-1084A-								
12H-6, 140-143	210	3.1	30.4	170	350	1400	0.55	15.4
25X-3, 20-23	44	n.a.	n.a.	180	360	850	0.58	16.1
51X-3, 20-23	13	n.a.	n.a.	68	140	180	0.74	21.2
175-1085A-								
11X-3, 20-23	12	6.9	30.4	8.6	17	300	0.68	19.3
50X-3, 20-23	13	5.1	30.2	9.5	19	80	0.84	24.0

Notes: n.a. = not applicable because of too low concentration; n.d. = not detected; tr. = trace amount

[a] $CPI = \frac{1}{2}\Sigma(X_i+X_{i+2}+..+X_n)/\Sigma(X_{I-1}+X_{i-1}+..+X_{n-1})+\frac{1}{2}\Sigma(X_i+X_{i+2}+..+X_n)/\Sigma(X_{I+1}+X_{i+3}+..+X_{n+1})$.

[b] ACL (average chain length) $= \Sigma(iX_i)/\Sigma X_i$

[c] U^K_{37}' (ketone unsaturation index) $= [C_{37:2}]/([C_{37:2}]+[C_{37:3}])$.

[d] Temperature calculated using the equation from Müller et al. (1998): $U^K_{37}' = 0.033\ T + 0.044$.

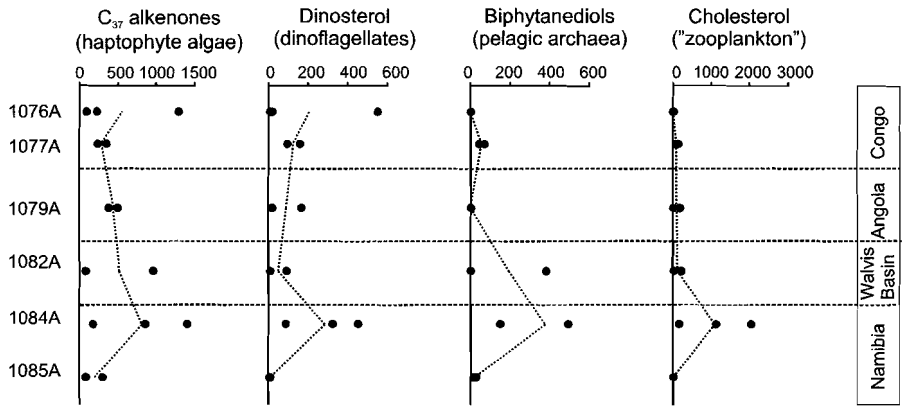

Figure 2.8 continued.

Table 2.4 continued.

Core section, Interval (cm)	Taraxerol	Loliolide	Dinosterol	Cholesterol	C_{30} diol	Biphytane-diols
175-1076A-						
4H-2, 75-77	6	0.7	18	5.4	34	n.d.
7H-2, 75-77	230	3.6	8	9.7	270	n.d.
15H-2, 75-77	1400	25	550	25	740	n.d.
175-1077A-						
9H-2, 75-77	120	0.4	96	130	260	43
13H-2, 75-77	380	0.6	160	67	220	69
175-1079A-						
2H-4, 46-49	12	39	19	6.8	29	n.d.
13H-4, 46-49	99	7.5	170	180	190	n.d.
175-1082A-						
6H-1, 105-108	n.d.	15	89	210	60	380
53X-3, 27-30	n.d.	0	7.9	10	5.2	n.d.
175-1084A-						
12H-6, 140-143	n.d.	63	450	1100	150	500
25X-3, 20-23	n.d.	56	320	2000	210	500
51X-3, 20-23	n.d.	8.5	86	150	53	150
175-1085A-						
11X-3, 20-23	n.d.	0.9	5.6	5.6	8.7	27
50X-3, 20-23	n.d.	0	9	5.8	4.5	12

Sediments at **Site 1082** in the Walvis Basin were reported to receive abundant biological material from displaced upwelling filaments (Wefer et al., 1998). The elevated organic carbon content of the studied samples (Table 2.1) may therefore reflect a strong phytoplankton signal. Most commonly, upwelling induces high diatom productivity. Only low amounts of loliolide are present in the sediments. However, HBI thiolanes clearly indicate significant supply of diatom-derived lipid material. The average concentration of alkenones in the sediments is relatively high (Fig. 2.8). Biphytanediols are present in significantly elevated amounts, in contrast to the more northern sites. Other biomarkers only contribute small to minor quantities. Especially the terrigenous lipid contribution is very low: the concentrations of *n*-alkanes are low, and taraxerol is absent (Table 2.3). The *n*-alkanes at this location are most probably predominantly wind-derived, whereas mangrove lipids are probably absent in the samples due to lack of coastal mangrove vegetation in this area and due to the ABF in the north inhibiting southward transport.

Investigated sediments from **Site 1084** off Lüderitz Bay contain the highest amount of organic carbon of all studied samples (up to 13 %, Table 2.1). Sediments from this site should contain the most pronounced coastal upwelling signal because of their close vicinity to the Lüderitz upwelling cell (Wefer et al., 1998). This is well expressed in the lipid geochemistry of these samples. Sediment from Site 1084 contains the highest concentrations of biphytanediols, long-chain alkenones, loliolide, and cholesterol. Alkyl diols and dinosterol are present in elevated amounts (Table 2.4, Fig. 2.8). The presence of other plankton-derived compounds, like mid-chain hydroxy fatty acids, sterols, sterol ethers, hopanoids, isoprenoid thiophenes, and sulphurised HBIs, also indicates the importance of plankton biomass contribution. The investigated sediments from Site 1084 contain the highest amounts of phytoplankton, pelagic archaea, and zooplankton markers of all investigated samples. Land-derived lipids are present only in trace amounts. The *n*-alkanes exhibit only small concentrations. Taraxerol, like at Site 1082, is absent. Of all studied samples, the sediments from Site 1084 contain the most diverse upwelling-derived lipids. The organic geochemical phytoplankton signals are much more pronounced than at Site 1082.

Site 1085 is located in the southern Cape Basin, situated under a seasonal upwelling regime. Its sediments show less-pronounced upwelling signals than those at Site 1084. The contribution of marine-derived compounds, like alkenones, loliolide, alkyl diols, and dinosterol, is on average smaller than at Site 1084 and in the same range as at Site 1082. The presence of elevated amounts of sterols and sterol ethers, however, suggests phytoplankton production with subsequent zooplankton grazing. The sediments from Site 1085 contain only trace quantities of *n*-alkanes, indicating negligible transfer of material from the nearby Orange River. Taraxerol could not be detected in this setting, which agrees with the present absence of mangrove vegetation in southern Africa. The lipid compositions of sediments from Site 1085 resemble those of sediments from Site 1082. Both settings receive their biological signal from seasonal upwelling or mixing of upwelled, nutrient-rich waters with low-productivity surface waters, in contrast to the persistent year-round upwelling at Site 1084.

2.4. Conclusions

- The lipid biomarker content in selected sediments from several sites along the southwestern African margin reflects different marine environments. The majority of the extracted lipids in all samples is of marine origin, with varying contributions of terrigenous lipids. It should be noted that the limited sample number restricts detailed paleoceanographic interpretations and this study is solely intended to be inventory.
- In general, two main areas can be distinguished, separated by the Angola-Benguela Front (ABF). Elevated concentrations of terrigenous lipids and lipids from eustigmatophyte algae were only observed north of the ABF, whereas lipids from archaea and zooplankton are only present in significantly elevated amounts south of it.
- The sediments below the Congo River freshwater plume received a large contribution of lipids from terrestrial higher plants and mangroves. The contribution of terrigenous lipids is suggested to decrease with increasing distance from the river mouth. At the shallower site, marine lipids were mainly derived from haptophyte algae, diatoms, dinoflagellates, and eustigmatophyte algae. Lipids of these algae were less abundant in samples from the deeper site, whereas the contribution from pelagic archaea and zooplankton were slightly higher. The changes in lipid composition with distance from the river mouth suggest variation of plankton communities with reduction of river influence.
- The investigated sediments on the Angola margin received a small amount of terrigenous lipids. A highly productive plankton community of haptophyte algae, diatoms, dinoflagellates, and unidentified, keto-ol-producing microalgae probably caused the elevated sedimentary organic carbon contents. Supply of nutrients from the nearby Angola Dome may sustain high productivity.
- Walvis Basin sediments received an upwelling signal transported by the Benguela Current. Major contributors of marine lipids were haptophyte algae and pelagic archaea. Diatom lipids were detectable in low concentrations as sulphurised compounds.
- Persistent coastal upwelling off Lüderitz Bay is well reflected in the sedimentary lipids. The investigated samples contain the highest lipid contributions of pelagic archaea, haptophyte algae, dinoflagellates, diatoms, and zooplankton. Anoxic sedimentary conditions were most probably caused by a large supply of labile organic matter.
- In the southern Cape Basin, sediments probably received plankton material from seasonal upwelling, indicated by their content of sterols and sterol ethers. Their marine lipid content is comparable to the lipids of the sediments in the Walvis Basin. The nearby Orange River did not cause elevated concentrations of terrigenous lipids in the investigated samples.

Acknowledgements

The authors thank Marianne Baas and Hanno Kinkel for technical assistance. The Ocean Drilling Program (ODP) is thanked for providing samples.

Chapter 3

Carbon isotope analysis of *n*-alkanes in dust from the lower atmosphere over the central eastern Atlantic

Enno Schefuß, Volker Ratmeyer, J. H. Fred Jansen and Jaap S. Sinninghe Damsté

Revised manuscript re-submitted to *Geochimica et Cosmochimica Acta*

Abstract

Atmospheric dust samples collected along a transect off the West African coast have been investigated on their lipid content and compound-specific stable carbon isotope compositions. The saturated hydrocarbon fractions of the organic solvent extracts consist mainly of long-chain *n*-alkanes derived from epicuticular wax coatings of terrestrial plants. Backward trajectories for each sampling day and location were calculated using a global atmospheric circulation model. The main atmospheric transport took place in the low-level trade-wind layer, except in the southern region, where long-range transport in the mid-troposphere occurred. Changes in the chain-length distributions of the *n*-alkane homologous series are probably related to aridity, rather than temperature or vegetation type. The carbon preference of the leaf-wax *n*-alkanes shows significant variation, attributed to a variable contribution of fossil fuel- or marine-derived lipids. The effect of this non-wax contribution on the $\delta^{13}C$ values of the two dominant *n*-alkanes in the aerosols, *n*-C_{29} and *n*-C_{31} alkane, is, however, insignificant. Their $\delta^{13}C$ values were translated into a percentage of C_4 versus C_3 plant type contribution, using a two-component-mixing-equation with isotopic end-member values from the literature. The data indicate that only regions with a predominant C_4 type vegetation, i.e., the Sahara, the Sahel and Gabon, supply C_4 plant-derived lipids to dust organic matter. The stable carbon isotopic compositions of leaf-wax lipids in aerosols mainly reflect the modern vegetation type along their transport pathway. Wind abrasion of wax particles from leaf surfaces, enhanced by a sandblasting effect, is most probably the dominant process of terrigenous lipid contribution to aerosols.

3.1. Introduction

Atmospheric transport has long been recognised as an important transport mechanism of continental-derived material to the oceans (Darwin, 1846). Observations of dust storms in arid areas of North Africa (Fig. 3.1) led to the conclusion that a large portion of marine sediments could be of eolian origin (Radczewski, 1939). Sampling of eolian dust itself has enhanced insight into its characteristics, enabling the assignment of source regions (Chester et al., 1972; Chester and Johnson, 1971).

Organic geochemical analyses of dust led to the recognition of lipids derived from various sources, e.g., terrestrial higher plants, microbial activity, sea spray, vehicle exhaust (Cox et al., 1982; Simoneit, 1977; Simoneit et al., 1977). Homologous series of long-chain *n*-alkanes, *n*-alcohols and fatty acids are typical lipids found in dust (Cox et al., 1982; Eichmann et al., 1979; Gagosian et al., 1981; Lepple and Brine, 1976; Simoneit et al., 1977) and marine sediments (Bird et al., 1995; Huang et al., 2000; Kuypers et al., 1999; Poynter et al., 1989). These lipids are abundant constituents of terrestrial higher plant epicuticular waxes (Eglinton and Hamilton, 1963), occurring as protective coating on leaves and stems. The wax layer sustains the water balance of the plant under dry conditions (Hall and Jones, 1961). The wax particles are easily sloughed off the surface of the leaves by wind, especially by a sandblasting effect, and can become airborne (Simoneit, 1977). Alternatively, decaying plant organic matter in soils can be lifted during dust storms and transported by wind. Plant-wax lipids are therefore commonly found in dust above remote ocean areas, i.e., the North Pacific (Gagosian and Peltzer, 1986; Gagosian et al., 1981), the South Pacific (Gagosian et al., 1987), the eastern Atlantic (Cox et al., 1982; Lepple and Brine, 1976; Simoneit, 1977; Simoneit et al., 1977; Simoneit et al., 1988), and the western South Atlantic (Simoneit et al., 1991). The combined occurrence of *n*-alkanes, *n*-alcohols and fatty acids in aerosol samples is strong evidence for a common terrestrial origin of the leaf-wax compounds (Eglinton and Hamilton, 1963; Kolattukudy, 1980). Occurrence of short-chain fatty acids and *n*-alcohols may indicate an additional marine source, probably introduced to the atmosphere via sea spray (Gagosian et al., 1987; Gagosian et al., 1981; Simoneit, 1977; Simoneit et al., 1991). A major fraction of the fatty acids are present as salts in the aerosol samples (Peltzer and Gagosian, 1987). Oxygenated compounds, like triterpenols and phytosterols, are rapidly altered or degraded during atmospheric transport (Simoneit et al., 1991; Simoneit and Mazurek, 1982). The non-functionalised *n*-alkanes, however, are relatively refractory compounds. Therefore, they probably constitute the best biomarkers for terrestrial-derived vegetation waxes in dust. Leaf waxes of terrestrial higher plants contain predominantly odd-numbered *n*-alkanes and even-numbered fatty acids and *n*-alcohols (Eglinton and Hamilton, 1963; Kolattukudy, 1980; Mazurek and Simoneit, 1984; Tulloch, 1976). This is expressed as Carbon Preference Index (CPI, equation given in Table 3.1; Kolattukudy, 1976). Natural vegetation waxes have high (>5) CPI (Eglinton and Hamilton, 1963; Mazurek and Simoneit, 1984), while petroleum-derived *n*-alkanes $>C_{23}$, on the other hand, have a lower odd-over-even carbon number predominance (Simoneit, 1984). The distribution of the *n*-alkanes, therefore, enables the recognition of fossil fuel- or marine-derived contributions to the aerosol lipids (Simoneit, 1977). However, no diagnostic features in the terrigenous lipid distributions, thus far, enable the separation of contributions by different plant types (Collister et al., 1994; Eglinton and Hamilton, 1963). The chain-length distribution of *n*-alkanes is thought to be influenced by conditions other than

vegetation type, like aridity or growing-season temperature (Cranwell, 1973; Gagosian and Peltzer, 1986; Poynter et al., 1989).

Compound-specific carbon isotope analyses of leaf-wax lipids provides information on the carbon-fixation pathway utilized during photosynthesis. *n*-Alkanes from plants using the Calvin-Benson cycle (C_3 plants) have *n*-alkane $\delta^{13}C$ values around -36 ‰ (-31 to -39 ‰ vs. PDB), while plants utilising the Hatch-Slack (or dicarboxylic acid) cycle (C_4 plants) have *n*-alkane $\delta^{13}C$ values around -21.5 ‰ (-18 to -25 ‰). The third type, CAM (Crassulacean Acid Metabolism) plants, can use both carbon-fixation pathways, so their $\delta^{13}C$ values are intermediate (-25 to -27 ‰; Collister et al., 1994; O'Leary, 1981; Rieley et al., 1993). Virtually all trees, most shrubs, and cool-season grasses and sedges use the C_3 pathway, while C_4 photosynthesis is found in warm-season grasses and sedges. CAM plants include many succulents, such as cacti (Cerling et al., 1993; Spicer, 1989). C_4 plants are thus predominantly found in tropical savannas, temperate grasslands and semi-deserts (Cerling et al., 1993). Most African grasslands, like the Sahel and the grass savannahs, are presently dominated by C_4 plant vegetation (Collatz et al., 1998). CAM plants do not form a significant part of the West African vegetation (Winter and Smith, 1996). The stable carbon isotope compositions of *n*-alkanes in marine sediments have been used to determine contributions by C_3/C_4 plant type organic material to marine sediments off NW-Africa (Bird et al., 1995; Huang et al., 2000; Kuypers et al., 1999). To date no survey of their distribution and stable carbon isotope composition in dust has been conducted.

Here we present data on lipid distributions and compound-specific stable carbon isotope compositions of 24 aerosol samples collected on a transect from 30°N to 10°S (D1 to D25) along the African west coast in February and March 1998 (Fig. 3.2). The variations in carbon isotope compositions of the *n*-alkanes are ascribed to varying relative amounts of C_4 plant-derived material in the dust particulate organic matter and are discussed relative to the vegetation zones and climatic conditions on the adjacent continent. These data provide insight into the sources and transport pathways of terrigenous lipid material in dust and the vegetation signal carried out to the ocean.

3.2. Regional setting

The phytogeographical zonation in West Africa shows essentially latitudinal extending belts of vegetation (Fig. 3.2; White, 1983). In the north, at the Mediterranean Sea, the Mediterranean forest (Med) is dominated by C_3 plants. The transition to the Sahara desert, the Mediterranean-Saharan transitional steppe (MST), is vegetated by a mixed C_3/C_4 plant vegetation. The Sahara desert is sparsely vegetated, and is supplying vast amounts of lithogenic dust to the atmosphere (Chester et al., 1972; Chester and Johnson, 1971; Sarnthein et al., 1981). The satellite picture from the sampling time clearly shows the intense dust outbreaks from the Sahara and Sahel zone and into the Gulf of Guinea during February/March 1998 (Fig. 3.1). Main dust source areas are dried lake deposits and deflations basins (Gasse et al., 1989). The sparse vegetation is mainly of C_4 plant type. Southwards, the Sahel zone is a semi-desert, mainly vegetated by grasses. A main dust source area is the alluvial plain of the Faya Largeau in Chad (Kalu, 1979; Petit-Marie, 1991). Its vegetation consists mainly of C_4 plants. Further south, vegetation belts are formed of grass savannah and tree savannah, containing a mixture of grasslands and semi-deciduous woodlands. Here, mixed C_3/C_4 plant vegetation occurs. In equatorial Africa, between 10°N and 5°S, tropical rain forest is the dominant vegetation type. It is dominantly of C_3 plant

type. South of the tropical rain forest this series of vegetation belts essentially is reversed (White, 1983). From 8°S to 20°S the vegetation consists of transitional dry forest and woodland, intercalated with grass savannah. It is of mixed C_3/C_4 plant type. Along the Atlantic coast to the south stretches a zone of grass-dominated semi-desert, which is succeeded by the coastal Namib Desert further southwards. Both desert types are, if at all, vegetated by C_4 plants.

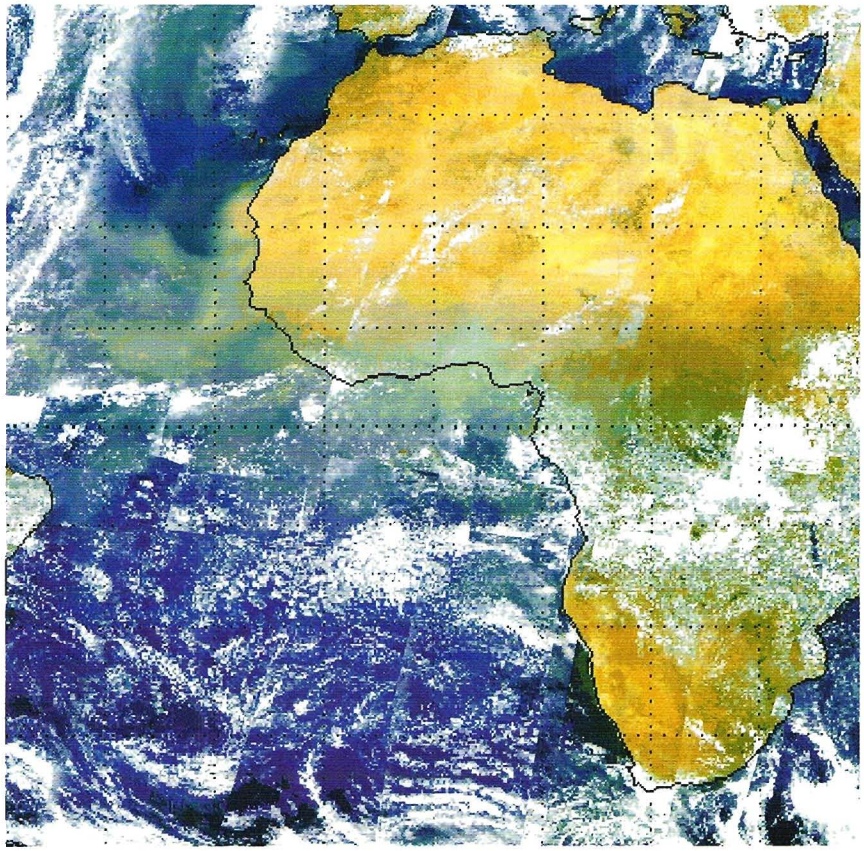

Figure 3.1: Quasi-true-colour satellite composite-picture for the sampling period (February-March 1998). Processed by Peer Helmke (University of Bremen).

Generally, the Sahara and the Sahel region are the main source regions of eolian transported material over the Atlantic Ocean (Schütz, 1980). During Northern Hemisphere summer, the main axis of the Saharan dust plume is directed westward at about 20°N, while during winter, associated with the southward migration of the Intertropical Convergence Zone (ITCZ), the main plume axis is located at about 5°N, directed southwards across the equatorial Atlantic (Fig. 3.1, 3.2; Kalu, 1979; Pye, 1987; Schütz, 1980). Three distinct wind systems are transporting dust from West Africa to the adjacent eastern Atlantic. The shallow (500-1500 m) trade-wind layer transports dust from the northwestern Sahara in southwestern direction parallel to the coast to the Canary and Cape Verde Islands (Sarnthein et al., 1981). The mid-tropospheric (at ca. 3 km) African Easterly Jet (AEJ) transports dust-laden Saharan air

above the trade-wind layer across the Atlantic (Prospero and Carlson, 1972). Part of the AEJ is deflected off the African coast to the northwest and then also transports dust to the Canary Islands (Tetzlaff and Wolter, 1980). During winter, when the ITZC is in its southernmost position, southeasterly cold dry surface winds (the Harmattan) transport dust from the Faya Largeau area of Chad southwards into the Gulf of Guinea (Kalu, 1979). Southern Hemisphere trade winds south of the ITZC blow from southern Africa in northwesterly direction to the equatorial Atlantic (Biscaye et al., 1974; Jansen et al., 1989). Distinct dust outbreaks can be seen in the satellite picture from the sampling time (Fig. 3.1) off the Sahara and Sahel in NW-Africa and in the Gulf of Guinea, there transported by the Harmattan.

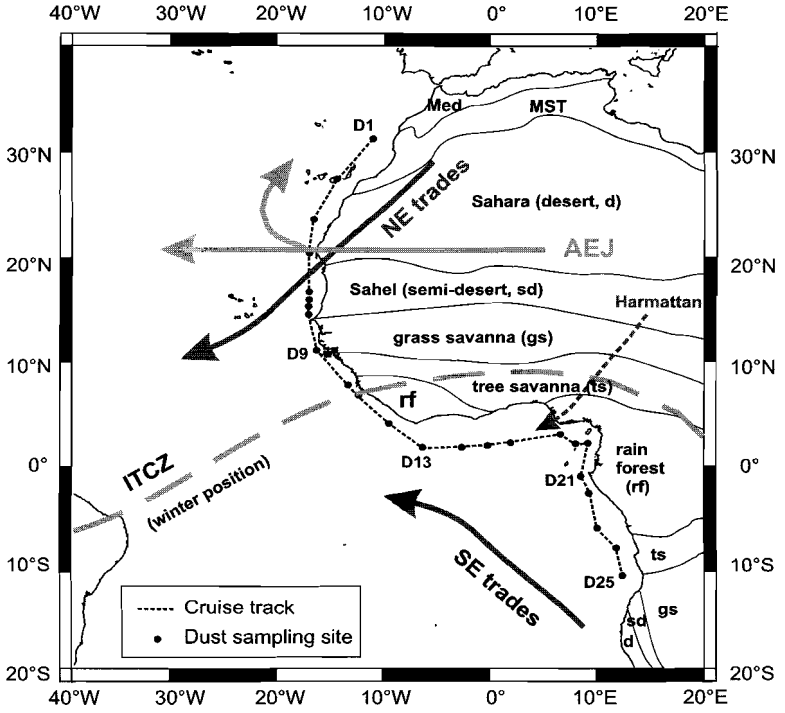

Figure 3.2: Ship track and dust sampling sites of *RV Meteor* cruise M41/1 along the W-African margin. Phytogeographical zonation of Africa is taken from White (1983): Med = Mediterranean vegetation; MST = Mediterranean-Saharan transition; d = desert; sd = semi-desert; gs = grass savannah; ts = tree savannah; rf = rain forest. Major wind systems are drawn after Kalu (1979), Tetzlaff and Wolter (1980), and Sarnthein et al. (1981) (see text for explanation). Note that samples D19 and D20 were taken at almost the same location.

3.3. Experimental

3.3.1. Samples

24 eolian dust samples were collected during *R/V Meteor* cruise M41/1 in February and March 1998 (Schulz et al., 1998). The cruise track stretched from 30°N to 10°S along the African coast (see Fig. 3.2 for sampling locations). Sampling was conducted with Andersen high-volume particulate matter dust samplers installed on the ship's tower. To avoid contamination of the samples by pollution from the ship's chimney

samples were only collected when the ship was moving and the wind direction was not deviating more than 50° from the direction of the ship's heading. Dust samples for organic analyses were collected on pre-combusted glass-fibre filters. The filters collect particles >10 μm. After sampling, the filters were wrapped in aluminium foil and stored at -20°C. Procedural blanks have been carried as unopened filters onboard the ship and were analysed along with the samples. Due to the breakdown of the flow measurement onboard, absolute compound quantification (in μg m^{-3} air) was not possible.

3.3.2. Sample extraction and compound isolation

Dust filters were extracted using an ultrasonication disruptor probe and successively less polar solvent mixtures (CH_3OH, CH_3OH/CH_2Cl_2 1:1, CH_2Cl_2), each for 5 min. The extracts were combined, the solvents were removed by rotary evaporation to near dryness at 30°C, and the extracts taken up in CH_2Cl_2 and dried over anhydrous Na_2SO_4. A known amount of standard, perdeutero-*n*-C_{24} alkane, was added and used as reference for quantification of each compound per filter. Saturated hydrocarbon fractions were obtained by column chromatography (activated Al_2O_3) using four column volumes of hexane.

3.3.3. Gas chromatography (GC) and GC-mass spectrometry (GC-MS)

Analyses were performed on a Hewlett Packard 5890 series II gas chromatograph equipped with an on-column injector and fitted with a fused-silica capillary column (25 m x 0.32 mm) coated with CP Sil 5 (film thickness 0.12 μm). helium was used as carrier gas. The GC oven was heated from 70°C to 130°C at 20°C/min, followed by 4°C/min to 320°C (10 min holding time). Effluents were detected using flame ionisation (FID). GC-mass spectrometry (GC-MS) was performed using the same type of gas chromatograph and conditions to check compound identifications in selected samples. The chromatographic column was directly inserted into the electron impact ion source of a VG Autospec Ultima mass spectrometer operated with an ionisation energy of 70 eV, scanning over a mass range of *m/z* 50-800 with a cycle time of 1.8 seconds. Compound identifications are based on comparison of relative GC retention times and mass spectra published in the literature. Quantification of compounds was performed by peak area integration in FID chromatograms. Data were acquired and integrated using ATLAS analytical software.

3.3.4. GC-isotope ratio monitoring-MS (GC-irm-MS)

GC-isotope ratio monitoring-MS has been used to measure the carbon isotopic composition of the individual compounds (Hayes et al., 1990). The Hewlett Packard 5890 Series II GC was equipped with a fused silica capillary column (25 m x 0.32 mm) coated with CP-Sil 5 (film thickness 0.12 mm). The carrier gas was helium and on column injection was applied. The oven-heating program was the same as for GC analyses, except for a longer (30 min) isothermal holding time. CO_2 gas with pre-calibrated isotopic composition was used as standard. The GC was connected via a combustion interface to a Finnigan delta C mass spectrometer. The isotopic compositions of individual compounds were calculated by integration of the mass 44, 45 and 46 ion currents (Merrit et al., 1994). Analyses were done in duplicate or

triplicate with standard deviations (±σ) better than 0.5 ‰. $\delta^{13}C$ values are expressed versus PDB.

3.3.5. Trajectory computations

Four-day backward trajectories were calculated for each sampling location for the specific dates at 850 and 500 hPa barometric levels with a global two-dimensional isobaric model at the Department of Geosciences of Bremen University, based on a model developed at the Norwegian Meteorological Institute (NMI; Eliassen, 1976). The wind fields used for trajectory calculation were generated with the ECHAM 3 atmospheric circulation model (Lorenz et al., 1996). The model computes trajectories from zonal and meridional wind components (Petterssen, 1956). Wind data were obtained from the European Centre for Medium Range Weather Forecast (ECMWF).

3.4. Results

3.4.1. Saturated hydrocarbon lipids in dust samples

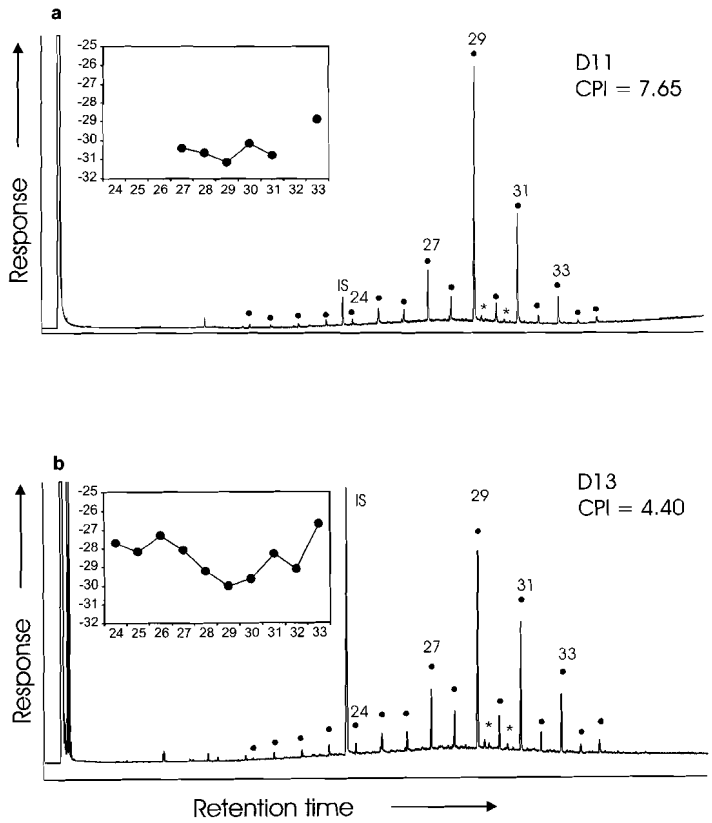

Figure 3.3: Gas chromatographic traces of saturated hydrocarbon fractions of organic solvent extracts of aerosol samples with a) high and b) low CPI (above: D11, CPI = 7.65; below: D13, CPI = 4.40). Dots indicate *n*-alkanes, stars indicate 17α,21β(H)-hopanes. Insets show stable carbon isotopic compositions (in ‰) versus chain length of *n*-alkanes.

Lipids in the saturated hydrocarbon fractions of the organic solvent extracts of the dust samples are dominated by homologous series of *n*-alkanes (Fig. 3.3). The *n*-alkanes range in carbon number from *n*-C_{24} to *n*-C_{35} with a predominance of the odd over the even-carbon-numbered homologues. A significant change in the carbon number of the most abundant homologue could be detected. Northern samples, D3 to D8, have the *n*-C_{31} alkane as most abundant homologue, while distributions in all other samples are dominated by the *n*-C_{29} alkane. This change is well reflected in the ratio of the *n*-C_{31} to the *n*-C_{29} alkane (31/(29+31)), which has maximum values in samples off Senegal around 15°N (Table 3.1; Fig. 3.4a). The average chain length (ACL) does not show a related shift. Significant variation was detected in the carbon preference index (CPI) of the *n*-alkanes series, ranging from 2.40 to 7.65 (Table 3.1; Fig. 3.4b). The highest CPI is found in a sample off Liberia (D11), while lowest values were detected in samples collected off Morocco (D1 to D4), Senegal (D9) and Gabon (D21 to D23, D25). Distribution parameters of the *n*-alkanes in the investigated dust samples are summarised in Table 3.1. Additionally, small amounts of 17α,21β(H)-hopanes were detected in all samples. 18(α)-oleanane is present in some samples. In the analytical blanks some minor contaminants were detected, identified as phthalate esters. No *n*-alkanes were detected.

Table 3.1: Locations and distribution parameters of *n*-alkanes in the dust samples.

Sample	Latitude		Longitude		Date	Range[a]	C_{max}[b]	ACL[c]	31/(29+31)[d]	CPI[e]
D1	30.44	N	11.72	W	15.2.98	24-35	29	27.6	0.48	2.40
D3	22.89	N	17.44	W	17.2.98	24-35	31	27.6	0.57	2.45
D4	19.74	N	17.91	W	17.2.98	24-35	31	26.9	0.60	2.24
D5	16.00	N	17.93	W	18.2.98	24-35	31	29.2	0.62	3.43
D6	15.29	N	17.92	W	18.2.98	24-35	31	29.3	0.61	4.23
D7	14.70	N	17.92	W	18.2.98	24-35	31	28.8	0.60	3.83
D8	13.93	N	17.92	W	18.2.98	24-33	31	29.1	0.55	4.39
D9	10.44	N	17.19	W	19.2.98	24-35	29	28.7	0.44	3.16
D10	7.26	N	14.19	W	20.2.98	24-33	29	28.8	0.28	5.79
D11	6.29	N	13.09	W	20.2.98	24-35	29	29.2	0.31	7.65
D12	3.71	N	10.23	W	21.2.98	24-33	29	28.8	0.33	5.09
D13	1.30	N	6.94	W	22.2.98	24-35	29	29.0	0.36	4.40
D14	1.32	N	2.86	W	23.2.98	24-31	29	27.0	0.12	3.71
D15	1.52	N	0.60	W	24.2.98	24-35	29	29.2	0.31	5.87
D16	1.76	N	1.64	E	24.2.98	24-35	29	29.2	0.33	5.48
D17	2.61	N	6.54	E	26.2.98	24-35	29	28.8	0.30	4.68
D18	1.68	N	7.97	E	27.2.98	24-33	29	28.4	0.24	6.09
D19	1.74	N	9.14	E	28.2.98	24-35	29	29.1	0.37	4.55
D20	1.65	N	9.11	E	1.3.98	24-33	29	28.7	0.25	5.17
D21	1.38	S	8.54	E	4.3.98	24-35	29	27.7	0.35	2.81
D22	2.91	S	9.21	E	5.3.98	24-31	29	26.0	0.15	3.23
D23	6.18	S	10.05	E	7.3.98	24-35	29	27.5	0.32	3.11
D24	8.00	S	11.86	E	8.3.98	24-35	29	28.8	0.39	4.37
D25	10.69	S	12.50	E	11.3.98	24-35	29	28.5	0.50	3.01

[a] The detected carbon number range of *n*-alkanes

[b] Carbon number of the homologue with highest abundance.

[c] Average chain length = $\Sigma(iX_i)/\Sigma X_i$, where X is abundance and i ranges from 25 to 35.

[d] Ratio of the *n*-C_{31} to the sum of the *n*-C_{29} and *n*-C_{31} alkane.

[e] CPI = $\frac{1}{2}\Sigma(X_i+X_{i+2}+..+X_n)/\Sigma(X_{i-1}+X_{i+1}+..+X_{n-})+\frac{1}{2}\Sigma(X_i+X_{i+2}+..+X_n)/\Sigma(X_{i+1}+X_{i+3}+..+X_{n+1})$, i = 25 and n = 33.

3.4.2. Stable carbon isotopic compositions of *n*-alkanes

The stable carbon isotopic compositions of all detected *n*-alkanes (*n*-C_{24} to *n*-C_{35}) in the aerosol samples fall in the range between -25 to -33 ‰ (Table 3.2). The odd-numbered *n*-alkanes are relatively more depleted in ^{13}C with increasing chain length. In general, the *n*-C_{29} or *n*-C_{31} alkanes are the most ^{13}C-depleted compounds in each sample. The longer-chain odd-numbered compounds, *n*-C_{33} and *n*-C_{35}, if present, are isotopically enriched relative to *n*-C_{29} or *n*-C_{31}. The even-numbered *n*-alkanes generally fall into this trend, but show an irregular scatter, which could indicate their higher sensitivity to contamination, due to their low abundance in plant waxes (Eglinton and Hamilton, 1963). The insets in Fig. 3.3 show examples of the stable carbon isotope compositions of *n*-alkanes versus carbon number.

3.4.3. 4-day backward trajectories

Atmospheric dust transport is known to occur either in the Saharan Air Layer (the African Easterly Jet, Fig. 3.2) above the trade-wind inversion (at pressure levels around 500 hPa), or in the trade-wind layer (the NE and SW trades and the Harmattan, at about 850 hPa) below 2 km altitude (Carlson and Prospero, 1972). Recent studies point to the significance of low-level dust transport, particularly for locations of less than 1500 km off the coast (Chiapello et al., 1997), with a direct impact on the Al-, mineral and grain size distribution of the deep-sea particle inventory and the underlying sediment (Ratmeyer et al., 1999). From the computed backward trajectories (Fig. 3.5) the dust samples can generally be subdivided into three distinctive groups. Dust material collected in samples D1 to D13, collected off Morocco to the Ivory Coast, was most likely transported in the low-level trade-wind layer. Backward trajectories of the mid-tropospheric 500 hPa level are starting far out over the Atlantic Ocean and are thus not likely to be transport pathways of continental-derived dust. For the dust samples collected in the Gulf of Guinea, D14 to D20, backward trajectories in both pressure levels direct approximately to the same continental source area, the Faya Largeau region in Chad. The southernmost dust sampling sites, D21 to D25, have only short backward trajectories in the trade-wind layer, which originate offshore. Only the trajectories in the higher 500 hPa level originate landinwards in southern equatorial Africa.

3.5. Discussion

3.5.1. Distributions of plant-wax *n*-alkanes

It has often been suggested that distributions of vascular plant-wax lipids may potentially be useful for taxonomic purposes. However, despite striking similarities in the *n*-alkane distributions of certain *Crassulaceae* species (Eglinton et al., 1962), such a conclusion is not supported by botanical investigations of plant lipids. Plants of widely divergent families have cuticle waxes of almost the same composition (Eglinton and Hamilton, 1963), while plants of the same species show strong variations in their leaf-wax lipid distributions (Borges Del Castillo et al., 1967; Eglinton and Hamilton, 1963). It has been inferred that the *n*-alkane distributions in plant waxes are not sufficiently diagnostic as taxonomic indicators (Borges Del Castillo et al., 1967). Alternatively, the composition of leaf-wax lipids may be strongly dependent on environmental factors due to their biological functionality to control the water balance of the plant (Hall and Jones, 1961). This may explain the

corresponding plant lipid distributions of the *Crassulaceae* species (Eglinton et al., 1962). These species are all adapted to warm and extremely dry climate conditions and all possess substantial amounts of wax coating. All of those investigated species show a strong predominance of the *n*-C_{31} and *n*-C_{33} alkanes with almost negligible amounts of other homologues (Eglinton and Hamilton, 1963).

The *n*-alkanes extracted from the dust samples depict a clear shift in their distribution, with the *n*-C_{31} dominating over the *n*-C_{29} in the northern samples, D3 to D8 (Table 3.1, Fig. 3.4a). Changes in the modal chain length of *n*-alkane distributions in dust samples (Gagosian and Peltzer, 1986; Simoneit et al., 1991; Simoneit et al., 1988) and in sediments (Poynter et al., 1989) have as yet mainly been explained by differences in growing-season temperature of the source regions. It has been assumed that in warmer tropical climates longer-chain compounds are biosynthesised as wax lipids, whereas in cooler temperate regions predominantly shorter chain compounds are produced (Gagosian and Peltzer, 1986). Our data partly contradict this hypothesis. The shift to more *n*-C_{29} dominated *n*-alkanes in dust samples collected off the rain forest areas of equatorial Africa (Fig. 3.4a) cannot be explained by a decrease in growing-season temperature. However, this region is strongly influenced by a vast moisture influx from the equatorial Atlantic with the monsoon (Leemans and Cramer, 1991). We thus suggest a large influence of the regional precipitation regime on the chain-length distribution of leaf-wax lipids, in accordance with their biological functionality as regulators of the plant's moisture balance. The chain-length distribution of *n*-alkanes in dust could thus reflect more an aridity- than a temperature-signal.

The CPI of the *n*-alkanes in the dust samples shows a significant variation from 7.65 to 2.40 (Table 3.1, Fig. 3.4b). Contributions of homologous series of *n*-alkanes with a low CPI to the dust in addition to plant waxes with a high (>5) CPI would lower the CPI. The sources of such *n*-alkanes could be vehicle exhaust (Simoneit, 1984), fuel or wood burning (Standley and Simoneit, 1987) or even marine sources (Lichtfouse et al., 1994). Lower temperature fires (e.g., brush fires) essentially steam-distill the vascular plant lipids into the smoke (Simoneit, 1985), while high-temperature fires can result in decrease of the CPI (Standley and Simoneit, 1987). Marine-derived *n*-alkanes can enter the lower atmosphere via sea spray.

The distribution of the CPI values along the coast (Fig. 3.4b) indicates a potential explanation for their variations. Lowest CPI values were found off the arid regions, the Sahara and Sahel and off the coast of Gabon, areas which are sparsely vegetated. Highest CPI values were found off the tropical rainforest regions. This suggests that the *n*-alkane distributions are sensitive to the contribution of fossil fuel- or marine-derived compounds when the fluxes of the plant waxes are low due to a low vegetation density in the source regions. Unfortunately, we cannot support this suggestion with actual flux data due to breakdown of the flux measurement onboard. When, on the other hand, atmospheric transport of plant waxes is presumably high, as in the rainforest regions, the CPI of the *n*-alkanes in the dust remains high.

The contribution of petroleum-derived compounds is confirmed by the presence, albeit in small amounts, of a series of 17α,21β(H)-hopanes in the saturated hydrocarbon fractions (Fig. 3.3). These compounds are geologically mature compounds and unambiguous fossil biomarkers for petroleum (Ensminger et al., 1974). The same triterpenoids have been previously identified in Harmattan aerosols from Nigeria and urban aerosols from Los Angeles and attributed to the contribution of petroleum residues (Simoneit, 1984; Simoneit et al., 1988). Their occurrence in aerosols was inferred to indicate the adsorption of lubricating oils to dust particulates,

as these higher-molecular weight compounds are not constituents of refined gasoline or diesel (Simoneit, 1984). Interestingly, 18(α)-oleanane, identified in some of the investigated dust samples, has earlier been identified as indicator for Nigerian crude oil products in Harmattan aerosols (Simoneit et al., 1988). The petroleum-derived compounds in aerosols could either be derived from the ship itself via contamination of the samples by chimney smoke or derived from fuel-burning processes in urbanised areas along the coast, possibly related to oil production activities. Contamination by the ship itself cannot completely ruled out, but seems unlikely due to the installed shut-down system of the dust samplers, stopping sampling of aerosols when the ship was not moving or the wind direction was deviating more than 50° from the ship's heading.

3.5.2. C_4 plant-derived wax lipids in dust

The detected range of stable carbon isotopic compositions of *n*-alkanes in the aerosol samples ($\delta^{13}C$ = -25 to -33 ‰) indicates that all the dust lipids consist of varying relative amounts of C_3 and C_4 plant-derived leaf-wax lipids. However, a significant contribution of fossil fuel/marine derived *n*-alkanes might potentially alter the stable carbon isotope compositions of the plant wax-derived lipids. To estimate, whether a potential fossil fuel/marine-contribution of *n*-alkanes, detected as a decrease in the CPI, has a significant effect on the stable carbon isotope composition of the dominant *n*-alkane homologues, *n*-C_{29} and *n*-C_{31} alkane, we applied a mass-balance approach, as described by Huang et al. (2000). We assume that the $\delta^{13}C$ value of the fossil fuel/marine contribution to equal the $\delta^{13}C$ value of the *n*-C_{24} alkane in each sample (Table 3.2). *n*-C_{24} alkane occurs in most saturated hydrocarbon fractions from the dust samples but is generally absent in plant waxes (Eglinton et al., 1962; Eglinton and Hamilton, 1963; Eglinton and Hamilton, 1967; Tulloch, 1976; Tulloch, 1984). For that purpose, we thus assume that *n*-C_{24} alkane originates from fossil fuel/marine sources in the dust samples. Furthermore we assume for this calculation, that the CPI of fossil fuel/marine-derived *n*-alkanes is 1 and that the CPI of plant waxes, uncontaminated by fossil fuel/marine sources is 7.65, the highest CPI detected in the dust *n*-alkanes (sample D11, Table 3.1). Both values are assumptions and we are aware that CPI of natural vegetation as well as that of fossil fuel/marine-derived *n*-alkanes can vary significantly in Nature. The calculated correction for fossil fuel/marine influence on the $\delta^{13}C$ values is small, ≤ 0.8 ‰, with only one exception (3.1 ‰ for *n*-C_{31} alkane in sample D14; Table 3.2) due to its relatively low concentration in this sample. If the weighted-average $\delta^{13}C$ value of the *n*-C_{29} alkane and *n*-C_{31} alkane for each sample is calculated and compared with the uncorrected value, only a minor deviation of ≤ 0.4 ‰ (Table 3.2) is detected. The correction of the stable carbon isotope compositions of the dominant plant-wax *n*-alkanes via the CPI is, thus, insignificant and, therefore, not required. This indicates that fossil fuel/marine-derived *n*-alkanes only significantly influence the CPI but not the $\delta^{13}C$ values of the dominant plant-wax compounds.

Table 3.2: Stable carbon isotopic analyses of *n*-alkanes in the dust samples (in ‰ PDB).

Sample	$\delta^{13}C_{24}$	$\delta^{13}C_{25}$	$\delta^{13}C_{26}$	$\delta^{13}C_{27}$	$\delta^{13}C_{28}$	$\delta^{13}C_{29}$	$\delta^{13}C_{30}$	$\delta^{13}C_{31}$	$\delta^{13}C_{32}$	$\delta^{13}C_{33}$
D1	n.d.	n.d.	n.d.	-28.8	n.d.	-30.1	n.d.	-28.9	n.d.	n.d.
D3	n.d.	-27.5	n.d.	-28.1	n.d.	-28.1	n.d.	-27.3	n.d.	-32.4
D4	-28.3	-27.2	-27.4	-26.9	-27.7	-28.7	-28.6	-27.7	-28.9	-29.3
D5	-27.9	n.d.	-26.9	-27.6	-28.9	-30.1	-28.9	-28.5	-30.7	-27.4
D6	-26.8	-32.6	-27.3	-27.4	-28.0	-29.3	-27.4	-27.8	-29.9	-26.0
D7	n.d.	-27.1	n.d.	-28.1	n.d.	-29.2	n.d.	-27.9	n.d.	n.d.
D8	n.d.	n.d.	-25.2	-27.4	-27.1	-29.1	-27.9	-27.1	n.d.	n.d.
D9	n.d.	-29.3	-26.7	-27.7	-29.1	-29.3	n.d.	-28.1	n.d.	-26.6
D10	-26.6	n.d.	-28.2	-29.6	-29.8	-31.2	-30.0	-31.0	n.d.	-29.5
D11	n.d.	n.d.	n.d.	-30.4	-30.6	-31.2	-30.2	-30.8	n.d.	-28.9
D12	-28.6	-28.7	-28.1	-27.6	-28.8	-30.4	-29.0	-30.2	-29.5	-28.8
D13	-27.7	-28.2	-27.3	-28.1	-29.3	-30.0	-29.7	-28.3	-29.1	-26.7
D14	-26.8	-30.3	-28.6	-29.5	-30.1	-31.5	-28.9	-30.2	n.d.	n.d.
D15	-29.3	-29.0	-29.4	-28.9	-29.9	-31.3	-31.2	-31.1	-31.3	-28.7
D16	-28.8	n.d.	-28.4	-29.0	-30.3	-31.5	-31.3	-31.7	-31.1	-30.0
D17	-27.3	-28.6	-27.4	-28.4	-29.3	-30.4	-29.7	-30.4	n.d.	-29.1
D18	-28.1	n.d.	-28.8	-29.0	-29.5	-31.4	-29.0	-31.6	n.d.	-29.5
D19	n.d.	n.d.	n.d.	-28.9	-29.8	-31.2	-32.2	-30.2	n.d.	-27.3
D20	-28.4	-29.2	-28.3	-28.5	-29.1	-30.9	-28.9	-30.4	-29.9	-27.3
D21	n.d.	-27.9	n.d.	-29.7	-32.5	-30.4	n.d.	-29.9	n.d.	-28.2
D22	-28.6	-27.6	-30.0	-28.9	-29.7	-30.2	n.d.	n.d.	n.d.	n.d.
D23	-27.1	n.d.	-28.9	-29.4	-31.1	-30.9	n.d.	-30.9	n.d.	-29.9
D24	-27.4	-28.3	-27.6	-27.9	-28.3	-29.8	-27.8	-28.0	-27.9	-28.9
D25	n.d.	n.d.	n.d.	-28.1	-27.5	-29.2	n.d.	-27.2	n.d.	-28.6

n.d. = not determined; stable carbon isotope values for *n*-C_{34} and *n*-C_{35} alkanes could only been detected in very few samples, therefore, they have been omitted.

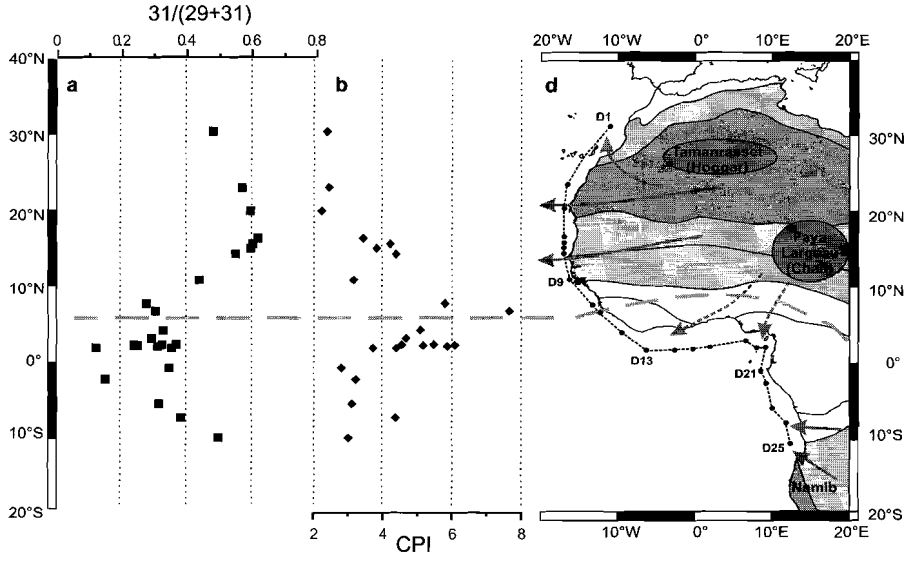

Figure 3.4: a) The variation in the ratio of the two dominant *n*-alkane homologues *n*-C_{31}/(*n*-C_{29}+ *n*-C_{31}) and b) the CPI of *n*-alkanes in the aerosol samples versus latitude. Note that sample D2 is missing. The grey stippled line indicates the position of the ITCZ.

Table 3.2 continued: The C_4 plant-derived fraction of *n*-alkanes in the dust samples.

Sample	$\delta^{13}C_{WM}$ [a]	C_4 %[b]	$\delta^{13}C_{29}$corr.[c]	$\delta^{13}C_{31}$corr.[c]	$\delta^{13}C_{WM}$ corr.[a]	C_4 % corr.[b]	ΔC_4 %
D1	-29.6	44	-30.1	-28.9	-29.5	44	0
D3	-27.7	58	-28.1	-27.3	-27.7	58	0
D4	-28.1	55	-29.1	-27.5	-28.1	54	1
D5	-29.1	47	-30.5	-28.5	-29.3	47	0
D6	-28.4	52	-29.6	-27.8	-28.5	51	1
D7	-28.4	53	-29.2	-27.9	-28.4	53	0
D8	-28.0	55	-29.1	-27.1	-28.0	55	0
D9	-28.7	50	-29.3	-28.1	-28.7	50	0
D10	-31.1	34	-31.2	-31.5	-31.3	33	1
D11	-31.0	34	-31.2	-30.8	-31.0	34	0
D12	-30.3	39	-30.4	-30.4	-30.4	39	0
D13	-29.4	45	-30.0	-28.4	-29.4	45	0
D14	-31.3	32	-31.5	-33.3	-31.7	30	2
D15	-31.2	33	-31.3	-31.2	-31.3	33	0
D16	-31.5	31	-31.5	-32.0	-31.6	30	1
D17	-30.4	38	-30.4	-30.9	-30.6	37	1
D18	-31.5	31	-31.4	-32.1	-31.6	30	1
D19	-30.8	36	-31.2	-30.2	-30.8	36	0
D20	-30.8	36	-30.9	-30.8	-30.9	36	0
D21	-30.2	40	-30.4	-29.9	-30.2	40	0
D22	-30.2	40	-30.2	n.d.	-30.2	40	0
D23	-30.9	35	-31.0	-31.7	-31.2	33	2
D24	-29.1	48	-29.8	-28.1	-29.2	47	1
D25	-28.2	54	-29.2	-27.2	-28.2	54	0

[a] Weighted-mean of the $\delta^{13}C$ values of the *n*-C_{29} and *n*-C_{31} alkane.
[b] Percentage of C_4 plant-derived *n*-alkanes in aerosols.
[c] $\delta^{13}C$ corrected for fossil fuel-/marine contribution (see text for explanation).

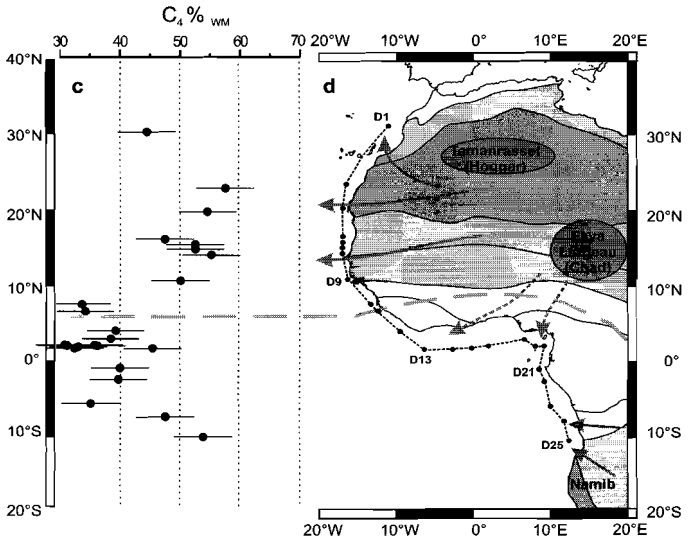

Figure 3.4 continued: c) C_4 plant-derived fraction of *n*-alkanes in the aerosols versus latitude. d) Vegetation zones on the continent with mixed C_3/C_4 plant vegetation are light shaded, the Sahara and Namib desert with sparse, but predominant C_4 plant vegetation are dark shaded. Major dust source regions and schematic transport pathways are indicated.

The weighted-mean uncorrected $\delta^{13}C$ values of the *n*-C_{29} alkane and *n*-C_{31} alkane (Table 3.2) are used to estimate the contribution of *n*-alkanes by C_4 plants using a two-component mixing equation. The end-member values for the mixing equation were taken from stable carbon isotope values of plant lipids reported in the literature: C_4 plant *n*-alkanes = -21.5 ‰ and C_3 plant *n*-alkanes = -36.0 ‰ (Collister et al., 1994; Rieley et al., 1993). This results in estimates of C_4 plant contribution varying from 31-58 % (Table 3.2, Fig. 3.4c). A significantly elevated input of C_4 plant-derived wax *n*-alkanes is only found in dust samples collected off the Sahara and the Sahel (samples D3 to D9), as well as off Gabon (samples D24 and D25). Slightly higher input of *n*-alkanes with a C_4 plant-wax signature is found off Morocco and off the Ivory Coast, and to a lesser extent, in the Gulf of Guinea.

Only few compound-specific isotope analyses of leaf-wax lipids in aerosol samples have yet been reported (Huang et al., 2000; Simoneit, 1997). Mean stable carbon isotopic compositions of *n*-alkanes in lipids from Harmattan aerosols from Nigeria vary from -27.7 to -30.9 ‰, in accordance with a vegetation composite ($\delta^{13}C$ = -28.9 ‰; Simoneit, 1997). This agrees quite well with the $\delta^{13}C$ of the weighted-mean of the *n*-C_{29} and *n*-C_{31} alkanes collected in the dust samples D17 to D20 off Nigeria. *n*-Alkanes in an aerosol sample collected in the eastern equatorial Atlantic (Simoneit, 1977) show an enriched mean stable carbon isotopic composition ($\delta^{13}C$ = -26.9 ‰; Simoneit, 1997), in accordance with their inferred transport via the SW trade winds from SW-African grasslands (Simoneit, 1977; Simoneit, 1997). This sample would thus likely be more comparable to the southernmost sample (D25) of our transect ($\delta^{13}C_{WM}$ = -28.2 ‰), which has an inferred origin in the SW-African savannahs, dominated by C_4 plant vegetation.

There is only a moderate correlation between the weighted-mean $\delta^{13}C$ of the two dominant homologues (*n*-C_{29} and *n*-C_{31} alkane) and the ratio of those compounds (*n*-C_{31}/(*n*-C_{29}+*n*-C_{31})), (r^2 = 0.69). This indicates the influence of other factors than photosynthesis type on the chain-length distribution of leaf-wax lipids (see section 3.5.1.). Interestingly, it can be seen from our data, that the $\delta^{13}C$ of the *n*-C_{31} alkane is increasingly more depleted than the *n*-C_{29} alkane when the $\delta^{13}C$ of the weighted-mean decreases (Table 3.2). The *n*-alkane isotopic values of C_3 plants usually become depleted with increasing carbon number, while C_4 plants produce *n*-alkanes of nearly constant isotopic composition with increasing chain length (Collister et al., 1994; Kuypers et al., 1999). The observed large isotopic difference between the *n*-C_{29} and *n*-C_{31} alkanes in samples D10-D23, thus, also indicates a higher contribution of C_3 plant *n*-alkanes to the dust.

3.5.3. Transport trajectories and vegetation sources

The Intertropical Convergence Zone (ITCZ) is the thermal equator of the Earth and moves seasonally with the latitudinal insolation shift. The trade winds generally blow in the direction of the ITCZ, either from the north in the Northern Hemisphere or from the south in the Southern Hemisphere. At the ITCZ, large-scale uplift of the converging air masses occurs, associated with a prominent precipitation maximum (Riehl, 1979). The wind field distribution is rather symmetrical around the ITCZ, similar to the climatological zones and vegetation belts. On their path towards the ITCZ, the low-altitude winds pick up organic material beside the inorganic dust components. The vegetation signal which is measured in the dust organic matter will therefore depend on the kind of vegetation present in that area and how rapidly this signal is overprinted on the existing signal, which was taken up during the previous

flow path. It will also reflect the relative importance of the modern vegetation signal versus the signal of older organic material in soils or dried lakes, reflecting a "fossil" vegetation.

When the relative amounts of C_4 plant-derived *n*-alkanes in dust (Fig. 3.4c) are compared with the vegetation zonation on the continent (Fig. 3.2) it is rather obvious, that a large C_4 plant-derived fraction of the leaf lipids could only be detected when there is a C_4 plant dominated vegetation present on the adjacent continent (Fig. 3.4d). This suggests that wind abrasion of leaf lipids and entrainment en route, possibly by a sandblasting effect, have a stronger effect than the lifting of sedimentary leaf waxes with desiccated soil material or from dried-up lake beds. However, this can only be confirmed when the isotopic signature of "old" leaf lipids in soil or lake bed material is significantly different from the recent vegetation. Soil organic matter should be quite sub-recent and thus not carry a significantly different isotopic signature than the recent vegetation.

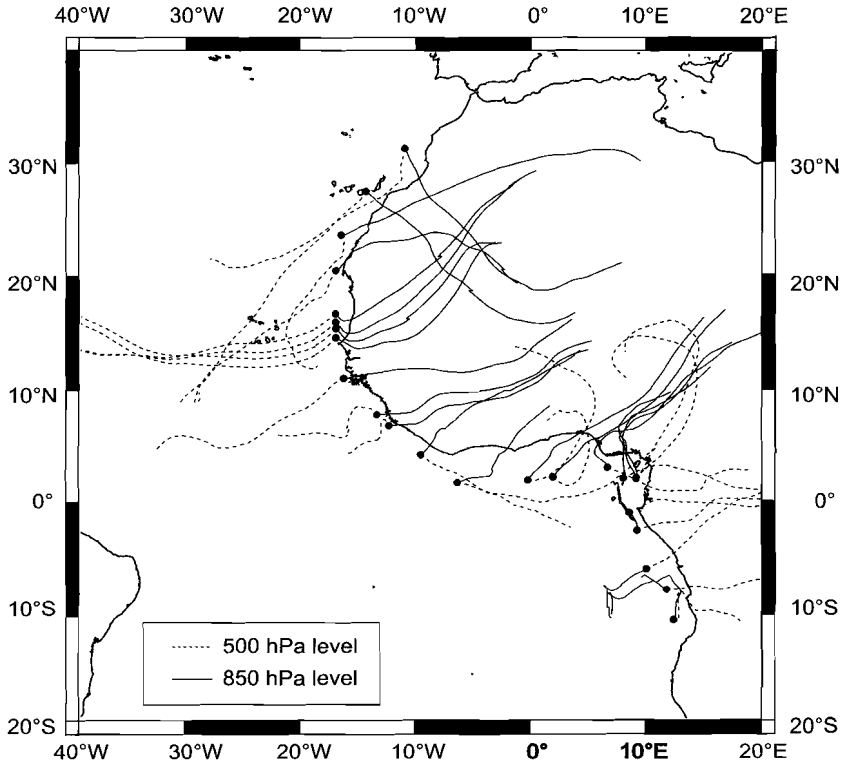

Figure 3.5: Four-day atmospheric backward trajectories computed for each sample, for the respective location and time of sampling. Calculated with a global two-dimensional isobaric model at the Department of Geosciences of Bremen University. Shown are trajectories for the 850 hPa (solid lines) and 500 hPa (stippled lines) barometric levels. Wind data were obtained from the European Centre for Medium Range Weather Forecast (ECMWF).

Lakes, however, were present in North Africa as far as 27°N and grasslands as far as 23°N during the African Humid period (14.8 to 5.5 kyr BP; de Menocal et al., 2000), while desert plants were restricted to the area north of 20°N (Joussaume et al., 1999).

It has been suggested, that these extensively vegetated areas were largely covered with C_4 plant dominated vegetation (Petit-Marie, 1991). If that was the case, transport of lake bed-derived material from the Faya Largeau region in Chad, which is transported to the Gulf of Guinea (Fig. 3.1, 3.5), should result in a C_4 plant isotopic signature of the dust lipids collected there. No significant ^{13}C-enriched leaf-wax lipids have been detected in those samples. Therefore, we suggest that leaf-wax lipids in aerosols largely reflect the contemporary vegetation along the transport pathways over the continent. Most probably, the isotopic signature of "old" leaf lipids from soils or lake beds gets rapidly overprinted by abrasion and entrainment of lipids from living plant leaves. The same conclusion has been drawn from a comparison of lipid contents of urban aerosol samples and that of samples downwind of the urban area, indicating a rapid dilution of the anthropogenic components (Simoneit et al., 1988). This interpretation fits with our data in so far, that we have inferred predominant low-level transport of dust for all collected samples collected north of the equator (see section 3.4.3). Thus, there is no need to invoke an additional source of ancient lipid material to explain the observed vegetation signal in dust, which leads us to suggest that in our sample set the recent vegetation is the main source. An unambiguous separation between modern and ancient sources of leaf-wax components can only be obtained by compound-specific ^{14}C-dating of leaf lipids in aerosols (Eglinton et al., 1997). The southernmost dust samples (D21 to D25) were probably transported in higher-altitude air layers (Fig. 3.5), and they exhibit an isotopically enriched leaf-wax signature, which does not reflect the contemporary vegetation on the adjacent continent (rain forest and woodland; Fig. 3.4c). For those samples we infer a longer-range transport of dust material and a source region that is probably located further south in the grass-savannahs, steppes or desert of SW-Africa (Kalahari or Namib desert). Based on these findings, we infer, that low-level transport of plant-wax lipids mainly reflects the modern vegetation at the last part of the transport trajectory, a signal which is rapidly overprinted onto an existing vegetation signal or that of ancient lipid material from soils or dried lakes.

The investigated aerosol samples reflect only the situation at the sampling time, during the winter season, when the ITCZ and the North African dust plume are in their southernmost position. However, the results are in good agreement with a study of $\delta^{13}C$ of *n*-alkanes in surface sediments off NW-Africa by Huang et al. (2000). These authors reported isotopically enriched leaf lipids only in sediments off the coast of the Sahara and Sahel, where they determined a C_4 plant-wax contribution of about 50 %, highly consistent with our data. It was concluded that the major contribution of leaf lipids was most probably derived from contemporary vegetation sources on the continent (Huang et al., 2000), which is now supported by our data.

3.6. Conclusions

- Aerosols sampled along a transect off the African West Coast from 30°N to 10°S were investigated on their lipid content and compound-specific stable carbon isotope compositions.
- Saturated hydrocarbon fractions contain predominantly long-chain *n*-alkanes with a strong dominance of odd-carbon-numbered compounds. These lipids are derived from epicuticular waxes of terrestrial plants and indicate the importance of vegetation sources for organic matter in dust.
- Backward trajectories confirm that atmospheric transport mainly took place in the low-level trade-wind layer (below 2 km), except for the southernmost samples, which are influenced by long-range transport from the SW-African steppe and savannahs.
- The chain length distribution of the *n*-alkanes is most likely a function of the aridity of the source region, in accordance with their biological functionality to regulate the moisture balance of the plant.
- The carbon preference of the *n*-alkanes, indicating the contribution of plant waxes, is higher in dusts from densely vegetated source areas, than from arid regions. This is attributed to a higher sensitivity of aerosols from dry areas with a lower leaf-wax content to fossil fuel or marine lipid contributions.
- A significant contribution of C_4 plant-derived wax lipids is detected only off regions with predominant C_4 plant type vegetation, the Sahara and Sahel in NW-Africa and Gabon in South Africa. Contributions of fossil fuel- or marine-derived lipids have no significant effect on the stable carbon isotope composition of the dominant plant-wax lipids.
- The leaf-wax lipids were mainly derived from the contemporary vegetation or sub-recent soil organic matter presumably via wind abrasion or sandblasting of leaf surfaces. Input of ancient lipid material, i.e., from dried-up lakes, cannot be confirmed and is apparently rapidly overprinted by the isotopic signature of the modern vegetation.
- The findings are highly consistent with studies of *n*-alkanes in surface sediments off NW Africa (Huang et al., 2000) and provide a basis for the reconstruction of vegetation sources by distribution parameters and compound-specific isotope analyses of leaf-wax lipids.

Acknowledgements

We are grateful to Jan-Berend Stuut (University of Utrecht) and Gaute Lavik (University of Bremen) for supply of the dust samples. We highly appreciate the effort of Ralph Schneider to enable the dust sampling. Horst Schulz is thanked as chief scientist of *RV Meteor* cruise 41/1. Peer Helmke (University of Bremen) generously supplied the satellite composite picture. Special thanks are given to Ulrike Wyputta for substantial support during trajectory analysis and preprocessing of windfield data.

Chapter 4

Lipid biomarkers as major source and preservation indicators in SE Atlantic surface sediments

Enno Schefuß, Gerard J. M. Versteegh, J. H. Fred Jansen, Jaap S. Sinninghe Damsté

Submitted to *Deep-Sea Research, Part I*

Abstract

Surface sediments from the eastern South Atlantic were investigated on their bulk organic geochemical characteristics and lipid biomarker contents to assess the sources, transport pathways and preservation of various organic components. Marine and terrestrial-derived organic carbon contents were estimated using the stable carbon isotopic composition of total organic matter. Normalisation of lipid biomarker concentrations on organic carbon content largely compensates for the differential effects of oxic degradation on organic carbon and lipid biomarkers. Principal component analysis enabled the identification of several groups of bulk and molecular parameters based on their spatial distributions. These patterns were combined with information on lipid sources to evaluate the controlling mechanisms of lipid distributions in the surface sediments. Wind-driven deep upwelling activity, river supply of terrigenous material, eolian contribution of plant waxes derived from dry continental areas and marine productivity related to river-induced mixing and oceanic upwelling or shallow coastal upwelling could be distinguished. Each source is reflected by characteristic bulk and molecular organic geochemical parameters. The spatial compound distributions provide a basis for paleoenvironmental reconstructions inferred from lipid biomarker distributions in ancient marine sediments.

4.1. Introduction

Distributions of lipid biomarkers in sediments can provide valuable information concerning the origin and transport pathways of organic matter and the conditions of past oceans (e.g., temperature, nutrient level, stratification etc.). Various phytoplankton groups contribute to the primary produced organic matter, largely depending on the nutrient conditions of the surface waters (Boon et al., 1979; Brown et al., 1991; Chyong, 1971; Falkowski et al., 1998; Hinrichs et al., 1999; Schubert et al., 1998; Shannon and Pillar, 1986; Volkman, 1986; Volkman et al., 1998; Westerhausen et al., 1993). Allochthonous lipids, on the other hand, are transported to the tropical marine realm by freshwater runoff or wind and thus carry information of continental aridity and wind strength (Cox et al., 1982; Gagosian and Peltzer, 1986; Huang et al., 2000; Simoneit, 1977; Simoneit et al., 1991; Simoneit et al., 1977; Westerhausen et al., 1993). During transport to the sediments these signals can be modified by zooplankton feeding and microbial degradation (Conte et al., 1995; Gagosian et al., 1983; Hedges and Prahl, 1993; Prahl et al., 1989; Sinninghe Damsté et al., 1997; Sinninghe Damsté et al., 2002b; Sun and Wakeham, 1994; Teece et al., 1994; Wakeham et al., 1998; Wakeham et al., 1997). For the proper understanding of paleoclimatic changes and interpretation of biomarker records in sediment cores, it is necessary to study the modern spatial distribution of biomarkers.

We aim to identify production and transport patterns of lipid biomarkers in surface sediments of the eastern South Atlantic to provide a base for the application of lipid distributions in paleoenvironmental reconstructions. The eastern South Atlantic consists of several distinct surface-water environments, i.e., a region influenced by strong perennial upwelling, several shallow and seasonal upwelling cells and an area influenced by a high freshwater runoff from the Congo River (Berger, 1989; Eisma and van Bennekom, 1978; Falkowski et al., 1998; Hinrichs et al., 1999; Jansen et al., 1984; Lutjeharms and Stokton, 1987; Peterson and Stramma, 1991; Schneider et al., 1994; Shannon, 1985; van Bennekom and Berger, 1984). All these settings are expected to be reflected in the composition of the organic matter of the surface sediments.

In this study we characterise the various depositional environments in the eastern South Atlantic by a combination of bulk organic geochemistry and lipid biomarkers. For this purpose, we measured several bulk and molecular organic geochemical parameters in a set of surface-sediment samples. We utilized statistical analysis to identify groups of parameters with similar spatial distributions. Five groups could be detected which reflect the modern environmental settings with regard to production, transport and preservation of organic compounds.

4.2. Setting

The modern surface and shallow subsurface hydrography of the eastern South Atlantic (Peterson and Stramma, 1991; van Bennekom and Berger, 1984) creates several distinct oceanographic regimes, which support different kinds of surface-water productivity in that area (Fig. 4.1a). The eastward-flowing South Equatorial Counter Current (SECC) in the north feeds the warm, nutrient-poor Angola Current (AC), which flows southwards along the western African margin. At about 15°-17°S it converges with the northward-flowing cold, nutrient-rich Benguela Coastal Current (BCC) and is deflected to the northwest. A frontal zone, the Angola-Benguela Front

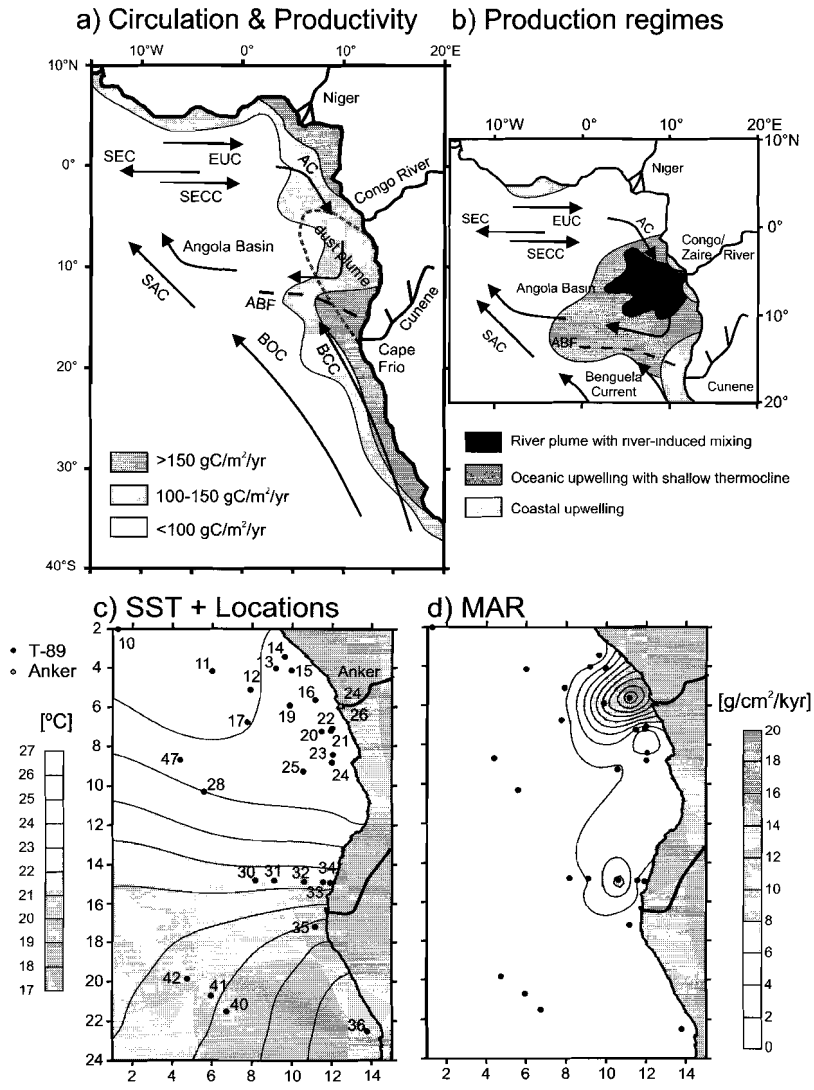

Figure 4.1: a) Surface and shallow subsurface circulation pattern in the eastern Atlantic summarized after Schneider et al. (1995) and productivity estimates after Falkowski et al. (1998). SEC = South Equatorial Current, SECC = South Equatorial Counter Current, EUC = Equatorial Undercurrent, AC = Angola Current, ABF = Angola-Benguela Front, BOC = Benguela Oceanic Current, BCC = Benguela Coastal Current, SAC = South Atlantic Current. The area surrounded by the stippled line, stretching from the Angolan coast to the northwest, indicates the dust plume as present during June to August. b) Production regimes in the Angola Basin, redrawn after Schneider et al. (1994). c) Modern sea-surface temperature field (in °C; Levitus and Boyer, 1994) and sample locations (Eisma et al., 1978; Jansen et al., 1990). The sample locations are given in each plot to give an indication of the statistical reliability. d) Mass accumulation rates of the T89-surface sediments (in g/cm^2/kyr).

(ABF), is established and extends to a distance of up to 1000 km off the coast (Meeuwis and Lutjeharms, 1990). The ABF effectively forms a barrier for surface-ocean mixing, as does the Walvis Ridge for deeper waters. The ABF also delineates the northern boundary of the zonally directed annual trade-wind field. North of the ABF, the weaker trade winds blow in a more meridional direction (Schneider et al., 1995). At about 30°S, the Benguela Current splits into the Benguela Oceanic Current (BOC), the main current in northwestern direction, and the Benguela Coastal Current (BCC), flowing as a sluggish, wide current along the continental margin (van Bennekom and Berger, 1984). Both are driven by the predominantly southerly and southeasterly trade winds (Shannon, 1985).

Off the coast of South Africa and Namibia, these winds drive coastal upwelling of cold, nutrient-rich South Atlantic Central Water (Shannon, 1985). In the upwelling zone, primary productivity reaches high rates of over 200 $gC/m^2/yr$ (Berger, 1989; Shannon et al., 1987). In the upwelling cell near Lüderitz Bay, persistent coastal upwelling causes high rates of sedimentary accumulation of phytoplankton biomass (Brown et al., 1991). Filaments of cold, nutrient-rich waters, extending up to 600 km offshore (Lutjeharms and Stokton, 1987), mix with low-productivity waters and sustain intermediate productivity. Elevated coastal productivity north of the ABF is restricted to two separated small-scale, coastal upwelling cells north and south of the Congo River mouth at 5°S and 7°S. The shallow upwelling activity has the strongest effect on nitrate and lesser on phosphate concentrations, while its effect on silicate concentrations is much smaller (van Bennekom et al., 1978). However, south of the Congo River plume, the primary production is relatively high (Chyong, 1971; van Bennekom and Berger, 1984). Estimates of primary productivity in the eastern South Atlantic are shown in Fig. 4.1a (Falkowski et al., 1998).

In the Angola Basin, the cyclonic gyre circulation causes shoaling of the thermocline and a seasonal supply of nutrients to the photic zone, supporting elevated phytoplankton productivity (Fig. 4.1b; Lutjeharms and Stokton, 1987). During austral winter (June to August), the Intertropical Convergence Zone (ITCZ) is furthest north (~20°N) and strong Southern Hemisphere trade winds cause oceanic upwelling by surface divergence in the equatorial Atlantic Ocean (Philander and Pacanowski, 1986). The upwelling intensity correlates to the zonal velocity of the southern trades (Philander and Pacanowski, 1986). SSTs in the eastern equatorial Atlantic are at their annual minimum, while surface-water productivity reaches its annual maximum during austral winter (Katz and Garzoli, 1982). Offshore oceanic upwelling outside the Congo River plume (Fig. 4.1b) induces moderate to high primary productivity of 125 to 180 $gC/m^2/yr$ (Berger, 1989).

At about 5°S, the low-salinity plume of the Congo (Zaire) River is superimposed on the cyclonic gyre of the Angola Basin and can be detected up to 800 km offshore from the river mouth. The variation in discharge is associated with the monsoonal circulation and precipitation (Eisma and van Bennekom, 1978; van Bennekom and Berger, 1984). During austral summer (December to February) the ITCZ is in its southernmost position (5°-10°N), causing maximum monsoon conditions in equatorial Africa with a large influx of moisture-laden air and high precipitation (Hsü and Wallace, 1976). The maximum extension of the Congo River plume occurs in February-March, later than the maximum discharge in December (van Bennekom and Berger, 1984) and is associated with the highest annual sea-surface temperatures (SST) in the equatorial Atlantic (Katz and Garzoli, 1982). The Congo River water flows rapidly in a thin surface layer into the ocean. Together with the large depth of the estuary, this leads to an extremely stratified condition with low vertical mixing.

Entrainment of subsurface waters with elevated concentrations of nitrate and phosphate to the silicate-rich river water causes river-induced productivity (van Bennekom et al., 1978). The river plankton consists largely of the freshwater diatom *Melosira granulata* and green algae which, however, rapidly die in the ocean (Cadée, 1978). About 100 to 200 km offshore the plume broadens. Entrainment of subsurface waters from below the shallow nutricline supplies additional nitrate and phosphate to the surface. A marine phytoplankton bloom develops in the inner plume area, but it takes some time to build up a high population. A maximum of primary productivity is found in a narrow meridional zone between salinities of 28 and 32, around 10 to 11°E (Fig. 4.1b; Cadée, 1978). The main phytoplankton bloom thus develops around a salinity of 30 (Cadée, 1984). Here about 40 to 90 % of the dissolved silica advected by the Congo River is taken up by diatoms (van Bennekom and Berger, 1984). surface-water productivity off the Congo River mouth reaches values of 90 to 125 $gC/m^2/yr$ (Berger, 1989) sustained by river-induced upwelling and mixing of river- with marine-derived nutrients (van Bennekom and Berger, 1984). Phytoplankton

Table 4.1: Sample locations, bulk parameters and SST estimates from alkenone unsaturation

Sample	Latitude	Longitude	Water depth (m)	MAR (g/cm^2/ kyr)	TOC (wt%)	$\delta^{13}C_{org}$ (‰)	terr. OC (wt%)	mar. OC (wt%)	SST (°C)
T89-10	2°4.6'S	1°19.3'E	2088	0.34	0.1	-20.4	0.0	0.1	26.8
T89-11	4°14.8'S	6°2.7'E	4627	1.22	0.7	-21.4	0.1	0.6	25.9
T89-12	5°12'S	7°58.4'E	4068	1.51	1.0	-20.9	0.1	0.9	26.0
T89-13	4°6.4'S	9°14.3'E	3092	2.52	2.1	-21.1	0.3	1.8	25.5
T89-14	3°30.5'S	9°41.4'E	868	0.84	2.5	-21.5	0.5	2.0	25.4
T89-15	4°12.8'S	10°1.3'E	1930	6.04	2.5	-21.5	0.5	2.0	25.9
T89-16	5°42.3'S	11°13.7'E	826	20.5	3.6	-23.8	1.9	1.7	25.8
T89-17	6°49.1'S	7°48.3'E	4253	0.78	0.8	-21.5	0.2	0.6	26.4
T89-19	6°2.6'S	9°57.3'E	3140	13.8	2.0	-23.2	0.9	1.1	25.0
T89-20	7°18.4'S	11°32.2'E	1080	2.2	2.2	-21.9	0.6	1.6	24.4
T89-21	7°16.5'S	11°59.6'E	490	0.42	3.8	-22.4	1.3	2.5	25.6
T89-22	7°7.8'S	12°4'E	200	3.36	0.7	-22.1	0.2	0.5	26.5
T89-23	8°30.8'S	12°6.5'E	796	1.45	4.8	-21.6	1.1	3.7	25.1
T89-24	8°54.4'S	12°3.5'E	2157	4.6	2.2	-20.8	0.3	1.9	26.6
T89-25	9°22.1'S	10°36.5'E	4164	1.71	1.2	-21.1	0.2	1.0	26.5
T89-28	10°23.2'S	5°38.2'E	5307	0.39	0.8	-21.3	0.1	0.7	24.2
T89-30	14°52.6'S	8°13.2'E	4752	1.65	0.4	-20.3	0.0	0.4	22.0
T89-31	14°53.6'S	9°10.2'E	4293	2.01	0.6	-19.8	0.0	0.6	22.6
T89-32	14°57.6'S	10°40.1'E	3342	7.14	0.9	-19.6	0.0	0.9	24.8
T89-33	14°58.4'S	11°37.2'E	2027	1.25	1.5	-20.0	0.0	1.5	24.1
T89-34	15°0.6'S	11°58'E	999	0.73	2.4	-20.4	0.1	2.3	24.4
T89-35	17°17.6'S	11°13.7'E	802	0.22	1.4	-20.8	0.2	1.2	22.2
T89-36	22°36.1'S	13°50.3'E	131	2	17.6	-20.4	1.0	16.6	17.1
T89-40	21°37'S	6°46.9'E	3060	1.65	0.1	-20.3	0.0	0.1	21.3
T89-41	20°48.5'S	6°0.3'E	4282	1.62	0.2	-20.1	0.0	0.2	20.3
T89-42	19°56'S	4°47.3'E	5265	0.37	0.2	-20.8	0.0	0.2	21.3
T89-47	8°47.2'S	4°25.6'E	5362	0.28	0.9	-20.3	0.0	0.9	25.3
Anker 24	6°2'S	12°34'E	5	n.d.	2.9	-26.4	2.6	0.3	n.d.
Anker 26	6°3'S	12°29'E	6	n.d.	0.1	-26.9	0.1	0.0	n.d.

Note: SST are calculated via U^K_{37}' (ketone unsaturation index) = $[C_{37:2}]/([C_{37:2}]+[C_{37:3}])$, using the equation of Müller et al. (1998): $U^K_{37}' = 0.033\ T + 0.044$.

productivity in the inner Congo River plume is dominated by a very high diatom production, accounting for 40 to 60 % of the total productivity (van Bennekom and Berger, 1984). Diatoms, particularly *Chaetoceros spp.*, form the bulk of this

phytoplankton bloom (Cadée, 1984). High amounts of *Chaetoceros* resting spores have been found in the underlying sediments (Jansen and van Iperen, 1991; van Iperen et al., 1987). The level of primary productivity in the outer Congo River plume decreases due to the subsequent dilution of the river-derived nutrients. The in-situ primary production in the outer plume reaches values hardly or not above those in the ocean outside the plume (Cadée, 1978).

4.3. Material and Methods

The investigated surface-sediment samples (Fig. 4.1c, Table 4.1) were collected during the *RV Tyro* cruise in the eastern South Atlantic during fall 1989 (Jansen et al., 1990). The box-cores were stored frozen at -20°C afterwards and the uppermost 1-1.5 cm were used for analyses. The two samples from the estuary of the Congo River, 'Anker 24' and 'Anker 26', were taken as grab samples (Eisma et al., 1978) and stored as dried sediment in dark PE-containers before analyses.

4.3.1. Bulk analyses

Total organic carbon (TOC) contents were measured after decalcification of the samples on a Fisons Instruments NCS-1500 Elemental Analyser using flash combustion at 1030°C. Standard deviations of duplicate measurements were better than 0.3 %. Stable carbon isotope compositions of the TOC have been determined using the same machine, connected via a ConFlo II interface to a Delta plus Finnigan MAT mass spectrometer. CO_2 was used as the reference gas. Standard deviations of duplicate and triplicate measurements were always better than 0.2 ‰ vs. PDB.

4.3.2. Lipid analyses

Sediment samples were freeze-dried and finely ground in an agate mortar, and subsequently extracted ultrasonically using 40 ml of methanol (MeOH) (3x), 40 ml of dichloromethane (DCM):MeOH (1:1, v/v) (3x), and 40 ml of DCM (3x), each for 5 min. For each sample, the extracts were combined and concentrated with a rotary evaporator at 35°C. Salts were removed by washing with double-distilled H_2O in a separatory funnel and extraction of the lipids with DCM (3x). For total lipid analysis known aliquots of the extracts with an added amount of standard (2,3-dimethyl-5-1',1'-D_2-hexadecyl-thiophene) were methylated with diazomethane after drying with anhydrous Na_2SO_4. Before silylation with bis(trimethyl-silyl)trifluoro-acetamide in pyridine (1 hr at 60°C), very polar compounds were removed on a silica-gel column eluted with ethyl acetate. Saturated hydrocarbon fractions were collected by column-separation on a small column (4 x 0.3 cm) packed with $AgNO_3$-impregnated, activated Al_2O_3 by elution with four column volumes of hexane:DCM (9:1, v/v). Gas chromatography (GC) was performed on a Hewlett Packard 5890 series II chromatograph equipped with an on-column injector and fitted with a fused-silica capillary column (25 m x 0.32 mm) coated with CP Sil 5 (film thickness 0.12 μm). helium was used as carrier gas, and the oven was programmed from 70°C to 130°C at 20°C/min, followed by 4°C/min to 320°C (10 min holding time). Effluents were detected using flame ionisation (FID). GC-mass spectrometry (GC-MS) was performed using the same type of gas chromatograph and the conditions described above. The chromatographic column was directly inserted into the electron impact ion source of a VG Autospec Ultima mass spectrometer operated with an ionisation

energy of 70 eV and scanned over a mass range of *m/z* 50-800 with a cycle time of 1.8 s. Compound identifications are based on comparison of relative GC retention times and mass spectra with those in the literature.

Quantification of long-chain alkenones was performed by integration of their peaks and those of internal standards in FID chromatograms of the total lipid extracts, while *n*-alkanes were quantified in saturated hydrocarbon fractions. Data acquisition and integration was done using Atlas analytical software. Other lipid biomarkers were quantified using characteristic fragment ions in mass chromatograms of GC-MS analyses. Resulting abundance values were converted to concentrations by compound-specific correction factors determined from clean mass spectra and comparison with GC-FID responses. The relative precision of the entire analytical procedure, based on duplicate sediment extraction, was around 10 %.

The U^{K}_{37}'-index is calculated as the ratio of the di- to the sum of the di- and tri-unsaturated C_{37} alkenones. The conversion of U^{K}_{37}' values to sea-surface temperature estimates was done using the calibration by Müller et al. (1998), based on an extensive set of core-tops from the South Atlantic: SST (°C) = (U^{K}_{37}' - 0.044) / 0.033. The standard error of this relationship is ±1.0°C. The standard deviation (±σ) based on duplicate and triplicate analyses of the sea-surface temperature estimates of our samples is 0.3°C (or 0.01 U^{K}_{37}' units).

GC-combustion-isotope ratio monitoring-MS was performed to measure the stable carbon isotopic composition of the individual *n*-alkanes and was described by Hayes et al. (1990). The Hewlett Packard 5890 Series II GC was equipped with a fused silica capillary column (25 m x 0.32 mm) coated with CP-Sil 5 (film thickness 0.12 mm). The carrier gas was helium and on column injection with continuos flow was applied. The oven-heating program was the same as for GC analyses, except for a longer (30 min) isothermal holding time. CO_2 gas with pre-calibrated isotopic composition was used as standard. The GC was connected via a combustion-interface to a Finnigan delta C mass-spectrometer. The isotopic compositions of individual compounds were calculated by integration of the mass 44, 45 and 46 ion currents (Merrit et al., 1994). Analyses were done in duplicate or triplicate with standard deviations (±σ) better than 0.5 ‰. $\delta^{13}C$ values are expressed versus PDB. The C_4 plant-derived percentage of the *n*-alkanes was calculated in the same way as described by Huang et al. (2000) and Schefuß et al. (re-submitted). In short, the $\delta^{13}C$ values of the C_{29} and C_{31} *n*-alkanes were corrected for the influence of marine- or fossil fuel-derived *n*-alkanes via a simple mass balance approach (Huang et al., 2000). For the correction, we assumed that the sample with the highest *n*-alkane CPI holds the most pure plant-wax signal, i.e., a CPI of 6.4 in sample "Anker 24" from the Congo estuary, that the *n*-alkane contribution of non-plant origin has a CPI of 1, and that the $\delta^{13}C$ value of the C_{24} *n*-alkane in each sample represents the stable carbon isotope composition of the non-plant-wax *n*-alkanes (Huang et al., 2000). These corrected $\delta^{13}C$ values of the C_{29} and C_{31} *n*-alkanes were than weight-averaged and converted into a C_4 plant-derived fraction via a binary mixing model. End-member values for this mixing equation were taken from the literature (Collister et al., 1994; Rieley et al., 1993): C_3 plant-derived *n*-alkanes = -36.0 ‰ vs. PDB, C_4 plant-derived *n*-alkanes = -21.5 ‰ vs. PDB. The applied correction of the $\delta^{13}C$ values results in a lowering of the C_4 plant estimate depending on the CPI of each sample. In case of the two samples with the lowest CPI values, the C_4 plant estimate is decreased by 11 % due to this correction, but for the samples with a CPI ≥ 4 almost no change occurs.

4.3.3. Principal component analysis

Principal component analysis (PCA) was performed to distinguish groups of the bulk and molecular geochemical variables with similar spatial distribution. The method assigns a loading to each variable, i.e., parameter, on each factor, representing the degree to which the variable is influenced by that factor, i.e., that environmental process. A commonly employed sub-routine is VARIMAX-rotation of the calculated factor loading. This calculation method involves the rotation of the factor-axes in a multi-dimensional space, which results in the simplest composition of factors, with either minimum or maximum loading of each variable on the extracted factors while preserving trends. The Systat software package was used for all PCA calculations (Wilkinson, 1988).

4.3.4. Mapping

The spatial distributions of bulk parameters and lipid biomarker concentrations are presented as maps, which have been produced with the Surfer software program. To interpolate the irregularly spaced and anisotrope data set, we utilized the gridding method of kriging. Kriging is a procedure that is used to estimate values of a surface at the nodes of a regular grid from irregularly spaced data points (Krige, 1951). It makes explicit use of the specific auto-correlation between observations on the surface being mapped. The procedures incorporate measures of error and uncertainty when determining estimations. Optimal weights are assigned to known values in order to calculate unknown ones. A more detailed description can be found in Deutsch and Journel (1992). A linear variogram model with no drift has been used in the kriging technique. The resulting contour maps have not been edited further.

4.4. Results and Discussion

4.4.1. Bulk parameters

Several bulk parameters (Table 4.1) have been measured in twenty-nine surface-sediment samples used in this study (Fig. 4.1c). The mass accumulation rates (MAR) of the investigated surface sediments (Table 4.1, Fig. 4.1d) were derived from radiocarbon dating, oxygen isotope data and core-to-core correlation of calcium carbonate profiles measured with the CORTEX XRF-scanner (Jansen et al., 1998). The differences between the MAR are large, i.e., they vary from 0.22 to 20.5 $g/cm^2/kyr$ (Table 4.1), thus by a factor of >90. The dominant feature in the spatial MAR distribution is the high MAR in the Congo fan (Fig. 4.1d), due to the large contribution of sedimentary material supplied by the Congo River. A small, secondary maximum in the MAR distribution is detected on the Walvis Ridge (sample T89-32). However, the reasons for the high MAR at this location are not known.

The total organic carbon content (TOC) of the surface sediments varies from 0.1 to 17.6 wt% (Table 4.1, Fig. 4.2a). Generally, elevated TOC values are found near the continent. The highest TOC value is detected for sample T89-36 located off Lüderitz Bay, in a region that is dominated by strong perennial upwelling (Shannon et al., 1987). We infer that the highest TOC values are caused by high accumulation of phytoplankton-derived organic material in the Benguela upwelling area (Brown et al., 1991). A secondary maximum, although below 5 wt% TOC, is found south of the Congo River, an oceanic upwelling region influenced by elevated phytoplankton productivity (Lutjeharms and Stokton, 1987). However, right at the mouth of the

Congo River, a minimum of TOC % is found. This is most likely caused by a dilution effect due to the high contribution of inorganic material right in front of the Congo River mouth (Jansen et al., 1984).

The stable carbon isotope composition of bulk organic matter ($\delta^{13}C_{org}$, Table 4.1, Fig. 4.2b) in the surface sediments shows minimum values right off the Congo River mouth. The two samples taken in the Congo estuary, Anker 24 and Anker 26, have a $\delta^{13}C_{org}$ between -26 and -27 ‰ vs. PDB, consistent with measurements on particulate organic carbon transported by the Congo River and entering the Angola Basin ($\delta^{13}C$ = -26.7 ‰; Mariotti et al., 1991). The stable carbon isotopic signature of terrigenous

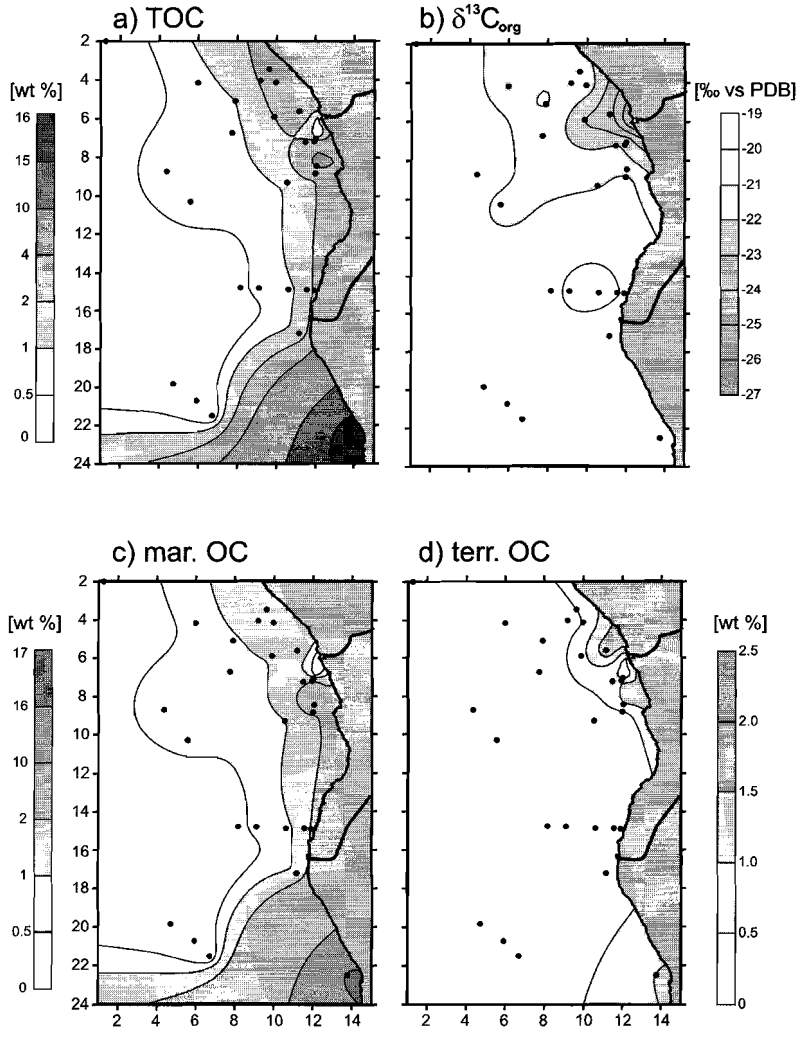

Figure 4.2: Spatial distribution of a) TOC values, b) $\delta^{13}C_{org}$ values, c) marine organic matter and d) terrigenous organic matter of the surface sediments.

organic matter differs for C_3 and C_4 plants. C_3 plant-derived organic matter generally has bulk $\delta^{13}C$ values around -27.0 ‰ (-25.5 to -29.3 ‰), while C_4 plants have $\delta^{13}C$ values around -12.0 ‰ (-8.0 to -19.0 ‰; Sackett, 1989; Tyson, 1995). This suggests an almost pure terrestrial C_3 plant source, i.e., rainforest vegetation, of the bulk organic matter supplied by the Congo River (Sackett, 1989; Tyson, 1995). The $\delta^{13}C_{org}$ values of the investigated surface sediments ($\delta^{13}C$ = -26.9 to -19.6 ‰) all fall between the values of terrestrial C_3 plant-derived and marine organic matter. The marine isotopic end-member falls in the range of -18.5 to -21.5 ‰, as confirmed by measurements on plankton samples (Westerhausen et al., 1993), sediment trap samples (Fischer et al., 1998), and surface sediments from the low- to mid-latitude ocean (Goñi et al., 1998; Tyson, 1995).

4.4.2. Marine vs. terrestrial OC

In order to gain more insight into the distribution of marine- and terrestrial-derived organic matter, the TOC contents of the surface sediments (Fig. 4.2a) were separated into a marine and terrestrial fraction utilising the $\delta^{13}C_{org}$ values (Fig. 4.2b). We have estimated the portions of marine- and terrestrial-derived organic matter with a simple binary mixing model, assuming a terrigenous C_3 plant-derived ($\delta^{13}C$ = -27.0 ‰) and a marine end-member ($\delta^{13}C$ = -20.0 ‰). It should be noted that a change of 1 ‰ in the assumption for the marine end-member results in a change of 12 % in the relative proportions of marine and terrestrial organic matter.

The marine organic matter content (Fig. 4.2c) shows generally elevated values along the coast. Along the northern coastline the marine organic matter is >1 wt%, while south of the Congo River mouth even values >2 wt% are found. The maximum of the marine OC content is, however, found for sample T89-36 from below the Benguela upwelling. Here, the marine fraction is about 94 % of the TOC. The OM from the Congo estuary contains hardly any marine organic carbon. The dilution of organic material by inorganic sedimentary input (Jansen et al., 1984) further explains the low marine OC values in the Congo fan area.

The contribution of terrigenous organic matter is high around the mouth of the Congo River (Fig. 4.2d), but as for TOC and marine OC, it is diluted with inorganic material in the Congo fan area. The terrigenous OC content is generally low far away from the continent. For the sample with the highest TOC value, sample T89-36 located below the Lüderitz upwelling cell, a relatively large terrestrial organic carbon content (>1 wt%) is calculated. This, however, is attributed to the error in the isotopic end-members.

A combination of several processes therefore explains the distribution of TOC and $\delta^{13}C_{org}$ values. A generally elevated input of marine-derived organic matter occurs near the coast (Fig. 4.2c). This finding is consistent with the general elevated marine primary productivity along the SW-African coast (Berger, 1989; Falkowski et al., 1998). The dominant contribution of terrestrial organic matter is via the Congo River freshwater outflow (Fig. 4.2d). This material unambiguously carries a C_3 plant isotopic signature and reflects the sole contribution of rainforest vegetation. Right off the mouth of the Congo River, lowered TOC values are found (Fig. 4.2a), caused by the predominant deposition of inorganic material (Jansen et al., 1984). Elevated phytoplankton productivity causes elevated TOC values in the oceanic upwelling region off the Congo River (Lutjeharms and Stokton, 1987) and, especially, in the Benguela upwelling area (Brown et al., 1991; Falkowski et al., 1998; Lutjeharms and Stokton, 1987).

Diagenesis potentially alters the organic matter composition and its isotopic signature. The terrigenous organic matter probably experienced extensive degradation, i.e., in tropical soils, prior to discharge into the marine environment. This implies that the more refractory terrestrial organic matter enters into the sediments. Marine organic matter, on the other hand, consists for a substantial part of labile components, which are rapidly degraded under oxic conditions (Hartnett et al., 1998; Hedges and Prahl, 1993). It can be expected, therefore, that diagenetic degradation of marine organic matter will take place along the coast, where the contribution of marine OC contents is large (Fig. 4.2c). Its strongest effect, however, can be expected for sediments below the Benguela upwelling system. The extraordinary high marine OC content of sample T89-36 may, however, point at a less severe degradation of labile marine organic matter due to suboxic bottomwater conditions associated with the upwelling-related high productivity (Canfield, 1989; Canfield, 1994; Schulz et al., 1994). Potential diagenetic effects on organic matter content and lipid biomarkers will be addressed in more detail below (see next section).

4.4.3. Lipid biomarkers

A wide variety of lipid compounds was identified in the total lipid fractions of the investigated surface sediments as illustrated by two GC-FID-traces (Fig. 4.3; Table 4.2). In principle, biomarker accumulation rates provide insight in the absolute fluxes into the surface sediments. However, because of the strong differences in MAR (Fig. 4.1d) in this specific setting the spatial distributions of all biomarker accumulation rates are very similar. From detailed investigations of organic carbon burial rates in the Congo fan area, it was already concluded, that these are mainly controlled by the MAR via a so-called 'sealing-effect' (Jansen et al., 1984; Sarnthein et al., 1987). We, therefore, decided to normalize the specific biomarker data to the TOC content of the surface sediments (Table 4.1). It appears that this normalisation partly compensates for the oxic degradation effects on TOC and lipid biomarkers. The extent of degradation of TOC and lipid biomarkers predominantly depends on the oxygen exposure time (Hartnett et al., 1998; Sinninghe Damsté et al., 2002b). Assuming, that pore-water oxygen is not completely consumed in the uppermost centimetres of the investigated sediments, which is true for 26 of the 29 investigated samples (A.J. van Bennekom, unpublished results), we should therefore find a strong influence of the MAR. That is indeed the case, as all biomarker accumulation rates show the same, MAR-dominated, distribution pattern. However, if the oxic degradation would considerably affect the TOC-normalised values, their spatial distributions would also resemble the MAR pattern. Since this is not the case, we conclude that the TOC normalisation largely masks the effect of oxic degradation.

There are, however, differences in the preservation potential of various lipid compounds during oxic degradation. The lipids of epicuticular plant waxes, are reported to be enriched during differential degradation processes (Sinninghe Damsté et al., 1997; Sinninghe Damsté et al., 2002b; Wakeham et al., 1998; Wakeham et al., 2002), being in part protected by the resistant character of the plant particles themselves and in part by the water-insoluble nature of the wax compounds (Gagosian and Peltzer, 1986; Kolattukudy, 1976). Degradation efficiencies of lipid biomarkers are highly variable, but always high (Wakeham et al., 1998; Wakeham et al., 2002). The general pattern of lipid preservation potential is that long-chain *n*-alkanes are most stable, followed by long-chain alkenones, which are equally resistant as long-

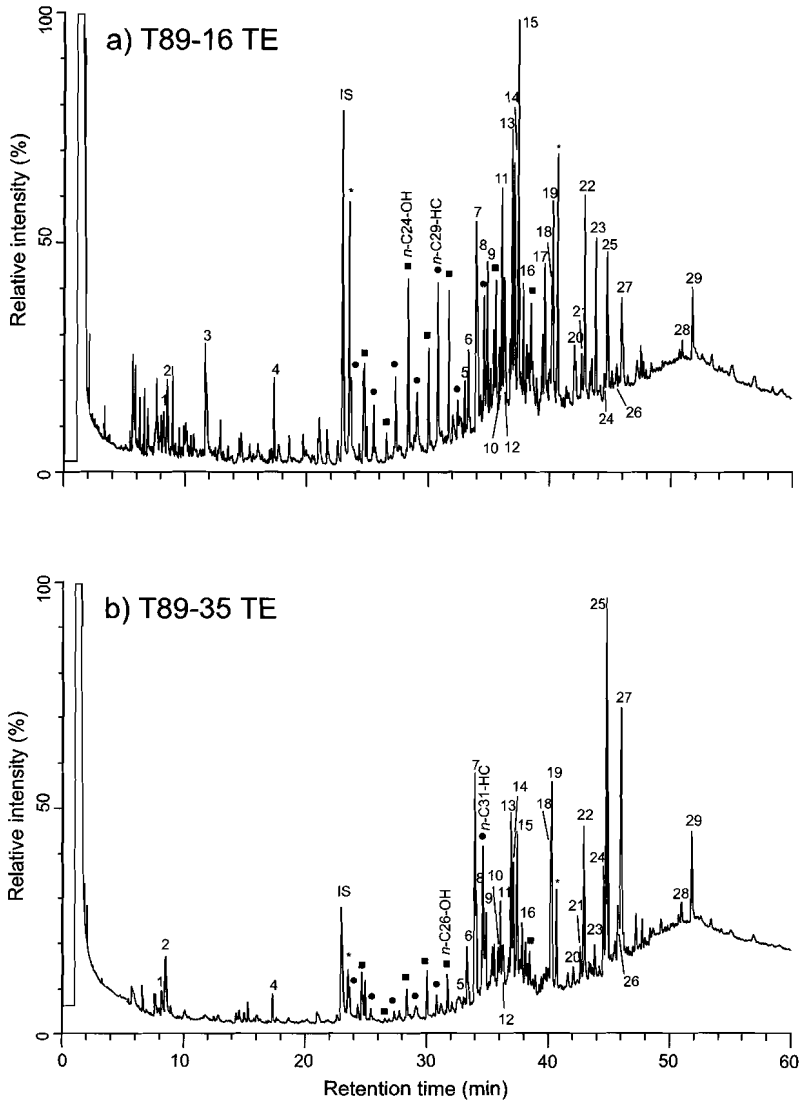

Figure 4.3: GC-FID traces of total lipid extracts of surface samples a) T89-16 and b) T89-35. Numbers indicate compound identifications as listed in Table 4.2, IS = internal standard, * = contamination, black squares = *n*-alkanols, black dots = *n*-alkanes.

chain diols, and with steroid compounds as least stable against oxic degradation (Hoefs et al., 2002; Sinninghe Damsté et al., 2002b). If the differences in preservation potential would determine the spatial distribution of the TOC-normalised lipid biomarker concentrations, we would expect a grouping resulting from PCA, which resembles the different stability of the compound classes. This is not the case, as will be seen in section 4.4.5. Only the compounds ascribed to an input of terrigenous plant waxes, long-chain *n*-alkanes, fatty acids and *n*-alkanols, are statistically grouped. This, however, can be explained by their common terrestrial origin and transport

mechanism and does not necessarily relate to a similar preservation potential. We, thus, conclude that differential oxic degradation efficiencies play only a minor role in the spatial distributions of the TOC-normalised lipid concentrations. For surface sediments that accumulated under anoxic conditions, on the other hand, the TOC-normalised concentrations might be affected by less degradation of labile organic matter. TOC normalisation does not compensate for this effect. Comparison of oxic samples with those deposited under anoxic conditions might thus not be applicable, as will be discussed later (section 4.4.5.2.).

Table 4.2: Lipid compounds identified in GC-FID and GC-MS traces.

Number	Compound
1	*Iso*-loliolide
2	Loliolide
3	*n*-Hexadecanoic acid
4	*n*-Octadecanoic acid
5	Cholesta-5,22-diene-3β-ol (Δ22-cholesterol)
6	5α-Cholest-22-ene-3β-ol
7	Cholest-5-ene-3β-ol (cholesterol)
8	5α-Cholestan-3β-ol
9	24-Methylcholesta-5,22-diene-3β-ol (diatomsterol)
10	24-Methylcholesta-5,24(28)-dien-3β-ol (fucosterol)
11	24-Methylcholest-5-ene-3β-ol
12	Taraxer-14-en-3β-ol (taraxerol)
13	24-Ethylcholest-5-ene-3β-ol (β-sitosterol)
14	24-Ethyl-5α-cholestan-3β-ol
15	4α,23,24-Trimethylcholest-22-en-3β-ol (dinosterol)
16	Octacosane-1,14-diol
17	Hopan-22-ol (diplopterol)
18	*n*-Triacontan-1-ol-x-one; x = 13, 15
19	Triacosane-1,x-diol; x = 13, 14, 15
20	17β,21β(H)-h*omo*-hopan-31-ol
21	*n*-Dotriacontan-1-ol-x-one; x = 13, 15
22	Dotriacontane-1,15-diol
23	17β,21β(H)-d*ihomo*-hopan-32-ol
24	$C_{37:3}$ methyl ketone
25	$C_{37:2}$ methyl ketone
26	$C_{38:3}$ methyl + ethyl ketones
27	$C_{38:2}$ methyl + ethyl ketones
28	C_{40} dicyclic biphytanediol
29	C_{40} tricyclic biphytanediol

Normalising biomarker concentrations to TOC has the disadvantage that TOC can be derived from various potential sources, i.e., marine and terrestrial. A marine-derived lipid biomarker normalised to TOC shows a change in its relative contribution, when solely the terrestrial component of TOC changes. A significant contribution of terrestrial organic carbon, however, can only be detected in the vicinity of the Congo River mouth, i.e., where the $\delta^{13}C_{org}$ values are low. Significant changes of the distribution patterns caused by the normalisation method, either on TOC or on marine OC, will thus mainly affect lipid biomarker concentrations that are related to the freshwater outflow of the Congo River, but not of terrestrial origin. As will be seen later (section 4.4.5.1.), only one group of lipid biomarkers is affected by the kind of normalisation.

4.4.4. Biomarker sources and distributions

4.4.4.1. Alkenones

C_{37} long-chain alkenones occur ubiquitously and are sometimes the most abundant biomarker compounds (Fig. 4.3b). They are exclusively biosynthesised by some Haptophyte algae, the most prominent are *Emiliania huxleyi* and *Gephyrocapsa spp.* (Marlowe et al., 1984; Volkman et al., 1995; Volkman et al., 1980), and occur widespread in marine sediments, including the South Atlantic (Brassell et al., 1986a). Changes in coccolithophore assemblage composition seem not to affect the alkenone production pattern (Müller et al., 1997). Sedimentary alkenone concentrations have been used as an indicator for marine primary productivity (Hinrichs et al., 1999; Schubert et al., 1998; Villanueva et al., 1998). The spatial distribution of the C_{37} alkenones (Fig. 4.4a) shows elevated concentrations in two distinct areas north and south of the Congo River mouth with higher concentrations in the more southern area. Both of these areas are constrained by two or three data points. The concentrations of C_{37} alkenones reach a maximum off the coast at Cape Frio at 18°S.

The ratio of the di- to the sum of the di- and tri-unsaturated C_{37} alkenones, the U^K_{37}'-index is used as a sea-surface temperature estimate (Brassell, 1993; Müller et al., 1998). The reconstruction of the SST field in the southeastern Atlantic via the U^K_{37}'-index agrees quite well with the modern spatial SST distribution (Fig. 4.1c; Levitus and Boyer, 1994). The lowest SST estimate was detected in the centre of the Benguela upwelling region and the highest estimate in the sample nearest to the equator (Fig. 4.4b). Alkenone-derived SST estimates are inferred not to be significantly affected by diagenetic processes when oxygen exposure time is not extensive (Sinninghe Damsté et al., 2002b). Assuming a dry bulk density of 0.5 g/cm^3, all 1.5-cm thick surface-sediment layers would have maximum oxygen exposure times <3500 years, assuming that pore water oxygen is not depleted in the uppermost 1.5 cm, which is true for most of the samples (A.J. van Bennekom, unpublished results). For the great majority of the sample locations, oxygen exposure times are even <1000 years. The investigated samples cover a large range of MAR (Table 4.1, Fig. 4.1d). These large differences, however, apparently do not significantly influence the SST estimates, as seen in the good agreement with the modern observed SST field. This calculation also indicates i) that our sample density is sufficient to reconstruct the modern SST distribution and ii) the samples represent the mean late Holocene values. We presume this to be valid also for other lipid biomarkers.

4.4.4.2. Sterols

The occurrence of C_{28} 24-methylcholesta-5,22-dien-3β-ol (diatomsterol) in sediments was long thought to be characteristic for a lipid contribution from diatoms (Patterson, 1987; Volkman, 1986), but in a survey of 14 marine diatom species, it was only found to be a minor constituent in three species (Barrett et al., 1995). It was, however, also detected in cultures of dinoflagellates (Goad and Whithers, 1982; Teshima et al., 1980) and Haptophyte algae (Marlowe et al., 1984; Volkman et al., 1998) and, in the water column, after massive blooms of *Emiliania huxleyi* (Conte et al., 1995). It has been inferred that Haptophyte algae are the more likely source of 24-methylcholesta-5,22-dien-3β-ol in sediments underlying oligotrophic, non-upwelling waters (Volkman, 1986). Diatomsterol is a minor compound in our sample set (Fig. 4.3a, 4.3b) and has its highest TOC-normalised abundance in a zone around 10°E about 150 to 200 km to the west or southwest from the Congo River mouth (Fig.

4.4c). Elevated concentrations are found also off the Angolan coast and off Cape Frio, although not as high as off the Congo River mouth.

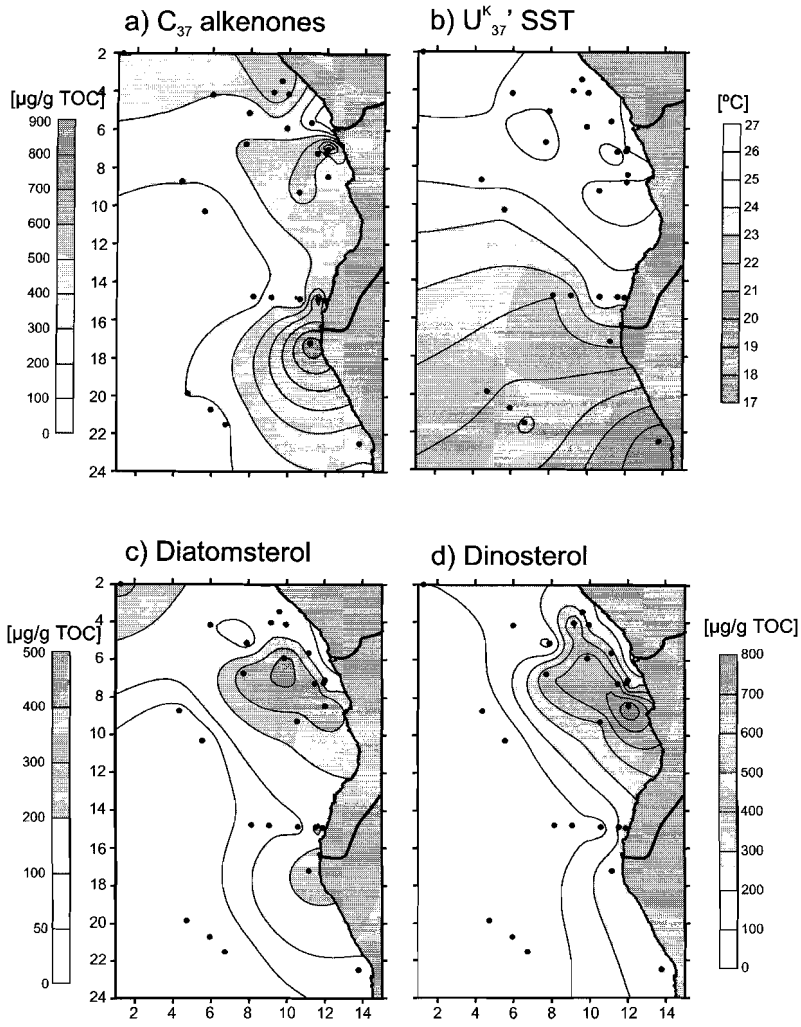

Figure 4.4: Spatial distribution of a) the sum of the C_{37} alkenones, b) the sea-surface temperature (SST) estimates. The spatial distribution of the TOC-normalised concentrations of c) diatomsterol and d) dinosterol.

Cholesta-5-en-3β-ol (cholesterol) occurs in high amounts in the investigated samples (Fig. 4.3a, 4.3b) and is derived from a variety of planktonic organisms, including dinoflagellates, diatoms and haptophyte algae (Volkman, 1986). It has been found to be a common sterol in diatoms, although most species do not contain large amounts (Volkman, 1986). Zooplankton was found to be a major source of cholesterol in the Peru upwelling system through dietary alteration of phytosterols (Volkman et al., 1987). A more non-specific origin must therefore be favoured. Its spatial distribution pattern (not shown) closely resembles that of 24-methylcholesta-5,22-

dien-3β-ol (diatomsterol) with maximum concentration shifted slightly southwards towards the Angolan coast.

Cholesta-5,22-dien-3β-ol is not a common sterol in unicellular algae, as well as in the investigated sediments. It occurs in some pennate diatom species (Barrett et al., 1995; Volkman, 1986; Volkman et al., 1980), but has also been reported from dinoflagellates and red algae (Beastall et al., 1974). It has been inferred that its occurrence in phytoplankton samples is most likely related to the presence of diatoms (Volkman, 1986), while significant amounts in sediments are more likely derived from zooplankton faeces (Gagosian et al., 1983). Its spatial distribution pattern (not shown) closely resembles that of 24-methylcholesta-5,22-dien-3β-ol (diatomsterol).

24-Methylcholesta-5,24(28)-dien-3β-ol (fucosterol) was found to be the major sterol compound in many diatom species (Patterson, 1991), appearing to be more prevalent in centric species (Barrett et al., 1995; Patterson, 1991; Volkman, 1986). It has been suggested that this sterol could be more indicative for a lipid contribution from diatoms than 24-methylcholesta-5,22-dien-3β-ol (Volkman et al., 1998). The spatial distribution of its TOC-normalised concentrations (not shown) is very similar to that of the C_{37} alkenones (Fig. 4.4a), with the difference, that maximum abundance is centred in the area south of the Congo River mouth. Its concentrations in the surface samples are, however, smaller than those of the C_{37} alkenones (Fig. 4.3a, 4.3b; Table 4.3).

24-Ethylcholest-5-en-3β-ol (β-sitosterol) is one of the major sterols found in terrestrial higher plants (Goad and Goodwin, 1972; Huang and Meinschen, 1976) and often one of the major peaks in the GC-traces of the investigated samples (Fig. 4.3a, 4.3b). Its occurrence in high productive oceanic settings, however, is often attributed to a contribution by non-specific planktonic sources (Volkman, 1986). The compound has been reported from diatoms, green algae and cyanobacteria (Barrett et al., 1995; Volkman, 1986) and is thus not necessarily indicative for a terrestrial input. The distribution of the TOC-normalised β-sitosterol concentration (not shown) shows a broad maximum off the Congo River and slightly elevated concentrations off Cape Frio. It thus resembles the distribution pattern of diatomsterol (Fig. 4.4c). The question, in how far the compound is indicative for a terrigenous input will be addressed later.

4α,23,24-Trimethylcholest-22-en-3β-ol (dinosterol) is almost uniquely produced by dinoflagellates (Boon et al., 1979; Robinson et al., 1984), with minor quantities also occurring in diatoms (Volkman et al., 1993). Some dinoflagellate species, however, do not contain this sterol (Goad and Withers, 1982). It occurs as a major compound in all surface sediments (Fig. 4.3a, 4.3b). Its spatial distribution pattern (Fig. 4.4d) is similar to that of diatomsterol, but with its maximum occurrence located more towards the coast.

4.4.4.3. Diols

The major source of long-chain saturated 1,13-, 1,14- and 1,15-C_{28} to C_{32} alkyl diols are probably yellow-green microalgae of the class *Eustigmatophyceae* (Volkman et al., 1992, 1999), but other microalgal species may also be a source (Volkman et al., 1992). Alkyl diols have been reported from sediments from various areas (de Leeuw et al., 1981; Versteegh et al., 1997). The distribution of the C_{28}-C_{32} alkyl diols (not shown) closely resembles that of diatomsterol (Fig. 4.4c), with a broad maximum off the Congo River centred at about 10°E.

Two C_{40} cyclic biphytanediols were identified in the surface sediment as the C_{40} dicyclic and tricyclic biphytanediol (Schouten et al., 1998). These compounds are

known from sediments in different regions, the Indian Ocean, Arabian Sea, Angola Basin, Walvis Bay, and Madeira Abyssal Plain (Schouten et al., 1998; Schouten et al., 2000a). From its structural similarities with sedimentary C_{40} ether-bound biphytanes, it was proposed that biphytanediols are biosynthesised by marine archaea (Hoefs et al., 1997; Schouten et al., 1998). Their high abundance in water-column particulates from the Black Sea and the Cariaco Basin (Hoefs et al., 1997) indicates that they are already produced in the water column. The carbon skeleton structure of the sedimentary $C_{40:3}$ biphytanediol differs from that of thermophilic archaea (Schouten et al., 1998). Therefore, it is assumed that these compounds derive from non-thermophilic planktonic archaea (Hoefs et al., 1997) that are possibly associated with low-oxygen conditions (Hoefs et al., 1997). Analyses of the structurally-related intact tetraether membrane lipids revealed evidence for widespread occurrence of the marine non-thermophilic archaea (Schouten et al., 2000b). Depth distributions in particulate material indicate that the marine archaea are not restricted to the photic zone and are probably facultative anaerobes (Sinninghe Damsté et al., 2002a). The TOC-normalised biphytanediol concentrations in the investigated surface sediments (Fig. 4.5a) are high along the coast. Their absolute maximum is, however, not found in the centre of the Benguela upwelling region, but north of it, in the region influenced by seasonal upwelling.

4.4.4.4. Loliolide and *iso*-loliolide

Loliolide and *iso*-loliolide are end products of anaerobic degradation of some carotenoids, like fucoxanthin (Klok et al., 1984; Repeta, 1989). Fucoxanthin is the major carotenoid in diatoms and haptophytes. Loliolide and *iso*-loliolide have been reported from sediments receiving abundant marine phytoplankton biomass, like the Mediterranean sapropels (ten Haven et al., 1987a), the Namibian (Klok et al., 1984), and the Peruvian shelf (Repeta, 1989). The potential of loliolide as productivity indicator was pointed out by Hinrichs et al. (1999), based on its correlation with gross productivity estimates in sediments from the Angola Basin. This correlation can be confirmed by comparison of the spatial distribution of the TOC-normalised loliolide concentrations (Fig. 4.5b) with that of the TOC (Fig. 4.2a) and marine OC contents (Fig. 4.2c). Loliolide shows its highest abundance values in the centre of the Benguela upwelling region and elevated concentrations all along the coast with a slight offshore extension off the Congo River mouth. Whether loliolide concentrations are potentially indicative for gross productivity will be discussed later.

4.4.4.5. Terrestrial biomarkers

Homologous series of long-chain *n*-alkanes, *n*-alkanols and fatty acids are typical terrigenous lipids found in marine sediments (Bird et al., 1995; Huang et al., 2000; Kuypers et al., 1999; Poynter et al., 1989). These lipids are abundant constituents of terrestrial higher plant epicuticular waxes (Eglinton and Hamilton, 1963), occurring as protective coating on leaves and stems. Leaf waxes of terrestrial higher plants contain predominantly odd-numbered *n*-alkanes and even-numbered *n*-alkanols and fatty acids (Eglinton and Hamilton, 1963; Kolattukudy, 1980; Mazurek and Simoneit, 1984; Tulloch, 1976). The odd-number predominance of the *n*-alkanes is expressed as Carbon Preference Index ($CPI = \frac{1}{2}\Sigma(X_i+X_{i+2}+..+X_n)/\Sigma(X_{i-1}+X_{i+1}+..+X_{n-1}) + \frac{1}{2}\Sigma(X_i+X_{i+2}+..+X_n)/\Sigma(X_{i+1}+X_{i+3}+..+X_{n+1})$; Kolattukudy, 1976). Higher plant waxes generally have high (>5) CPI values (Eglinton and Hamilton, 1963; Mazurek and Simoneit, 1984). Petroleum- or marine-derived *n*-alkanes longer than C_{23}, on the other

Table 4.3: Lipid biomarker concentrations normalised to TOC (in µg compound per g TOC).

Sample	Diatomsterol	Dinosterol	ΣC_{28}-C_{32} diols	Cholesterol	Δ22-cholesterol	β-Sitosterol
T89-10	330	99	170	570	50	610
T89-11	100	130	260	110	41	390
T89-12	53	51	130	160	22	260
T89-13	180	550	390	170	49	460
T89-14	200	270	270	220	33	260
T89-15	100	240	240	98	21	320
T89-16	150	330	85	130	25	210
T89-17	380	500	360	250	73	910
T89-19	450	580	380	270	110	950
T89-20	350	550	540	360	160	660
T89-21	95	180	93	69	19	100
T89-22	170	320	120	120	85	300
T89-23	410	830	450	220	69	380
T89-25	240	390	620	460	62	1000
T89-28	n.d.	n.d.	200	52	n.d.	78
T89-30	69	31	270	90	6.8	190
T89-31	90	95	190	100	15	370
T89-32	72	61	320	63	7.4	220
T89-33	230	230	350	490	68	590
T89-34	130	220	150	92	20	200
T89-35	280	290	190	300	47	230
T89-36	75	270	44	43	18	110
T89-40	n.d.	n.d.	n.d.	9.8	n.d.	15
T89-41	13	n.d.	2.2	24	9.5	52
T89-42	n.d.	n.d.	32	71	n.d.	160
T89-47	30	14	43	92	5.9	530
Anker 24	51	11	41	45	8.5	250
Anker 26	n.d.	n.d.	4.7	20	17	96

Note: Lipids in T89-24 could not be quantified due to standard loss.

Table 4.4: *n*-Alkane data, concentrations in µg/g TOC, $\delta^{13}C$ values in ‰ vs. PDB.

Sample	ΣC_{25}-C_{35} odd *n*-alkanes	CPI *n*-alkanes	$\delta^{13}C_{24}$ (‰)	$\delta^{13}C_{29}$ (‰)	$\delta^{13}C_{31}$ (‰)
T89-10	550	2.44	-27.4	-28.6	-27.6
T89-11	800	3.04	-25.5	-30.2	-26.7
T89-12	600	3.02	-29.9	-29.2	-26.7
T89-13	650	3.86	-27.6	-29.6	-27.3
T89-14	230	4.44	n.d.	-30.1	-29.5
T89-15	440	3.85	-28.3	-29.6	-28.9
T89-16	330	3.35	-29.2	-32.1	-31.7
T89-17	1100	3.11	-28.5	-29.5	-26.9
T89-19	2000	3.74	-25.8	-33.4	-32.1
T89-21	250	4.29	n.d.	-31.3	-30.5
T89-22	940	3.15	-28.5	-31.2	-35.7
T89-23	190	4.26	n.d.	-29.9	-29.6
T89-24	-	2.49	-25.8	-29.7	-30.0
T89-25	1000	2.82	-26.3	-29.6	-27.4
T89-28	640	4.30	-29.4	-26.8	-25.5
T89-30	560	4.04	-28.0	-26.5	-25.8
T89-31	710	5.40	-29.3	-27.8	-26.3
T89-33	1600	3.89	-25.1	-28.4	-26.8
T89-35	190	5.38	-24.7	-26.5	-25.0
T89-36	44	5.33	n.d.	-26.5	-24.3
T89-40	400	1.40	-21.5	-23.1	-27.6
T89-47	730	3.34	-27.3	-27.5	-25.1
Anker 24	850	6.44	-30.1	-35.1	-36.0
Anker 26	180	2.27	-27.0	-29.2	-34.6

Note: Apolar fractions of T89-20, -32, -34, -41, -42 were contaminated and not measured.

Table 4.3 continued: Lipid biomarker concentrations (in µg per g TOC).

Sample	Fucosterol	C_{37} alkenones	Loliolide	LCOH	LCFA	Biphyt.
T89-10	230	410	18	48	76	n.d.
T89-11	87	300	47	170	300	n.d.
T89-12	73	190	33	130	80	n.d.
T89-13	110	500	150	310	n.d.	42
T89-14	110	490	100	240	170	47
T89-15	180	410	130	270	240	51
T89-16	150	100	100	260	87	40
T89-17	330	330	120	290	230	n.d.
T89-19	330	260	170	2300	1500	40
T89-20	160	500	130	630	n.d.	40
T89-21	78	290	47	140	130	53
T89-22	1300	850	230	250	800	93
T89-23	290	370	170	310	230	110
T89-25	210	430	92	360	n.d.	n.d.
T89-28	64	120	7.1	82	22	10
T89-30	49	150	13	130	n.d.	27
T89-31	84	280	38	210	n.d.	45
T89-32	n.d.	180	35	280	n.d.	19
T89-33	170	670	200	820	470	110
T89-34	51	280	120	280	n.d.	44
T89-35	170	900	270	160	n.d.	200
T89-36	73	320	1200	24	180	140
T89-40	n.d.	190	58	9.9	n.d.	20
T89-41	14	170	13	6.1	38	28
T89-42	160	200	3.7	34	32	34
T89-47	670	210	7.6	33	96	38
Anker 24	35	n.d.	6.2	710	76	n.d.
Anker 26	81	n.d.	13	28	59	n.d.

LCOH: C_{24}+C_{26}+C_{28} *n*-alkanols, LCFA: C_{24}+C_{26}+C_{28} fatty acids, Biphyt.: C_{40} biphytanediols.

Table 4.4 continued: Fossil-fuel correction and calculation of C_4 %.

Sample	$\delta^{13}C_{29}$ corrected (‰)	$\delta^{13}C_{31}$ corrected (‰)	$\delta^{13}C_{WM(29,31)}$ (‰)	C_4 % *n*-alkanes
T89-10	-28.9	-27.6	-28.3	53
T89-11	-30.8	-26.9	-29.0	48
T89-12	-29.1	-26.1	-27.7	57
T89-13	-29.8	-27.2	-28.6	51
T89-14	-30.1	-29.5	-29.8	43
T89-15	-29.7	-29.0	-29.3	46
T89-16	-32.4	-32.1	-32.3	26
T89-17	-29.7	-26.5	-28.3	53
T89-19	-33.4	-32.6	-33.1	20
T89-21	-31.3	-30.5	-31.0	35
T89-22	-31.6	-37.3	-34.3	12
T89-23	-29.9	-29.6	-29.8	43
T89-24	-30.5	-31.5	-30.9	35
T89-25	-30.2	-27.7	-29.1	48
T89-28	-26.6	-25.4	-25.9	70
T89-30	-26.3	-25.7	-26.0	69
T89-31	-27.7	-26.3	-26.9	63
T89-33	-29.7	-27.2	-28.3	53
T89-35	-26.7	-25.0	-25.6	72
T89-36	-26.5	-24.3	-25.0	76
T89-40	-24.3	-29.5	-27.3	60
T89-47	-27.5	-24.9	-26.1	68
Anker 24	-34.9	-36.2	-35.4	4
Anker 26	-29.7	-37.5	-33.2	19

$\delta^{13}C$ values were corrected for fossil fuel contribution (see text for details).

hand, have essentially no odd-over-even carbon-number predominance. They generally have a CPI of unity and show a smooth distribution (Simoneit, 1984). Alkane distributions, therefore, enable the recognition to what degree terrigenous plant-wax contributions or other sources, either marine alkanes or contamination, influence the sedimentary alkanes. The CPI of the long-chain *n*-alkanes in the investigated surface sediments from the South Atlantic is, with a single exception, between 2 and 7. Its spatial distribution (not shown) reveals elevated CPI values along the coast. Maximum values are found off Namibia, indicating that the purest plant-wax material is found at the sites of strong wind-driven upwelling and, therefore, suggesting a predominant eolian supply. The distribution of the CPI agrees therefore with that of the TOC values or that of the SST estimates. The generally elevated CPI values indicate that the majority of the long-chain *n*-alkanes are derived from terrestrial sources.

Plant waxes can be washed off the leaf surface by rain and are expected to be transported into the ocean by freshwater runoff (Bird et al., 1995). However, the wax particles are also easily sloughed off the surface of the leaves by wind and can become airborne (Simoneit et al., 1977). Alternatively, decaying plant organic matter in soils can be lifted during dust storms and combustion (bush fires) or washed away after heavy rainfall. Plant-wax lipids are found in aerosol samples from remote ocean areas, i.e., the North Pacific (Gagosian and Peltzer, 1986; Gagosian et al., 1981), the South Pacific (Gagosian et al., 1987), the western South Atlantic (Simoneit et al., 1991), and the eastern Atlantic (Cox et al., 1982; Lepple and Brine, 1976; Schefuß et al., re-submitted; Simoneit, 1977; Simoneit et al., 1977; Simoneit et al., 1988). The spatial distribution of the long-chain odd-numbered *n*-alkanes resembles a broad plume, connected to the grass savannah along the Angolan coast (Fig. 4.5c) and stretching out into the South Atlantic below the main trade-wind trajectory. This distribution strongly suggests that most of the plant wax-derived compounds were not transported by river runoff, but via eolian transport. A small secondary maximum, off the Congo River, is much more reflected in the distributions of the long-chain even-numbered fatty acids and *n*-alkanols than in that of the *n*-alkanes, indicating a relatively higher contribution of these more polar lipids by the freshwater outflow of the Congo River. The spatial distribution of the plant-wax lipids thus closely resembles the distribution of opal phytoliths in surface sediments of the Congo fan (Jansen et al., 1989).

Compound-specific carbon isotope analyses of leaf-wax lipids can provide information on the carbon-fixation pathway utilized during photosynthesis (Collister et al., 1994; O'Leary, 1981; Rieley et al., 1993). *n*-Alkanes from plants using the Calvin-Benson cycle (C_3 plants) have $\delta^{13}C$ values around -36 ‰ (-31 to -39 ‰ vs. PDB), while plants utilising the Hatch-Slack (or dicarboxylic acid) cycle (C_4 plants) fractionate less against $^{13}CO_2$ of air and have $\delta^{13}C$ values around -21.5 ‰ (-18 to -25 ‰ vs. PDB; Collister et al., 1994; O'Leary, 1981; Rieley et al., 1993). Virtually all trees, most shrubs, and cool-season grasses and sedges use the C_3 photosynthetic pathway, while C_4 plant photosynthesis is found in warm-season grasses, warm-season sedges, *Amaranthaceae* and *Chenopodiaceae* (Cerling et al., 1993). C_4 plants are thus predominantly found in tropical savannahs, temperate grasslands and semi-deserts (Cerling et al., 1993). Most African grasslands, like the Sahel and the grass savannahs, are presently dominated by C_4 plant vegetation (Collatz et al., 1998). In marine sediments, the stable carbon isotope composition of *n*-alkanes has been used to determine the contributions by C_3 and C_4 plant type organic material (Bird et al., 1995; Huang et al., 2000; Kuypers et al., 1999). Compound-specific stable carbon isotopic analyses of *n*-alkanes in dust collected over the eastern Atlantic has shown,

that the eolian-transported *n*-alkanes are almost exclusively derived from the contemporary vegetation on the continent (Schefuß et al., re-submitted). The spatial distribution of the C_4 plant-derived percentage shows a clear pattern (Fig. 4.5d) of predominant C_3 plant-derived *n*-alkanes offshore the Congo River mouth. Here, the distribution of the stable carbon isotope compositions of the *n*-alkanes resembles those of the bulk organic matter (Fig. 4.2b). Plant-wax *n*-alkanes at the remaining sample locations mainly carry a C_4 plant signature. The gross amount of the long-

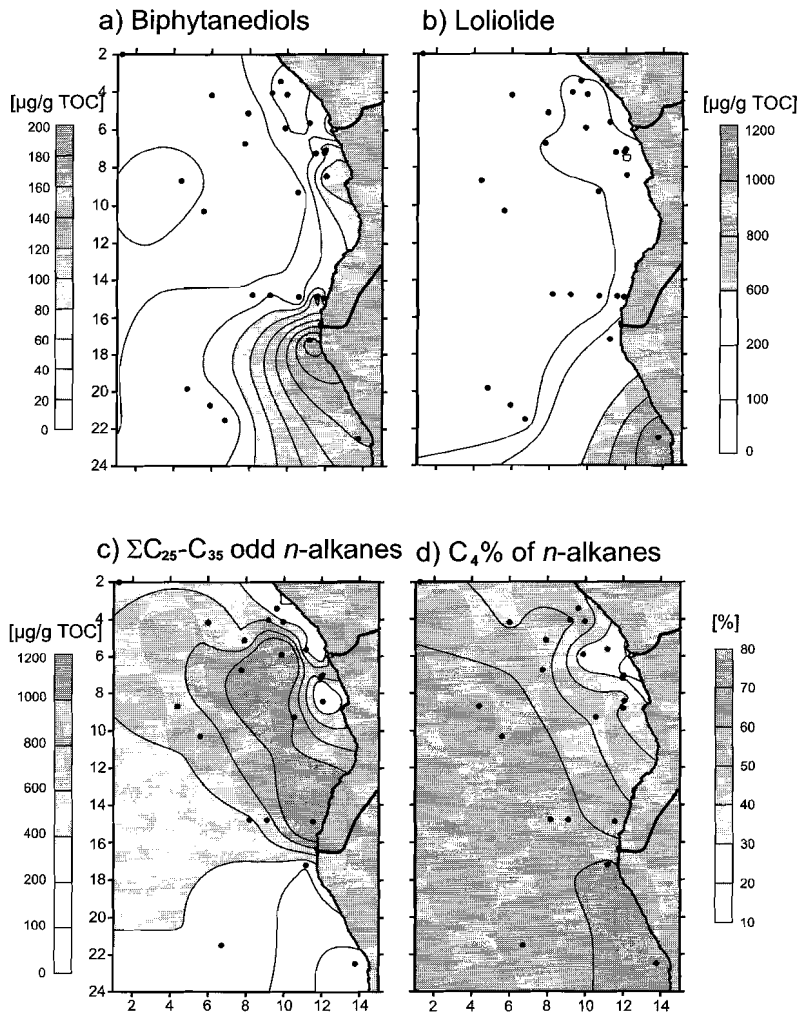

Figure 4.5: Spatial distributions the TOC-normalised concentrations of a) the C_{40} biphytanediols, b) loliolide, c) the sum of the C_{25} to C_{35} odd-numbered *n*-alkanes, and d) the C_4 plant-derived percentage of the *n*-alkanes.

chain *n*-alkanes thus has a stable carbon isotope signature that indicates a >50 % C_4 plant origin (compare Fig. 4.5c and 4.5d). This strongly supports the Angolan and Namibian grass savannahs as a source area from where the overwhelming portion of

the plant-wax lipids are transported by wind. By comparison with the distribution of the bulk $\delta^{13}C_{org}$ values (Fig. 4.2b), we infer, that there is apparently no significant influence of C_4 plant-derived bulk organic matter, which should resemble the spatial distribution of the long-chain *n*-alkane concentrations. We therefore conclude that our assumption of a binary-mixing model for the bulk organic matter with a terrestrial C_3 plant and a marine end-member is valid and that an additional source of C_4 plant-derived terrestrial bulk organic matter is not required. However, there is a contribution of C_4 plant-derived *n*-alkanes to the sediments, but its influence on bulk organic stable carbon isotope compositions is insignificant because they represent only a very small fraction of the total organic matter. We infer that the *n*-alkanes, which are most likely eolian-transported and not river-supplied, are not accompanied with a contribution of C_4 plant-derived macro-molecular organic matter.

4.4.5. PCA: Controls and processes

We performed principal component analysis (PCA) to identify groups of the bulk and molecular geochemical parameters with a similar spatial distribution. Based on these groups we identified common processes, which presumably control these distributions. As the data input for the PCA we used the absolute portions of marine-derived (Fig. 4.2c) and terrestrial-derived OC content (Fig. 4.2d), the TOC-normalised biomarker concentrations, and the MAR, $\delta^{13}C_{org}$ values, CPI and C_4 plant-derived percentage of the long-chain *n*-alkanes, and SST estimates (Table 4.1 and 4.4). The PCA (Table 4.5) reveals five dominant factors (groups), each with a latent root (eigenvalue) >1, which explain a cumulative 85 % of the total variance. The first three factors each explain about 20 % of the total variance. The fourth and fifth factors explain about 15 % and 10 %, respectively, of the total variance.

4.4.5.1. River-plume production and oceanic upwelling

PCA factor 1 explains about 20 % of the total variance in the data (Table 4.5). Its score shows a broad maximum offshore the Congo River mouth around 10°E, which stretches towards the Angolan coast. Slightly elevated factor-scores are found also off Cape Frio (Fig. 4.6a). All the major sterols, except fucosterol, and the sum of the C_{28}-C_{32} alkyl diols are statistically grouped in this principal component. All these compounds, except perhaps for β-sitosterol, are exclusively derived from marine sources, like diatoms, haptophyte algae, dinoflagellates or zooplankton, grazing on the phytoplankton. To a lesser extent the concentration of the C_{37} alkenones, the SST estimates and also the long-chain *n*-alkanes and *n*-alkanols show a moderate loading on PCA factor 1 (Table 4.5). However, the influence of the land-derived plant-wax compounds, and thus probably also of the terrigenous fraction of β-sitosterol, is apparently of minor importance. Obviously, the distribution patterns of these compounds are most likely the result of productivity of planktonic organisms. Interestingly, the TOC and marine OC contents do not correlate with this PCA factor (Table 4.5). This suggests that the process that determines this PCA factor only influences the composition of the marine planktonic ecosystem without significantly changing the gross productivity. The abundance patterns of the individual lipid concentrations contributing to this factor suggest that these compounds originate from either river-induced mixing of river nutrients with marine nutrients or from wind-driven oceanic upwelling in the region of a shallow thermocline. It is not possible to differentiate between these two sources, because both are separated only in season, but not spatially. The strong southeast trades drive maximum oceanic upwelling

during austral winter, while river runoff is largest during the Southern African monsoon season in austral summer. We suggest, however, that the contribution of diatom-derived lipids is largest during maximum river-induced productivity, sustained by a strong silicate enrichment of surface waters, while the other lipids are mainly produced during the non-monsoon season. The abundance patterns of the lipid biomarkers correlate well to the modern situation, as river-induced phytoplankton productivity is found at some distance from the river mouth and the level of bulk marine productivity in the outer Congo River plume is hardly higher than in the surrounding oceanic waters (Cadée, 1978; Cadée, 1984). On the molecular level, the combined occurrence of 24-methylcholesta-5,22-dien-3β-ol (diatomsterol) and 24-ethylcholest-5-en-3β-ol (β-sitosterol) suggests a large contribution of diatom lipids to the surface sediments. *Chaetoceros sp.* is the dominant diatom in phytoplankton samples (Cadée, 1984) and *Chaetoceros* resting spores are the main sedimentary diatom remains underlying the inner Congo River plume (Jansen and van Iperen, 1991; van Iperen et al., 1987). The sterol distribution of *Chaetoceros sp.* (Volkman, 1986) with β-sitosterol as major and diatomsterol as minor constituent agrees quite well with these findings.

This group of lipid biomarkers, making up this PCA factor, is the only group with distribution patterns that are significantly altered by the normalisation to the marine OC content compared to the TOC values. When normalised to the marine OC content, the maximum concentrations of its biomarkers shift towards the river mouth. The considered compounds, however, are almost certainly not related to terrestrial input, as they only occur in the offshore plume area and almost all of them are exclusively marine. Moreover, the statistical grouping of these compounds is independent of the normalisation method. The compounds group in one PCA factor, even when normalised on the marine OC content and do not mix with parameters that indicate river transport. The spatial distributions of all other PCA factors are not significantly altered on change of the normalisation method.

4.4.5.2. Strong upwelling and anoxia

PCA factor 2, explaining about 22 % of the total variance, consists of the SST estimates (Fig. 4.4b), the TOC-normalised biphytanediol concentration (Fig. 4.5a), the loliolide concentration (Fig. 4.5b), the marine OC content (Fig. 4.3c), the TOC content (Fig. 4.3a), and the CPI of the *n*-alkanes (Fig. 4.5c). It has elevated values along the coast, especially in the southern part. Maximum values are restricted to the centre of the Benguela upwelling area (Fig. 4.6b). This suggests that this PCA factor is determined by upwelling activity causing a large accumulation of marine organic material, dominating the TOC signal, and which is associated with a lowering of the SST. As mentioned above, the high loading of the *n*-alkane CPI in this PCA factor suggests that wind-driven upwelling is connected to the supply of relatively pure plant-wax material. The only biomarker concentrations that correlate with this PCA factor, are the loliolide and the biphytanediol concentrations. We suggest, however, that this does not mean that marine planktonic archaea and fucoxanthin-producing algae are the dominant primary producers in the Benguela upwelling area. Both, loliolide and biphytanediols, are to some extent connected to anoxic conditions. Loliolide and *iso*-loliolide are the degradation products of fucoxanthin under anoxic sedimentary conditions (Klok et al., 1984; Repeta, 1989). The biphytanediols are labile compounds, their occurrence appears to be related to less degradation under anoxic or sub-oxic conditions (Hoefs et al., 1997; Sinninghe Damsté et al., 2002b). We therefore attribute the relatively high abundance of these compounds to anoxic or

low-oxygen conditions in the water column and pore waters of the surface sediment. Loliolide variations were suggested to be indicative of productivity variations from its correlation with TOC-based productivity estimates (Hinrichs et al., 1999). This correlation, however, is indirect. Fucoxanthin is a labile compound and only survives under anoxic bottomwater conditions before it is transferred into loliolide (Repeta, 1989). The low degradation of labile marine organic matter under anoxic conditions thus dilutes all TOC-normalised lipid biomarker concentrations, which explains why none of the marine planktonic biomarkers is detected as primary producer responsible for the enhanced TOC values. It is thus rather unclear from our biomarker data, which phytoplankton group causes the high TOC values. The PCA factor 2 is clearly dominated by the composition of sample T89-36 taken close to the largest and most active upwelling centre, the Lüderitz cell. Upwelling in this area is characterised by year-round very high primary productivity (Berger, 1989; Sackett, 1989; Shannon et al., 1987), and phytoplankton assemblages are generally dominated by diatoms (Shannon and Pillar, 1986). Diatom-derived lipids are, however, not at all represented in this PCA factor. This does, however, not indicate that the statistical analysis, or the TOC normalisation, is not valid or not applicable. It indicates that the comparison of TOC-normalised lipid concentrations only reflects the phytoplankton classes if the preservation/degradation effects on lipids are minor or insignificant.

Table 4.4: Loadings on the five factors explaining a cumulative 85 % of the total variance.

Factor	**1**	**2**	**3**	**4**	**5**
Latent Roots (Eigenvalues)	6.86	4.53	3.08	1.78	1.54
"Variance" Explained by Rotated Components	4.2	4.6	3.7	2.3	3.0
Percent of Total Variance Explained	20.0	22.1	17.6	10.8	14.1
Parameter	**VARIMAX-Rotated Loading Matrix**				
$\Sigma(C_{28}\text{-}C_{32}$ diols)/TOC	**0.875**[1]	-0.123	-0.030	-0.123	0.105
Diatomsterol/TOC	**0.846**	0.036	0.238	0.207	0.225
Cholesterol/TOC	**0.765**	-0.161	-0.217	0.136	0.116
β-Sitosterol/TOC	**0.733**	-0.242	-0.048	-0.047	0.490
Dinosterol/TOC	**0.722**	0.241	0.485	0.173	0.053
Δ22-cholesterol/TOC	**0.695**	-0.022	0.246	0.424	0.486
Loliolide/TOC	-0.052	**0.935**	0.000	0.086	0.096
marine OC (wt%)	-0.094	**0.928**	0.061	-0.103	-0.045
TOC (wt%)	-0.087	**0.917**	0.184	-0.116	-0.062
SST (°C)	0.356	**-0.776**	0.321	0.180	-0.023
Biphytanediols/TOC	0.071	**0.708**	-0.024	0.555	-0.129
n-Alkane CPI	0.086	**0.652**	-0.029	0.084	-0.191
$\delta^{13}C_{org}$ (‰)	-0.065	0.121	**-0.942**	-0.070	-0.130
terrestrial OC (wt%)	0.001	0.363	**0.885**	-0.138	-0.143
MAR (g/cm^2/kyr)	-0.037	0.000	**0.787**	-0.161	0.311
C_4 % of *n*-alkanes	-0.155	0.302	**-0.758**	-0.365	-0.281
C_{37} alkenones/TOC	0.357	0.147	-0.196	**0.841**	-0.060
Fucosterol/TOC	-0.068	-0.179	0.136	**0.781**	0.298
$\Sigma(C_{25}\text{-}C_{35}$ odd *n*-alkanes)/TOC	0.329	-0.297	-0.070	0.033	**0.855**
$\Sigma(C_{24}+C_{26}+C_{28}$ fatty acids)/TOC	0.153	0.053	0.367	0.313	**0.825**
$\Sigma(C_{24}+C_{26}+C_{28}$ *n*-alkanols)/TOC	0.383	0.036	0.315	-0.033	**0.791**

[1] Values >0.65 in bold for comparison.

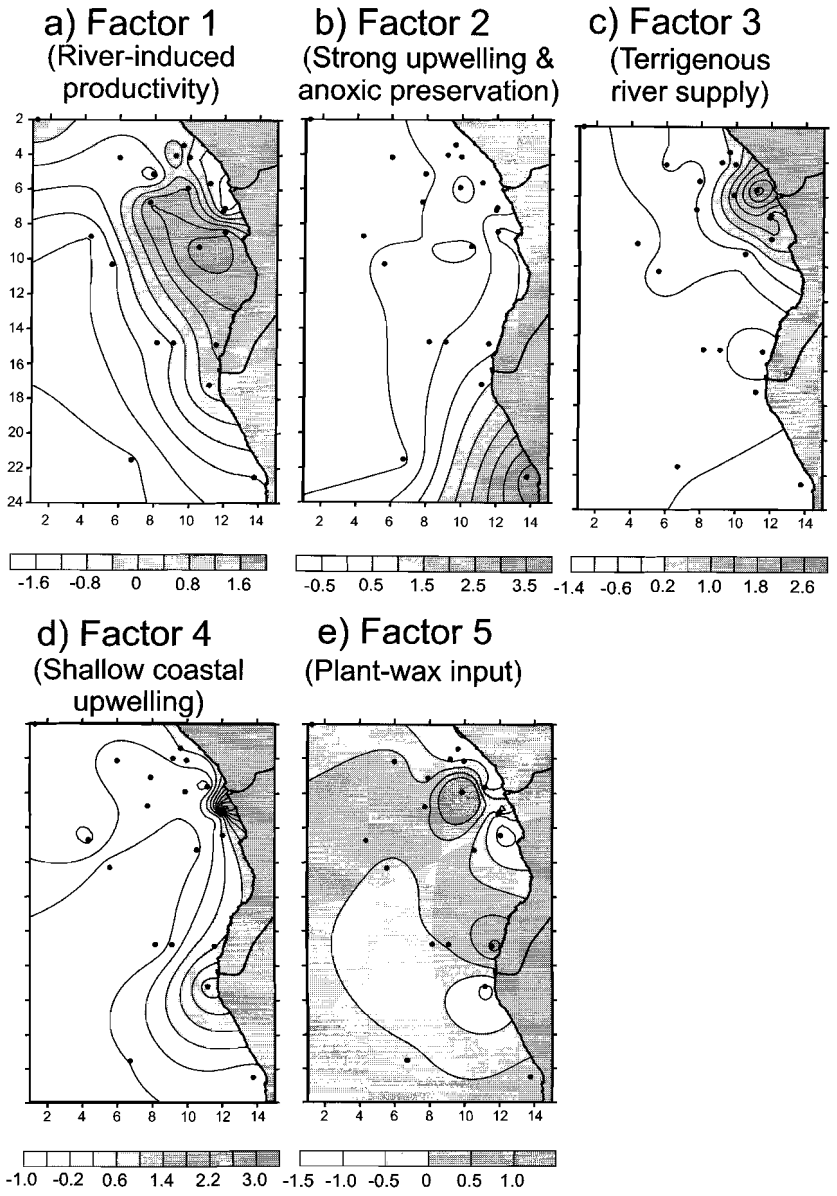

Figure 4.6: Spatial distributions of the factor-scores of each PCA factor with a latent root (eigenvalue) >1.

4.4.5.3. Terrigenous OM river supply

PCA factor 3, which explains about 18 % of the total variance (Table 4.5), is determined by the variations in the stable carbon isotope composition of the bulk organic matter ($\delta^{13}C_{org}$, Fig. 4.3b), the terrigenous OC content (Fig. 4.3d), the MAR (Fig. 4.1d) and the contribution of C_3 plant waxes to the *n*-alkanes, indicated as negative C_4 plant-derived percentage (Fig. 4.5d). The spatial distribution of the factor-

score is dominated by a strong maximum at the Congo River fan (Fig. 4.6c). Apparently, this PCA factor reflects the contribution of organic and inorganic material by the Congo River. The Congo River is thus the only significant source of terrestrial organic material, which influences the stable carbon isotope composition of the bulk organic matter and the plant wax-derived *n*-alkanes with a predominant C_3 plant, i.e., rainforest-, isotopic signature. The Congo supply, however, has only a minor influence on the *n*-alkane concentration, which has a small loading on this factor, in contrast to the moderate contribution by the long-chain *n*-alkanols and fatty acids (Table 4.5). This corroborates once more the validity of the binary mixing model to distinguish between C_3 plant-derived terrestrial and marine organic matter (see section 4.4.4.5.).

4.4.5.4. Coastal shallow upwelling

PCA factor 4, explains about 11 % of the total variance of all the data included in the principal component analysis (Table 4.5). It shows a high score along the coast, mainly south of the Congo River mouth and also offshore Cape Frio (Fig. 4.6d). The only parameters that are significantly associated with PCA factor 4, are the TOC-normalised concentrations of the C_{37} alkenones (Fig. 4.5a) and 24-methylcholesta-5,24(28)-dien-3β-ol (fucosterol). Their spatial distribution patterns remain stable with respect to different ways of normalisation, i.e., on TOC or on marine OC. This indicates that processes connected to the outflow of river-water do not influence their distributions. The C_{37} alkenones and fucosterol are lipid biomarkers unambiguously produced by marine organisms. In combination with their spatial distributions, this suggests that this PCA factor reflects intermediate coastal upwelling. Both north and south of the Congo River mouth small-scale upwelling cells are present. The upwelled waters are derived from a shallow depth-range, thus affecting preferentially the nitrate and phosphate concentrations, but not the silicate concentrations (van Bennekom et al., 1978). Therefore, the small cell north of the Congo River, off Pointe Noire, mainly reflects phytoplankton production of small flagellates with a subordinate role of diatoms (Cadée, 1978). South of the Congo River mouth, the upwelling activity is apparently stronger, or transporting deeper waters to the surface, so primary production levels are relatively elevated and show a more substantial role of diatoms (Chyong, 1971; van Bennekom and Berger, 1984). These findings agree well with the lipid biomarker distributions. The contribution of Haptophyte-derived lipids is high in the northern cell (Fig. 4.4a), while a larger input of diatom lipids is confirmed for the southern cell. The concentrations of the C_{37} alkenones are also slightly correlated with the sterol concentrations, ascribed to the river-induced productivity (see above). In general, however, it can be stated that the phytoplankton associations in the shallow coastal upwelling cells and the river-induced productivity zone are distinguishable by molecular means. The elevated concentrations of the C_{37} alkenones and fucosterol off Cape Frio can be explained by filaments of upwelled waters, displaced by the Benguela Current and the wind to the north and northwest (Lutjeharms and Stokton, 1987), which cause elevated productivity at that location, similar to the findings from the sterols of PCA factor 1.

4.4.5.5. Plant-wax input by dust and river

PCA factor 5 (Table 4.5) explains about 14 % of the total variance in the data. The distribution of the factor-score shows essentially two areas of a high abundance, off Cape Frio and off the Congo River mouth (Fig. 4.6e). This PCA factor is determined by the TOC-normalised concentrations of the long-chain odd-numbered *n*-alkanes and

their even-numbered *n*-alkanol and fatty acid analogues. All these compounds are common constituents of terrestrial higher plant epicuticular waxes (Eglinton and Hamilton, 1963). The co-occurrence of all the detected plant-wax lipids, odd-numbered *n*-alkanes, even-numbered *n*-alkanols and fatty acids, in one PCA factor stresses their common origin. Their distribution is not affected by any change in the normalisation-method. A secondary maximum for PCA factor 5 is detected off the Congo River mouth. As mentioned above, this is due to the moderate loading of the long-chain fatty acids and *n*-alkanols on PCA factor 3, inferred to reflect river-transported terrestrial material (Table 4.5). The distribution of the long-chain odd-numbered *n*-alkanes resembles more a broad plume, connected to the grass savannah along the Angolan coast and stretching out onto the South Atlantic to the northwest (Fig. 4.5b). This suggests, that the plant wax-derived *n*-alkanes are not predominantly river-transported, but eolian-transported along the path of the main trade winds. Moreover, the gross amount of the long-chain *n*-alkanes has a stable carbon isotope signature that indicates a >50 % C_4 plant origin (Fig. 4.5c and 4.5d). This strongly supports the Angolan and Namibian grass savannahs as the suggested source area. Apparently, the overwhelming portion of the plant-wax *n*-alkanes originates from dry areas and is transported by the wind. This pattern closely resembles the distribution of the freshwater diatoms in South Atlantic coretops (Jansen et al., 1989; Pokras and Mix, 1985), inferred to be indicative of eolian dust transport. Satellite images of the atmospheric aerosol contents (e.g., from the SeaWiFS Project) show that dust transport over the eastern South Atlantic occurs mainly during Southern Hemisphere winter (June to August) in a pattern that closely resembles the spatial distribution of the long-chain *n*-alkanes in the surface sediments (Fig. 4.1a).

4.5. Conclusions

- Lipid biomarker concentrations, normalised to total organic carbon content (TOC), reflect the relative contributions of specific compounds or compound classes to the organic matter. The normalisation on TOC largely compensates for the effects of differential oxic degradation of TOC and lipid biomarkers. Principal component analysis separates five main factors that explain a cumulative 85 % of the total variance. These factors indicate similarities in sources, transport pathways or preservation of the biomarker compounds.
- Factor 1 represents marine productivity off the Congo River either induced by outflow of nutrient-rich river waters or by wind-driven oceanic upwelling of nutrients from below a shallow thermocline. Both processes take place in the eastern Angola Basin in the upwelling season (austral winter) or the monsoon season (austral summer). Factor 1 groups diatomsterol, dinosterol, β-sitosterol, cholesterol, Δ22-cholesterol and the C_{28} to C_{32} alkyl diols.
- Factor 2 represents strong upwelling, predominantly influencing the total organic carbon content, the marine-derived organic carbon content, the U^{K}_{37}'-derived sea-surface temperature estimates, and the abundance of loliolide and C_{40} biphytanediols. The preservation of labile organic matter and biomarkers in areas underlying strong upwelling activity is increased by anoxic sedimentary conditions.
- Factor 3 represents river supply of terrigenous material. This factor determines the distribution of the bulk stable carbon isotopic compositions, the terrigenous organic carbon content, the mass accumulation rate and, negatively, the percentage of the C_4 plant-derived *n*-alkanes. The contribution of organic material with a C_3 plant, i.e., rainforest, signature by the Congo River is the main process, which influences the bulk stable carbon isotopic values of the surface sediments.
- Factor 4 represents the coastal upwelling cells north and south of the Congo River mouth, supporting the productivity of Haptophyte algae and diatoms to a different extent as indicated by variable abundance of the C_{37} alkenones and fucosterol. The distributions of compounds produced during coastal upwelling and river-induced productivity depend on the availability of dissolved silicate.
- Factor 5 represents the majority of the terrigenous long-chain *n*-alkanes, derived from epicuticular plant waxes. They carry a C_4 plant isotopic signature and are predominantly eolian transported from the Angolan and Namibian grass savannahs in a NW-directed plume below the trade-wind trajectory.
- Enhanced preservation of labile organic matter under anoxic sedimentary conditions prohibits the comparison with sediments deposited under oxic conditions and the identification of molecular indicators of phytoplankton production. This investigation of spatial distributions of lipid biomarkers in the eastern South Atlantic provides a basis for paleoenvironmental reconstructions in ancient marine sediments.

Acknowledgements

We are grateful to the Captain and crew of the *RV Tyro* for all support during sampling. Gijs Nobbe (University of Utrecht) is thanked for providing the possibility for total organic carbon analyses. Discussions with Johan van Bennekom, Stefan Schouten and Jan W. de Leeuw significantly improved the manuscript.

Chapter 5

Forcing of tropical Atlantic sea-surface temperatures during the Mid-Pleistocene Transition

Enno Schefuß, Jaap S. Sinninghe Damsté, J. H. Fred Jansen

Submitted to *Paleoceanography*

Abstract

A sea-surface temperature (SST) record from the south-eastern tropical Atlantic ODP Site 1077 covering the Mid-Pleistocene Transition (MPT) is compared with the changes in orbital insolation, global ice volume and Atlantic deepwater ventilation. The MPT is the change from an obliquity-dominated to an eccentricity-dominated cyclicity in global ice-volume variations, significantly preceded by an increase of the mean global ice mass. The tropical SSTs did not vary independently from these high-latitude climate changes. The 100-kyr variations increased concurrently in the SST and ice-volume changes at about 650 kyr BP. In both the obliquity and eccentricity cycles, the tropical SST significantly led over the high-latitude ice-volume changes. Such an early response is not detected for SST variations in a transitional 80-kyr cycle, presumably forced by ice-volume changes directly and not preceded by an insolation change. The precessional variability of tropical SST changes seems to be suppressed during times of enlarged global ice volume, possibly due to the increased zonal trade-wind velocity. The long-term development of the tropical SSTs is linked to the strength of North Atlantic Deep-Water (NADW) formation. The increase of global ice volume around 900 kyr BP led to the most severe reductions in NADW formation during the MPT over the last 3 Ma, likely caused by the re-adjustment of the enlarged ice sheets. These reductions initiated a long-term warming of the tropical Atlantic Ocean during the MPT.

5.1. Introduction

5.1.1. The Mid-Pleistocene Transition

The Mid-Pleistocene Transition (MPT) led to the development of the Late Pleistocene ice-ages with an increased mean global ice volume changing in a sawtooth-pattern in near-100-kyr cycles (Mudelsee and Schulz, 1997; Prell, 1982). Records related to ice volume are dominated by 41-kyr variations before the 100-kyr rhythm became dominant (Pisias and Moore, 1981; Ruddiman et al., 1989a; Shackleton and Opdyke, 1976). Time-series analyses of orbitally-tuned $\delta^{18}O$ records of deep-sea carbonates showed that the increase in mean continental ice mass significantly preceded the increase in spectral power of the 100-kyr cycle (Mudelsee and Schulz, 1997). The increase in mean ice mass has been reported to be an abrupt event at 900 kyr BP (Maasch, 1988; Prell, 1982), while later studies favour an increase lasting from about 920 to 900 kyr BP (Berger and Jansen, 1994) or from 942 to 902 kyr BP (Mudelsee and Schulz, 1997), i.e., occurring essentially during marine isotope stage (MIS) 24. It has been suggested that the increase in ice volume was mainly due to the growth of shelf based ice sheets in high-latitude regions (Berger and Jansen, 1994). The change in the frequency domain, the transition from the predominant 41-kyr cycle to the predominant 100-kyr cycle, has also been considered both gradual and abrupt. A gradual increase in power of the 100-kyr cycle was favoured by Ruddiman et al. (1989) and Berger and Jansen (1994). They placed it between 900 and 400 kyr BP, with the strongest change occurring between 700 and 600 kyr BP. Park and Maasch (1993) concluded that the transition occurred gradually between 1000 and 500 kyr BP. Bolton et al. (1995) inferred a stepwise transition with strongest changes around 750 kyr BP. An abrupt increase in power of the 100-kyr cycle, on the other hand, was placed at 900 kyr BP (Pisias and Moore, 1981), at 700 kyr BP (Lau and Weng, 1995), and at 641 kyr BP (Mudelsee and Schulz, 1997). In either way, it is generally agreed that the increase of mean global ice mass significantly preceded the full establishment of the 100-kyr cycle in ice-volume variations.

5.1.2. Deepwater linkage

It has been suggested that the MPT was connected to a perturbation of the global thermohaline circulation (THC). Calculation of Atlantic-Pacific $\delta^{13}C$ gradients of deep-sea carbonate showed that North Atlantic Deep-Water (NADW) formation was severely weakened during the Mid-Pleistocene relatively to the early and late Pleistocene (Raymo et al., 1997; Raymo et al., 1990). Reduced bottomwater ventilation led to more corrosive bottomwaters and therefore decreased the carbonate accumulation rates in the deep South Atlantic (Schmieder et al., 2000). These authors also suggested that the lag between ice-volume increase and onset of 100-kyr cyclicity may reflect an 'interim state' of the THC at the onset of the Late Pleistocene ice-age cycles. The nature of this transitional state remained, however, unexplained.

5.1.3. Surface-ocean & terrestrial linkage

Reduced NADW formation is expected to decrease the northward heat export from the South Atlantic, and to accumulate heat in the tropical Atlantic surface waters (Crowley, 1992). This process has been inferred from climate models (Manabe and Stouffer, 1988) and detected for short-term Late Pleistocene climate variations

(Crowley, 1992; Rühlemann et al., 1999). Warming of the tropical Atlantic, in turn, should influence the influx of moist air into equatorial Africa, either via the land-sea temperature gradient (de Menocal and Rind, 1993; Druyan, 1989; Lough, 1986; Mulitza and Rühlemann, 2000) or by influencing the tropical precipitation-evaporation balance (Ganopolski et al., 1998). A terrestrial vegetation change in tropical areas associated with an increase in global aridity has indeed been suggested for the MPT (Raymo et al., 1997). Pollen records from tropical mountain ecosystems (Hooghiemstra et al., 1993) and from equatorial Africa (Dupont et al., 2001) have confirmed a shift to more arid conditions. Tropical sea-surface temperatures therefore link the development of high-latitude continental ice volume to the terrestrial aridity in the tropics.

5.1.4. Scope

Although the most striking feature of the Mid-Pleistocene Transition is the growth of additional ice mass in the Northern Hemisphere (Berger and Jansen, 1994), the transition had important climatic connections on the global scale. To examine the effect of the main climatic forcing mechanisms during the MPT on the low-latitudes, we developed a SST record of the tropical Atlantic Ocean (ODP Site 1077) from 1250 to 450 kyr BP. This record is compared with the history of continental ice volume, orbital insolation changes and variations in Atlantic deepwater ventilation. The development of the SST during the MPT is complex and can only be explained by the interference of the various controlling factors. We show that a prominent long-term surface-water warming took place in the tropical Atlantic Ocean that is linked to the strong reduction of the THC during the MPT.

5.1.5. Current and paleoceanographic setting

The modern surface and shallow subsurface circulation in the Angola Basin consists of a cyclonic gyre circulation (Fig. 5.1) connected to the tropical Atlantic warm pool. Warm tropical waters flow eastward in the South Equatorial Counter Current (SECC) and feed the Angola Current (AC) flowing southwards along the African margin. Between 14°S to 17°S its tropical warm waters converge with the northward-flowing cold Benguela Current (BC), establishing the Angola-Benguela Front (ABF). The Benguela Current is deflected to the northwest and becomes part of the South Equatorial Current (SEC) directing to the equator. The surface circulation of the Angola Basin is overprinted by the influence of the Congo (Zaire) River, the World's second largest river with an average annual freshwater discharge of 1.3 x 10^{12} m^3/yr (van Bennekom and Berger, 1984). Its low-salinity plume can be detected as far as 800 km offshore (van Bennekom and Berger, 1984). The seasonal variation in discharge is associated with the monsoonal circulation and precipitation (Eisma and van Bennekom, 1978; van Bennekom and Berger, 1984). During austral summer (December to February) the Intertropical Convergence Zone (ITCZ) is in its southernmost position (5°-10°N), causing maximum monsoon conditions in southern equatorial Africa with a large influx of moisture-laden air and high precipitation (Hsü and Wallace, 1976). The maximum extension of the Congo River plume occurs in February-March, later than the maximum discharge in December (van Bennekom and Berger, 1984) and is associated with the highest annual sea-surface temperatures (SST) in the equatorial Atlantic (Katz and Garzoli, 1982). The outflow of Congo

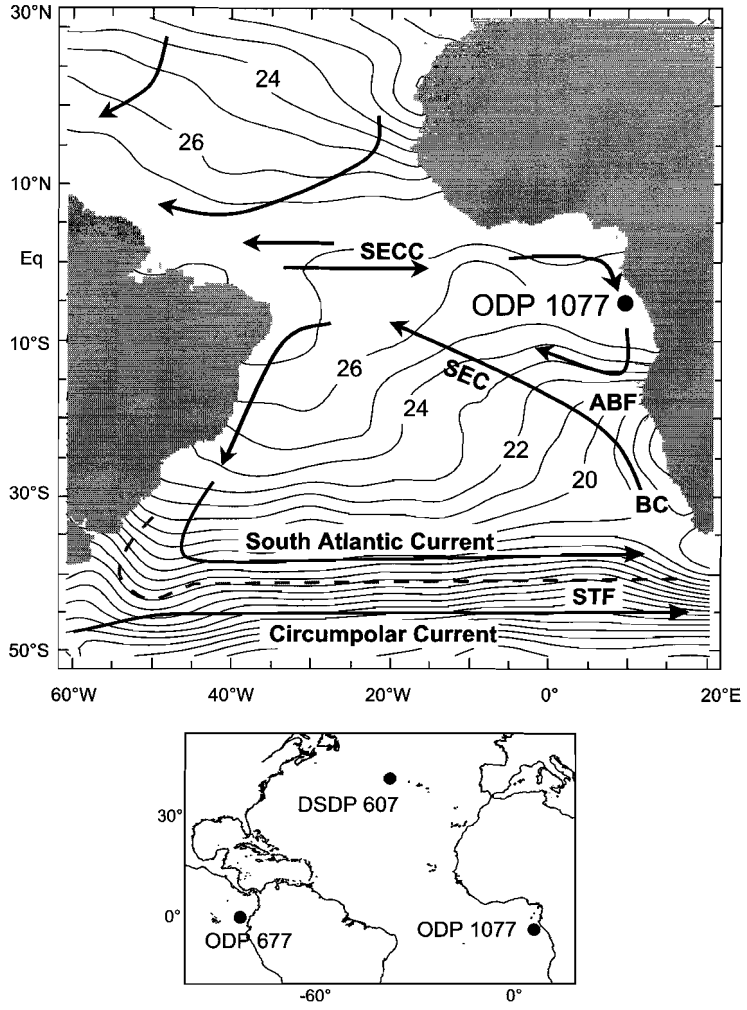

Figure 5.1: Map showing the location of ODP Site 1077 in the Angola Basin and surface and shallow subsurface currents in the South Atlantic Ocean. BC = Benguela Current, SEC = South Equatorial Current, SECC = South Equatorial Countercurrent, ABF = Angola-Benguela Front, STF = subtropical front. The thin lines are isotherms of modern annual mean SST (Levitus and Boyer, 1994). The small map shows the locations of the other sites, DSDP 607 (North Atlantic) and ODP 677 (Panama Basin).

River water in the narrow estuary is rapid and causes river-induced upwelling by the entrainment of subsurface oceanic nutrients (Eisma and van Bennekom, 1978; van Bennekom et al., 1978). During austral winter (June to August), the ITCZ is furthest north (~20°N) and strong Southern Hemisphere trade winds cause oceanic upwelling by surface divergence in the equatorial Atlantic Ocean (Philander and Pacanowski, 1986). The upwelling intensity correlates to the zonal velocity of the southern trades (Philander and Pacanowski, 1986). SSTs in the eastern equatorial Atlantic are at their annual minimum, while surface-water productivity reaches its annual maximum (Katz and Garzoli, 1982). Offshore oceanic upwelling outside the Congo River plume

induces moderate to high primary productivity (Berger, 1989). Coastal upwelling in the Angola Basin is restricted to two small areas south and north of the mouth of the Congo River.

A comparison of two Late Quaternary sedimentary records, one located at the lower Congo fan and one off the coast of Angola, showed that the Congo freshwater outflow, in contrast to other major river systems, had only a minor effect on the planktonic foraminiferal $\delta^{18}O$ values (Schneider et al., 1994) and on alkenone-SST variations (Schneider et al., 1995). The two SST records co-vary strongly and exhibit the same range, about 21-27°C, during the Late Quaternary (Schneider et al., 1995). The minor SST differences between these two cores have been explained by latitudinal movements of the Angola-Benguela Front over the southern core location (Jansen et al., 1996). The two SST records also closely resemble the SST estimates from sites located below the South Equatorial Countercurrent (SECC), derived by a transfer function technique using planktonic foraminiferal assemblages (Mix et al., 1986; Schneider et al., 1995). Consequently, the SST variations in the Angola Basin and off the Congo River were considered to generally follow the SST development in the eastern equatorial Atlantic.

The Late Quaternary alkenone-SST changes in the Angola Basin were dominated by periods of 100- and 23-kyrs, while variance in the 41-kyr cycle was absent (Schneider et al., 1995, 1996, 1999), similarly to the results obtained from the eastern equatorial Atlantic (McIntyre et al., 1989; Mix et al., 1986). These SST changes were attributed to variations in wind-forced upwelling intensity and advection of cold Benguela Current waters from southern high latitudes to the tropical Atlantic (Jansen et al., 1996), relating to the zonality and intensity of the south-easterly trade-wind system. The pronounced 23-kyr cycle observed in Late Quaternary SST records from the eastern equatorial Atlantic has been attributed to the influence of the African monsoon. When boreal summer insolation is at its maximum, North African monsoon is strongest. The austral trade winds are then deflected northwards, suppressing the upwelling intensity in the eastern equatorial Atlantic in the precessional cycle (McIntyre et al., 1989). The eastern equatorial Atlantic SST changes slightly lag the Southern Hemisphere SST, but significantly lead over the high-latitude Northern Hemisphere SST and ice volume (McIntyre et al., 1989; Schneider et al., 1996). In the eccentricity cycle, the Late Quaternary tropical Atlantic and Angola Basin SST changes also have been found to significantly lead over the sea-level movements and melting of continental ice sheets (Schneider et al., 1996, 1999). It has been suggested that the early tropical warming was caused by i) enhanced subsurface return flow of warm tropical waters with the SECC into the Angola Basin or ii) heat storage in the tropical oceans due to reduced cross-equatorial heat transport during peak glacial times (Schneider et al., 1996). The sole occurrence of the 100- and 23-kyr cycles, and absence of the 41-kyr period, in SST records of the tropical Atlantic, combined with the early warming preceding ice-volume change, led to the suggestion that tropical SST variations are a direct response to low-latitude insolation forcing and independent of high-latitude climate changes (Schneider et al., 1999). An active role of the tropics as amplifier of climate change by exporting this signal to higher latitudes has therefore been proposed (Schneider et al., 1999). The establishment of a tropical SST record extending far beyond the 100-kyr dominance in high-latitude climate forcing enables us to test these hypotheses.

5.2. Material and Methods

The samples for this study were acquired from the Ocean Drilling Program (ODP) Site 1077 (Fig. 5.1). The uppermost sample investigated is 175-1077-B-8-H-1-17 cm, in 62.77 meters below sea floor (mbsf) and the lowermost sample is 175-1077-B-17-H-6-33 cm, in 155.93 mbsf. The core is located at 10°26.2'E, 5°10.8'S, in 2382 m water depth about 275 km off the mouth of the Congo River (Wefer et al., 1998). The sedimentation rates are high, around 12 cm/kyr, and quite constant as a result of a sustained supply of fine, suspended material from the river and the high productive overlying waters (Berger et al., 1998; Dupont et al., 2001; Jansen et al., 1984).

5.2.1. SST estimates

SST estimates were determined with the alkenone-unsaturation method (Brassell et al., 1986a). About 5 to 10 g of freeze-dried and ground sediments were ultrasonically extracted using 40 ml of methanol (MeOH), 40 ml of dichloromethane (DCM):MeOH (1:1, v/v), and 40 ml of DCM, each for 5 min. For each sample, the extracts were combined and rotary-evaporated to near-dryness at 35°C. Salts were removed by washing with double-distilled H_2O in a separatory funnel and lipids were extracted with DCM. The desalted lipid extracts were again rotary-evaporated and methylated with diazomethane after drying over anhydrous Na_2SO_4. Before silylation with bis(trimethyl-silyl)trifluoro-acetamide in pyridine (1 hr at 60°C), very polar compounds were removed on a silica-gel column eluted with ethyl acetate. For gas chromatographic analyses extracts were concentrated to about 1 mg/ml. Capillary gas chromatography was performed using a Hewlett Packard 5890 series II chromatograph equipped with an on-column injector and fitted with a fused-silica capillary column (25 m x 0.32 mm) coated with CP Sil 5 (film thickness 0.12 μm). helium was used as carrier gas, and the oven was programmed from 70°C to 130°C at 20°C/min, followed by a heating of 4°C/min to 320°C (10 min holding time). Components were detected using a flame ionisation detector (FID). Compound identification and purity was checked on randomly selected samples with GC-mass spectrometry (GC-MS). GC-MS was performed using the same type of gas chromatograph and the conditions described above. The chromatographic column of the GC was directly inserted into the electron impact ion source of a VG Autospec Ultima mass spectrometer, operated with an ionisation energy of 70 eV and scanning over a mass range of *m/z* 50-800 with a cycle time of 1.8 seconds. Compound identifications were based on comparison of relative GC retention times and mass spectra published in the literature (de Leeuw et al., 1980).

For SST estimation, we used the simplified unsaturation index of the C_{37} alkenones (U^K_{37}'; Prahl and Wakeham, 1987), calculated from the peak areas of the di- and triunsaturated C_{37} alkenones in FID chromatograms. The conversion of U^K_{37}' values to sea-surface temperature estimates was done using the global calibration by Müller et al. (1998), based on an extensive set of core-tops. This equation: SST (°C) = (U^K_{37}' - 0.044) / 0.033 is identical to a calibration derived from Haptophyte laboratory cultures (Prahl et al., 1988). The standard error of estimate of this relationship is ±1.0°C. The standard deviation (±σ) based on duplicate and triplicate analyses of the SST estimates of our samples is 0.3°C (or 0.01 U^K_{37}' units). An extensive study of Müller et al. (1998) showed that the alkenone-derived SST estimates generally reflect the annual mean mixed-layer temperatures. This is corroborated by data from surface sediments off Congo and Angola analysed by Schneider et al. (1995) that are in

excellent agreement with the mean annual SST values given by Levitus and Boyer (1994). Changes of alkenone-producing haptophyte species assemblages, growth rates and nutrient availability have shown not to exert a significant effect on U^{K}_{37}' values (Müller et al., 1997). The high sedimentation rates of the sediments result in a rapid removal of the alkenones from the zone of oxic porewaters, causing short oxygen-exposure times (OET), unlikely to cause significant diagenetic alteration of the alkenone-derived SST estimates (Sinninghe Damsté et al., 2002b).

5.2.2. Spectral analyses

Records of orbital variance, Atlantic deepwater ventilation and global ice volume are used for comparison with the SST record to identify forcing factors and phase relations. For this purpose, we have calculated an artificial record of orbital variance, ETP, containing equal power in all orbital frequencies, i.e., eccentricity (E), obliquity (T) and precession (P), based on the values by Berger and Loutre (1991) and using the calculation-method described in Imbrie et al. (1984). It is considered the forcing function for orbital insolation changes. High values indicate maximum interglacial forcing. Spectral analyses of the proxy records were carried out with the SPECTRUM program (Schulz and Statteger, 1997) using a Siegel-test to identify significant periodic variations. The level of significance was kept at 0.05, the oversampling-factor was set to 4, and the high frequency-factor set to 1 in the calculations. Cross-spectral analyses between the signals sharing significant variance in similar frequencies were performed to reveal whether the detected cycles are coherent and to detect their phase relations. The phase angles are given as lag. The level of significance for the cross-spectral analyses was 0.1, other parameters were the same as in the power spectra calculations. A Welch-window and 2 segments with 50 % overlap were used. Gaussian filtering of the records has been performed to investigate changes in the amplitude of the 41- and 100-kyr cycles and to isolate the long-term trend of each of the time-series. The bandwidths of the filters had been adjusted to solely pass the period under consideration and to suppress other orbital frequencies. The filters used were a 41-kyr filter with a central frequency of 0.0244 and a bandwidth of 0.003 cycles/kyr. The 100-kyr filter has a central frequency of 0.0103 and a bandwidth of 0.002 cycles/kyr. The long-term filter has a central frequency of 0.004 and a bandwidth of 0.004 cycles/kyr. The used filter characteristics are slightly modified after Ruddiman et al. (1989).

5.3. Results & Discussion

5.3.1. Age model

The stratigraphy of ODP Site 1077 was initially based on orbital tuning of the magnetic susceptibility record of the neighbouring Site 1075 and correlation to Site 1077 (Berger et al., 1998; Wefer et al., 1998). This age model was largely confirmed by an oxygen-isotope record using planktonic foraminifera (only *Globigerinoides ruber* (pink) was consistently present) and correlation to the benthic oxygen isotope record of the eastern Pacific ODP Site 677 (Fig. 5.2a; Dupont et al., 2001; Shackleton et al., 1990). The oxygen-isotope variations of *G. ruber* have been shown to be an useful stratigraphic tool off the Congo River (Schneider et al., 1994, 1995, 1996). The $\delta^{18}O$ record of benthic foraminifera at ODP Site 677 (01°12'N, 83°44'W, Panama Basin; Shackleton et al., 1990) is used as the age-model reference for all records considered in this study (Fig. 5.2a). It has a sufficiently high temporal resolution (average sample spacing = 2.7 kyr) across the MPT and was therefore chosen as an

equivalent to the Late Pleistocene SPECMAP ice-volume stack (Imbrie et al., 1989). The oxygen isotope curve from Site 1077, however, shows gaps for MIS 13, MIS 25-28 and MIS 36 (Fig. 5.2a). Based on this stratigraphy, the samples cover the time interval from MIS 12 to 37 (from 457 to 1250 kyr BP). The ages for all 214 samples were determined by linear interpolation between the tie points using the revised composite depth scale (Jansen and Dupont, 2001). The average time resolution of the SST record is 3.9 kyr.

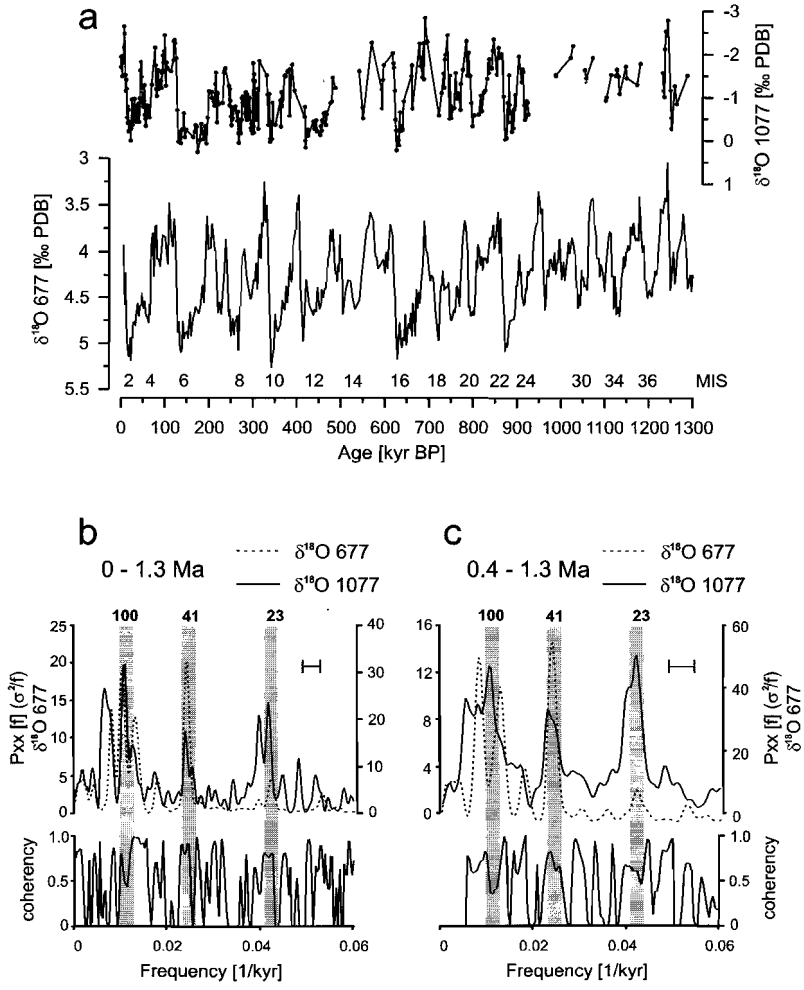

Figure 5.2: a) Oxygen isotope stratigraphy of Ocean Drilling Program (ODP) Site 1077 (above) based on *Globigerinoides ruber* (pink) and of benthic foraminifera from ODP Site 677 (below). b) Results of cross-spectral analyses between the $\delta^{18}O$ record of benthic foraminifera at Site 677 and the oxygen isotope record from Site 1077 for the last 1300 kyr. Horizontal bar is 6 dB bandwidth. Autospectra of each record above and coherency between records in each orbital frequency (shaded) below. c) Same as in b), but restricted to the period from 400 to 1300 kyr BP.

To investigate the accuracy of the age model we conducted cross-spectral analyses between the oxygen isotope records of Site 1077 and Site 677. The results show that the foraminiferal isotope records exhibit similar periodic variations (Fig. 5.2b) in the eccentricity- and obliquity-band. The higher precessional variance in the Site 1077 $\delta^{18}O$ record can be explained by the use of a planktonic foraminiferal species, which records a precessional signal in the low-latitudes. The $\delta^{18}O$ variations of ODP Site 1077 is in all main Milankovitch bands (1/100, 1/41, 1/23 1/kyr) highly coherent (Table 5.1) and in phase with the variations of the $\delta^{18}O$ record of ODP Site 677 in the eccentricity and obliquity cycle. The phasing in the precessional band might as well be induced by the interference with the planktonic low-latitude signal recorded at ODP Site 1077. This calculation confirms the general accuracy of the age model for the last 1.3 Ma. For the more detailed phase-investigations in the considered period of 400 to 1300 kyr BP we performed a cross-spectral analysis between the oxygen isotope records of Site 1077 and Site 677 restricted to this time interval. The autospectra of the $\delta^{18}O$ records differ somewhat from each other (Fig. 5.2c) and from the spectra over the last 1.3 Ma (Fig. 5.2b). The Site 677 $\delta^{18}O$ record contains no spectral variance centred on the 100-kyr cycle, which was not present before 641 kyr BP (Mudelsee and Schulz, 1997). Instead, a high spectral power is detected for a 78-kyr cycle, reported to be present in several benthic $\delta^{18}O$ records from the mid-Pleistocene (Mudelsee and Schulz, 1997). The power spectrum of the Site 1077 planktonic $\delta^{18}O$ record from the mid-Pleistocene contains, as in the last 1.3 Ma, a large precessional variance, which is not present in the benthic $\delta^{18}O$ record. Since precessional variations in the low-latitudes are amplitude-modulated by the eccentricity, it is most likely, that also the 100-kyr cycle detected in the $\delta^{18}O$ record of Site 1077 in the mid-Pleistocene resulted from the low-latitude influence on the isotopic variations of the planktonic foraminifera. In the mid-Pleistocene, the two isotope records are coherent in the eccentricity- and obliquity-band (Table 5.2), while coherency is low for the precessional cycle. The mid-Pleistocene oxygen-isotope variations in the main Milankovitch cycles are in phase within errors (Table 5.2). Due to the weak coherency in the precessional band in the mid-Pleistocene, however, we decided not to conduct statistical phase determinations in that cycle.

Table 5.1: Results of cross-spectral analyses between the benthic foraminiferal $\delta^{18}O$ record of ODP 677 (Shackleton et al., 1990) and $\delta^{18}O$ record of *G. ruber* in ODP 1077 (Dupont et al., 2001) for the last 1300 kyr.

$\delta^{18}O$ 677 vs. $\delta^{18}O$ 1077	Coherency k	Phase, deg.	Lag, kyr
1/100 1/kyr	0.81	-6 ± 25	-1.7 ± 6.9
1/41 1/kyr	0.93	1 ± 14	0.1 ± 1.6
1/23 1/kyr	0.79	-27 ± 26	-1.7 ± 1.7

Table 5.2: Same as in Table 5.1, but restricted to the period from 400 to 1300 kyr BP.

$\delta^{18}O$ 677 vs. $\delta^{18}O$ 1077	Coherency k	Phase, deg.	Lag, kyr
1/100 1/kyr	0.80	16 ± 26	4.4 ± 7.2
1/41 1/kyr	0.82	4 ± 24	0.5 ± 2.7
1/23 1/kyr	0.60	-29 ± 42	-1.9 ± 2.7

Non-zero coherency k_0 is 0.96 for all cycles. A negative lag denotes lead.

5.3.2. Tropical Atlantic SST during the MPT

A large temperature range, between 19.5 to 27.6°C, was detected for the ODP Site 1077 SST record for the Mid-Pleistocene in the tropical South Atlantic Angola Basin (Fig. 5.3a), the total SST amplitude being thus about 8°C. SSTs are generally lower in glacial stages than during interglacials. The largest absolute temperature change, a warming of 5.8°C, occurred during deglaciation of MIS 22. About 2°C higher SSTs than the modern annual mean SST, of 25.8°C (Fig. 5.1), occurred during MIS 15, while the lowest SST occurred during MIS 12, 6°C lower than the modern annual mean SST. Remarkably, the SST development does not follow the sawtooth-like pattern observed in the record of the benthic oxygen isotopes of Site 677 (Fig. 5.3c); the glacials show relatively short-lived and sharp drops in SST. From 1250 kyr BP (MIS 37) to about 930 kyr BP (MIS 25), a slight long-term decline in SST is detected. Only during MIS 30, at 1050 kyr BP, lower SSTs prevailed for about 10 kyr. During MIS 24 and 22, at 925 and at 860 kyr BP respectively, SSTs as low as those during the last glacial maximum, ca. 21°C (Schneider et al., 1995) were reached. SST remained generally low until the end of MIS 22 (at about 860 kyr BP), with a short warming during MIS 23. After MIS 22, a long-term increase in SST is observed, mainly caused by higher glacial minimum SSTs. This warming trend ends with a strong glacial cooling at the end of MIS 16, at about 640 kyr BP. The following glacial MIS 14 and 12 show a reversed trend to subsequently lower minimum SST.

5.3.3. $\delta^{18}O$ record of ice volume during the MPT

The Pacific ODP 677 benthic $\delta^{18}O$ record (Fig. 5.3c) serves as the age model template and also as the proxy record for the global ice volume (Shackleton, 1987) in the mid-Pleistocene. It differs significantly from the SST record at Site 1077 in the tropical Atlantic (Fig. 5.3a). There is no or only a slight increase in average ice volume from MIS 37 to MIS 24. The first high $\delta^{18}O$ values were abruptly reached during MIS 22, so after the main drop in SST during MIS 24. Afterwards, the glacial $\delta^{18}O$ values tend to be higher, the highest values occurring at the end of MIS 16. The shift to generally enriched $\delta^{18}O$ values can be detected during MIS 22. From MIS 24 onward, a sawtooth-pattern is observed in the $\delta^{18}O$ record, most clearly expressed in the glacial MIS 24, 20, 16 and 12. From MIS 22 to MIS 16, however, a long-term reversal as detected in the SST record, is not observed. This indicates that the long-term warming of the tropical Atlantic surface ocean was not accompanied by a long-term decrease in global ice volume.

5.3.4. $\delta^{13}C$ record of Atlantic deepwater ventilation

The $\delta^{13}C$ record of carbonate tests of the benthic foraminifer *C. wuellerstorfi* at DSDP Site 607 (North Atlantic) is used as a proxy for the extent of deep-water ventilation of the Atlantic Ocean (Fig. 5.3d; Raymo et al., 1997; Ruddiman et al., 1989a; Wara et al., 2000). The record displays the $\delta^{13}C$ composition of dissolved inorganic carbon ($\delta^{13}C_{DIC}$) that is primarily determined by the proportions of NADW (North Atlantic Deep-Water) and AABW (Antarctic Bottom Water) at this site. The mixture of AABW from the south, having relatively low $\delta^{13}C_{DIC}$ values, and NADW from the north, with relatively high $\delta^{13}C_{DIC}$ values, determines the $\delta^{13}C_{DIC}$ and thus

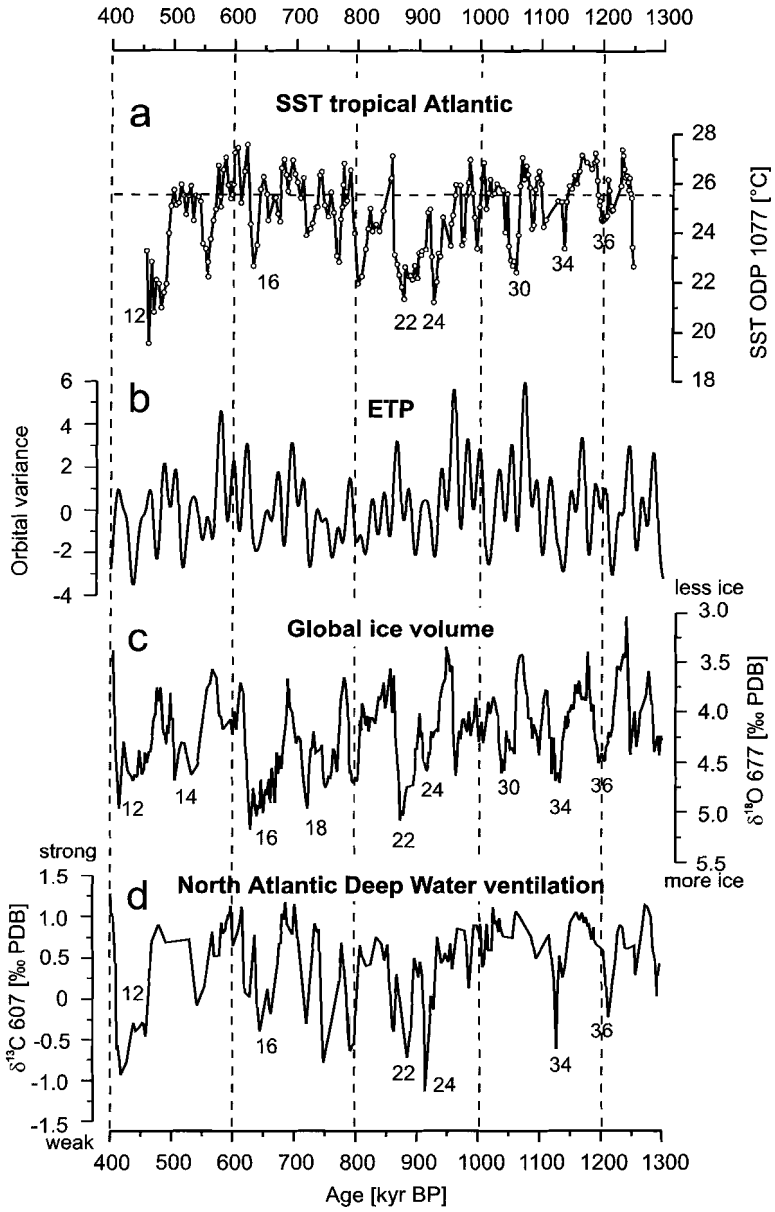

Figure 5.3: The investigated records for the Mid-Pleistocene Transition, a) the Site 1077 SST record, b) the calculated ETP record of orbital variance as summed-unit variance (Berger and Loutre, 1991; Imbrie et al., 1984), c) the Site 677 benthic $\delta^{18}O$ record for global ice volume (note axis orientation; Shackleton et al., 1990), and d) the Site 607 benthic $\delta^{13}C$ record for North Atlantic Deep-Water (NADW) ventilation (Raymo et al., 1997; Ruddiman et al., 1989a). The horizontal broken line in a) is the modern annual mean SST at the location of core ODP 1077 (Levitus and Boyer, 1994). Numbers indicate marine isotope stages (MIS).

the $\delta^{13}C$ of benthic foraminifera at this site (Kroopnick, 1985; Ruddiman et al., 1989a). It is therefore implicitly assumed that any changes in preformed $\delta^{13}C_{DIC}$ of NADW and changes in the mean ocean $\delta^{13}C_{DIC}$ were small relative to the variations caused by deepwater circulation changes. The original stratigraphy of DSDP Site 607 (Ruddiman et al., 1989a) was adjusted to the stratigraphy of ODP Site 677 by Raymo et al. (1997). The Site 607 $\delta^{13}C$ record of benthic foraminifera (Fig. 5.3d) shows a distinct development during the MPT. The values are relatively stable from MIS 37 to MIS 25, with minor brief excursions to more depleted values. At MIS 24 a major decrease in $\delta^{13}C$ occurred, the most pronounced decrease in $\delta^{13}C$ since 3 Ma BP (Raymo et al., 1997). From this time on, the $\delta^{13}C$ values are relatively depleted during each glacial stage, but subsequently become more enriched until MIS 14. At the end of MIS 12, again very low $\delta^{13}C$ values were detected. In the Late Pleistocene, similar low values were only observed for meltwater events during deglaciations, but they never again became as low as during MIS 24 (Raymo et al., 1997).

5.3.5. Power spectra

The spectral analysis of the SST record reveals the strongest power in a 450-kyr cycle (Fig. 5.4a). Clearly, the length of the SST record, about 800 kyr, is not long enough to reliably attribute a 450-kyr cycle to orbital forcing, but, obviously, this long cyclicity reflects the long-term trend in the SST record. An 80-kyr cyclicity contains the second most power in the SST record. Some spectral power also occurs in a 41-kyr cycle. The artificial ETP record is calculated to contain equal power in all orbital bands (Fig. 5.4b). The Pacific (ODP Site 677) benthic $\delta^{18}O$ record for the Mid-Pleistocene period contains dominant power in the 100-kyr cycle (Fig. 5.4c). Also the 41-kyr cycle is strongly present. Remarkably, a 76-kyr cycle is present in this record, possibly related to the 80-kyr cycle found in the 1077 SST record. Besides, 23- and 19-kyr cycles are present. In the power spectrum of the North Atlantic (DSDP Site 607) benthic $\delta^{13}C$ record (Fig. 5.4d) most power could be detected in the 100-kyr cycle. Again, a long-term cyclicity with a 450-kyr period is detected. The power spectrum of the $\delta^{13}C$ record also shows periods of 70, 41, 31, 27 and 23 kyrs.

5.3.6. Precession

In the power spectrum of the ODP Site 1077 SST record (Fig. 5.4a) no significant power in the precessional band (23-kyr period) can be detected. Visual inspection of the record (Fig. 5.3a), however, reveals some high-frequency variations, most probably related to precessional cycles. From the investigation on the accuracy of the age model we inferred that it is not justified to address the phasing in the precessional band. It is, however, possible to investigate the amplitude variations of the precessional cycles by filtering. Gaussian-filtering of the 1077 SST record for the 23-kyr period (Fig 5) shows that the amplitude of the precessional SST variations has varied significantly. Large variations occurred from 1100 to 900 kyrs BP and from 650 to 600 kyrs BP. By comparison with the calculated variations of the orbital precession index (Fig. 5.5; Berger and Loutre, 1991), it appears that the precession and the 23-kyr SST variations were in anti-phase when the 23-kyr SST amplitudes were high. When both records were not in anti-phase the precessional SST amplitudes appeared to be low. The alternating phase relation explains the absence of a 23-kyr peak in the SST power spectrum (Fig. 5.4a).

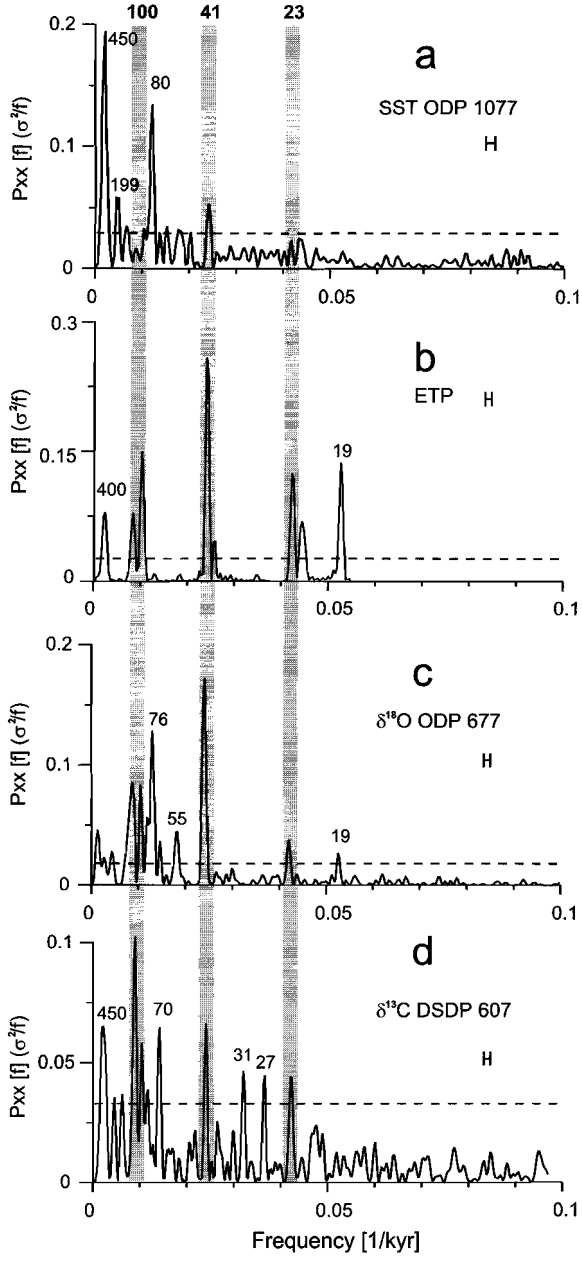

Figure 5.4: Power spectra of the investigated records in the Mid-Pleistocene time interval (1300 - 400 kyr BP), for a) the Site 1077 SST record, b) the calculated ETP record, c) the Site 677 benthic $\delta^{18}O$ record for the global ice volume, and d) the Site 607 benthic $\delta^{13}C$ record for the Atlantic deepwater ventilation. Small horizontal bar marks the 6 dB bandwidth for each calculation. Dashed lines indicate the periodicity significance level based on a Siegel-test. Orbital periodicities for eccentricity (100), obliquity (41) and precession (23) are indicated by grey bars. Other significant peaks are labelled separately.

The precessional SST variations in the equatorial Atlantic east of 15°W were inferred to be mainly a wind-forced phenomenon (Schneider et al., 1996). Upwelling due to equatorial divergence is thought to respond almost immediately to the change in the direction and strength of the trade-wind vector by monsoonal forcing (Imbrie et al., 1989). Every 23 kyrs, when the precession index was at a minimum, the boreal summer (June 21) insolation in northern Africa reached a maximum. This caused a maximum heating of the North African continent and the strongest development of the North African atmospheric low-pressure cell. In these situations, the trade winds north of 15°S were deflected to the north or northwest and blew in a more meridional direction, causing a reduced upwelling in the eastern equatorial Atlantic (de Menocal et al., 1993; McIntyre et al., 1989; Prell and Kutzbach, 1987). The low-latitude insolation thus plays a strong role in forcing the 23-kyr cyclic SST variations. However, changes in the thermal gradient of the Southern Hemisphere can interfere with this forcing (McIntyre et al., 1989). A steeper meridional thermal gradient during times of large ice volume compresses the atmospheric Hadley circulation and generally increases the zonal velocity of the trade winds (de Menocal and Rind, 1993; Manabe and Broccoli, 1985). This mechanism potentially increased the wind-driven upwelling and the advection of cold waters from high southern latitudes (Jansen et al., 1996; Schneider et al., 1996).

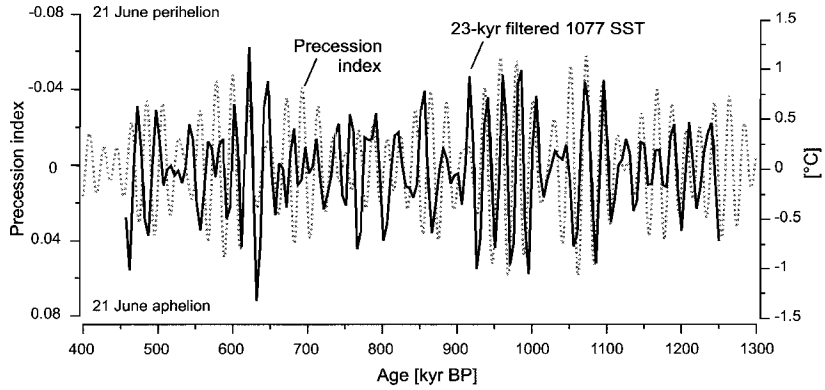

Figure 5.5: The 23-kyr-filtered SST record from ODP Site 1077 (central frequency = 0.0477 1/kyr and bandwidth = 0.02 1/kyr) to compare precessional SST variations (solid line) and variations in the orbital precession index (dotted line; Berger and Loutre, 1991). A minimum precession index results in maximum boreal summer insolation in North Africa, causing maximum monsoonal circulation (Prell and Kutzbach, 1987).

We suggest that the balance between these two processes has determined the precessional SST variability at Site 1077. During interglacial times with small ice volume, the low-latitude insolation was the prevalent forcing mechanism for precessional-related SST changes. We therefore detect high SST almost in phase with maximum boreal summer insolation, i.e., a minimum precession index (Fig. 5.5) during those times. When there was a generally increased ice volume, however, the precessional monsoon variability in the SST record is suppressed due to the increased zonal strength of the trade winds and advection from the south. The interference of the

upwelling and advection variability may therefore have caused the smaller amplitudes and the changing phase in the 23-kyr-filtered SST record.

5.3.7. Obliquity

In all power spectra of the investigated time-series, variance in the 41-kyr obliquity cycle can be detected (Fig. 5.4). Cross-spectral analyses between the ETP record and the SST, the $\delta^{18}O$, and the $\delta^{13}C$ records shows that all four records are coherent in the 41-kyr band (Table 5.3). A comparison of the 41-kyr-filtered SST and $\delta^{18}O$ records shows that the cycles follow each other with a consistent phasing (Fig. 5.6a). This confirms that the age-model of Site 1077 is accurate enough for a solid cross-spectral analyses in the 41-kyr cycle. The obliquity-related variations in the SST record consistently follow the changes in the Earth's tilt by 5.5 kyrs during the Mid-Pleistocene (Fig. 5.6b, Table 5.3). The global ice volume lags the ETP variations by about 8.9 kyrs (Fig. 5.6b, Table 5.3), consistent with the lag of about 8.0 kyrs assigned by orbital tuning (Imbrie et al., 1984; Shackleton et al., 1990). The $\delta^{13}C$ record shows a considerably larger phase-lag of about 12.9 kyrs relative to obliquity-related variations of ETP (Fig. 5.6b, Table 5.3). Cross-checking the obliquity phasing of the $\delta^{18}O$ record against the SST changes in the tropical Atlantic reveals a lead of SST by about 3.2 ± 1.0 kyrs (Table 5.3). A similar lead relative to ice-volume changes has been detected for alkenone SST variations at the Angolan margin during the Late quaternary (3.2 ± 2.3 kyrs, Table 5.3; Schneider et al., 1996).

The obliquity-related SST variability at Site 1077 cannot be explained by changes in low-latitude insolation, neither directly nor via the monsoonal atmospheric circulation, since there is no obliquity-related variability in the low-latitude insolation signal (Berger and Loutre, 1991). Two processes may be invoked to explain the obliquity-related SST variability in the tropical Atlantic: i) wind-driven upwelling and ii) advection of heat from high southern latitudes. Upwelling due to oceanic divergence depends on the zonal velocity of the trade winds, as described above for the precessional SST variations (Jansen et al., 1996; Schneider et al., 1996). The zonal strength of the trade winds is also in the obliquity cycle controlled by the atmospheric Hadley circulation, which is coupled to the Southern Hemisphere meridional thermal gradient (de Menocal and Rind, 1993; Manabe and Broccoli, 1985). The second potential process is the advection of heat from southern high latitudes. The South Atlantic exports surface water and heat to the North Atlantic, which is balanced by the inflow of surface water from the Indian and the Pacific Ocean (Hastenrath, 1982). Warm Indian Ocean waters are imported into the South Atlantic around the Cape of Good Hope (Lutjeharms and van Ballegooyen, 1988). The trapped heat is transported from the southern tip of Africa to the equator by the Benguela Current and the South Equatorial Current (Peterson and Stramma, 1991). When, during glaciations, the subtropical front moved north, this inflow of warm Indian Ocean waters was reduced and might even be pinched off, and cold waters from the Circum-Antarctic Current were shunted into the South Atlantic. The increased thermal surface gradient would then simultaneously strengthen the zonal trade winds and also enhance the transport of cold waters to the equator.

Both processes, equatorial upwelling and cold-water advection, thus depend on the position of the subtropical front in the Southern Ocean. They are connected to another and will influence the tropical Atlantic SST simultaneously (Schneider et al., 1996). SST records from the southern Indian Ocean and the subantarctic South Atlantic corroborate this explanation. These records, thought to reflect past frontal positions,

have a similar phase in the obliquity band as the Site 1077 SST record (Table 5.3; Brathauer and Abelmann, 1999; Howard and Prell, 1992). The variations in tropical Atlantic upwelling and heat advection intensity were therefore likely caused by shifts in the position of the Southern Ocean subtropical front, itself mainly controlled by, but preceding, the ice-volume changes (Imbrie et al., 1993).

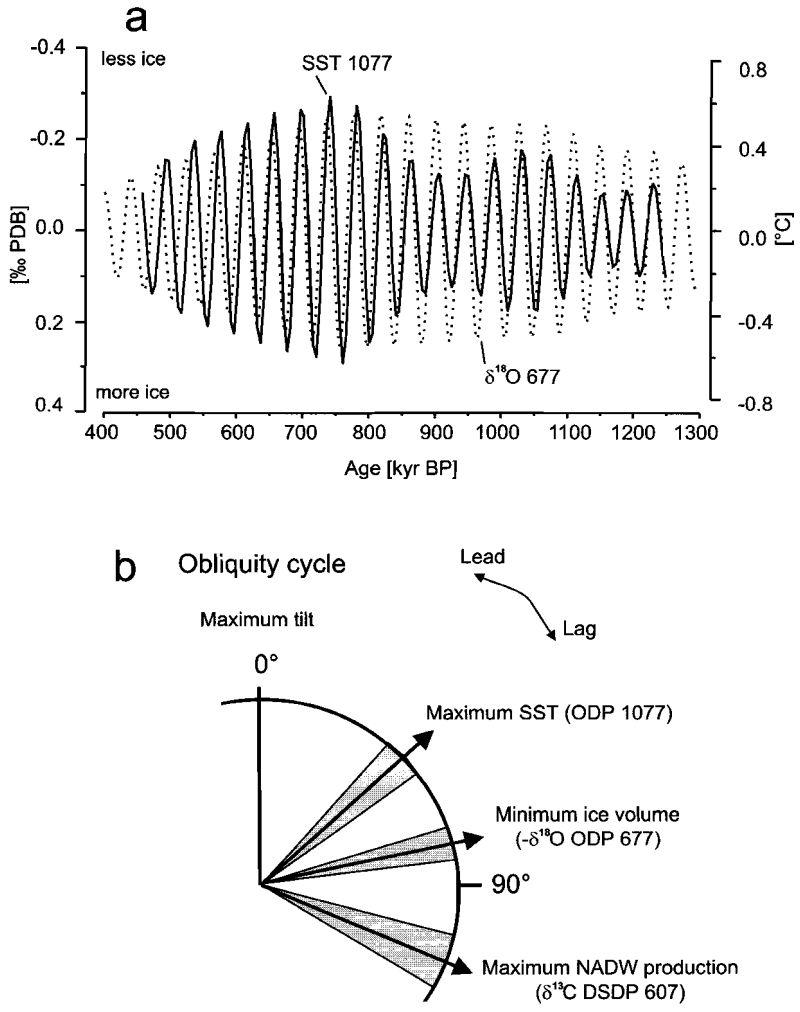

Figure 5.6: Results of the investigation of the 41-kyr cycle. **a)** The 41-kyr-filtered Site 1077 SST record (solid line) compared to the 41-kyr-filtered ice-volume signal, as represented by the Site 677 benthic $\delta^{18}O$ record (dotted line, note axis orientation). **b)** Phasing in the obliquity cycle shown in a phase wheel: maximum tilt is set to 0°, phase lag in degrees is clockwise. The shaded areas indicate the error estimates of the phase angles.

Table 5.3: Phase angles in the obliquity (41-kyr) cycle

Time series	coherency	Non-zero coherency (80 %)	Phase, deg.	Lag, kyr
ETP vs.				
ODP 1077 SST	0.99	0.96	48 ± 6	5.5 ± 0.7
ODP 677 $-\delta^{18}O_{bent.}$	0.99	0.96	78 ± 5	8.9 ± 0.6
DSDP 607 $\delta^{13}C_{wuell.}$	0.97	0.96	113 ± 9	12.9 ± 1.0
$-\delta^{18}O_{677}$ vs.				
ODP 1077 SST	0.99	0.96	-29 ± 8	-3.2 ± 1.0
-SPECMAP vs.				
GeoB 1016 SST Angola margin	0.76	0.64	-28 ± 20	-3.2 ± 2.3
E45-29/E49-18 SST (44°-46°S) South Indian fronts	0.86	0.65	-27 ± 15	-3.1 ± 1.7
PS2082-1 SST (43°S) South Atlantic fronts	0.92	0.73	-18 ± 12	-2.1 ± 1.4

ETP describes summed orbital variance following the convention by Imbrie et al. (1989) using the data of Berger and Loutre (1991). Data of ODP 677 $\delta^{18}O$ are from Shackleton et al. (1990), of DSDP 607 $\delta^{13}C$ are from Ruddiman et al. (1989a) with the stratigraphy of Raymo et al. (1997). SPECMAP data are from Imbrie et al. (1984), data of GeoB 1016 are from Schneider et al. (1995), data for E45-29/E49-18 are from Howard and Prell (1992) and data from PS2082-1 are from Brathauer and Abelmann (1999). A negative lag denotes lead.

5.3.8. 80-kyr cycle

During the Mid-Pleistocene Transition, much spectral power is observed in an 80-kyr cyclicity. It is distinct in our SST record and has also been detected in benthic foraminiferal $\delta^{18}O$ records from various locations, i.e., DSDP 552, DSDP 607, ODP 659, ODP 677 and ODP 806 (Mudelsee and Schulz, 1997). While some authors have explained this cyclicity as a doubling of the 41-kyr cycle (Berger et al., 1998), others attribute it to premature calving events of enlarged ice sheets during the transition from a 41-kyr to a 100-kyr cyclicity (Mudelsee and Schulz, 1997). To gain more insight into the phasing, we filtered the records with an 80-kyr filter with a central frequency of 0.0125 and a bandwidth of 0.001 cycles/kyr. The signals after filtering (Fig. 5.7) are almost in phase. This is confirmed by cross-spectral analysis of the $\delta^{18}O$ and $\delta^{13}C$ records versus the SST record (Table 5.4). The ETP record has no power in an 80-kyr cycle, so that the SST record was chosen as cross-spectral reference for that cycle. All three filtered records show a general increase in amplitude from 1300 to about 900 kyr BP (Fig. 5.7). Then, the 80-kyr power in the $\delta^{18}O$ and the $\delta^{13}C$ record decreases and is almost disappeared at 600 kyr BP, but this is not the case for the filtered SST record. The proposed transitional occurrence of the 80-kyr cycle during the MPT (Mudelsee and Schulz, 1997) can be confirmed for the global ice-volume and deepwater ventilation signal. It remains enigmatic, however, why the 80-kyr amplitude in the SST record is still large even after 600 kyr BP. Based on their strong

in-phase variation we suggest, nevertheless, that the 80-kyr SST cycles are also caused by the ice-volume variations. The zero phase relation between the 80-kyr-filtered records suggests that there is no orbital forcing involved. In contrast to the insolation-forced 41-kyr and 100-kyr cycle (see below), in which the tropical SST variations precede the ice-volume changes, no such early response is detected in the 80-kyr cycle, excluding the possible explanation by a doubling of the 41-kyr cycle. The 80-kyr cycle in SST is therefore likely an immediate response on the variations of ice volume during the MPT, involving only rapid oceanic and atmospheric reorganisations.

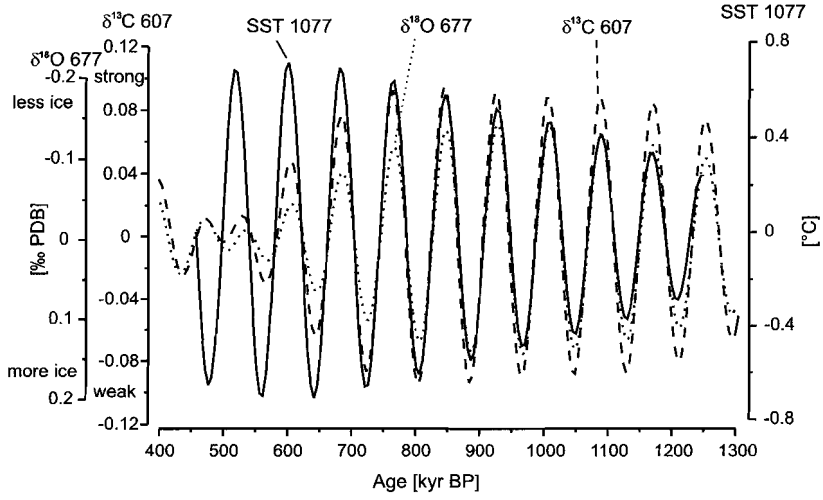

Figure 5.7: Comparison of 80-kyr cyclic variations in the Site 1077 SST record (solid line), the Site 677 benthic $\delta^{18}O$ record (dotted line) and the Site 607 benthic $\delta^{13}C$ record (broken line) to show the relative synchrony of the variations.

Table 5.4: Phase angles in the 80-kyr cycle

Time series	coherency	Non-zero coherency (80 %)	Phase, deg.	Lag, kyr
SST vs.				
ODP 677 $-\delta^{18}O_{bent.}$	0.83	0.96	-1 ± 23	-0.2 ± 5.1
DSDP 607 $\delta^{13}C_{wuell.}$	0.95	0.96	4 ± 12	0.9 ± 2.7

Data of ODP 677 $\delta^{18}O$ are from Shackleton et al. (1990), of DSDP 607 $\delta^{13}C$ are from Ruddiman et al. (1989) with the stratigraphy of Raymo et al. (1997). A negative lag denotes lead.

5.3.9. 100-kyr cycle

The 100-kyr-filtered SST record (Fig. 5.8a) shows the increasing power of the 100-kyr cyclicity at the end of the MPT. From 1250 to 650 kyr BP the filtered SST record contains only small variations in the 100-kyr-frequency band. From about 650 kyr BP, however, the amplitude of the 100-kyr-filtered signal becomes significantly larger than the envelope of the variations before (Fig. 5.8a). After that, the eccentricity-

related power in the Site 1077 SST record continued to increase. The 100-kyr-filtered $\delta^{18}O$ signal from Site 677 increased in power at approximately the same time (Fig. 5.8a; Chen et al., 1995). Because the 100-kyr cycle in the SST, as well as in the $\delta^{18}O$ record is absent from the older part of the record, we restricted cross-spectral analyses in the eccentricity band to the interval from 900 to 450 kyr BP (Table 5.5). In the 100-kyr cycle, the SST signal is rather in phase with insolation forcing and precedes the $\delta^{18}O$-signal by 8.6 kyrs. The eccentricity-related SST variability in the tropical Atlantic during the Late Quaternary had, within error limits, the same phasing with global ice-volume changes (Schneider et al., 1996). Like for the obliquity cycles, these SST changes were found to be in phase with the SST variability in the southern Indian Ocean and the subantarctic Atlantic, inferred to reflect past frontal movements in the high southern latitudes (Brathauer and Abelmann, 1999; Howard and Prell, 1992). Similar to the conclusions from the SST variability in the obliquity cycle (above), we therefore suggest a dominant control of eccentricity-related SST

Table 5.5: Phase angles in the eccentricity (100-kyr) cycle from 900 to 450 kyr BP

Time series	coherency	Non-zero Coherency (80 %)	Phase, deg.	Lag, kyr
ETP vs.				
ODP 1077 SST	0.96	0.96	-8 ± 10	-2.2 ± 2.8
DSDP 607 $\delta^{13}C_{wuell.}$	0.93	0.96	5 ± 14	1.4 ± 3.9
ODP 677 -$\delta^{18}O_{bent.}$	0.98	0.96	24 ± 8	6.7 ± 2.2
-$\delta^{18}O_{677}$ vs.				
ODP 1077 SST	0.91	0.96	-31 ± 16	-8.6 ± 4.4
-SPECMAP vs.				
GeoB 1016 SST	0.92	0.64	-14 ± 15	-3.9 ± 4.2
Angola margin				
E45-29/E49-18 SST	0.81	0.65	-18 ± 18	-5.0 ± 5.0
(44°-46°S)				
South Indian fronts				
PS2082-1 SST (43°S)	0.97	0.73	-18 ± 6	-5.0 ± 1.7
South Atlantic fronts				

ETP describes summed orbital variance following the convention by Imbrie et al. (1989) using the data of Berger and Loutre (1991). Data of ODP 677 $\delta^{18}O$ are from Shackleton et al. (1990), of DSDP 607 $\delta^{13}C$ are from Ruddiman et al. (1989a) with the stratigraphy of Raymo et al. (1997). SPECMAP data are from Imbrie et al. (1984), data of GeoB 1016 are from Schneider et al. (1995), data for E45-29/E49-18 are from Howard and Prell (1992) and data from PS2082-1 are from Brathauer and Abelmann (1999). A negative lag denotes lead.

variations in the equatorial Atlantic by changes in the Southern Hemisphere thermal gradient. Since these changes preceded the global ice-volume development, they caused the lead of the tropical SST variations over the high-latitude signal. With the onset of the 100-kyr cycle as predominant cyclicity of high-latitude ice-volume variations, and sea-ice extension, also tropical Atlantic upwelling and heat advection variability became dominated by this frequency. While the overall rhythm of longer period (100- and 41-kyr) climate cycles is thus set by the ice-volume variability in the

high latitudes, the tropics fulfil the role of an important amplifier of global climate change due to their early response on orbital forcing compared to the ice sheets.

These findings about the onset of the 100-kyr variability in tropical SST variations at 650 kyr BP support the observations of Mudelsee and Schulz (1997) on the global climate evolution during the MPT (Fig. 5.8c). The coherent increase in eccentricity-related power in the SST and the $\delta^{18}O$ record indicates that the SST in the tropics have not changed independently from the high-latitude ice-volume signal, in other words, both exhibit the same, changing pattern during the MPT. This contradicts the conclusion by Schneider et al. (1999), that the tropical SST variations are exclusively forced by changes in the tropical insolation. However, also a pure passive role of the tropics with regard to the high latitudes may not be inferred, as demonstrated by the lead of the tropical SST over the ice-volume signal.

5.3.10. Long-term trend

The long-term trend of the Site 1077 SST record (Fig. 5.8b), explaining a significant portion of the signal, differs significantly from the long-term development of the orbital forcing and the global ice volume. While the long-term minimum of ETP is centered around 800 kyr BP, the long-term SST in the tropical Atlantic reached a minimum around 900 kyr BP and can, therefore, not be explained by orbital forcing. The long-term SST minimum, however, coincides well with the start of the period of substantially larger mean global ice volume (Mudelsee and Schulz, 1997) (Fig. 5.8c). Besides a maximum around 900 kyr BP, however, the long-term trend of the global ice volume shows a second, even stronger maximum around 650 kyr BP, which is not at all reflected in the SST record. This excludes the global ice volume as the only cause of the long-term forcing of the tropical SST. The Site 607 $\delta^{13}C$ record, on the other hand, shows a similar long-term trend as the tropical Atlantic SST record during the MPT (Fig. 5.8b), suggesting a link between the strength of the thermohaline ventilation of the deep Atlantic Ocean and long-term tropical SST variations.

The MPT is a period of strong breakdown of NADW formation, unprecedented during the last 3 Ma (Raymo et al., 1997), as seen by the extremely low $\delta^{13}C$ values, which occur in the last 500 kyrs only during the meltwater events when the large 100-kyr ice sheets collapsed. The long-term amplitude of about 0.8 ‰ in the $\delta^{13}C$ record of benthic foraminifera (Fig. 5.8b) is much larger than the inferred mean ocean $\delta^{13}C_{DIC}$ change of about 0.3 ‰ during the MPT (Raymo et al., 1997) and consequently reflects primarily a change in the Atlantic deepwater ventilation. The long-term minimum of the Atlantic thermohaline deep ventilation is confirmed by the occurrence of a long-term minimum in carbonate deposition in the South Atlantic at the same time, attributed to a stronger influence of more aggressive, southern-source deepwaters (Schmieder et al., 2000). The first occurrence of low tropical SST (Fig. 5.3a) coincided with the first strongly decreased Atlantic deep convection (Fig. 5.3d), and with the inferred increase of the global ice volume during MIS 24 (Mudelsee and Schulz, 1997). It was, however, not simultaneous with the first maximum global ice mass, that occurred during MIS 22 (Fig. 5.3c).

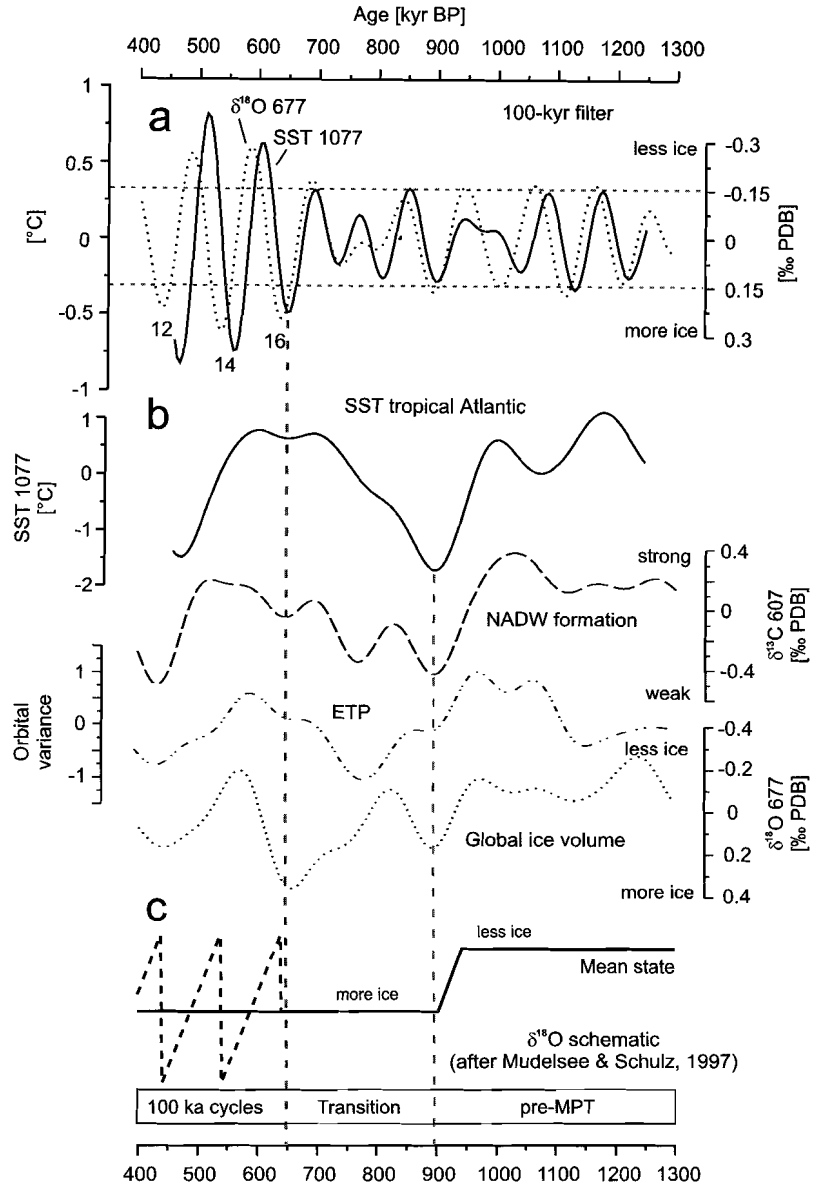

Figure 5.8: **a**) Results of the investigation of the 100-kyr cycle. The 100-kyr-filtered Site 1077 SST record (solid line) compared with the 100-kyr-filtered Site 677 benthic $\delta^{18}O$ record (dotted line, note axis orientation). The horizontal broken lines denote the envelope for 100-kyr SST variations before the amplitude increase. **b**) The long-term trend of the Site 1077 SST (solid line) compared with the long-term trends of the Site 607 benthic $\delta^{13}C$ (broken line), the calculated ETP record (dashed-dotted line), and the Site 677 benthic $\delta^{18}O$ record (dotted line, note axis orientation). **c**) The schematised development of $\delta^{18}O$ from statistical analyses (Mudelsee and Schulz, 1997). The vertical broken lines indicate the correlation of the discussed events.

A direct forcing of long-term tropical SST by the long-term North Atlantic deepwater formation during the MPT, however, cannot be inferred. This process assumes a warming of the tropical Atlantic surface ocean, during reduced North Atlantic Deep-Water formation (Crowley, 1992; Rühlemann et al., 1999), which is not the case. More likely, the two similar long-term developments, the tropical SST and NADW formation, were controlled by a common cause. We suggest that this cause was the growth of additional global ice volume at the start of the MPT.

Presently, the formation of deepwater in the North Atlantic leads to a vigorous thermohaline deepwater circulation (THC) in the Atlantic (Schmitz, 1995). Paleoceanographic data from the last glacial indicate that the THC in the Atlantic was approximately 30 % weaker than today (Sarnthein et al., 1994), while a total inhibition of NADW formation was caused by meltwater injection into the North Atlantic during deglaciations (Seidov and Haupt, 1997). Analogously, the strong glacial decreases of the Site 607 $\delta^{13}C$ values after MIS 24 suggests that each glacial during the MPT was in a meltwater mode. The enlarged ice mass, established around 900 kyr BP (Berger and Jansen, 1994; Maasch, 1988; Mudelsee and Schulz, 1997; Prell, 1982), was probably not in a stable configuration before 650 kyr BP and constantly melting. The severe glacial shutdowns of the Atlantic deep ventilation led to the accumulation of heat in the tropical Atlantic during each glacial in the MPT. This inference is corroborated by the increasingly warmer glacial SSTs from 900 to 650 kyr BP (Fig. 5.3a), resulting into a constant interglacially-warm tropical Atlantic during glacials, especially at the end of the MPT. At 650 kyr BP, when the 100-kyr cycle increased in power, the enlarged ice sheets presumably had adjusted to their new, lower, resonance frequency and reduced NADW formation had become established during glacials. Tropical surface-water heat was exported again during the glacials and the glacial minimum SSTs significantly decreased (Fig. 5.3a). During the following glacial, MIS 14 around 550 kyr BP, the long-term warming trend ended (Fig. 5.8b). While the MPT was thus initially caused by the mean-state change of the high-latitude ice sheets, it led to a pronounced long-term warming in the low-latitude Atlantic Ocean due to the strong decrease of NADW formation during the MPT glacials.

5.4. Conclusions:

- During the MPT, orbitally-driven SST variations in the tropical Atlantic show a prevalent 41-kyr cyclicity. The 100-kyr SST variability increased at 650 kyr BP, coinciding with the amplification of the 100-kyr ice-volume changes. The tropical SST variations followed a rhythm paced by the ice-sheet behaviour in the high latitudes, and were not exclusively forced by direct tropical insolation changes. In both the 41-kyr and 100-kyr cycle, however, the tropical SST responded significantly earlier on changes in the Earth's orbit than global ice volume. This early reaction is likely caused by rapid atmospheric and oceanic responses on changes in insolation. The SST variations in the 41-kyr and 100-kyr cycle are in phase with inferred frontal movements in the subantarctic Atlantic. Consequently, we attribute the obliquity- and eccentricity-related SST variability to changes in the thermal gradient of the South Atlantic, modulating the strength and zonality of the trade-wind system and thus controlling the wind-driven equatorial upwelling and heat advection in the tropical surface ocean. The early response stresses the role of the tropics as an important amplifier of orbital-driven climate changes.
- The tropical SST variations during the mid-Pleistocene show a strong 80-kyr cyclicity. This cycle is likely forced directly by premature calving events of the enlarged global ice mass during the MPT, as no early response relative to the ice-volume changes is detected and since it is not supported by orbital insolation changes.
- Strong precessional variations in the tropical SST record occurred only during times of small global ice volume. A stronger Hadley circulation caused by a steeper pressure gradient at times of a large global ice volume presumably suppressed the effect of low-latitude insolation forcing on the equatorial upwelling intensity.
- The long-term development of the tropical SST record shares a number of important features with the long-term benthic $\delta^{13}C$ record of the North Atlantic Ocean (Raymo et al., 1997). Both records show minimum values around 900 kyr BP and a subsequent long-term increase until around 550 kyr BP. The significant long-term SST development is, therefore, most probably linked to the strength of the Atlantic deep ventilation. We suggest that the mean-state change in the high latitudes, i.e., the increase of the mean ice volume, caused the SST minimum around 900 kyr BP and initiated the strongest reduction of NADW formation during the MPT over the last 3 Ma. Afterwards, each glacial during the MPT was most probably in a meltwater mode associated with a severely decreased NADW formation. Surface-water heat accumulated in the tropical Atlantic Ocean, causing the long-term warming between 900 and 550 kyr BP. The 250 kyr lag of the onset of the 100-kyr cyclicity after the growth of additional ice mass was probably due to the re-adjustment of the enlarged ice sheets and the thermohaline circulation system to the changed climatic boundary conditions at the MPT.

Acknowledgements

We gratefully thank the Ocean Drilling Program (ODP) for the supply of samples. We are indebted to Lydie Dupont (University of Bremen) and Lucas Lourens (University of Utrecht) for help with the stratigraphy.

Chapter 6

Aridity controls African C_4 plant abundance

Enno Schefuß, Stefan Schouten, J.H. Fred Jansen & Jaap S. Sinninghe Damsté

Submitted to *Nature*

The dominant forcing factors for large-scale vegetation changes in the past are still widely debated. The emergence and abundance of C_4 plants, adapted to dry and warm or low pCO_2 conditions (Collatz et al., 1998), has been inferred to be controlled by substantial changes in environmental conditions. The relative impacts of changes in aridity, temperature (Huang et al., 2001; Pagani et al., 1999) and of pCO_2 (Cerling et al., 1993; Kuypers et al., 1999) are, however, not yet well understood. Here, we present a 750-kyr long record of relative C_4 plant abundance derived from compound-specific carbon isotope analyses of wind-transported terrigenous plant waxes, reflecting large-scale African vegetation changes. These changes do not correlate with the development of global ice volume, and the inferred parallel pCO_2 variations, but are highly correlated with sea-surface temperatures (SST) in the tropical Atlantic. Changes in atmospheric moisture content, driven by tropical SST changes and the African monsoon, appear to be the dominant control of African aridity, in line with recent modelling efforts (Ganopolski et al., 1998), and thus control the large-scale C_3 to C_4 plant vegetation changes during the mid-Pleistocene.

Two main carbon-fixation pathways of plant photosynthesis, the Calvin-Benson (C_3) and the Hatch-Slack (C_4) cycles, occur in natural ecosystems (O'Leary, 1981). Nearly all trees, cold-season grasses and sedges use the C_3 pathway, while C_4 photosynthesis is found in warm-season grasses and sedges (Cerling et al., 1997). C_4 plants are, thus, predominantly found in tropical savannahs, temperate grasslands and semi-deserts (Cerling et al., 1997). Most African grasslands are presently dominated by C_4 plant vegetation (Collatz et al., 1998). C_4 plants utilise a CO_2-concentrating mechanism, which gives them advantage over C_3 plants at low atmospheric pCO_2 (Ehleringer et al., 1997) and causes them to be isotopically enriched in ^{13}C (Cerling et al., 1993). At high pCO_2, however, C_3 plants will outcompete C_4 plants due to the higher energy need of C_4 plants during photosynthesis (Ehleringer et al., 1997). The crossover between C_3 and C_4 plants depends also on the daytime growing-season temperature, with higher temperatures favouring C_4 plants (Cerling et al., 1997; Ehleringer et al., 1997). Other factors, however, may interfere. Where precipitation and nutrient availability permit trees to grow, C_3 trees will outcompete C_4 grasses, like in the tropical forests (Collatz et al., 1998). The significance of the climatic factors controlling the large-scale C_4 plant abundance is, due to these interferences, still not well understood, but insights may be gained from past C_3 to C_4 plant vegetation changes through the analysis of fossil plant remains.

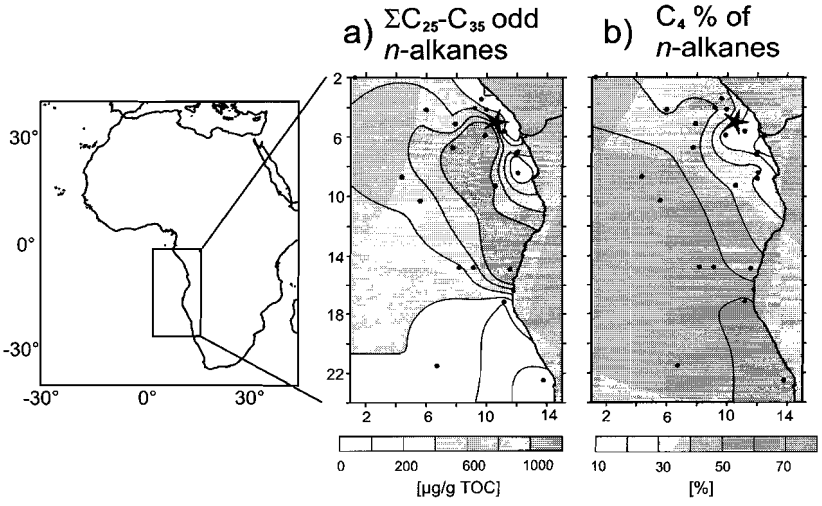

Figure 6.1: Spatial distribution of a) the TOC-normalised concentrations of the C_{25} to C_{35} odd-numbered *n*-alkanes and b) the C_4 plant fraction of the *n*-C_{31} alkane in surface sediments. Black dots are locations of *RV Tyro* '89 surface samples. The star indicates the location of ODP Site 1077.

Long-chain, odd-numbered C_{25} to C_{35} *n*-alkanes are major lipid constituents of the epicuticular wax layer of terrestrial plants (Eglinton and Hamilton, 1967). These plant waxes are easily removed from the leaf surface by rain or wind, especially by sandblasting during dust storms. They are, therefore, common organic components of eolian dust (Schefuß et al., re-submitted). In surface sediments of the eastern South Atlantic the plant-wax *n*-alkanes exhibit a moderate to high odd-over-even

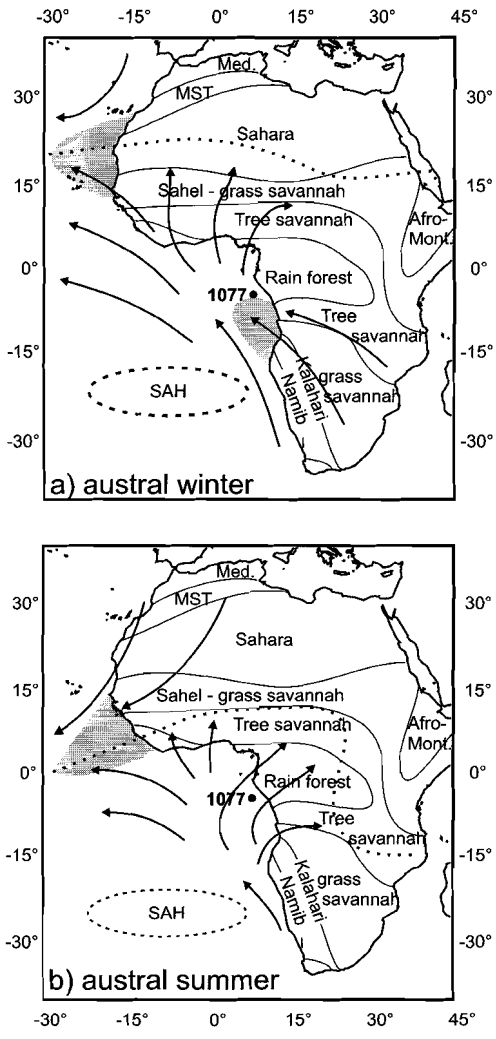

Figure 6.2: General pattern of present-day atmospheric circulation over Africa and the Southeast Atlantic Ocean in a) austral winter (June to August) and b) austral summer (December to February). SAH = South Atlantic high-pressure cell. The dotted lines indicate the Intertropical Convergence Zone (ITCZ). Dust plumes are shaded. Areas in Africa indicate vegetation zones. Med.: Mediterranean vegetation,
MST: Mediterranean-Saharan transitional vegetation,
Afro-Mont.: Afro-Montane vegetation zone. The location of ODP Site 1077 is indicated.

carbon number predominance (Carbon Preference Index = 2.3-6.4) and thus predominantly represent leaf waxes of terrestrial higher plants (Eglinton and Hamilton, 1967). Their plume-like distribution in surface sediments (Fig. 6.1a) indicates that they are mainly supplied by south-easterly winds from the dry areas in southern Africa, the Kalahari savannah and Namib Desert. During the austral winter (June to August, Fig. 6.2a) the strong Southern Hemisphere trade winds transport large amounts of dust north-westwards over the eastern South Atlantic. In the austral summer (December to February), during the southern African monsoon season, the trade winds are deflected landinwards (Fig. 6.2b). We estimated the C_4 plant percentage of the leaf-wax *n*-alkanes in surface sediments using the stable carbon isotopic composition ($\delta^{13}C$ in ‰ vs. PDB) of the predominating *n*-C_{31} alkane and a binary mixing equation, assuming $\delta^{13}C_4$ leaf-wax lipids = -21.5 ‰ and $\delta^{13}C_3$ leaf-wax lipids = -36.0 ‰ (Collister et al., 1994). The results (Fig. 6.1b) show that the leaf-wax *n*-alkanes in the surface sediments of the eastern South Atlantic mainly reflect the contemporary vegetation zones on the adjacent continent (Fig. 6.2) and the, primarily eolian, transport pathway. This finding is supported by the $\delta^{13}C$ of plant-wax lipids in atmospheric dusts collected off the African coast (Schefuß et al., re-submitted). The atmospheric plant-wax lipids show a C_4 plant contribution of about 55 % in dust from the southern African dry areas, while off the tropical rainforest regions

the C_4 plant fraction is only 30 - 40 % (Schefuß et al., re-submitted).

Based on these insights into the present-day system, we reconstructed the mid-Pleistocene African C_3 to C_4 plant vegetation changes with a plant-wax $\delta^{13}C$ record from ODP Site 1077 (10°26.2'E, 5°10.8'S, 2382 m water depth) in the eastern tropical Atlantic Angola Basin (Fig. 6.1). This site is located at the northern edge of the modern Southern Hemisphere dust plume during the austral winter (Fig. 6.2a) and is thus sensitive to changes in its strength and position. It is, therefore, an ideal recorder of the southern African vegetation signal transported with plant-wax lipids in dust. We investigated the period from 1.2 million years to 450 thousand years ago (kyr BP), including the Mid-Pleistocene Transition (MPT), which led to the establishment of the well known 100-kyr rhythm of the Late Pleistocene ice ages around 650 kyr BP. Before that, a 41-kyr cyclicity was prevalent. During the MPT, from about 920 to 650 kyr BP, the global ice-volume variations increased in amplitude (Shackleton and Opdyke, 1976), which led to a substantial perturbation of the climate system, probably by re-adjustment of the enlarged Late Pleistocene ice sheets (Mudelsee and Schulz, 1997). The global oceanic thermohaline circulation was severely weakened by a strong reduction of North Atlantic Deep-Water formation (Raymo et al., 1997), causing a long-term surface-water warming of the tropical Atlantic Ocean (Fig. 6.3b). This temporary deviation from the cyclic climate behaviour during the MPT provides the possibility to distinguish between the various climatic factors controlling large-scale vegetation changes.

The *n*-alkanes in the sediments of ODP Site 1077 are predominantly derived from higher plant waxes (CPI = 2.1-5.3). The mid-Pleistocene record of the relative C_4 plant contribution at ODP Site 1077 shows large deviations (from 20 to 70 %, Fig. 6.3a) from the present-day value (about 35 %, Fig. 6.1b). The record of the C_4 plant contribution shows no correlation with the changes in *n*-alkane accumulation rates (Fig. 6.3c). The *n*-alkane accumulation rates were generally low before the growth of the global ice volume at around 900 kyr BP. The increase of *n*-alkane accumulation rates after 900 kyr BP suggests a response of the eolian plant-wax transport to changes in the trade-wind system. An increase of eolian terrigenous accumulation off NW-Africa caused by the expansion of the mean global ice volume at 900 kyr BP was attributed to the compression and strengthening of the atmospheric circulation cells (de Menocal, 1995). The *n*-alkane accumulation rates presumably depended also on the supply of plant waxes by the vegetation cover. However, the eolian transport became sensitive to ice-volume changes only after the mean global ice mass had increased to its enlarged Late Pleistocene volume (Mudelsee and Schulz, 1997). If an increased eolian flux of C_4 plant *n*-alkanes by dust would have determined the C_4 plant record, elevated *n*-alkane accumulation rates should have led to a higher fraction of C_4 plant lipids, which is obviously not the case (Fig. 6.3). Therefore, the C_4 plant record reflects true changes in the vegetation cover of southern Africa. But, what was the driving force behind these large changes? Several factors, i.e., variations of atmospheric pCO_2, continental temperature and aridity (Cerling et al., 1993; Huang et al., 2001; Kuypers et al., 1999; Pagani et al., 1999), have been put forward to explain large-scale C_3 to C_4 plant vegetation changes in Earth's history.

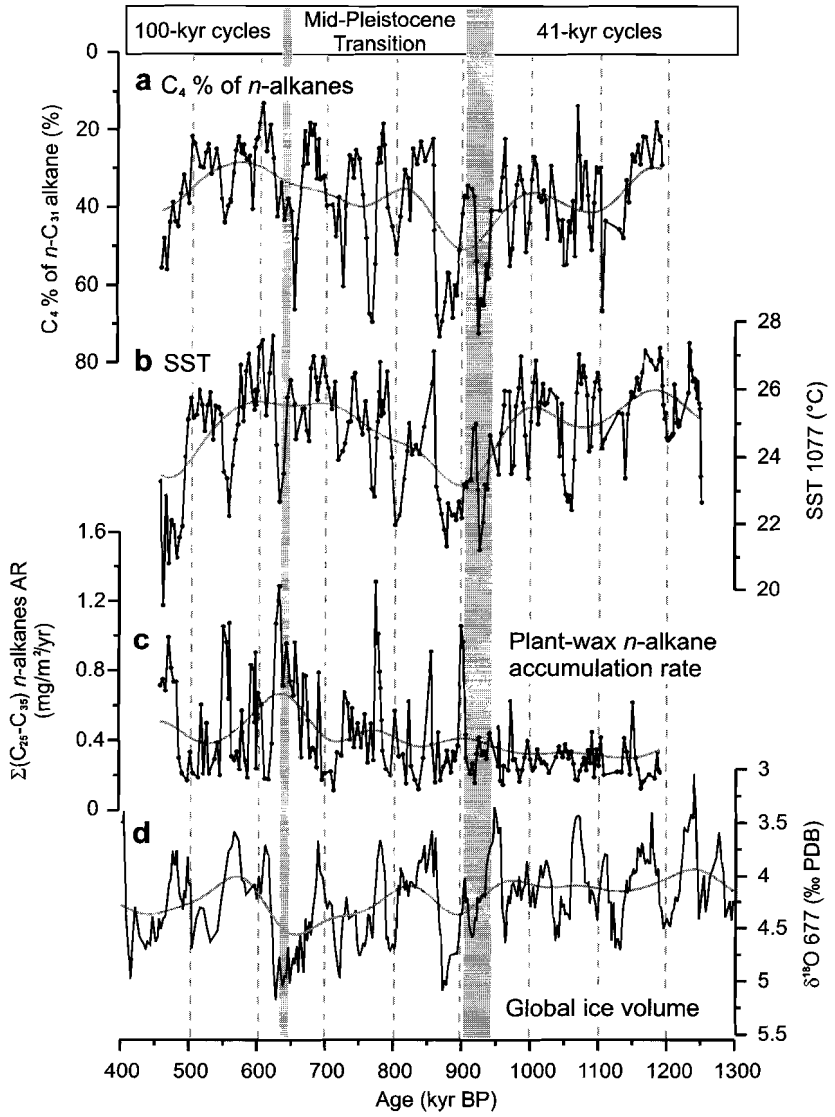

Figure 6.3: Mid-Pleistocene records of a) the C_4 plant fraction of the plant-wax *n*-alkanes using $\delta^{13}C$ values of the *n*-C_{31} alkane (note axis orientation); b) the alkenone-derived SST record at ODP Site 1077; c) the accumulation rates of plant wax-derived long-chain C_{25} to C_{35} odd-numbered *n*-alkanes; and d) the global ice-volume evolution, reflected by the oxygen-isotope values of benthic foraminifera at ODP Site 677 (note axis orientation; Shackleton et al., 1990). The grey lines behind the records are the long-term trends (bandpass-filters with a central frequency of 0.004 (250 kyr period) and a bandwidth of 0.004 cycles/kyr). The stratigraphy of ODP Site 1077 is based on oxygen-isotope analyses of *G. ruber* (pink) by correlation to the stratigraphy of ODP Site 677 (Dupont et al., 2001). Ages for all samples were determined by linear interpolation using the revised composite depth scale (Jansen and Dupont, 2001). The division into pre-MPT, transition and post-MPT is based on Mudelsee and Schulz (1997).

The C_4 plant record shows no general correlation with the global ice volume as reflected by the $\delta^{18}O$ signal of benthic foraminifera (Fig. 6.3d), indicating that the observed large-scale C_3 to C_4 plant abundance changes were also not primarily triggered by variations of atmospheric pCO_2. Over the last 420 kyrs, the ice core records of pCO_2 (Petit et al., 1999) show a strong correlation with the ice-volume records (Mudelsee, 2001) and we assume that this correlation was also valid for the mid-Pleistocene, although the mechanistic linkage between the two climate parameters still remains unexplained. The conclusion, that C_3 to C_4 plant abundance changes were not controlled by variations of pCO_2, is supported by a recent reconstruction of pCO_2 for the Miocene, when C_4 grasses had widely expanded (Cerling et al., 1997) without an accompanying decrease in atmospheric CO_2 concentrations (Pagani et al., 1999).

Table 6.1: Results of cross-spectral analyses

		1/100 1/kyr		1/41 1/kyr		1/23 1/kyr	
Data	k_0	k	Phi°	k	Phi°	k	Phi°
C_4 percentage	0.96	0.97	174±9	0.98	-132±8	0.97	-34±9
SST ODP 1077	0.96	0.96	-8±10	0.99	48±6	0.94	-22±13
ΣC_{25}-C_{35} *n*-alkanes AR	0.96	0.85	126±21	0.94	144±14	0.99	122±4
$-\delta^{18}O$ ODP 677	0.96	0.98	24±8	0.99	78±5	1.00	87±2

Variables are crossed with the summed orbital variance record ETP (eccentricity, tilt and precession) based on data from Berger and Loutre (1991). Given are the nonzero coherency at the 80 % level (k_0), the coherencies (k) and phase angles (Phi) with 80 % confidence interval. Positive phase angles indicate that a variable lags the maximum interglacial forcing, negative phases indicate a lead of a variable over maximum interglacial forcing. Benthic $\delta^{18}O$ data of ODP 677 are from Shackleton et al. (1990).

The C_4 plant record, however, correlates strongly with the SST development at ODP Site 1077 (Fig. 6.3b). Cross-spectral analyses of the C_4 plant, SST and *n*-alkane flux records with the ETP record, i.e., the summed variance of Eccentricity, Tilt, and Precession of the Earth's orbit, confirm that the C_4 plant changes occurred out of phase with the variations of global ice volume and the *n*-alkane accumulation rates in all orbital cycles (Table 6.1). In the two longer orbital periods, eccentricity (1/100 1/kyr) and obliquity (1/41 1/kyr), and also in the long-term development (Fig. 6.3a, 6.3b), maximum C_4 plant occurrence coincided with minimum SST values (Table 6.1). In contrast, in the precessional cycle (1/23 1/kyr) the C_4 plant maximum corresponded with the SST maximum. The coincidence of maximum C_4 plant abundance and maximum SST in the precession cycle can be explained by the common low-latitude insolation forcing of the African monsoon and equatorial Atlantic upwelling (de Menocal, 1995; McIntyre et al., 1989; Prell and Kutzbach, 1987), which both are mainly controlled by the precession (Berger and Loutre, 1991). Subtropical southern Africa receives its main precipitation in the monsoon season during the austral summer (DJF, Fig. 6.2b; Hsü and Wallace, 1976), while equatorial upwelling in the tropical Atlantic is strongest during the austral winter (JJA, Fig. 6.2a; Katz and Garzoli, 1982; Philander and Pacanowski, 1986). Due to the geometry of the orbital precession, changes in summer insolation are in anti-phase between the hemispheres (Berger and Loutre, 1991). This means that southern African monsoon is strongest when the monsoon in northern Africa is weakest, i.e., when equatorial upwelling is strongest. The most humid periods in southern Africa,

favourable for C_3 plants, therefore coincide with periods of enhanced equatorial upwelling and lowered tropical SST (Katz and Garzoli, 1982; McIntyre et al., 1989; Philander and Pacanowski, 1986) in the precessional cycle. The short-term C_3 to C_4 plant variations in subtropical southern Africa are thus explained by changes in monsoonal precipitation, driven by the low-latitude insolation changes.

In the two longer orbital cycles and in the long-term development, however, the opposite phasing between SST and C_4 plant abundance (Table 6.1, Fig. 6.3) requires a different explanation since the low-latitude insolation changes do contain neither an obliquity nor an eccentricity component (Berger and Loutre, 1991). SST variations at these timescales did not directly control the observed C_3 to C_4 plant vegetation changes. If air temperatures over sea and the SST variations were directly connected, the air temperatures over subtropical Africa would have changed in the same way as in the tropical area, possibly with an even larger amplitude. Lower growing-season temperatures, however, favour C_3 plants and do not lead to more C_4 plants, as detected in these cycles (Table 6.1). Consequently, aridity changes must also be the driving force for the large-scale C_4 plant abundance changes in subtropical southern Africa observed in the longer orbital cycles and in the long-term development. We therefore propose that the tropical SST is an important factor determining the continental aridity and, thus, the C_4 plant abundance. During the mid-Pleistocene, the tropical SST (Fig. 6.3b) decreased by up to 5°C during glacials. Contrary to former CLIMAP estimates (CLIMAP Members, 1981), it has been shown that the tropical SST has fallen several degrees also during the last glacial maximum (Schneider et al., 1995). Lower tropical SST reduced the tropical evaporation and atmospheric moisture, the main source of precipitation for the monsoon. The lower content of atmospheric water vapour, a major greenhouse gas, presumably led to a further cooling. This scenario has recently been simulated with a coupled ocean-atmosphere model (Ganopolski et al., 1998), showing an overall decrease in summer precipitation in the African tropics driven by reduced tropical SST during the last glacial maximum. The SST variations in the equatorial Atlantic were thus the dominant control of the continental aridity changes in southern Africa on timescales when variations in the strength of the monsoon where absent. These occurred solely in the precession cycle and overruled the weaker SST forcing.

It has recently been shown that a low global atmospheric pCO_2 alone is unable to trigger the C_4 plant expansions in the icehouse world, and that aridity drives C_3 to C_4 plant abundance changes on a regional scale (Huang et al., 2001). Our results indicate that aridity is the dominant climatic control of C_4 plant abundance on a large, continental scale and various time-scales. The vegetation changes in Africa were thus primarily forced by the strength of the monsoon and atmospheric moisture changes controlled by the tropical SST and insolation. The significance of the low-latitude sea-surface conditions for large-scale environmental changes in the past and future may thus be far more important than previously thought.

Methods

Dried and ground sediment samples were ultrasonically extracted (3x) using successively less polar solvent mixtures (CH_3OH, CH_3OH/CH_2Cl_2 1:1, CH_2Cl_2). Extracts of each sample were combined and rotary-evaporated to near dryness. Salts were removed by washing with double-distilled H_2O in a separatory funnel and extraction of the lipids with CH_2Cl_2 (3x). Extracts were rotary-evaporated again, taken up in CH_2Cl_2 and dried over anhydrous Na_2SO_4. A known amount of standard, (2,3-dimethyl-5-1',1'-d_2-hexadecyl-thiophene), was added and used for compound quantification. Saturated hydrocarbon fractions were obtained by column-chromatography over $AgNO_3$-impregnated, activated Al_2O_3 eluted with hexane: CH_2Cl_2 (9:1). Compounds were analysed on a Hewlett Packard 5890 series II gas chromatograph using flame ionisation detection (FID). Compound identifications were mainly based on relative GC retention times and GC-mass spectrometry (GC-MS) analyses of selected samples. Quantification of compounds was performed by peak area integration in FID chromatograms. The compound-specific stable carbon isotopic composition of the *n*-alkanes was measured via GC-isotope ratio monitoring-MS (GC-irm-MS) with a Finnigan Delta C mass-spectrometer. CO_2 gas with known isotopic composition was used as reference. Analyses were done at least in duplicate. Standard deviations of $\delta^{13}C$ values ($\pm\sigma$) were better than 0.5 ‰ vs. PDB.

Chapter 7

Tropical environmental changes at the Mid-Pleistocene Transition: insights from lipid biomarkers

Enno Schefuß, J. H. Fred Jansen, Jaap S. Sinninghe Damsté

In preparation for *Quaternary Science Reviews*

Abstract

We examined mid-Pleistocene (1250-450 kyr BP) lipid biomarker accumulation rates and bulk organic geochemical records from the Angola Basin (ODP Site 1077, eastern tropical Atlantic) to assess the low-latitude environmental changes associated with the onset of the Late Pleistocene ice ages. Five groups of molecular and bulk parameters with a similar temporal development were identified by principal component analysis and, combined with information on lipid sources, used to evaluate the main forcing factors of changes in phytoplankton productivity and lipid transport pathways. Cross-spectral analyses reveal the phasing in orbital-driven climatic cycles. The absolute level of total marine production was high and unchanged over the mid-Pleistocene, however, the relative lipid contributions indicate a change in the primary producing plankton ecosystem. Before the growth of the mean global ice volume, monsoonal variations in river runoff periodically increased the availability of dissolved silicate in the Congo River plume, leading to siliceous marine production, while variations in trade-wind zonality controlled marine production by oceanic upwelling. Both processes were forced by precessional insolation changes, but were suppressed by the large ice mass. The eolian transport of terrigenous plant waxes and the production of biomarkers by wind-driven upwelling were strongly increased after the onset of the 100-kyr cyclicity. The terrestrial vegetation signal is linked to the tropical sea-surface temperature, directly or via the continental aridity.

7.1. Introduction

The Mid-Pleistocene Transition (MPT) resulted in the development of the Late Pleistocene ice ages with an increased mean global ice volume changing in a sawtooth-pattern in 100,000-year (100-kyr) cycles (Mudelsee and Schulz, 1997; Prell, 1982). Records related to ice volume are dominated by 41-kyr variations before the 100-kyr rhythm became dominant (Pisias and Moore, 1981; Ruddiman et al., 1989a; Shackleton and Opdyke, 1976). Time-series analyses of $\delta^{18}O$ records of deep-sea carbonates, reflecting the global ice-volume development, showed that the increase in mean continental ice mass significantly preceded the increase in spectral power of the 100-kyr cycle (Mudelsee and Schulz, 1997). It has been suggested that the increase in ice volume was mainly due to the growth of shelf based ice sheets in high-latitude regions (Berger and Jansen, 1994). Both the increase in mean global ice mass and the change in the frequency domain, the transition from a prevalent 41-kyr cycle to the predominant 100-kyr cycle, were considered to have been either abrupt or gradual (Berger and Jansen, 1994; Bolton et al., 1995; Maasch, 1988; Mudelsee and Schulz, 1997; Park and Maasch, 1993; Prell, 1982). It is, however, generally agreed that the increase of mean global ice mass significantly preceded the full establishment of the 100-kyr cycle in ice-volume variations. For this study, we follow the conclusions from the most recent statistical examination of the evolution of the global ice volume (Mudelsee and Schulz, 1997). These findings favour a gradual increase in global ice mass lasting from 942 to 902 kyr before present (BP) and a rather abrupt onset of the 100-kyr cyclicity in ice-volume variations at 641 kyr BP. The MPT was associated with a substantial perturbation of the global thermohaline circulation (THC). Atlantic-Pacific $\delta^{13}C$ gradients of deep-sea carbonate show that North Atlantic Deep-Water (NADW) formation was most severely weakened during the MPT over the last 3 Ma (Raymo et al., 1997; Raymo et al., 1990). Reduced bottomwater ventilation led to more corrosive bottomwaters and decreased the carbonate accumulation rates in the deep South Atlantic during the MPT (Schmieder et al., 2000). The reduced NADW formation also decreased the northward heat export from the South Atlantic, and caused the long-term accumulation of surface-water heat in the tropical Atlantic during the MPT (Schefuß et al., submitted-b).

In order to examine the remote effects of the high-latitude ice-volume changes, occurring during the MPT, on the tropical Atlantic marine environment, we conducted a lipid biomarker study of sediments deposited at the lower Congo fan from 1300 to 450 kyrs BP. Lipid biomarker accumulation rates in sediments can be used to discriminate between the contributions of various phytoplankton sources to marine productivity (Boon et al., 1979; Hinrichs et al., 1999; Schubert et al., 1998; Volkman et al., 1998; Westerhausen et al., 1993) and to detect the contributions of allochthonous, land-derived lipids (Gagosian and Peltzer, 1986; Simoneit, 1977; Simoneit et al., 1991; Simoneit et al., 1977). Our goal is to assess amplitude and frequency changes in the contributions of terrigenous material, variations of the bulk marine productivity and in the planktonic community structure. We utilise lipid biomarker and total organic carbon accumulation rates and stable carbon isotope compositions of bulk organic matter and biomarkers to examine the response of various phytoplankton classes and the contributions of river-, as well as wind-transported terrigenous lipids during the onset of the Late Pleistocene ice ages.

7.2. Present-day and past oceanography of the Angola Basin
7.2.1. Modern seasonal circulation change

The modern surface and shallow subsurface circulation in the Angola Basin forms a cyclonic gyre connected to the tropical Atlantic (Fig. 7.1a; Peterson and Stramma, 1991; van Bennekom and Berger, 1984). The eastward-flowing South Equatorial Counter Current (SECC) in the north feeds the warm, nutrient-poor Angola Current (AC), which flows southwards along the western African margin. At about 15°-17°S it converges with the northward-flowing cold, nutrient-rich Benguela Coastal Current (BCC), is deflected to the north-west and becomes part of the South Equatorial Current (SEC) directing to the equator.

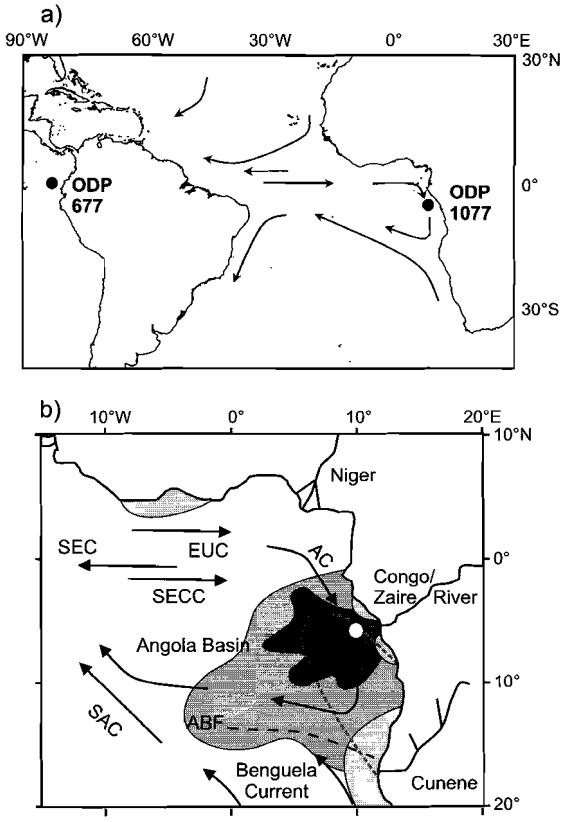

Figure 7.1: a) Overview map with the location of ODP Site 1077 and the present-day surface and shallow subsurface currents in the South Atlantic Ocean and the location of ODP Site 677 in the Pacific Panama Basin. b) Detailed map of the Angola Basin with the major currents: SAC = South Atlantic Current, SEC = South Equatorial Current, SECC = South Equatorial Countercurrent, ABF = Angola-Benguela Front. Shaded areas indicate elevated productivity (after Schneider et al., 1994). Dark shading: River-induced production, medium shading: oceanic upwelling with shallow thermocline, light shading: coastal upwelling cells. Location of ODP 1077 is indicated by the white dot in the river plume.

While the southerly trade winds drive intense upwelling off the coast of South Africa and Namibia (Shannon, 1985) and cause primary productivity rates of >200 $gC/m^2/yr$ (Berger, 1989; Shannon and Pillar, 1986), elevated coastal productivity in the Angola Basin is restricted to two small, coastal upwelling cells at 5 and 7°S, north and south of the Congo River mouth (Fig. 7.1b; Servain et al., 1982; Voituriez and Herbland, 1982). This shallow upwelling activity has the strongest effect on nitrate and lesser on phosphate concentrations, while its effect on silicate concentrations is much smaller (van Bennekom et al., 1978). However, south of the Congo River plume, the primary production is relatively high (Chyong, 1971; van Bennekom and Berger, 1984). Here, the cyclonic gyre circulation causes shoaling of the thermocline and seasonally elevated supply of nutrients to the photic zone, supporting an elevated phytoplankton productivity (Lutjeharms and Stokton, 1987).

At about 5°S, the surface circulation of the Angola Basin is superimposed by the low-salinity plume of the Congo (Zaire) River, the World's second largest river with an average annual freshwater discharge of 1.3×10^{12} m^3/yr. Its plume can be detected as far as 800 km offshore (van Bennekom and Berger, 1984). The seasonal variation in discharge is associated with the monsoonal circulation and precipitation (Eisma and van Bennekom, 1978; van Bennekom and Berger, 1984). During austral summer (December to February) the Intertropical Convergence Zone (ITCZ) is in its southernmost position (5°-10°N), causing maximum monsoon conditions in southern Africa with a large influx of moisture-laden air and high precipitation (Hsü and Wallace, 1976). The maximum extension of the Congo River plume occurs in February-March, later than the maximum discharge in December (van Bennekom and Berger, 1984) and is associated with the highest annual sea-surface temperatures (SST) in the equatorial Atlantic (Katz and Garzoli, 1982).

The Congo River water flows rapidly as a thin surface layer into the ocean. Together with the large depth of the estuary, this leads to an extremely stratified outflow with low vertical mixing. Entrainment of subsurface waters with elevated concentrations of nitrate and phosphate to the silicate-rich river water causes some river-induced productivity (van Bennekom et al., 1978). About 150 to 200 km offshore the plume broadens. Entrainment of subsurface waters from below the shallow nutricline supplies additional nitrate and phosphate to the surface. A marine phytoplankton bloom develops in the inner plume area, but it takes some time to build up a high population. A maximum of primary productivity is therefore found in a narrow meridional zone between a salinity of 28 and 32, around 10 to 11°E (Cadée, 1978; Cadée, 1984). Surface-water productivity off the Congo River mouth reaches values of 90-125 $gC/m^2/yr$ (Berger, 1989). Phytoplankton productivity in the inner Congo River plume is dominated by a very high diatom production, accounting for 40 to 60 % of the total productivity (van Bennekom and Berger, 1984). Offshore, the level of primary productivity in the Congo River plume decreases due to the subsequent dilution of the river-derived nutrients. The river-induced phytoplankton activity extends about 160 km beyond the shelf-edge, however the majority of the regionally enhanced productivity is not river-related (Jansen, 1985; Jansen et al., 1984).

During austral winter (June to August), the ITCZ is furthest north (~20°N) and strong Southern Hemisphere trade winds cause oceanic upwelling by surface divergence in the equatorial Atlantic Ocean (Philander and Pacanowski, 1986). The upwelling intensity correlates to the zonal velocity of the southern trades (Philander and Pacanowski, 1986). SSTs in the eastern equatorial Atlantic are at their annual minimum, while surface-water productivity reaches its annual maximum during

austral winter (Katz and Garzoli, 1982). Offshore oceanic upwelling outside the Congo River plume induces moderate to high primary productivity of 90-180 $gC/m^2/yr$ (Berger, 1989).

In a survey of bulk geochemical parameters and lipid biomarker distributions of surface sediments in the eastern South Atlantic, we have previously shown that various production, transport and preservation processes in the different oceanographic environments can be distinguished by the measurement of organic geochemical proxies (Schefuß et al., submitted-c). River-induced productivity and oceanic upwelling in the plume area leads to a high contribution of sterols from phyto- and zooplankton and long-chain diols, while river transport of terrestrial material can only be traced as terrigenous fraction of the bulk organic matter, based on its stable carbon isotopic composition. Strong coastal upwelling dominantly influences the content of total and marine-derived organic matter and the SST variations, and leads to enhanced preservation of labile organic compounds via lower oxygen exposure times of the lipids in the surface sediments. The small-scale coastal upwelling cells north and south of the Congo River mouth can be identified by their high production of long-chain alkenones and fucosterol, derived from Haptophyte algae and diatoms, respectively. Eolian transport of lipids can be recognised by elevated concentrations of plant-wax lipids, which stretch in a plume-like lobe from the dry areas in southern Africa below the trade-wind path towards the equator. These lipids are nowadays predominantly derived from C_4 plant vegetation, as indicated by their stable carbon isotopic signature (Schefuß et al., re-submitted; Schefuß et al., submitted-c).

7.2.2. Paleoceanography

Paleoenvironmental studies in the Angola Basin have, until the recent drilling of ODP Leg 175, mainly focused on the Late Quaternary. From investigations of diatoms in the Congo fan area it was inferred that coastal upwelling was strong during glacials and weak during interglacials, while oceanic upwelling was also strong during cold substages of interglacials (Jansen and van Iperen, 1991). From the ratio of opal phytoliths to freshwater diatoms it was concluded that equatorial Africa was more arid during glacial stages and substages and more humid during interglacial (sub)stages (Jansen et al., 1989). A detailed investigation of stable carbon isotopic gradients between planktonic foraminifera has shown that off the Congo River no large freshwater signal is recorded and that the isotopic records are mainly influenced by changes in upwelling intensity and biological productivity, as indicated by their correlation with the marine organic carbon record (Schneider et al., 1994). The planktonic $\Delta\delta^{13}C$ record contains a strong 23-kyr cyclicity, with minima of $\Delta\delta^{13}C$, i.e., maxima of upwelling, aligned to minima in the austral winter insolation over northern Africa, the inferred forcing function for precessional variations in upwelling and monsoon strength (Prell and Kutzbach, 1987). A comparison of TOC records with SST time series suggested that in the equatorial Atlantic east of 15°W wind-driven upwelling controls productivity and SST variability, generating mainly 100-kyr and 23-kyr cycles during the Late Quaternary (Schneider et al., 1996). It was suggested that the 'excess siliceous production' was elevated during increased northern African monsoonal precipitation, leading to a higher dissolved silicate load of the Congo discharge, but that the total paleoproductivity was controlled by the availability of marine nutrients, depending on the stronger upwelling at times of a low northern African insolation and a weak

monsoon (Schneider et al., 1997). The only organic geochemical study of a Late Quaternary sediment core off the coast of Angola yet (Hinrichs et al., 1999), showed, that the abundance of long-chain alkenones, long-chain diols and loliolide all correlate with estimates of paleoproductivity. Also the long-chain even-numbered fatty acids, presumably transported by dust, correlate with this group and were thus interpreted to reflect the wind strength, driving the coastal upwelling. The phytosterols and sterols from zooplankton did not correlate with the productivity-group and were therefore inferred to reflect a more non-specific, heterogeneous origin with unknown microalgae sources, which responded differently to the nutrient changes than the main primary producers (Hinrichs et al., 1999).

Records, which document the long-term climatic development in the eastern tropical Atlantic, were until recently mainly derived from ODP Leg 108 (Ruddiman et al., 1989b). The long-term records of biogenic and terrigenous fluxes show variability in all orbital frequencies, i.e., eccentricity-, obliquity- and precession-related. Thus, they were inferred to contain low-latitude, as well as high-latitude signals (de Menocal et al., 1993). It was suggested, that the low-latitude forcing was stronger in the absence of a high-latitude ice-volume influence, i.e., during times of lower ice volume (de Menocal et al., 1993). The terrigenous (eolian dust) and phytolith (grass cuticle) accumulation rates from these sites show longer periods and increasing amplitudes associated with the intensification of Northern Hemisphere glacial cycles at 2.8 Ma, 1.7 Ma and around 1.0 Ma (de Menocal, 1995; Tiedemann et al., 1994). The strong covariance between the records of organic carbon, biogenic opal and terrigenous matter in the 100- and 41-kyr cycles (de Menocal et al., 1993; Ruddiman and Janecek, 1989; Wagner, 2000) suggests that glacially enhanced dust supply and surface-water mixing caused productivity-driven deposition of marine organic matter.

Recently, sediments of the Congo fan were drilled during ODP Leg 175 (Wefer et al., 1998) enabling the establishment of long-term records from the Angola Basin. During the last 460,000 years, high abundance of diatoms, silicoflagellates and radiolarians point to increased productivity during glacials and cold substages of interglacials (Uliana et al., 2001). Organic carbon contents vary predominantly in precession-related cycles during the last 1 Ma (Holtvoeth et al., 2001). With regard to the MPT, it has been inferred from a statistical analysis of red/blue colour cycles of sediments from the Congo fan, likely indicating variations in primary productivity, that the inferred organic matter supply was higher during glacial periods in the 100-kyr and the 41-kyr cycle (Berger et al., 1998). Largest amplitudes of the colour cycles in the precessional and eccentricity-band occurred during the last 625 kyr BP suggesting that the enlarged variations in global ice volume generally increased the variability of organic matter supply (Berger et al., 1998). Palynological records from the Congo fan indicate an early cooling in the tropics around 1050 kyr BP and a subsequent reduction of the Congo River plume and associated river-induced productivity until around 900 kyr BP, which is interpreted as an aridification of tropical Africa (Dupont et al., 2001). After 900 kyr BP, the Congo River discharge was strongly decreased and an open vegetation developed during warm and dry interglacials (Dupont et al., 2001).

A study of SST variations associated with the MPT in the eastern tropical Atlantic (Schefuß et al., submitted-b) has shown that the tropics followed the climate development of the high latitudes, with a prevalent 41-kyr rhythm before the MPT and a contemporary onset of the 100-kyr cyclicity in SST and ice-volume changes at 650 kyr BP (Fig. 7.2a). In both the 41-kyr and 100-kyr cycles, however,

the tropical SST changes significantly led over the ice-volume variations, likely due to an early response of oceanic and atmosphere modulations on the orbital insolation changes. An 80-kyr cycle occurred in the SST record, likely connected to the 76-kyr transitional cyclicity observed in the mid-Pleistocene ice-volume record. This was likely caused by the re-organisation of the enlarged mean ice volume, which led to premature melting events during the MPT. In line with this interpretation, the 80-kyr SST and ice-volume changes were in phase. The enlarged ice volume suppressed the monsoonal, low-latitude forcing of the SST variations in the tropical Atlantic via compression and intensification of the atmospheric Hadley circulation (Schefuß et al., submitted-b). The long-term development of the SST in the mid-Pleistocene tropical Atlantic was apparently linked to the strength of the thermohaline circulation of the Atlantic. The strong reduction of the NADW formation during the MPT (Raymo et al., 1997) led to a pronounced long-term warming of the tropical Atlantic (Schefuß et al., submitted-b).

The tropical Atlantic SST development has influenced the continental aridity in equatorial Africa by changing the tropical precipitation-evaporation balance (Ganopolski et al., 1998; Schefuß et al., submitted-a). A terrestrial vegetation change in tropical areas associated with an increase in global aridity has earlier been suggested for the MPT (Raymo et al., 1997) and confirmed by pollen records from South America (Hooghiemstra et al., 1993) and equatorial Africa (Dupont et al., 2001). From investigations of C_3/C_4 plant abundance changes during the MPT we inferred that these reflect aridity variations, mainly driven by the tropical SSTs (Schefuß et al., submitted-a). The variations of atmospheric moisture content were controlled by the tropical evaporation-precipitation balance (Ganopolski et al., 1998), and, therefore, driven by the SST changes in the tropical Atlantic. So, the most arid conditions in equatorial Africa occurred at times with the lowest SST in the tropical Atlantic (Schefuß et al., submitted-a).

7.3. Material and Methods

7.3.1. Samples

The 214 samples for this study were obtained from the Ocean Drilling Program (ODP) Site 1077 (Fig. 7.1). The uppermost sample investigated is 175-1077-B-8-H-1-17 cm (62.77 meters below sea floor (mbsf)) and the lowermost sample is 175-1077-B-17-H-6-33 cm (155.93 mbsf). The core is located at 10°26.2'E, 5°10.8'S, in 2382 m water depth about 275 km off the mouth of the Congo River (Wefer et al., 1998).

7.3.2. Stratigraphy

The stratigraphy of ODP Site 1077 is based on a correlation of the oxygen isotope values of the planktonic foraminifer *G. ruber* (pink) to the oxygen isotope record of the eastern Pacific ODP Site 677 (Fig. 7.2b; Dupont et al., 2001; Shackleton et al., 1990). It is discussed in great detail in Schefuß et al. (submitted-b). The benthic $\delta^{18}O$ record of ODP Site 677 (Shackleton et al., 1990) is used as the age-model reference, and also, due to its high temporal resolution (average sample spacing = 2.7 kyr), as an equivalent to the Late Pleistocene SPECMAP ice-volume stack (Imbrie et al., 1989). Based on this stratigraphy, the samples cover the time interval from MIS 12 to 37 (from 457 to 1250 kyr BP). The ages for all 214 samples were determined by linear interpolation between the assigned age control points

resulting in an average time resolution of 3.9 kyr. Sedimentation rates (Fig. 7.2c, SR) were assumed to be linear between the age control points and on average are quite high, i.e., 12.4 cm/kyr. SRs are around 10-13 cm/kyr in the older interval (1300-870 kyr BP) and slightly elevated in the younger section, 14-16 cm/kyr (690-450 kyr BP). From 870 to 690 kyr BP the SRs were slightly lower, around 4-10 cm/kyr with some short periods of very high SRs, i.e., up to 30 cm/kyr around 780 kyr BP. The very high SRs in that period cause all accumulation rates of lipid biomarkers and bulk organic parameters to be elevated. This effect will, however, influence all calculated accumulation records to the same extent and will therefore not have a significant effect on the principal component analysis. Because the influence of the high SR spike is a single and non-periodic event in all records, it will also not substantially offset the spectral analyses and, thus, also not the cross-spectral examination. We will, therefore, not correct for this effect.

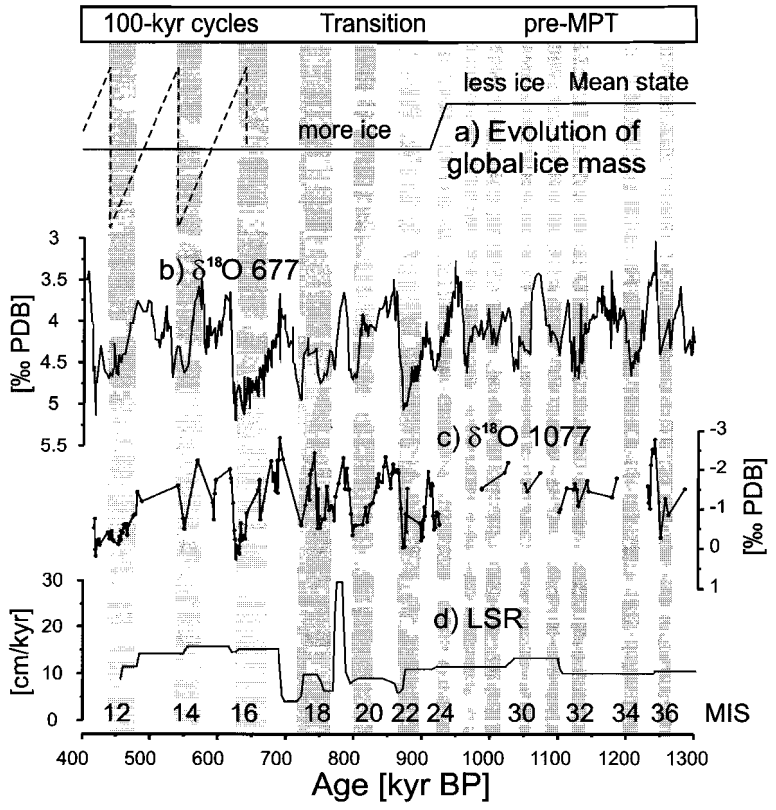

Figure 7.2: a) Schematic development of the global ice volume, based on investigation of several benthic ODP $\delta^{18}O$ records after Mudelsee and Schulz (1997). b) The benthic $\delta^{18}O$ record of ODP Site 677 (Shackleton et al., 1990), used as ice-volume proxy for the mid-Pleistocene and age model template. c) Oxygen isotope stratigraphy based on *Globigerinoides ruber* (pink) from ODP Site 1077 from Dupont et al. (2001). d) Linear sedimentation rates (LSR) based on the age model of ODP Site 1077 after Dupont et al. (2001). Grey bars indicate glacial marine isotope stages (MIS). Both isotope records and the scheme are oriented to less ice-volume conditions to the top.

The accuracy of the stratigraphy of ODP Site 1077 in the main orbital cycles was examined by Schefuß et al. (submitted-b). It was concluded that the age model is sufficiently accurate for phase investigations in the 100- and 41-kyr cycles. To increase the accuracy of the phase determinations in the 100-kyr cycle we decided to use only the younger part of the record, i.e., <900 kyr BP. This was done, because a large eccentricity-related variability of global ice-volume variations (Mudelsee and Schulz, 1997) and tropical SST changes (Schefuß et al., submitted-b) was present only since 650 kyr BP. The coherency between the precession cycles of ODP 1077 and ODP 677 is low, indicating that the precessional lipid biomarker and bulk geochemical signals might be shifted in phase with regard to an external signal, like the global ice-volume development or the orbital insolation forcing. Since, however, mainly records from only one core are compared, we decided to conduct also cross-spectral analyses in the precessional band, keeping in mind the potential phase error with the calculated record of orbital insolation or the $\delta^{18}O$ record of ODP Site 677.

7.3.3. Bulk analyses

Total organic carbon (TOC) contents were measured on a Fisons Instruments NCS-1500 Elemental Analyser. Standard deviations were better than 0.3 %. Stable carbon isotope compositions of the TOC have been determined using the same machine, connected via a ConFlo II interface to a Delta plus Finnigan MAT mass spectrometer. Standard deviations were always better than 0.2 ‰ vs. PDB. Conditions of the bulk measurements are described in Schefuß et al. (submitted-c).

7.3.4. Lipid analyses

Lipid exractions, analyses and identifications were performed following the same procedures as described in Schefuß et al. (submitted-c). The quantification of long-chain alkenones and biphytanediols was performed by integration of their peak areas and those of internal standards in FID chromatograms of the total lipid extracts, while *n*-alkanes were quantified in saturated hydrocarbon fractions. Data acquisition and integration was done using Atlas analytical software. Other lipid biomarkers were quantified using characteristic fragment ions in mass chromatograms of GC-MS analyses. Resulting abundance values were converted to concentrations by compound-specific correction factors determined from clean mass spectra and comparison with GC-FID responses. The relative precision of the entire analytical procedure, based on duplicate sediment extraction, was around 10 %.

The U^{K}_{37}'-index is calculated as the ratio of the di- to the sum of the di- and tri-unsaturated C_{37} alkenones. The conversion of U^{K}_{37}' values to SST estimates was done using the calibration by Müller et al. (1998): SST (°C) = (U^{K}_{37}' - 0.044) / 0.033. The standard error of this relationship is ± 1.0°C. The standard deviation (±σ) based on duplicate and triplicate analyses of the SST estimates of our samples is 0.3°C (or 0.01 U^{K}_{37}' units).

The stable carbon isotopic composition of the individual *n*-alkanes was measured with GC-combustion-isotope ratio monitoring-MS using a Finnigan delta C mass-spectrometer. The analytical procedure is described by Schefuß et al. (re-submitted; submitted-c). $\delta^{13}C$ values are expressed versus PDB. Standard deviations (±σ) were better than 0.5 ‰. The C_4 plant-derived percentage of the *n*-alkanes was calculated in the same way as described by Huang et al. (2000) and Schefuß et al. (re-

submitted). In short, the $\delta^{13}C$ values of the C_{31} *n*-alkanes were converted into a C_4 plant-derived fraction via a binary mixing model, assuming end-member values from the literature (Collister et al., 1994; Rieley et al., 1993): C_3 plant-derived *n*-alkanes = -36.0 ‰, C_4 plant-derived *n*-alkanes = -21.5 ‰.

7.3.5. Principal component analysis

Principal component analysis (PCA) was performed to distinguish groups of the bulk and molecular geochemical variables using the Systat software package (Wilkinson, 1988). The method assigns a loading to each variable, i.e., geochemical parameter, on each factor, representing the degree to which the variable is influenced by that factor, i.e., that environmental process. The calculated factor loadings are VARIMAX-rotated, resulting in the simplest composition of factors, with either minimum or maximum loading of each variable on the extracted factors while preserving trends.

7.3.6. Frequency analyses and filters

Spectral frequency analyses of the investigated records were carried out to determine the main periods, in which the parameters vary and to detect their significance. Analyses were done with the SPECTRUM program, which detects frequency spectra of unevenly spaced time series (Schulz and Statteger, 1997). A Siegel-test was used to identify significant periodic variations. Cross-spectral analyses between the signals were performed to obtain phase relations. The parameters of the spectral and cross-spectral analyses are similar to the procedures described in Schefuß et al. (submitted-b). Gaussian filtering of the records is performed to examine amplitude changes in the various orbital and non-orbital cycles and to isolate the long-term trend from the records. The bandwidths of the filters had been adjusted to solely pass the period under consideration and to suppress other frequencies. The filter characteristics are modified after Ruddiman et al. (1989a).

7.4. Results and Discussion

7.4.1. TOC and $\delta^{13}C_{org}$

Total organic carbon contents (TOC) in the sediments range from 0.8 to 4.0 wt% (Fig. 7.3a). Before 900 kyr BP, the TOC record shows pronounced high-frequency variations with periods around 20 to 25 kyr. After 900 kyr BP, a longer cyclicity is prevalent with generally higher TOC values during glacials and lower during interglacials (Fig. 7.3a). Sedimentary TOC variations are influenced by surface-water productivity, preservation and remineralisation of organic matter and dilution with non-organic constituents, i.e., terrigenous, siliceous material or carbonate. A number of studies have addressed the potential impacts of the various factors on TOC contents (Lyle, 1988; Müller et al., 1994; Sarnthein et al., 1988; Sarnthein et al., 1992; Westerhausen et al., 1993). To correct for the dilution effect by non-organic constituents we calculated the TOC accumulation rates (AR). These were calculated by multiplying the TOC concentrations by the dry bulk density and the linear sedimentation rates. The dry bulk density of the samples showed no large differences in the investigated depth interval and was therefore assumed to be

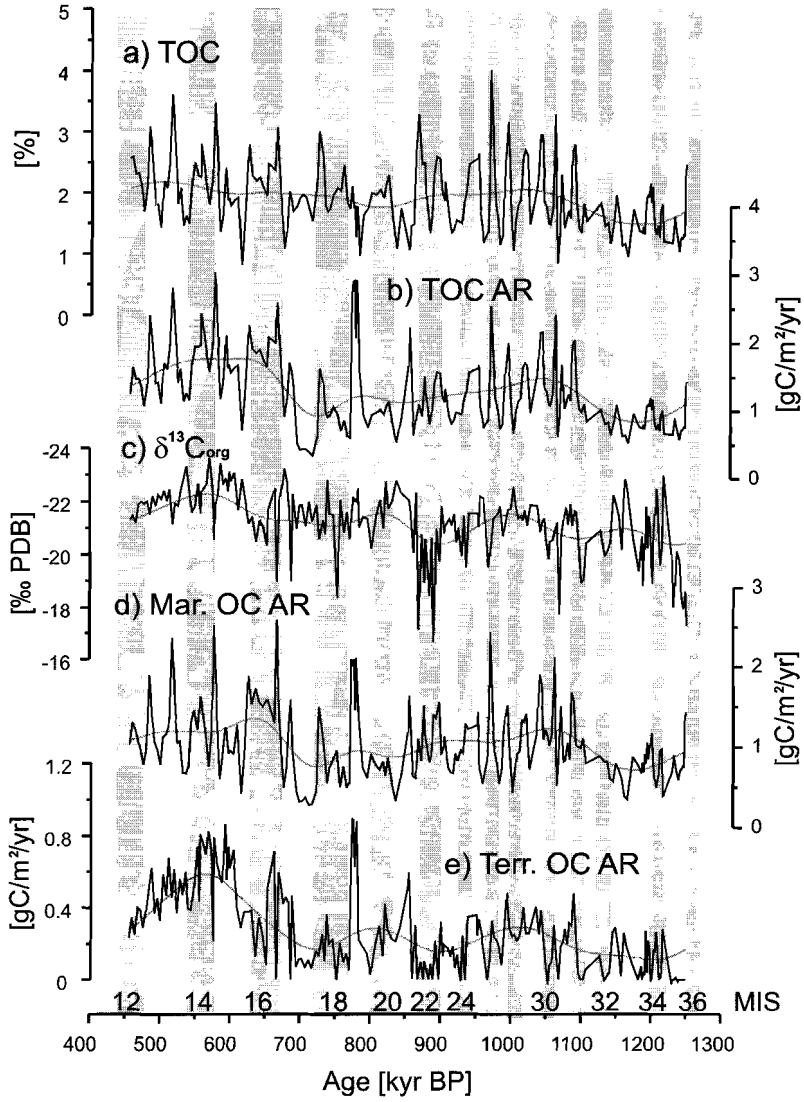

Figure 7.3: Mid-Pleistocene time series of a) TOC (%), b) the accumulation rate (AR) of TOC (gC/m^2/yr), c) the stable carbon isotope composition of the bulk organic material $\delta^{13}C_{org}$ (‰, note axis orientation, lowest values to the top), d) the calculated marine OC AR (gC/m^2/yr), and e) the calculated terrigenous OC AR (gC/m^2/yr). Grey line behind records is long-term-filtered trend (central frequency of 0.004, bandwidth of 0.004 cycles/kyr).

constant as 0.56 g/cm^3 (S. West, personal communication). The TOC AR (Fig. 7.3b) range between 0.4 and 3.0 gC/m^2/yr. The TOC AR record largely resembles the TOC record, because there are no large sudden SR changes in the largest part of the record. When these changes occurred, i.e., around 780 kyr BP, also the TOC ARs were high. During these times of high sediment deposition the preservation of TOC was enhanced by the sealing effect (Jansen et al., 1984; Sarnthein et al., 1992).

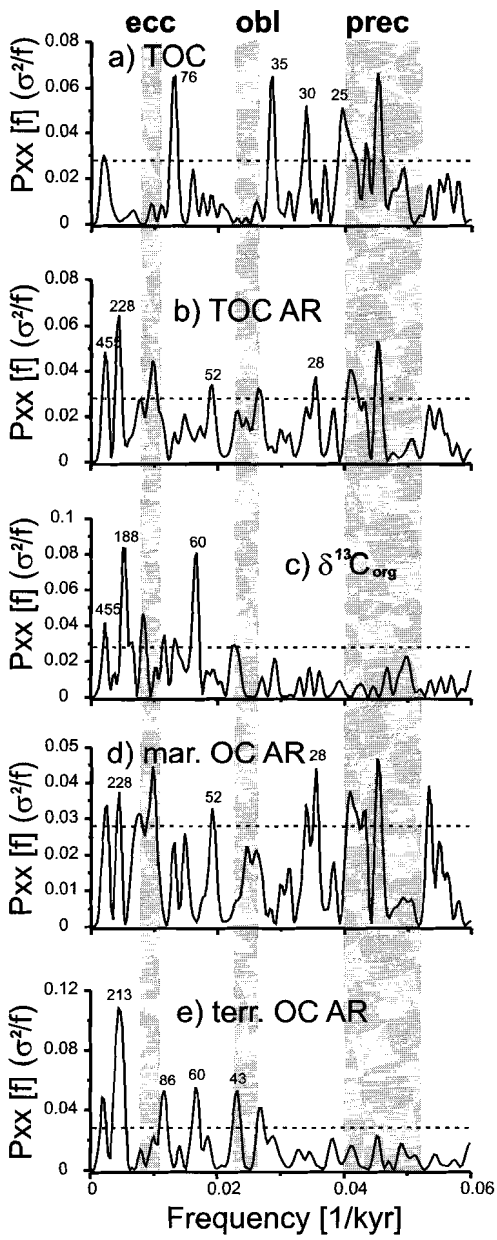

Figure 7.4: Frequency power spectra of the investigated records in the mid-Pleistocene period (400 - 1300 kyr BP), for a) TOC, b) TOC AR, c) $\delta^{13}C_{org}$, d) the marine OC AR, e) the terrigenous OC AR. Grey bars indicate orbital frequency bands. The stippled line is significance after Siegel.

In the frequency domain, the TOC record shows variance in the precessional band, although not centred on one frequency, but spread out over several periods between 22 and 25 kyrs (Fig. 7.4a). The distinct 76-kyr period is possibly related to the transitional 76/80-kyr period in the ice-volume and SST variations described for the MPT (Mudelsee and Schulz, 1997; Schefuß et al., submitted-b). This will be discussed below. The TOC AR frequency spectrum (Fig. 7.4b) contains, beside the precessional cycles, more power in the 100-kyr band and in long cycles, the latter representing the long-term trend. The long-term trend of the TOC AR, as well as the TOC, record explains a large portion of the signal variance (Fig. 7.3a,b). It shows high values between 1100 and 1000 kyr BP and from about 650 to 500 kyr BP.

The stable carbon isotope compositions ($\delta^{13}C_{org}$) provide insight in the nature of the organic matter and vary between -16.7 and -23.6 ‰ (vs. PDB, Fig. 7.3c). Over the whole investigated interval there appears to be a long-term decrease of the $\delta^{13}C_{org}$ values, overlain by a rather irregular scatter. An exception is detected between 890 and 868 kyr BP with the occurrence of substantially enriched values. The isotopic value for marine organic matter falls in the range of -18.5 to -21.5 ‰ (Fischer et al., 1998; Goñi et al., 1998; Tyson, 1995; Westerhausen et al., 1993). The $\delta^{13}C_{org}$ values of ODP 1077 therefore may indicate predominant marine sources of the organic matter. However, the

contribution of terrestrial organic matter is not easy to assess. The stable carbon isotopic signature of terrigenous organic matter differs for C_3 and C_4 plants. C_3 plant-derived organic matter has bulk $\delta^{13}C$ values around -27.0 ‰ (-25.5 to -29.3 ‰), while C_4 plants have $\delta^{13}C$ values around -12.0 ‰ (-8.0 to -19.0 ‰; Sackett, 1989; Tyson, 1995). Particulate organic matter which presently is transported by the Congo River outflow has an unambiguous C_3 plant, i.e., rainforest, isotopic signature ($\delta^{13}C$ = -26.7 ‰; Mariotti et al., 1991), which is also found in surface sediment of the Angola Basin (Schefuß et al., submitted-c). However, this could have been substantially different in the period under investigation. Indeed, we detect the largest expansion of C_4 plants during the interval from 890 to 861 kyr BP (Schefuß et al., submitted-a). This, however, is inferred from isotopic investigation of plant-wax lipids (see below), which are transported by wind and are not associated with bulk organic matter (Schefuß et al., submitted-c). During maximum C_4 plant expansion, however, a contribution of C_4 plant-derived bulk organic matter by the Congo River outflow might thus have been possible. A significant contribution of C_4 plant-derived organic matter during glacials was detected by microscopic maceral analyses of sedimentary organic matter in the equatorial Atlantic (Wagner, 2000) and inferred to be wind-transported, but was also found off the Congo River (Holtvoeth et al., 2001), possibly derived by freshwater outflow. It was thus concluded that the separation of marine and land-derived organic matter based on bulk stable carbon isotopic compositions alone leads to an underestimation of the terrigenous organic matter contribution (Holtvoeth et al., 2001; Wagner, 2000). In our study, however, we do not have an independent measure of the contribution of C_4 plant-derived bulk organic matter other than the $\delta^{13}C$ values available. Since the occurrence of more enriched $\delta^{13}C$ values than for the marine range of -18.5 to -21.5 ‰ is restricted to 10 out of a total of 214 samples, i.e., detected in less than 5 % of the samples, we infer that essentially the relative contributions of marine and C_3 plant-derived determine the $\delta^{13}C_{org}$ values. The exceptional period from 890 to 863 kyr BP will be considered later. In the frequency spectrum of the $\delta^{13}C_{org}$ record (Fig. 7.4c) no significant power can be detected in the orbital frequency bands. Large power occurs in a non-orbital 60-kyr cycle, which origin is unknown, and in the long-term trend showing decreasing $\delta^{13}C_{org}$ values in younger sediment layers.

7.4.2. Marine and terrestrial bulk organic matter

We divided the TOC AR of the sediments into a marine and terrestrial fraction utilising the $\delta^{13}C_{org}$ values and a binary mixing model, assuming a terrestrial C_3 plant ($\delta^{13}C$ = -27.0 ‰) and a marine end-member ($\delta^{13}C$ = -20.0 ‰). Negative values have been adjusted to zero. In this model a change of 1 ‰ in the assumed value of the marine end-member results in a change of 12 % in the proportions of marine and terrestrial organic matter.

Diagenetic alteration of organic material can change its composition and isotopic signature. Terrigenous organic matter experienced extensive degradation, i.e., in tropical soils, prior to its discharge into the marine environment via the Congo River. This implies that only the more refractory terrestrial organic matter ends up in the marine sediments. Marine organic matter is made up for a substantial part of labile components, which can be rapidly degraded under oxic conditions (Hartnett et al., 1998; Hedges and Prahl, 1993). If organic matter degradation would be the

dominant process determining the isotopic signature and composition of the TOC, we should find a general decrease of $\delta^{13}C_{org}$ with increasing depth. However, rather the opposite is observed (Fig. 7.3c). Consequently, organic matter degradation plays a minor role in controlling the isotopic composition of the bulk organic matter.

The marine OC AR (Fig. 7.3d), ranging between 0.3 and 2.6 $gC/m^2/yr$, closely resembles the record of TOC AR. As for the latter, we can detect high frequency, precessional variations in the older section from 1100 to 900 kyr BP, and more glacial-interglacial-related changes in marine OC AR in the younger part. The absolute amplitude of the marine organic carbon deposition in the two periods, however, does not differ substantially. In the frequency domain, the spectrum of the marine OC AR (Fig. 7.4d) is very similar to the spectrum of the TOC AR. Strong power is detected in various precessional-related cycles with periods from 19 to 25 kyrs. There is less power in the obliquity cycle, while the power of the 100-kyr cycle resembles that of the precessional cycles. The long-term trend shows relatively high values between 1100 to 1000 and 650 to 500 kyr BP. All these features are thus comparable to the TOC AR record.

Apparently, the mid-Pleistocene accumulation of marine OC and TOC depended on the same processes as in the Late Quaternary. Both times show a predominance of precession and eccentricity cycles (Schneider et al., 1994, 1996). In analogy, we suggest that the marine OC deposition, primarily reflecting marine productivity (Lyle, 1988; Sarnthein et al., 1988; Schneider et al., 1996; Wagner, 2000), was mainly driven by the strength and zonality of the trade winds during the mid-Pleistocene (Prell and Kutzbach, 1987). We infer that marine OC and TOC accumulations were mainly caused by wind-driven upwelling (Schefuß et al., submitted-b). The precessional variations in low-latitude insolation caused a cyclic variation of trade-wind zonality (McIntyre et al., 1989; Prell and Kutzbach, 1987), while the large ice volumes of the 100-kyr cycle caused increased zonal strength of the trades via a steeper thermal gradient of the Southern Hemisphere (de Menocal and Rind, 1993; Jansen et al., 1996; Manabe and Broccoli, 1985; McIntyre et al., 1989; Schneider et al., 1996). The variations in wind strength in the obliquity cycle were probably too small to exert a large effect on upwelling intensity in the tropics. Examination of the phasing in each cycle with respect to orbital forcing will be done below. The mid-Pleistocene marine OC AR record (Fig. 7.3d) can therefore roughly divided in two parts which are characterised by different a forcing mechanism. Before 900 kyr BP, precessional variability was strong, while after the growth of additional global ice volume, an interglacial-glacial rhythm was predominant. This suggests a weakening of the low-latitude insolation forcing by the increase of the mean global ice volume, already concluded from an examination of the mid-Pleistocene SST variability (Schefuß et al., submitted-b).

The record of the terrigenous OC AR (Fig. 7.3e) varies from 0 to 0.9 $gC/m^2/yr$. Its development is dominated by a long-term increase. Slightly elevated values found around 1000 kyr BP and a strong long-term increase is detected from 700 to 550 kyr BP (Fig. 7.3e). Its frequency spectrum (Fig. 7.4e) shows predominantly a long-term trend. The accumulation of C_3 plant terrigenous organic matter is obviously not primarily related to climatic variations in orbital cycles, either to changes in wind strength or direction or to changes in river runoff. The accumulation of terrestrial organic matter apparently only correlates with the contribution of bulk terrigenous material, i.e., inorganic and organic, as reflected by the sedimentation rate (Fig. 7.2c), even when taken into account that the terrestrial

organic carbon might be underestimated by neglecting the input of bulk C_4 plant-derived organic matter.

7.4.3. Lipid biomarkers

A wide variety of lipid biomarkers was identified and quantified. We determined biomarker accumulation rates to achieve insight into export production, transport and preservation pattern of the various lipid sources. Although the biomarker accumulation rates cannot be used as a direct measure of the number of contributing organisms, they are useful reconstructive tools to examine the temporal changes in the export flux of specific phytoplankton and changes in the flux of allochthonous, terrigenous compounds. An extensive discussion of the sources of the lipid biomarkers and their significance in the investigated area has been done in a study of their distribution in surface sediments (Schefuß et al., submitted-c), and will not be repeated here. We would like to draw the reader's attention to the detailed description in that paper, whenever more information is wanted.

7.4.3.1. Diagenesis

For any comparative organic geochemical study, it is crucial to account for potential diagenetic alteration of the lipid biomarker concentration or accumulation profiles. The preservation potential of lipid biomarkers during oxic degradation is highly variable, but always low (Wakeham et al., 1998; Wakeham et al., 2002). A general pattern of decreasing preservation potential has been established: the long-chain *n*-alkanes are most stable, followed by the long-chain alkenones, which are equally resistant as the long-chain diols, and the sterols are least stable against oxic degradation. The oxygen-exposure-time in the sediments has been shown to play the dominant role in determining the preservation of lipid biomarkers (Hartnett et al., 1998; Hoefs et al., 2002; Sinninghe Damsté et al., 2002b). In recent surface sediments from the area the penetration depth of pore water oxygen lies between 0.5 and 2 cm (J. van Bennekom, unpublished results). With the high sedimentation rates of ODP Site 1077, i.e., 12.4 cm/kyr on average, the oxygen exposure time would have been between 50 and 200 years. The lipid biomarkers were thus removed from the oxic surface-sediment layer quite rapidly, leading to a relatively good preservation of the primary signal. We conclude, therefore, that the biomarker ARs in ODP 1077 were mainly controlled by the primary production and variable contributions of allochthonous lipids, and that oxic degradation had only a minor influence.

7.4.3.2. Long-chain alkenones

C_{37} alkenones are exclusively biosynthesised by some Haptophyte algae, among which are the open marine species *Emiliania huxleyi* and *Gephyrocapsa spp.* (Marlowe et al., 1984; Volkman et al., 1995; Volkman et al., 1980), and occur widespread in marine sediments, including the South Atlantic (Brassell et al., 1986a). Because changes in coccolithophore assemblage composition does not seem to affect the alkenone production pattern (Müller et al., 1997), the sedimentary alkenone concentrations have been used as an indicator of Haptophyte productivity (Hinrichs et al., 1999; Schubert et al., 1998; Villanueva et al., 1998). The ARs of the C_{37} alkenones were relatively small and show small variations before 780 kyr BP (Fig. 7.5a). Afterwards, their ARs strongly increased. In the frequency spectrum we

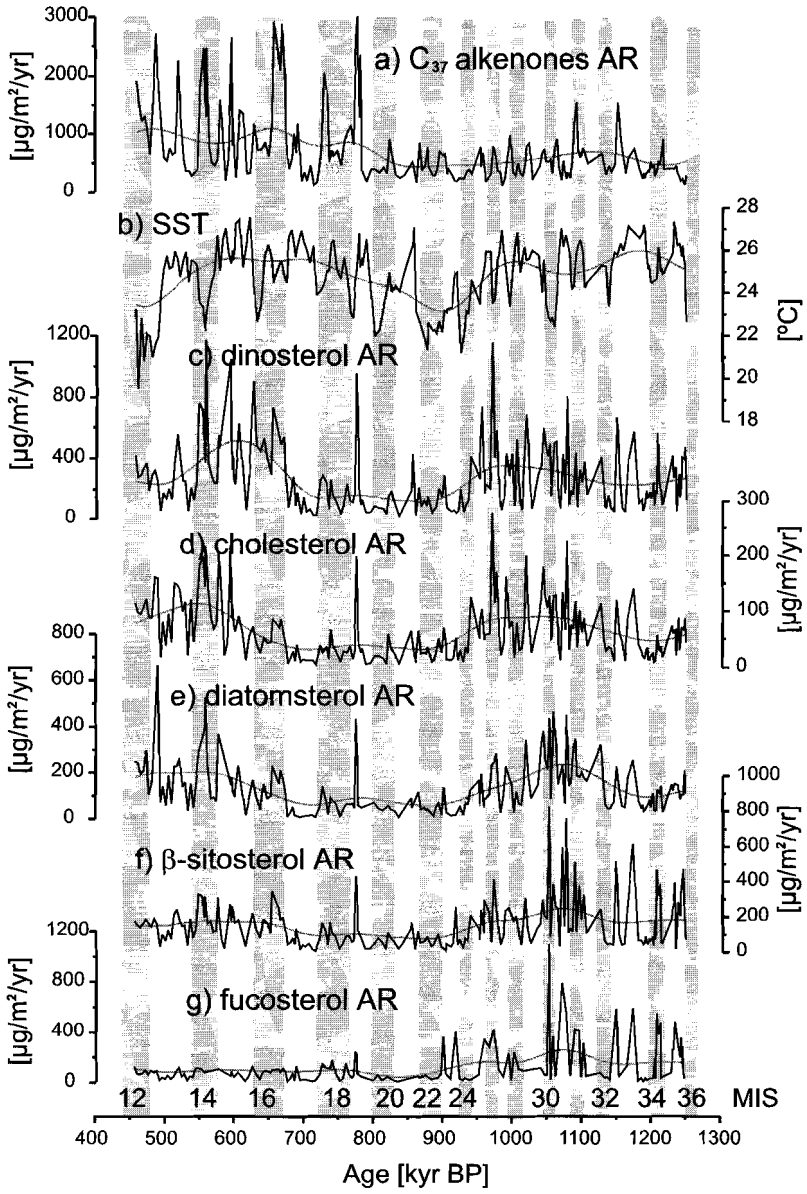

Figure 7.5: Times series of a) the C_{37} alkenone AR, b) the alkenone-based SST estimates (in °C), c) the dinosterol AR, d) the cholesterol AR, e) diatomsterol AR, f) β-sitosterol AR, g) fucosterol AR. All AR in µg/m^2/yr. Grey line behind records is long-term-filtered trend (central frequency of 0.004, bandwidth of 0.004 cycles/kyr).

detect strong power in a 100-kyr cycle (Fig. 7.6a), which indicates that the export flux of C_{37} alkenones substantially increased during the large 100-kyr glacials and responded to the growth of the global ice mass during the MPT, albeit with a delay. From the C_{37} alkenone distributions in surface sediments of the Angola Basin was

concluded that these compounds are mainly produced during coastal upwelling which does not lead to surface-water enrichment with dissolved silicate. The intensification of the 100-kyr cycle, therefore, presumably strengthened the coastal upwelling activity.

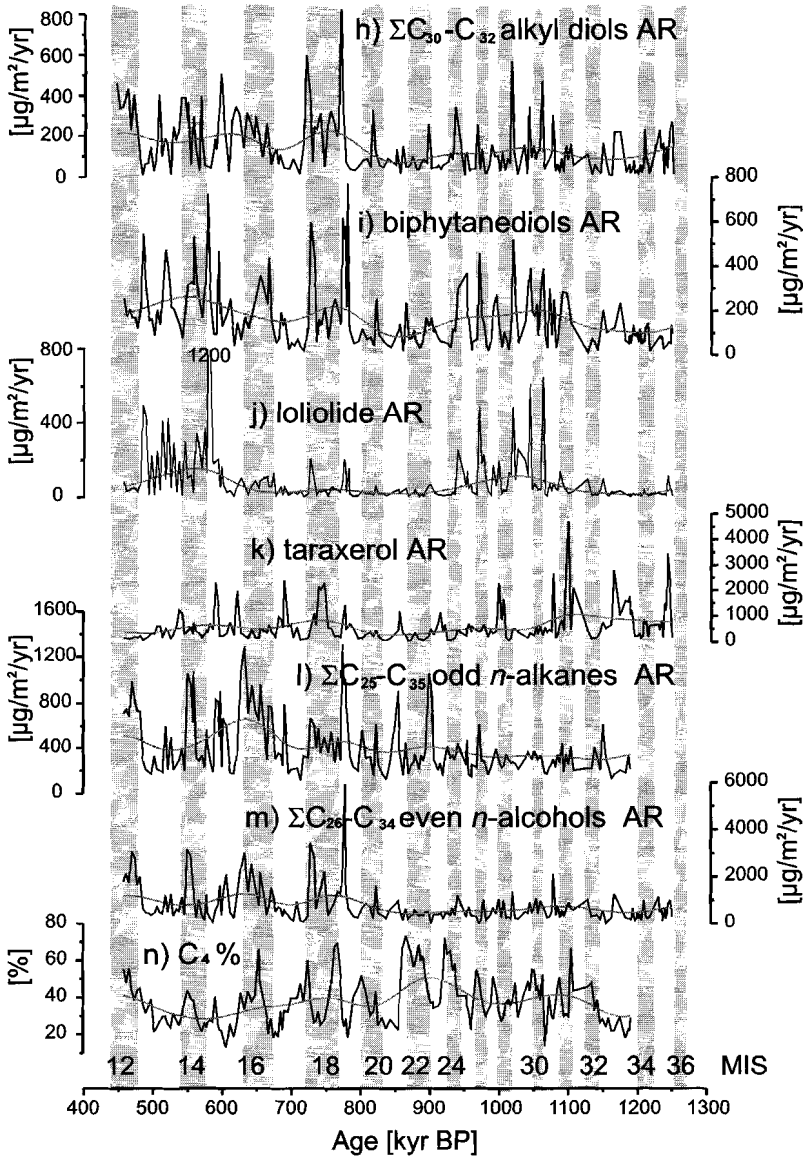

Figure 7.5 continued: Times series of h) the C_{30}-C_{32} alkyl diols AR, i) the biphytanediol AR, j) the loliolide AR, k) the taraxerol AR, l) the AR of the C_{25}-C_{35} odd-numbered *n*-alkanes, m) the C_{26}-C_{34} even-numbered *n*-alcohol AR, and n) the C_4 percentage of the *n*- alkanes (in %).

The ratio of the di- to the sum of the di- and tri-unsaturated C_{37} alkenones, the U^{K}_{37}'-index is used as a sea-surface temperature estimate (Brassell, 1993; Müller et al., 1998; Prahl and Wakeham, 1987). The SST record established from ODP 1077 (Fig. 7.5b) was examined in great detail with respect to forcing in orbital and non-orbital cycles (Schefuß et al., submitted-b). It was shown that the development of the tropical SSTs during the MPT were driven by an interaction of changes in insolation, global ice volume and thermohaline ventilation (Schefuß et al., submitted-b). In its frequency spectrum (Fig. 7.6b) a pronounced long-term trend, an 80-kyr and a 41-kyr cycle are detected. The increase in the 100-kyr amplitude is found at 650 kyr BP, coinciding with the increase in power of the 100-kyr ice-volume changes (Schefuß et al., submitted-b). The tropical SST variations thus followed the rhythm paced by the climate development in the high latitudes (Schefuß et al., submitted-b). In the two longer orbital cycles the tropical SST responded significantly earlier on changes in the Earth's insolation than global ice volume did, which is attributed to early changes in the thermal gradient of the South Atlantic (Schefuß et al., submitted-b). In the 80-kyr cycle, however, no early response is detected, likely because these variations result from ice-volume changes directly and were not preceded by an insolation change. Strong precessional variations in the tropical SST record occurred only during periods of small ice volume. A strengthened Hadley circulation at times of a large ice volume presumably suppressed the low-latitude insolation forcing of equatorial upwelling. The long-term development of SST is most probably linked to the strength of the Atlantic deep ventilation, which shows the strongest reduction during the MPT over the last 3 Ma (Raymo et al., 1997; Raymo et al., 1990; Schmieder et al., 2000). Surface-water heat accumulated in the tropical Atlantic Ocean over the course of the MPT, causing the long-term warming between 900 and 550 kyr BP (Schefuß et al., submitted-b).

7.4.3.3. Sterols

4α,23,24-Trimethylcholest-22-en-3β-ol (dinosterol) is almost uniquely produced by dinoflagellates (Boon et al., 1979; Robinson et al., 1984). Minor quantities occur in diatoms (Volkman et al., 1993) and some dinoflagellate species do not contain this sterol (Goad and Whithers, 1982). The dinosterol AR record (Fig. 7.5c) shows two periods with increased mean ARs, i.e., from 1300 to 950 kyrs BP and from 700 to 500 kyrs BP. Its frequency spectrum (Fig. 7.6c) contains, besides a strong long-term trend, variability in the 100-kyr cycle and also in precessional periods. Weak power is present in the obliquity band. The dinosterol distribution in the surface sediments shows that the contribution of dinosterol is related to wind-driven mixing of river nutrients with oceanic nutrients from below a shallow thermocline in the area of the river plume and oceanic upwelling (Schefuß et al., submitted-c). The abundance of dinosterol thus likely depends on two factors, i.e., the availability of river nutrients and wind-driven mixing. For this reason, we find high dinosterol ARs in the period before 900 kyr BP with a strong precessional variability in river runoff, as well as during period of strengthened trade winds after 900 kyr BP (Fig. 7.5c).

Cholesta-5-en-3β-ol (cholesterol) is produced by a variety of planktonic organisms, including dinoflagellates, diatoms and haptophyte algae (Volkman, 1986). It is a common sterol in diatoms, although most species do not contain large amounts (Volkman, 1986). Zooplankton was found to be a major source of cholesterol in the Peru upwelling system through dietary alteration of phytosterols (Volkman et al., 1987). Based on its surface-sediment distribution (Schefuß et al.,

submitted-c) it was concluded that cholesterol in the Congo River plume is primarily related to the recycling of the river-induced primary production by zooplankton. The record of the cholesterol AR (Fig. 7.5d), for this reason, resembles the dinosterol ARs (Fig. 7.5c), both being on average high at times of either high river-induced or high productivity by wind-driven upwelling. Also the frequency spectrum of the cholesterol AR (Fig. 7.6d) is very similar to that of dinosterol (Fig. 7.6c).

The occurrence of C_{28} 24-methylcholesta-5,22-dien-3β-ol (diatomsterol) in sediments is thought to be characteristic for diatoms (Patterson, 1987; Volkman, 1986). However, in a survey of 14 marine diatom species, it was only detected in three species (Barrett et al., 1995), and, moreover, occurs also in cultures of dinoflagellates (Goad and Whithers, 1982; Teshima et al., 1980) and Haptophyte algae (Marlowe et al., 1984; Volkman et al., 1998). In the water column, it was found after massive blooms of *Emiliania huxleyi* (Conte et al., 1995). From the surface sediments, however, it was concluded that diatomsterol might well be indicative for diatom production (Schefuß et al., submitted-c), relating strongly to the availability of dissolved silicate supplied by the Congo River. Its accumulation record (Fig. 7.5e) and frequency spectrum (Fig. 7.6e) are similar to that of dinosterol. However, contrary to the long-term trend of the dinosterol AR, the diatomsterol ARs are on average higher before the ice-volume growth at 900 kyr BP, i.e., during the time of a dominant precessional forcing (Fig. 7.5e). This suggests that the productivity of diatoms much more depends to the availability of dissolved silicate from Congo River runoff than on wind-driven surface-water mixing.

24-Ethylcholest-5-en-3β-ol (β-sitosterol) is one of the major sterols found in terrestrial higher plants (Goad and Goodwin, 1972; Huang and Meinschen, 1976). Its occurrence in highly productive oceanic settings, however, is attributed to non-specific planktonic sources (Volkman, 1986). This compound has been reported from diatoms, green algae and cyanobacteria (Barrett et al., 1995; Volkman, 1986). Based its surface-sediment distribution off the Congo River, it was inferred that the occurrence of β-sitosterol in this area is most likely related to diatom productivity, like diatomsterol (Schefuß et al., submitted-c). Its frequency spectrum (Fig. 7.6f) also resembles that of diatomsterol (Fig. 7.6e). The high ARs of β-sitosterol from 1300 to 900 kyr BP (Fig. 7.5f) indicate a large contribution of diatom lipids to the sediments during a time of high diatom productivity, associated with a high silicate availability in the surface waters due to large river runoff. However, contrary to diatomsterol, β-sitosterol seems to be even more indicative for a specific diatom input in this area. Its long-term ARs are far higher in the period of precession-dominated variability before 900 kyr BP, than during the wind-driven production regime afterwards.

An even more specific contribution of diatoms is probably indicated by 24-methylcholesta-5,24(28)-dien-3β-ol (fucosterol). It is the major sterol compound in many diatom species (Patterson, 1991), appearing to be more prevalent in centric species (Barrett et al., 1995; Patterson, 1991; Volkman, 1986). It has, therefore, been suggested that this sterol is more indicative for a lipid contribution from diatoms than 24-methylcholesta-5,22-dien-3β-ol (Volkman et al., 1998). In surface sediments off the Congo River, the occurrence of fucosterol was related to a shallow upwelling activity right in the vicinity of the river mouth, where high concentrations of dissolved silicate are available (Schefuß et al., submitted-c). The AR record of fucosterol (Fig. 7.5g) shows high ARs from 1250 to 1050 kyr BP, during the period

with a strong precessional cyclicity in marine productivity (Fig. 7.3d). This suggests a strong influence of monsoonal silicate supply on coastal productivity during that time.

All the AR records of the sterol biomarkers are generally produced in the zone of high marine productivity off the Congo River, however, depending to a different degree on one of the two processes, i.e., wind-driven oceanic upwelling of marine nutrients (nitrate and phosphate) from below a shallow thermocline and mixing with river nutrients (dissolved silicate) or supply of dissolved silicate with the Congo River runoff. The latter, apparently, mainly determines the accumulation of diatom lipids.

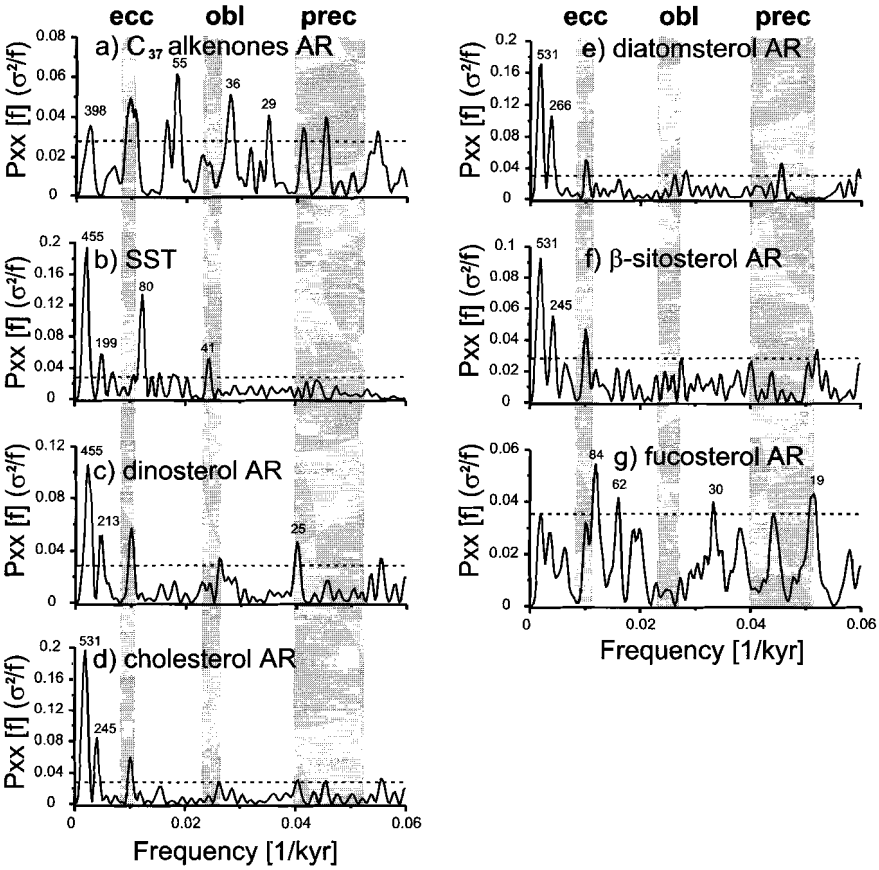

Figure 7.6: Frequency power spectra of a) the C_{37} alkenone AR, b) the alkenone-based SST estimates, c) the dinosterol AR, d) the cholesterol AR, e) diatomsterol AR, f) β-sitosterol AR, g) fucosterol AR. Grey bars indicate orbital frequency bands. The stippled line is significance-test after Siegel.

7.4.3.4. Diols

As major source of long-chain saturated C_{30} and C_{32} alkyl diols, yellow-green microalgae of the class *Eustigmatophyceae* have been indicated (Volkman et al., 1992, 1999). Recently, it has been shown that 1,14 C_{28} and 1,14 C_{30} alkyl diols are

produced by marine diatoms of the genus *Proboscia* (Sinninghe Damsté et al., in press). To prevent any misleading interpretations, we, therefore, have omitted the C_{28} diols from our considerations, although neither the C_{28}, nor the C_{30} alkyl diols contain a large fraction of the 1,14 isomer (E.S., unpublished results). The C_{30} and C_{32} alkyl diols have been detected in sediments from various areas, including the South Atlantic (de Leeuw et al., 1981; Versteegh et al., 1997). In the surface sediments from the Angola Basin the maximum abundance of these alkyl diols occur in the outer Congo River plume area (Schefuß et al., submitted-c).

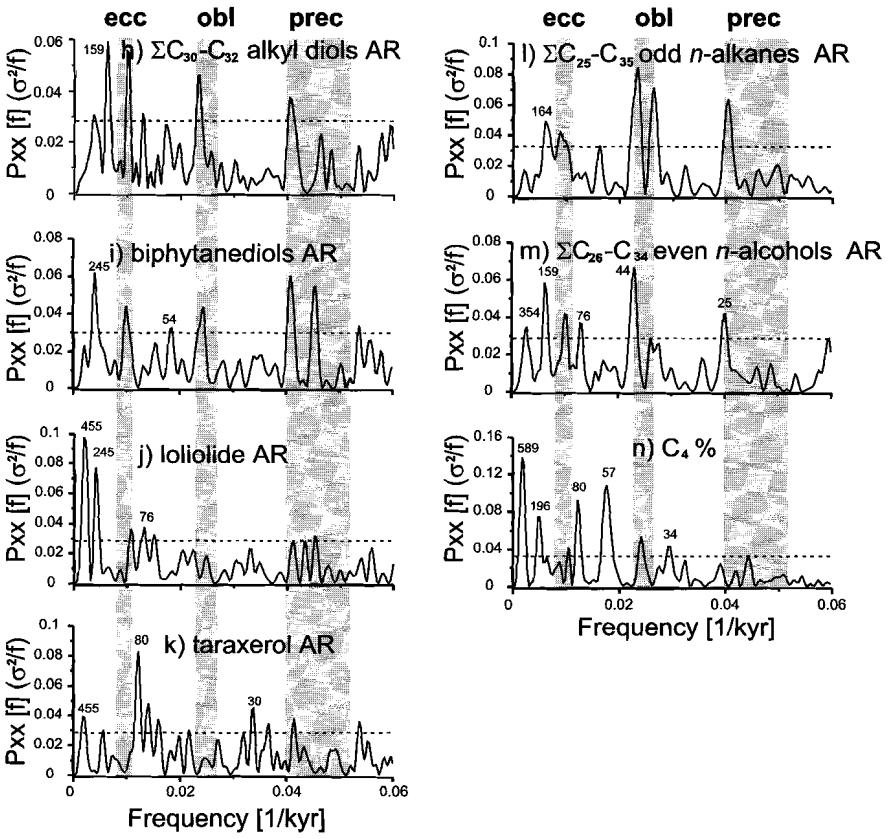

Figure 7.6 continued: Frequency power spectra of h) the C_{30}-C_{32} alkyl diols AR, i) the biphytanediol AR, j) the loliolide AR, k) the taraxerol AR, l) the AR of the C_{25}-C_{35} odd-numbered *n*-alkanes, m) the C_{26}-C_{34} even-numbered *n*-alcohol AR, and n) the C_4 percentage of the *n*-alkanes. Grey bars indicate orbital frequency bands. The stippled line is significancetest after Siegel.

The production of these compounds relates mainly to the wind-driven mixing of the surface waters with subsurface nutrients. Eustigmatophyte algae do not utilise silicate, so they do not depend on riverine supply of dissolved silicate. The ARs of the summed C_{30} to C_{32} alkyl diols (Fig. 7.5h) show some short increases, possibly precession-related, before 780 kyr BP. From that period onwards, the C_{30} to C_{32} alkyl diols-AR shows a 100-kyr rhythm with strongly increased AR values in

glacials. The frequency spectrum (Fig. 7.6h) contains the highest power in the eccentricity band. We infer that the AR of the alkyl diols relates to wind-driven oceanic upwelling without any significant surface-water enrichment with dissolved silicate. The productivity of eustigmatophyte algae was strongly enhanced by the strengthened zonal trade winds after the ice-volume growth at the MPT.

Two C_{40} cyclic biphytanediols in the samples were identified as the C_{40} dicyclic and tricyclic biphytanediol, biosynthesised by planktonic archaea in the water column (Hoefs et al., 1997; Schouten et al., 1998). These marine, non-thermophilic archaea occur widespread in the World's ocean (Schouten et al., 2000b). Depth distributions in suspended particulate material indicate that the occurrence of marine archaea is not restricted to the photic zone (Sinninghe Damsté et al., 2002a). The biphytanediols are labile compounds (Sinninghe Damsté et al., 2002a), their occurrence in surface sediments of the Angola Basin appears to be controlled by anoxic or sub-oxic conditions relating to a less intense oxic degradation of the organic matter (Schefuß et al., submitted-c). Elevated ARs of the biphytanediols occur between 1100 to 950 kyr BP and from about 550 kyr BP onwards (Fig. 7.5i). The frequency spectrum contains power mainly in the precession and eccentricity periods (Fig. 7.6i). The accumulation of biphytanediols was elevated during the period with a precession-dominated variability in marine OC AR, but also in the period of increased wind-driven upwelling. The biphytanediol AR record resembles the AR record of marine OC (Fig. 7.3d), TOC (Fig. 7.3b), but also of dinosterol (Fig. 7.5c), and, to a lesser extent, of cholesterol (Fig. 7.5d). This suggests that a higher abundance of biphytanediols is caused by less severe oxic degradation caused by high organic matter accumulation, as concluded already from the investigation of the distribution of biphytanediols in the surface sediments.

7.4.3.5. Loliolide and *iso*-loliolide

Loliolide and *iso*-loliolide are products of anaerobic degradation of some carotenoids, like fucoxanthin, the major carotenoid in diatoms and haptophytes (Klok et al., 1984; Repeta, 1989). Loliolide was inferred to be useful as indicator of elevated marine productivity (Hinrichs et al., 1999). Based on the examination of the lipid distributions in surface sediments, it was inferred, however, that the occurrence of loliolide, like that of the biphytanediols, was related to a less severe oxic degradation of labile organic matter and is not indicative for a specific phytoplankton input (Schefuß et al., submitted-c). Fucoxanthin is transformed into loliolide only under sub-oxic or anoxic conditions in the sediments (Klok et al., 1984; Repeta, 1989), which were likely to established by elevated organic carbon accumulation. Therefore, an indirect connection exists between elevated organic mater accumulation, often used to calculate productivity estimates, and the abundance of loliolide (Hinrichs et al., 1999). The record of loliolide ARs (Fig. 7.5j) partly resemble the record of the biphytanediol ARs (Fig. 7.5i). Its frequency spectrum is dominated by the long-term trend, with some small power found in eccentricity- and precession-related cycles (Fig. 7.6j). Elevated loliolide ARs occurred in two periods, from 1100 to 950 kyr BP and from 600 to 480 kyr BP. These times were characterised by enhanced marine OC AR (Fig. 7.3d), which presumably led to oxygen depletion in the surface sediments. Loliolide abundance may thus be very sensitive to variable oxygen exposure times, possibly even more than the biphytanediols.

7.4.3.6. Taraxerol

The pentacyclic triterpenol taraxer-14-en-3β-ol (taraxerol) occurs widespread in higher plants (Beaton et al., 1955; Killops and Frewin, 1994) and in marine sediments (Brassell and Eglinton, 1983; ten Haven and Rullkötter, 1988; Volkman et al., 1987). Mangrove vegetation appears to be a major source for taraxerol in marine sediments (Ghosh et al., 1985; Killops and Frewin, 1994). At present, the dominant mangrove species in the Congo area is *Rhizophora racemosa*, which inhabits the seaward edge of the mangrove belt (Breteler, 1969; Moguedet, 1980). We examined leaves of *R. racemosa*, collected in the vicinity of Libreville, Gabon, and found taraxerol as the most abundant compound in the inner-leaf fraction (E. Schefuß, unpublished results). In another widespread African mangrove species, *Rhizophora mangle*, taraxerol is a major constituent of the cutin fraction of the leaves (Frewin et al., 1993; Killops and Frewin, 1994). We, therefore, infer that the mangrove vegetation along the coast of equatorial Africa is the major source of taraxerol found in the sediments. Maximum concentrations of taraxerol have been detected in sediments off the Congo River mouth (Schefuß et al., 2001). We, therefore, suggest that the abundance of taraxerol in sediments is related to the extent of the mangrove vegetation along the coast. Two environmental factors have been inferred to primarily control the extension of mangroves, e.g., sea-level changes and sea-surface temperatures (SST) at the coast (Woodroffe and Grindrod, 1991). The ARs of taraxerol in the mid-Pleistocene ODP 1077 sediments show short periods of strongly increased values (Fig. 7.5k). These spikes are exceptionally large in the period before 900 kyr BP, while a second, although smaller, long-term maximum is found from 800 to 550 kyr BP. The frequency spectrum (Fig. 7.6k) shows some power in precession cycles. The largest power is, however, detected for a 82-kyr cyclicity. The 80-kyr cycle has also been detected in the mid-Pleistocene SST variations (Fig. 7.6b), and was concluded to be a direct response of the tropical SST on the ice-volume changes during the MPT (Schefuß et al., submitted-b). We will examine below (section 7.4.4.2.) what were the principal driving forces for variations of the taraxerol ARs, reflecting contribution changes from mangrove vegetation.

7.4.3.7. Plant-wax lipids

Homologous series of long-chain *n*-alkanes and *n*-alkanols are abundant constituents of terrestrial higher plant epicuticular waxes (Eglinton and Hamilton, 1963), occurring as protective coating on leaves and stems. These lipids are typical terrigenous lipids found in marine sediments (Bird et al., 1995; Huang et al., 2000; Kuypers et al., 1999; Poynter et al., 1989). Leaf waxes of terrestrial higher plants contain predominantly odd-numbered *n*-alkanes and even-numbered *n*-alkanols, which is expressed as high (>5) Carbon Preference Index (CPI; Eglinton and Hamilton, 1963; Kolattukudy, 1976; Mazurek and Simoneit, 1984; Tulloch, 1976). Marine-derived *n*-alkanes longer than C_{23} have essentially no carbon-number predominance (CPI $\approx$ 1). Plant waxes can be washed off the leaf surface by rain and transported into the ocean by freshwater runoff (Bird et al., 1995), but are also easily sloughed off by wind and can become airborne (Simoneit, 1977). Plant-wax lipids are found in aerosol samples from the eastern Atlantic (Cox et al., 1982; Lepple and Brine, 1976; Schefuß et al., re-submitted; Simoneit, 1977; Simoneit et al., 1977; Simoneit et al., 1988). The spatial distributions of the plant-wax lipids in surface sediments of the Angola Basin resemble a broad plume, originating in the dry grass savannahs of southern Africa and stretching out below the trade-wind

trajectory (Schefuß et al., submitted-c), indicating that most of the plant-wax compounds were wind-transported.

The *n*-alkanes in the investigated ODP 1077 sediments are predominantly derived from higher plant waxes (CPI = 2.1-5.3). The *n*-alkane ARs were small and show only minor variation before 900 kyr BP (Fig. 7.5l). From this time onwards, the accumulation of plant-wax alkanes strongly increased. The *n*-alkane ARs were thus apparently driven by ice-volume changes from 900 kyr BP onwards. However, they became sensitive to ice-volume changes only after the ice mass had grown to its enlarged Late Pleistocene mean volume. The first substantial increase in AR occurred right after the growth of additional ice mass at the MPT (Mudelsee and Schulz, 1997). The enhancement of dust-derived terrigenous accumulation at the increase of glacial climate amplitudes at 900 kyr BP has already been inferred from marine sediments off NW-Africa and in the equatorial Atlantic (de Menocal, 1995; de Menocal et al., 1993; Ruddiman and Janecek, 1989; Ruddiman et al., 1989a; Ruddiman et al., 1989b; Tiedemann et al., 1994; Wagner, 2000). The increases in *n*-alkane ARs might thus indicate stronger trade winds or a northward shift of the trade-wind belt. Most likely, a combination of both processes occurred. During periods of enlarged ice volume the South Atlantic high-pressure system was pushed northwards by an extra latitudinal shift of 3-5°, in addition to its seasonal shift of 6-8° (Imbrie et al., 1993), displacing the trade-wind belt northwards. The steeper pressure gradient over the South Atlantic compressed and intensified the atmospheric Hadley-circulation, strengthening the zonal trade-wind vector and enhancing the offshore-directed wind speed (de Menocal and Rind, 1993; Manabe and Broccoli, 1985). The increased *n*-alkane accumulation rates during glacials could, however, also be due to a shift in vegetation supplying a higher flux of plant waxes or a higher vegetation density in the more northern source area, causing an increased glacial *n*-alkane supply. Regardless of the exact combination of processes, the increased glacial *n*-alkanes fluxes after 900 kyr BP were the response on the enlarged mean ice volume since the MPT. The frequency spectrum of the *n*-alkane ARs during the MPT contains power in all orbital frequencies (Fig. 7.6l).

The accumulation of long-chain even-numbered *n*-alcohols in sediments of ODP 1077 (Fig. 7.5m) resembles the AR record of the plant-wax *n*-alkanes (Fig. 7.5l) due to their common origin. The increase in *n*-alcohol AR, however, appear to have occurred later than the shift to higher *n*-alkane ARs. Apparently, the AR of *n*-alcohols may be less sensitive to the increase in wind strength than of the *n*-alkanes. The differential response will be investigated later in the light of the phase relations between the global ice volume and the *n*-alkane and *n*-alcohol ARs. The frequency spectrum of the *n*-alcohol ARs (Fig. 7.6m) resembles that of the *n*-alkane ARs (Fig. 7.6l).

Compound-specific carbon isotope analyses of leaf-wax lipids can provide information on the carbon-fixation pathway utilised during plant photosynthesis (Collister et al., 1994; O'Leary, 1981; Rieley et al., 1993). *n*-Alkanes from plants using the Calvin-Benson cycle (C_3 plants) have $\delta^{13}C$ values around -36 ‰ (-31 to -39 ‰ vs. PDB), while plants utilising the Hatch-Slack (or dicarboxylic acid) cycle (C_4 plants) have $\delta^{13}C$ values around -21.5 ‰ (-18 to -25 ‰ vs. PDB; Collister et al., 1994; O'Leary, 1981; Rieley et al., 1993). Virtually all trees, most shrubs, and cool-season grasses and sedges use the C_3 pathway, while C_4 photosynthesis is found in warm-season grasses, warm-season sedges, *Amaranthaceae* and *Chenopodiaceae* (Cerling et al., 1993). C_4 plants are thus predominantly found in tropical savannahs, temperate grasslands and semi-deserts (Cerling et al., 1993). Most African

grasslands, like the Sahel and the grass savannahs, are presently dominated by C_4 plant vegetation (Collatz et al., 1998). In marine sediments, the stable carbon isotope composition of *n*-alkanes has been used to determine the contributions by C_3 and C_4 plant organic material (Bird et al., 1995; Huang et al., 2000; Kuypers et al., 1999). Compound-specific stable carbon isotopic analyses of *n*-alkanes in dust collected over the eastern Atlantic have shown that the eolian-transported *n*-alkanes primarily reflect the contemporary vegetation on the continent (Schefuß et al., re-submitted). Plant-wax lipids show a C_4 plant contribution of about 55 % in dust from the southern African dry areas, while off the tropical rainforest regions the C_4 plant-derived fraction in dust is only 30 - 40 % (Schefuß et al., re-submitted). The spatial distribution of the C_4 percentage of the long-chain *n*-alkanes in surface sediments revealed that the wind-transported *n*-alkanes in the surface sediments underlying the trade-wind plume are predominantly derived from C_4 plants mainly reflecting the contemporary vegetation in the source area, the Angolan and Namibian grass savannahs (Schefuß et al., submitted-c). By comparison with the distribution of the bulk $\delta^{13}C$ values, it was concluded that there is apparently no significant contribution of C_4 plant-derived bulk organic matter to the surface sediments associated with the eolian input of plant waxes (Schefuß et al., submitted-c).

The record of the relative C_4 plant contribution shows large variations, i.e., from 20 to 70 %, during the mid-Pleistocene (Fig. 7.5n). From 1200 to 900 kyr BP, the C_4 percentage increased, overlain by precessional variations. After ca. 860 kyr BP, the C_4 percentage decreased to a lower long-term level with some short-term increases afterwards. Besides the obvious long-term trend, the frequency spectrum (Fig. 7.6n) contains power in an 80-kyr, a 57-kyr and a 41-kyr cycle. In a detailed study we have investigated the controlling factors of the C_4 percentage variations (Schefuß et al., submitted-a). It is shown that the C_4 percentage of the *n*-alkanes reflects southern African vegetation changes, which are driven by continental aridity changes (Schefuß et al., submitted-a). These aridity changes are linked to the strength of the monsoon in the precession cycle and to the tropical SST development for longer time scales (Schefuß et al., submitted-a). The interference of the 41-kyr obliquity cycle with the 23-kyr cycle of the monsoonal strength results in the 57-kyr cycle, i.e., 1/57 1/kyrs = 1/23.7 - 1/41 1/kyrs. The tropical SST are coupled with longer-term African continental aridity changes via the evaporation-precipitation balance, as simulated for the last glacial maximum (Ganopolski et al., 1998). While the eolian transport of plant waxes is apparently highly sensitive to global ice-volume variations, the nature of the wind-blown plant material depends solely on the vegetation present on the continent.

The largest expansion of C_4 plant vegetation based on the stable carbon isotope composition of *n*-alkanes is detected for the period from 890 to 861 kyr BP. During this maximum of C_4 plant expansion a contribution of river-transported C_4 plant-derived bulk organic matter by the Congo River might have been possible, which could have led to the exceptionally high $\delta^{13}C_{org}$ values during that time (Fig. 7.3c). As mentioned above, the separation of marine and land-derived organic matter based on stable carbon isotopic compositions alone might underestimate the terrigenous organic matter contribution. Because the occurrence of $^{13}C_{org}$ values, which are higher than expected, is, however, restricted to a short period, we suggest that the contribution of C_4 plant-derived bulk organic matter on average was of limited significance during the mid-Pleistocene.

7.4.4. PCA: Controls and processes

We performed principal component analysis (PCA) to identify groups of molecular and bulk geochemical parameters that show a similar temporal development during the MPT. The PCA (Table 7.1) reveals five dominant factors (groups), each with a latent root (eigenvalue) >1, which explain a cumulative 82 % of the total variance. Based on these groups we identified common processes, which presumably control these developments. As data input for the PCA we used the lipid biomarker ARs, the SST estimates from the long-chain alkenones, the C_4 percentage of the long-chain *n*-alkanes, the TOC content, the TOC AR, the marine OC AR, the terrestrial-derived OC AR, and the $\delta^{13}C$ values of TOC.

Table 7.1: Compound loadings on the five PCA factors with a latent root >1.

Factor	**1**	**2**	**3**	**4**	**5**
Latent Roots (Eigenvalues)	7.62	2.85	2.27	1.64	1.18
"Variance" Explained by Rotated Components	3.6	2.2	3.2	4.5	2.1
Percent of Total Variance Explained	18.9	11.6	16.8	23.7	10.9
Parameter	**VARIMAX-Rotated Loading Matrix**				
ΣC_{26}-C_{34} even *n*-alcohols AR	**0.904**[1]	0.038	0.155	0.063	0.140
ΣC_{25}-C_{35} odd *n*-alkanes AR	**0.860**	-0.104	-0.020	0.207	0.022
ΣC_{30}-C_{32} alkyl diols AR	**0.806**	0.029	0.175	0.262	0.206
ΣC_{37} alkenones AR	**0.640**	-0.025	0.122	**0.542**	0.141
SST	-0.181	**0.871**	0.012	-0.086	0.113
C_4 percentage of *n*-alkanes	-0.023	**-0.814**	0.049	-0.069	-0.335
Taraxerol AR	0.159	**0.724**	0.295	-0.163	-0.102
β-sitosterol AR	0.138	0.151	**0.923**	0.106	0.020
Fucosterol AR	-0.042	0.104	**0.868**	-0.040	-0.184
Diatomsterol AR	0.183	-0.107	**0.706**	0.460	0.262
Cholesterol AR	0.179	-0.033	**0.681**	**0.528**	0.288
Dinosterol AR	0.428	0.053	**0.583**	0.483	0.147
Marine OC AR	0.301	-0.022	0.107	**0.880**	-0.200
TOC AR	0.383	0.037	0.105	**0.858**	0.117
TOC	0.140	-0.343	0.060	**0.793**	-0.089
Loliolide AR	-0.167	-0.050	0.174	**0.726**	0.387
Biphytanediols AR	0.448	0.062	0.273	**0.716**	0.089
$\delta^{13}C_{org}$	-0.152	-0.210	-0.020	0.128	**-0.904**
Terrigenous OC AR	0.363	0.153	0.044	0.346	**0.776**

[1] Values >0.5 in bold.

7.4.4.1. Eolian transport and ice-volume forced wind-driven upwelling

PCA factor 1 groups ARs of the long-chain even-numbered *n*-alcohols, the long-chain odd-numbered *n*-alkanes, the summed C_{30}-C_{32} alkyl diols and the long-chain C_{37} alkenones. To a lesser extent, dinosterol and biphytanediol ARs are grouped in this factor. PCA factor 1 explains 18.9 % of the total variance (Table 7.1). The factor score (Fig. 7.7a) is low and shows only small variations before 780 kyr BP, but it varies strongly in a 100-kyr cycle afterwards. A pronounced long-term increase is present. This is supported by the frequency spectrum of the PCA factor 1 score (Fig. 7.8a), revealing a prominent 100-kyr power peak additional to the long-term trend. Also, some variability around the 41-kyr cycle and small power in the precessional band is detected.

Freshwater inflow by the Congo River is the only source for dissolved silicate in the modern Angola Basin surface waters (van Bennekom and Berger, 1984), while the modern coastal upwelling only effects the nitrate and phosphate concentrations, but not the silicate concentrations (van Bennekom et al., 1978). We suggest that these processes were essentially unaltered during the last 1.2 million years. The intensity of the recent oceanic upwelling by surface divergence correlates mainly to the zonal velocity of the southern trades winds in austral winter (Katz and Garzoli, 1982; Philander and Pacanowski, 1986).

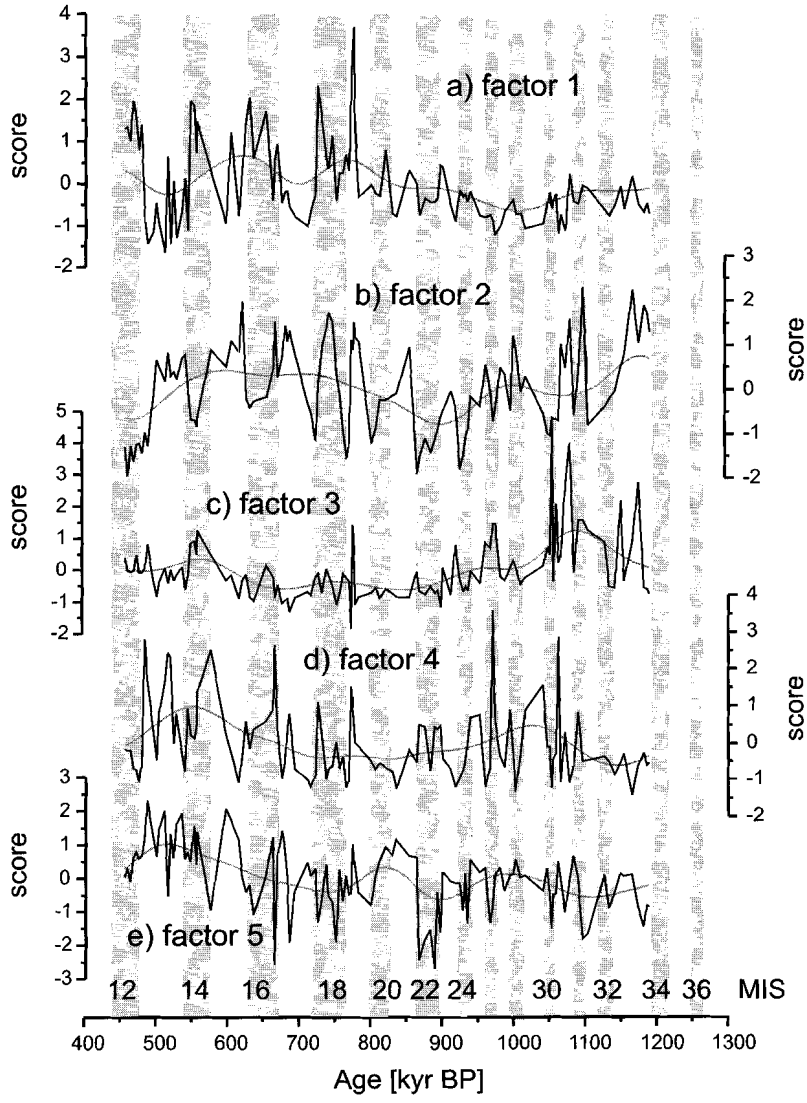

Figure 7.7: a-e) Factor score records of the five PCA factors with latent root >1 and long-term-filtered trends (central frequency of 0.004, bandwidth of 0.004 cycles/kyr).

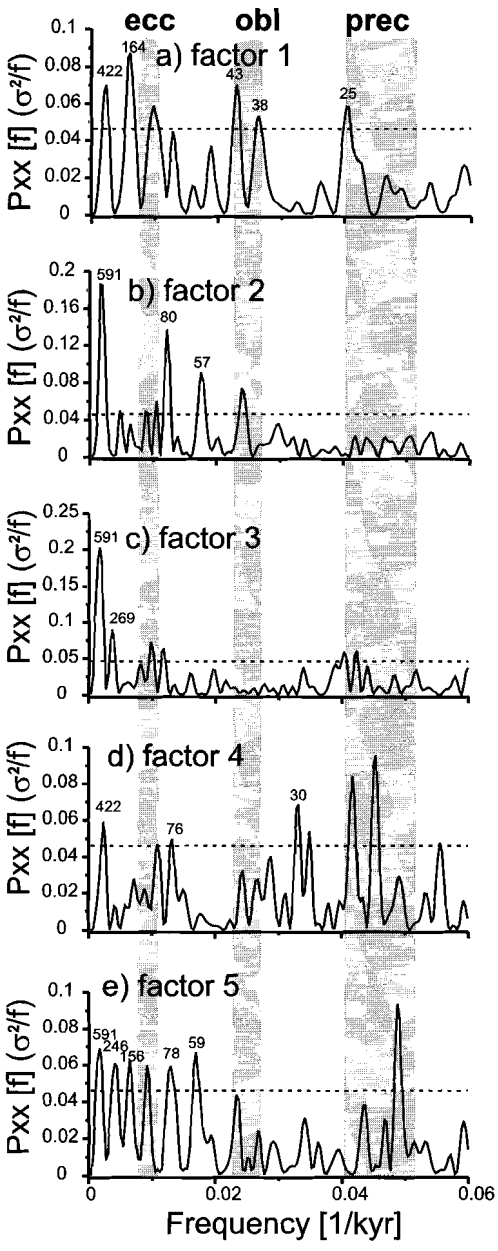

Figure 7.8: a-e) Power spectra of the five PCA factors. Grey bars indicate main orbital frequency bands. The stippled line is a significance-test after Siegel.

The compound classes grouped by PCA factor 1 are either indicative for an eolian contribution, as the plant-wax *n*-alkanes and *n*-alcohols, or derived from wind-driven upwelling activity, as the C_{37} alkenones, the alkyl diols and dinosterol. None of the phytoplankton classes, which are represented by the compounds of PCA factor 1, is indicative for surface-water enrichment by dissolved silicate from the Congo River. This supports the suggestion that factor 1 primarily reflects wind strength and zonality, which drive eolian transport and coastal and oceanic upwelling. Because the increase of the eolian transport of plant waxes and wind-driven upwelling after 900 kyr BP is apparently mainly related to the 100-kyr cycle (Fig. 7.7a, 7.8a) we compare the onset of the 100-kyr cyclicity in the signals grouped by PCA factor 1 (Fig. 7.9). The 100-kyr-filtered records start to increase in amplitude from 900 to 800 kyr onwards, earlier than the increased 100-kyr cyclicity in the SST record, that started only 650 kyr BP (Schefuß et al., submitted-b) (Fig. 7.9). These leads over SST probably indicates that the lipid biomarker ARs were more sensitive to the increased upwelling by stronger trade winds, caused by the increase in ice volume around 900 kyr BP, than the SST signal, which is also influenced by heat advection and insolation.

7.4.4.2. Sea-surface temperatures and continental vegetation signals

PCA factor 2 contains the alkenone-derived SST estimates, negatively, the C_4 percentage of the plant-wax *n*-alkanes and the

taraxerol AR (Table 7.1). It explains 11.6 % of the total variance in the data set. The record of the factor scores (Fig. 7.7b) shows a distinct long-term trend: a decrease from 1200 to 900 kyr BP followed by an increase until 600 kyr BP, and again a decrease afterwards. This long-term development contains the most dominant power in the frequency spectrum of the factor score (Fig. 7.8b). Other significant cyclicities are, in decreasing amplitude, an 80-kyr, a 57-kyr, and a 41-kyr cycle.

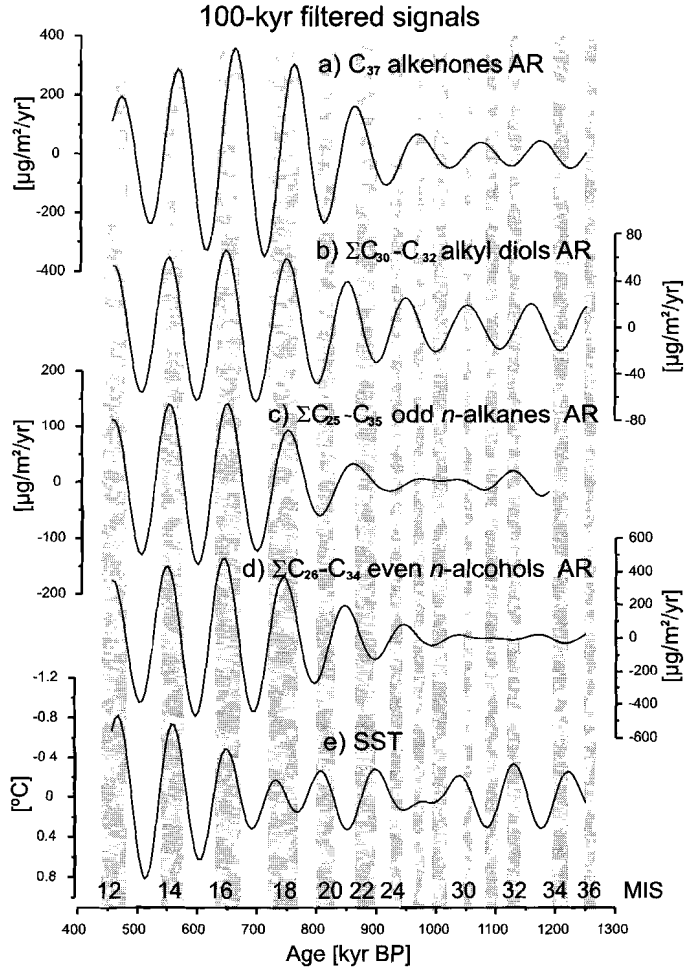

Figure 7.9: The onset of the 100-kyr variability in the records of PCA factor 1: a) the C_{37} alkenones AR, b) the C_{30}-C_{32} alkyl diols AR, c) the C_{25}-C_{35} odd-numbered *n*-alkane AR, d) the C_{26}-C_{34} even-numbered *n*-alcohol AR, and e) the 100-kyr-filtered SST record for comparison (note axis orientation, lowest SST to the top). The 100-kyr filter has a central frequency of 0.0103 and a bandwidth of 0.002 cycles/kyr.

While the 80-kyr and 41-kyr cycle are present in all three composing records, the 57-kyr cycle is only present in the C_4 percentage record, where it most likely results from an interference of the 41-kyr cycle with the 23-kyr monsoon cycle. From a detailed investigation of the SST development in the tropical Atlantic during the

mid-Pleistocene, it was inferred that a combination of factors controls the SST evolution (Schefuß et al., submitted-b). The pronounced long-term development was coupled to the strength of the Atlantic deep thermohaline ventilation. The 41-kyr cyclicity was caused by orbital forcing via the Southern Hemisphere thermal gradient, which controlled wind-driven upwelling and heat advection from high southern latitudes. The onset of a significant 100-kyr SST variability was detected only at 650 kyr BP (Fig. 7.9e; Schefuß et al., submitted-b). The 80-kyr cycle was found at the transition from a prevalent 41-kyr cyclicity to a predominant 100-kyr cycle in global ice-volume changes (Mudelsee and Schulz, 1997). The 80-kyr SST variability was detected to be in phase with the 76-kyr ice-mass changes (Schefuß et al., submitted-b). It was concluded, therefore, that the 80-kyr SST variability represents a direct response on ice-volume variations (Schefuß et al., submitted-b).

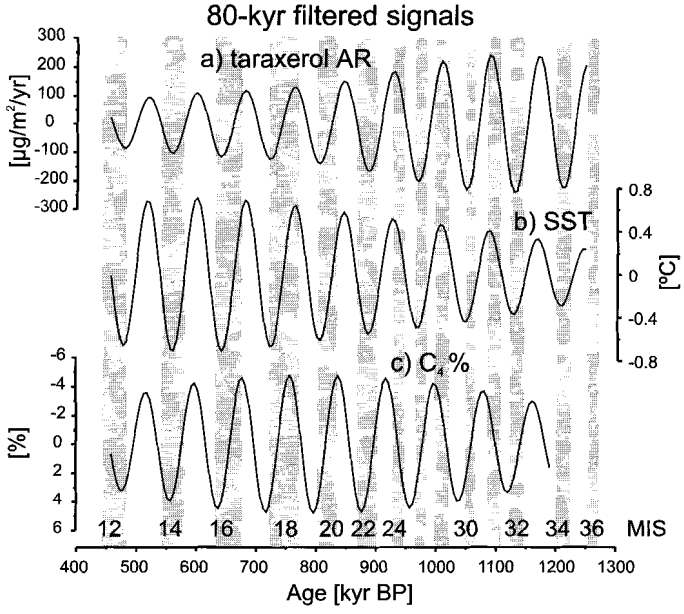

Figure 7.10: Comparison of the 80-kyr-filtered records of biomarkers determining PCA factor 2: a) the taraxerol AR, b) the SST estimates, and c) the C_4 percentage of the plant-wax *n*-alkanes (note axis orientation, maximum C_3 plant signal to the top). The 80-kyr filter has a central frequency of 0.0125 and a bandwidth of 0.001 cycles/kyr.

Table 7.2: Phase angles in the 80-kyr cycle

Time series	Coherency, k	Phase, deg.	Error, deg.	Lag, kyr	Error, kyr
SST vs.					
Taraxerol AR	0.784	-7	27	-1.5	6.0
$-\delta^{18}O$ ODP 677	0.833	-1	23	-0.2	5.1
$-C_4\ \% = C_3\ \%$	0.891	27	18	6.1	4.0

Non-zero coherency k_0 (80 %) is 0.963 for all calculations. Data of ODP 677 $\delta^{18}O$ are from Shackleton et al. (1990). A negative lag denotes lead.

The C_4 percentage record of the plant-wax *n*-alkanes was inferred to reflect southern African vegetation changes which were found to be closely coupled to the SST development (see above; Schefuß et al., submitted-a). The linkage is via a direct control of African aridity by tropical SST, as shown by modelling efforts for the last glacial maximum (Ganopolski et al., 1998).

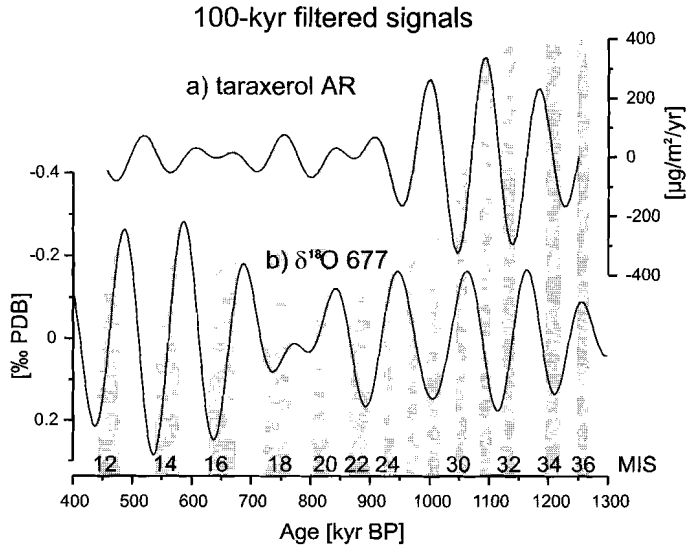

Figure 7.11: The 100-kyr-filtered a) taraxerol accumulation record and b) benthic $\delta^{18}O$ record of ODP Site 677 (Shackleton et al., 1990) as global ice-volume proxy (note axis orientation, low ice volume to the top), showing the independence of the taraxerol AR from the large sea-level changes in the 100-kyr cycle. The 100-kyr filter has a central frequency of 0.0103 and a bandwidth of 0.002 cycles/kyr.

The occurrence of taraxerol in sediments reflects the extent of mangrove vegetation along the coast of equatorial Africa, mainly controlled by SST changes in the absence of large sea-level fluctuations (Woodroffe and Grindrod, 1991). Mangrove vegetation is absent in areas where the mean annual SST is below 24°C (Barth, 1982), which is also the modern mean annual SST off the coast at Lobito, Angola (12°20'S; Levitus and Boyer, 1994), the southernmost modern occurrence of mangroves along the West African coast (Tomlinson, 1986). The occurrence of the distinct 80-kyr cycle suggests that the extension of mangrove vegetation was coupled to the SST development, directly or indirectly. By comparing the 80-kyr-filtered records (Fig. 7.10) we can detect a lead of the taraxerol AR and the SST signal over the C_4 record. Cross-spectral analyses over the time period from 1300 to 450 kyr BP confirm that the maximum taraxerol AR, the highest SST and the strongest deepwater ventilation (indicated by highest benthic foraminiferal $\delta^{13}C$ values of the North Atlantic DSDP Site 607) occur simultaneously (Table 7.2). This confirms the strong correlation of the SST with the taraxerol AR record in the 80-kyr cycle, but does not exclude a control by sea-level changes. The 100-kyr-filtered records of the taraxerol AR and the global ice-volume record, however, do not contain a significant eccentricity-related variability during most of the mid-Pleistocene (Fig. 7.11). The onset of 100-kyr cyclicity in the global ice-volume

variations around 650 kyr BP (Mudelsee and Schulz, 1997) is not recognised in the filtered taraxerol AR record. Instead, it shows a high eccentricity-related variability before 900 kyr BP. As a consequence, it was SST that determined the extension of mangrove vegetation along the coast and controlled the accumulation of taraxerol during the mid-Pleistocene. Summarising, the PCA factor 2 thus groups the environmental signals, SST and continental aridity, dominantly influencing the terrestrial vegetation.

7.4.4.3. Marine production induced by river runoff and oceanic upwelling

PCA factor 3 contains the ARs of the major sterols and explains 16.8 % of the variance (Table 7.1). The highest loadings on this factor have β-sitosterol and fucosterol, compounds inferred to be most characteristic for a lipid contribution by diatoms (Schefuß et al., submitted-c), while diatomsterol, cholesterol and dinosterol, which are less source-specific in this setting and derived from organisms not relying on high dissolved silicate concentrations (i.e., dinoflagellates or zooplankton), show a smaller loading on factor 3. Diatom productivity off the Congo relies on the availability of dissolved silicate, which is rather entirely supplied by the river outflow (van Bennekom and Berger, 1984). The score record of factor 3 (Fig. 7.7c) shows a very pronounced long-term trend, which dominates the frequency spectrum (Fig. 7.8c). The spectrum additionally reveals some power associated with the eccentricity and precession cycles. Power in the obliquity band is absent. The highest AR of the biomarkers determining factor 3 clearly occurred before 900 kyr BP, during the precession-dominated period with a smaller mean global ice volume (Mudelsee and Schulz, 1997). Afterwards, the score is strongly decreased until about 600 kyr BP, followed by a slight comeback thereafter (Fig. 7.7c). This suggests that the biomarkers determining factor 3 are mainly related to river-induced productivity or oceanic upwelling, both processes which are driven mainly by monsoonal changes in wind direction, controlled by the precession and amplitude-modulated by the eccentricity (Berger and Loutre, 1991). There was only a small response to the large 100-kyr upwelling cycles from 900 kyr BP onwards (see section 7.4.4.1.).

To compare the different amplitudes of the precessional responses in the time-domain, we investigated the 23-kyr-filtered biomarker records of PCA factor 3 (Fig. 7.12). For comparison the precessional index is also shown (Fig. 7.12a), the main forcing function of precessional variability in the upwelling intensity via the trade-wind zonality (Prell and Kutzbach, 1987). Largest precessional index means that the boreal summer, i.e., austral winter insolation over N-Africa is smallest, resulting in a minimum meridional deflection of the strong trade winds, which enter the Northern Hemisphere from the south. Therefore, the oceanic upwelling during austral winter is strongest during maximum precession (McIntyre et al., 1989; Prell and Kutzbach, 1987). For this reason, we observe a lower SST when the precessional index is high (Fig. 7.12b, note axis orientation). It was, however, observed that the simple low-latitude insolation forcing is suppressed by presence of a large global ice volume (Schefuß et al., submitted-b). During enlarged ice volume, a steeper meridional thermal gradient compressed the atmospheric Hadley cell circulation and increased the zonal velocity of the trade winds (de Menocal and Rind, 1993; Manabe and Broccoli, 1985). This suppression can be seen in the smaller amplitudes of the filtered SST record after 900 kyr BP (Fig. 7.12). Earlier, it was concluded that SST in the area east of 15°W in the equatorial Atlantic is

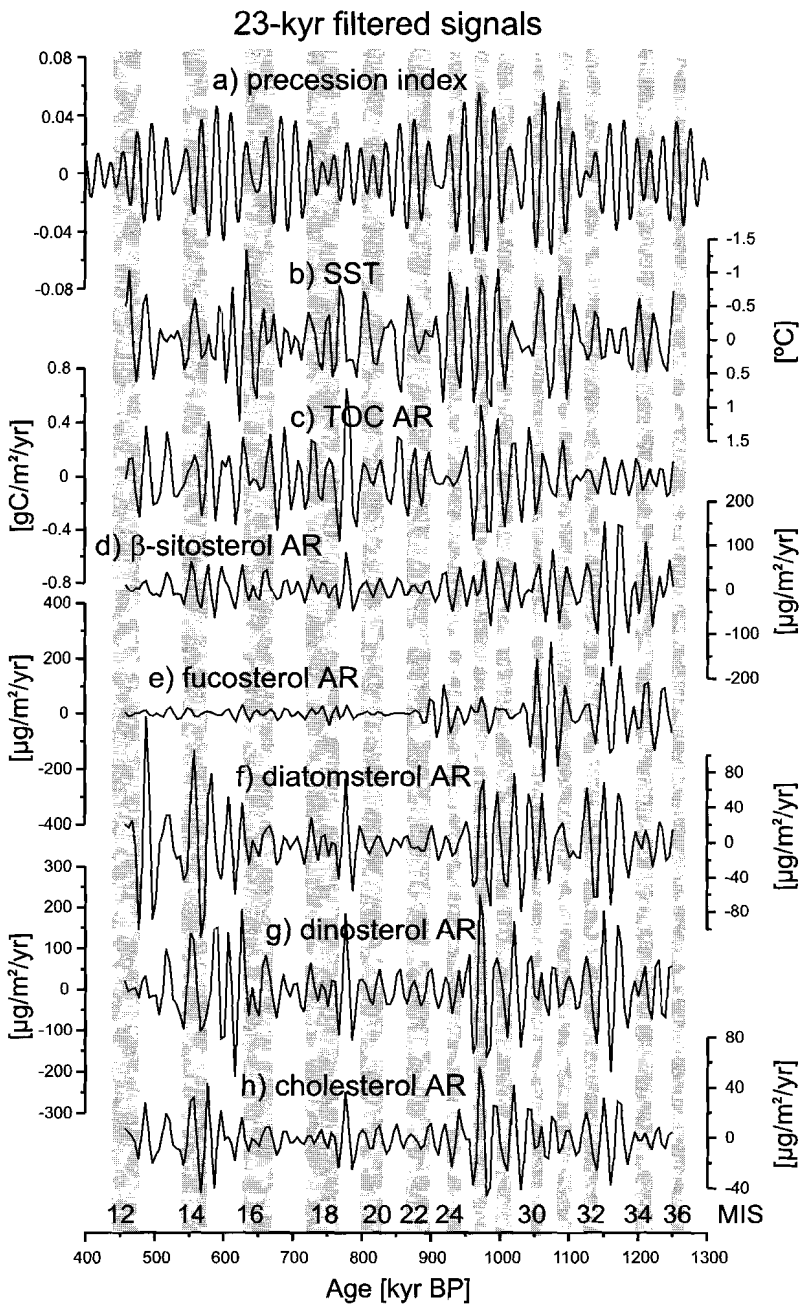

Figure 7.12: a) The precessional index (Berger and Loutre, 1991), with maximum values forcing strongest upwelling and highest monsoonal precipitation in southern Africa, compared with the 23-kyr-filtered b) SST record (note axis orientation, lowest SST to the top), c) TOC AR, d) β-sitosterol AR, e) fucosterol AR, f) diatomsterol AR, g) dinosterol AR, h) cholesterol AR, showing the differential response in the precessional band. The 23-kyr filter has a central frequency of 0.0477 and a bandwidth of 0.02 cycles/kyr.

controlled primarily by wind-driven upwelling (Schneider et al., 1996). The 23-kyr-filtered SST (Fig. 7.12b) and TOC AR (Fig. 7.12c) records are therefore mostly anti-correlated, indicating that total marine productivity was elevated during times of maximum trade-wind zonality (Schneider et al., 1994, 1996, 1997). All the 23-kyr-filtered records of the biomarkers determining PCA factor 3 show a general correlation with the TOC AR record, suggesting that the productivity of diatoms, dinoflagellates and zooplankton in the monsoonal cycle may also be primarily controlled by wind-driven upwelling (Fig. 7.12d-h). However, a different behaviour is detected for β-sitosterol (Fig. 7.12d) and fucosterol (Fig. 7.12e). These compounds only show a substantial 23-kyr cyclicity in their ARs before 900 kyr PB, suggesting a severe decrease in the availability of dissolved silicate in the surface waters associated with the onset of the mean enlarged global ice volume and increased aridity at the MPT.

7.4.4.4. Bulk marine productivity

PCA factor 4 explains the highest fraction of the total variance in the data set, i.e., 23.7 % (Table 7.1). It groups the AR of marine organic matter, the AR of total organic carbon, the TOC content and the ARs of the long-chain biphytanediols and loliolide. A smaller loading on this factor is detected for the long-chain C_{37} alkenones, cholesterol, dinosterol and diatomsterol AR. This suggests that the factor 4 describes the accumulation of marine organic matter and contains the lipid biomarkers from the main producing organisms. The lipids are either from the group of biomarkers that were derived from strong wind-driven coastal upwelling, as the C_{37} alkenones, or from oceanic upwelling, as diatomsterol, dinosterol and cholesterol. Interestingly, diatom-derived biomarkers like fucosterol and β-sitosterol are not included, indicating the independence of PCA factor 4 from silicate enrichment of the surface waters. We find a long-term maximum in the factor score (Fig. 7.7d) from 1100 to 950 kyr BP, in the precessional-dominated period, as well as in the interval from 650 to 500 kyr BP, when the 100-kyr cycle was established. This is reflected in the frequency spectrum of factor 4 (Fig. 7.8d). Beside the long-term trend, it contains power in precessional- and eccentricity-related cycles. The strong precessional power and the absence of unambiguously diatom-derived lipids indicate the importance of the oceanic upwelling activity during each precessional maximum for marine production. The maximum level of marine organic matter AR, however, is not significantly different in the two forcing regimes, i.e., controlled by low-latitude insolation or ice volume. The lipid biomarkers, which are mainly restricted to this PCA factor, are the biphytanediols and loliolide. In the surface sediments of the eastern South Atlantic these both compounds were also associated with high marine organic carbon contents (Schefuß et al., submitted-c). It was concluded, that high concentrations of the biphytanediols and loliolide in sediments are probably caused by a less severe oxic degradation of labile organic matter (Schefuß et al., submitted-c) due to low oxygen levels in the sediments caused by the high organic matter accumulation. The co-occurrence of the marine and total organic matter AR with the biphytanediols and loliolide AR suggests a similar control for the mid-Pleistocene. The indirect coupling to total organic matter ARs explains the reported correlation of loliolide with paleoproductivity estimates (Hinrichs et al., 1999). Since, however, also other factors might influence the oxygen content in the bottom or pore water, we infer that biphytanediols and loliolide cannot be used as productivity indicators.

7.4.4.5. Input of bulk terrigenous organic matter

The fifth PCA factor explains the smallest portion (10.9 %) of the total variance (Table 7.1). It is predominantly determined by the stable carbon isotopic composition of the total organic matter, and the derivative from $\delta^{13}C_{org}$ and TOC, the terrestrial OC AR. Apparently, PCA factor 5 reflects the terrestrial C_3 plant organic matter from the rainforest supplied by the Congo River. Although no significant influence on the AR of the plant-wax *n*-alkanes can be detected, it does show a small, negative influence on the C_4 percentage of the plant waxes (Table 7.1). The same was already concluded from investigation of surface sediments (Schefuß et al., submitted-c). The downcore record of the factor scores (Fig. 7.7e) reveals a long-term increase overlain by short-term variations. In the frequency spectrum (Fig. 7.8e), the long-term trend contains the largest power. The second largest power occurs in the precession cycle, and smaller amplitudes are detected for 110-, 78-, 89- and 42-kyr cycles. The frequency spectrum of factor 5 thus contains similar cycles as the spectrum of factor 2 representing SST, continental humidity and the AR of mangrove lipids. The striking difference with the factor 2, however, is the strong precessional power. The supply of terrigenous organic matter, apparently, relates mainly to monsoonal-driven river outflow, and to a lesser degree to the continental humidity on longer time scales.

7.4.5. Orbital phasing

In order to examine the phasing in the main orbital cycles, we conducted cross-spectral analyses between each geochemical signal and the ETP record of orbital variance. ETP was calculated to contain equal power in all orbital bands, i.e., eccentricity (E), obliquity (T) and precession (P), using the method described in Imbrie et al. (1984) and orbital data from Berger and Loutre (1991). Maximum ETP values indicates maximum interglacial forcing. The results of these analyses are shown in phase wheels according to SPECMAP convention with maximum interglacial forcing at 0° and a phase-lag clockwise (Imbrie et al., 1984).

7.4.5.1. Eccentricity

The cross-spectral analyses in the eccentricity cycle (Table 7.3, Fig. 7.13) have been restricted to the period from 900 to 450 kyr BP, because the 100-kyr cycle is only present in the younger part of the records (Fig. 7.9).

In the 100-kyr cycle, the SST maximum is in phase, within statistical error, with maximum interglacial-forcing (i.e., maximum eccentricity), a direct response on the changing Southern Hemisphere thermal gradient (Schefuß et al., submitted-b), and therefore in phase with frontal movements in the Southern Ocean (Brathauer and Abelmann, 1999; Howard and Prell, 1992). SST is also in phase, within statistical error, with the maximum C_3 plant signal of the plant-wax *n*-alkanes, since it directly controls continental humidity (Schefuß et al., submitted-a). Minimum ice volume (and thus maximum sea level) occurs significantly later by about 6.7 kyrs (Shackleton et al., 1990), in accordance with the phase assigned by orbital tuning (Imbrie et al., 1984). 3-4 kyr after maximum interglacial conditions, i.e., minimum benthic $\delta^{18}O$ values, the terrestrial OC AR is highest, indicating that the contribution of terrigenous organic material is largest during warm, humid climate conditions connected to a high sea level.

About 8 kyrs later, the maximum AR of total organic matter occurs and delayed by about 3 kyrs, also the AR of marine OC is largest. Coinciding with the maximum

of marine OC AR occur the highest biphytanediol AR, also in phase with the maximum AR of the long-chain alkenones. This confirms that the biphytanediol AR maximum is strongly linked to high marine OC accumulation. The maximum accumulation of marine OC likely indicates high rates of primary production, which are, as indicated by the coincidence with the alkenone AR maximum, probably associated with enhanced coastal upwelling. This suggests, that as soon as the ice mass grew in the 100-kyr cycle, the trade winds became stronger. The direction of the trades was not necessarily more zonal, as increased coastal upwelling occurs when the main winds blow parallel to the coast. Obviously, coastal upwelling induces maximum marine productivity in the eccentricity cycle and results in oxygen depletion in the bottom or pore waters. This also explains the contemporaneous occurrence of the maximum loliolide AR.

Table 7.3: Phase angles in the eccentricity- (100-kyr) cycle

Time series	Coherency, k	Phase, deg.	Error, deg.	Lag, kyr	Error, kyr
ETP vs.					
SST	0.964	-8	10	-2.2	2.8
$-\delta^{18}O$ ODP 677	0.978	24	8	6.7	2.2
Terrigenous OC AR	0.928	34	14	9.4	3.9
$-\delta^{13}C_{org}$	0.990	37	5	10.3	1.4
TOC AR	0.978	64	8	17.8	2.2
Biphytanediol AR	0.996	74	3	20.6	0.8
Marine OC AR	0.955	76	11	21.1	3.1
ΣC_{37} alkenones AR	0.990	81	5	22.5	1.4
Loliolide AR	0.854	83	21	23.1	5.8
Diatomsterol AR	0.976	92	8	25.6	2.2
Cholesterol AR	0.996	94	3	26.1	0.8
β-sitosterol AR	0.997	96	3	26.7	0.8
Dinosterol AR	0.956	103	11	28.6	3.1
Fucosterol AR	0.994	104	4	28.9	1.1
ΣC_{25}-C_{35} *n*-alkanes AR	0.851	126	21	35.0	5.8
ΣC_{30}-C_{32} alkyl diol AR	0.806	139	25	38.6	6.9
ΣC_{26}-C_{34} *n*-alcohol AR	0.862	144	20	40.0	5.6
-SST	0.964	172	10	47.8	2.8
C_4 percentage	0.972	174	9	48.3	2.5

Non-zero coherency k_0 (80 %) is 0.963 for all calculations. ETP describes summed orbital variance following the convention by Imbrie et al. (1989). Data of ODP 677 $\delta^{18}O$ are from Shackleton et al. (1990). A negative lag denotes lead.

Subsequently, a maximum contribution of diatom lipids is indicated by the AR maxima of diatomsterol, β-sitosterol, and fucosterol. Together with dinosterol and cholesterol, all these abundance maxima occur within a time span of 4 kyrs, indicating a fertilisation of the surface waters with dissolved silicate leading to higher diatom productivity. We hypothesise that the occurrence of silicate enrichment during the ice-volume growth in the 100-kyr cycle can be explained by the anomalous behaviour of the 100-kyr ice sheets. Taking the ice volume as forcing function for trade-wind strength and zonality, the 100-kyr cycle is not a real sinusoidal cycle, but follows a sawtooth-like development. In the enlarged 100-kyr cycle, the ice volume builds up slowly and melts rapidly, while in the smaller 41-kyr ice-volume cycle the ice mass reacts rather linearly on changes in orbital forcing (Imbrie et al., 1993). Therefore, the increase in strength and zonality in the 100-kyr cycle was delayed, compared with the more linear response in the 41-kyr cycle. When ice volume was slowly increasing in the 100-kyr cycle, the supply of

dissolved silicate with the Congo River outflow was presumably still high, while winds were already strengthened. The enhanced mixing of the silicate-enriched plume waters by the wind then resulted in a high production of diatom lipids.

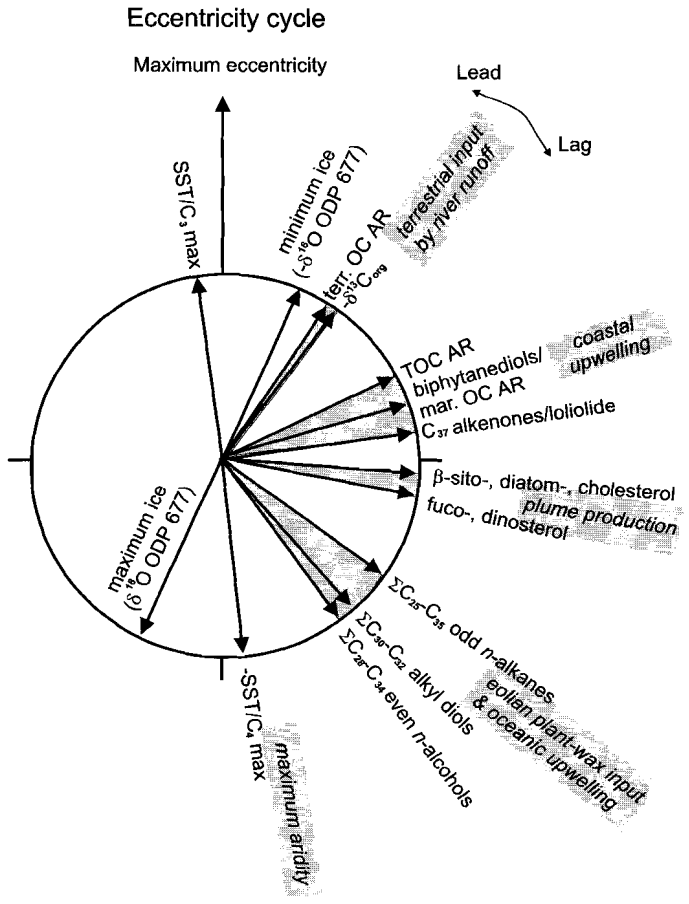

Figure 7.13: 100-kyr phase wheel depicting phasing of lipid accumulation records in the eccentricity band from 900 to 450 kyr BP. After SPECMAP convention a lag is clockwise (Imbrie et al., 1989). The benthic $\delta^{18}O$ record of ODP Site 677 (Shackleton et al., 1990) has been taken as the indicator for global ice volume. The arrows indicate maximum lipid-biomarker accumulation rate, if not otherwise indicated. Comments in italics in the outer circle are the interpretation of the groupings indicated by the shaded areas. Note that taraxerol is not coherent in the 100-kyr cycle from 900 to 450 kyr BP.

About 6 kyrs later, the maximum AR of the long-chain odd-numbered *n*-alkanes occurs. The high *n*-alkane AR indicates a maximum flux of plant waxes from the continent to the ocean, depending on two conditions: strong zonal winds and a vast supply of plant waxes. The latter could be due to a different vegetation type, a higher vegetation density or a major vegetation change. We suggest the plant-wax *n*-alkane ARs indeed reflect a vegetation change. Today, the zonal trade winds mainly transport plant waxes from dry southern African areas, i.e., the Kalahari

savannah or the Namib Desert (Schefuß et al., re-submitted; submitted-c). During the growth of the 100-kyr cycle ice mass the South Atlantic high-pressure system was pushed northwards by an extra latitudinal shift of 3-5° in addition to its seasonal shift of 6-8° (Imbrie et al., 1993), displacing the zonal trade-wind belt to the north. During those times, the strong winds will eventually blow over areas, which are vegetated by denser vegetation, possibly rainforest. The strong, offshore-directed winds will cause an aridification and de-stabilisation of the vegetation in the more northern source area and lead to the supply of large amounts of leaf waxes to the atmosphere. The maximum *n*-alkane AR, therefore, leads the occurrence of maximum aridity by about 13 kyrs. The most arid conditions are indicated by the highest C_4 percentage of the *n*-alkanes, occurring simultaneously with the lowest SST. Both parameters were inferred to be tightly coupled via the atmospheric moisture balance, directly influencing the continental aridity in subtropical Africa (Ganopolski et al., 1998; Schefuß et al., submitted-a). The lead of the plant-wax accumulation over the maximum aridity resembles the transport of the freshwater diatom *Melosira*, wind-blown from dried out lake beds, found to precede maximum aridity in the Late Quaternary (Pokras, 1987).

The maximum accumulation of the long-chain *n*-alkanes is followed by the highest contribution of the C_{30}-C_{32} alkyl diols, reflecting the highest productivity of eustigmatophyte algae at maximum oceanic upwelling. The process of offshore surface-water divergence and nutrient entrainment from subsurface waters depends on strong zonally-directed trade winds. The maximum of the *n*-alcohol AR is, within error, in phase with the C_{30}-C_{32} alkyl diols AR maximum. The long-chain *n*-alcohols should correlate to the long-chain *n*-alkanes due to their common origin. What, however, causes the phase lag between those compound classes is not known.

The sequence of AR maxima in the 100-kyr cycle thus points to the turning and strengthening of the mean trade-wind vector associated with the compression and intensification of the Hadley cell due to the increasing ice volume (de Menocal and Rind, 1993; Manabe and Broccoli, 1985) as the main process during this cycle.

7.4.5.2. Obliquity

Table 7.4: Phase angles in the obliquity- (41-kyr) cycle

Time series	Coherency, k	Phase, deg.	Error, deg.	Lag, kyr	Error, kyr
ETP vs.					
SST	0.986	48	6	5.5	0.7
C_3 percentage	0.976	48	8	5.5	0.9
terrigenous OC AR	0.735	55	31	6.3	3.5
$-\delta^{18}O$ ODP 677	0.992	78	5	8.9	0.6
Biphytanediols AR	0.786	102	27	11.6	3.1
TOC AR	0.733	107	31	12.2	3.5
$\delta^{13}C_{org}$	0.995	112	4	12.8	0.5
ΣC_{30}-C_{32} alkyl diol AR	0.867	115	20	13.1	2.3
ΣC_{37} alkenones AR	0.693	121	34	13.8	3.9
marine OC AR	0.820	126	24	14.4	2.7
ΣC_{26}-C_{34} *n*-alcohol AR	0.615	134	40	15.3	4.6
ΣC_{25}-C_{35} *n*-alkanes AR	0.935	144	14	16.4	1.6
-SST	0.986	228	6	26.0	0.7
C_4 percentage	0.976	228	8	26.0	0.9

Non-zero coherency k_0 (80 %) is 0.963 for all calculations. ETP describes summed orbital variance following the convention by Imbrie et al. (1989). Data of ODP 677 $\delta^{18}O$ are from Shackleton et al. (1990). A negative lag denotes lead.

In the obliquity cycle, maximum SST occurs 5.5 kyrs after the maximum tilt (Table 7.4, Fig. 7.14), simultaneous with the lowest C_4 percentage of the plant-wax *n*-alkanes. The SST development is thus, like in the 100-kyr cycle, in phase with movements of the subtropical convergence (Brathauer and Abelmann, 1999; Howard and Prell, 1992; Schefuß et al., submitted-b) and directly coupled to the continental aridity (Schefuß et al., submitted-a). The largest AR of terrestrial C_3 plant organic matter follows, indicating the maximum extension of C_3 plant vegetation in subtropical southern Africa during warm and humid times with a large

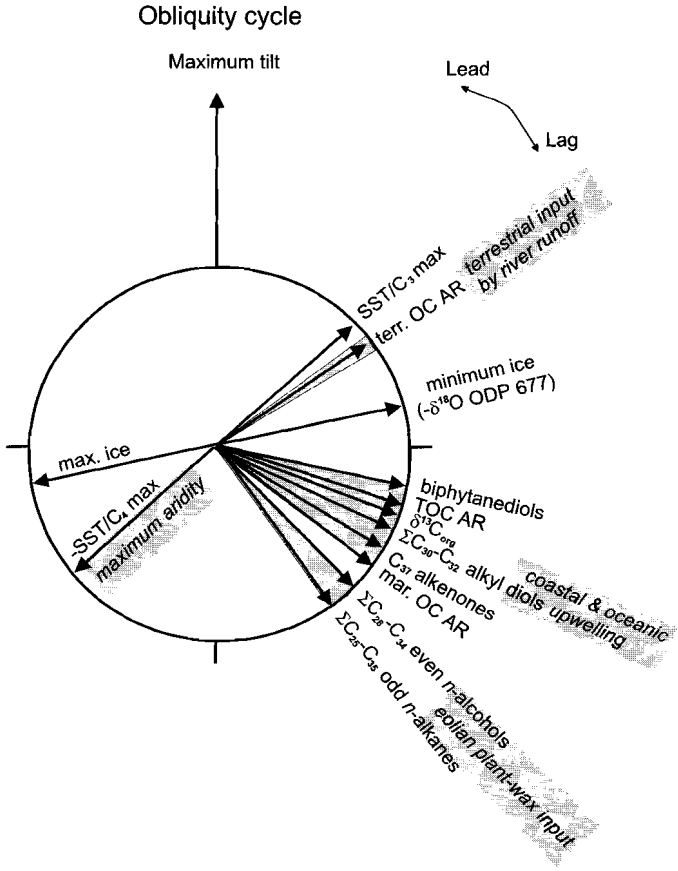

Figure 7.14: 41-kyr phase wheel representing phasing of lipid accumulation records in the obliquity band over the entire period from 1300 to 450 kyr BP. See legend of Figure 7.13 for more explanation. The accumulation records of β-sitosterol, fucosterol, diatomsterol, loliolide and the record of the $\delta^{13}C_{org}$ values are not coherent in the obliquity cycle.

river runoff (Schefuß et al., submitted-a). Minimum ice volume occurs about 3 kyrs later. During the 3 kyrs that followed, no crucial events occurred. In the following 3 kyrs thereafter, however, we detect the AR maxima of the biphytanediols, of TOC, of the C_{30}-C_{32} alkyl diols, of the C_{37} alkenones and of the marine OC. All these parameters indicate an elevated level of wind-driven upwelling, either coastal or oceanic. Following this group of upwelling-derived lipids we find maximum AR of

the plant-wax compounds, long-chain *n*-alcohols and *n*-alkanes, having peak accumulation at 16 kyrs after maximum tilt.

In contrast to the findings from the eccentricity cycle, we cannot detect biomarkers indicating river-induced production with a significant silicate enrichment of the surface waters. As suggested above, this is explained by the different behaviour of the ice sheets during the 41-kyr and 100-kyr variations. During the 41-kyr cycle, a combination of large river runoff and strong winds presumably never co-occurred, due to the rapid turning and increase in the trade-wind vector, responding rather linearly to the increasing ice volume. We suggest that this is the reason, why we do not detect a significant variability of diatom lipids, i.e., β-sitosterol, fucosterol, diatomsterol and loliolide, in the 41-kyr cycle. In the obliquity cycle, we can only detect biomarkers, indicative for wind-driven upwelling, with source organisms that are not depending on silicate availability, i.e., biphytanediols, C_{37} alkenones and C_{30}-C_{32} alkyl diols, indicating productivity of marine archaea, haptophytes and eustigmatophytes, respectively.

The maximum C_4 percentage of the *n*-alkanes occurred simultaneously with the lowest SST, about 10 kyrs later than the maximum of plant-wax AR. This lag is similar to the phasing in the 100-kyr cycle, suggesting that the largest transport of plant waxes occurred during de-stabilisation of the vegetation upon aridification and increasing wind strength, while the most arid conditions on the South African continent were established significantly later.

7.4.5.3. Precession

Table 7.5: Phase angles in the precessional- (23-kyr) cycle

Time series	Coherency, k	Phase, deg.	Error, deg.	Lag, kyr	Error, kyr
ETP vs.					
C_4 percentage	0.969	-34	9	-2.2	0.6
SST	0.938	-22	13	-1.4	0.8
Taraxerol AR	0.893	-22	18	-1.4	1.2
ΣC_{37} alkenones AR	0.819	64	24	4.1	1.5
$-\delta^{18}O$ ODP 677	0.998	87	2	5.6	0.1
Loliolide AR	0.965	91	10	5.8	0.6
ΣC_{30}-C_{32} alkyl diol AR	0.976	101	8	6.5	0.5
ΣC_{25}-C_{35} *n*-alkanes AR	0.992	122	4	7.8	0.3
β-sitosterol AR	0.993	123	4	7.9	0.3
Fucosterol AR	0.999	130	1	8.3	0.1
Cholesterol AR	0.964	132	10	8.4	0.6
Terrigenous OC AR	0.949	141	12	9.0	0.8
C_3 percentage	0.969	146	9	9.3	0.6
Biphytanediols AR	0.912	148	16	9.5	1.0
ΣC_{26}-C_{34} *n*-alcohol AR	0.971	153	9	9.8	0.6
-SST	0.938	158	13	10.1	0.8
TOC AR	0.985	159	6	10.2	0.4
Marine OC AR	0.986	160	6	10.2	0.4
Diatomsterol AR	0.962	169	10	10.8	0.6
Dinosterol AR	0.956	197	11	12.6	0.7
$\delta^{18}O$ ODP 677	0.998	267	2	17.1	0.1

Non-zero coherency k_0 (80 %) is 0.963 for all calculations. ETP describes summed orbital variance following the convention by Imbrie et al. (1989). Data of ODP 677 $\delta^{18}O$ are from Shackleton et al. (1990). A negative lag denotes lead.

Investigation of the accuracy of the age model of ODP Site 1077 has shown that there is a large uncertainty in the precessional phase versus orbital forcing, i.e., a low coherency in the 23-kyr band (Schefuß et al., submitted-b). The detected phase angles in the precessional cycle may thus possibly be shifted against independent records as ETP and the $\delta^{18}O$ record of ODP Site 677 due to this uncertainty (Table 7.5; Fig. 7.15). Precessional variations of $\delta^{18}O$ from ODP Site 677 have a phase angle of 87° with minimum precession, which is in accordance with the phasing expected from the SPECMAP stack (Imbrie et al., 1989), since it was assigned by orbital tuning (Shackleton et al., 1990).

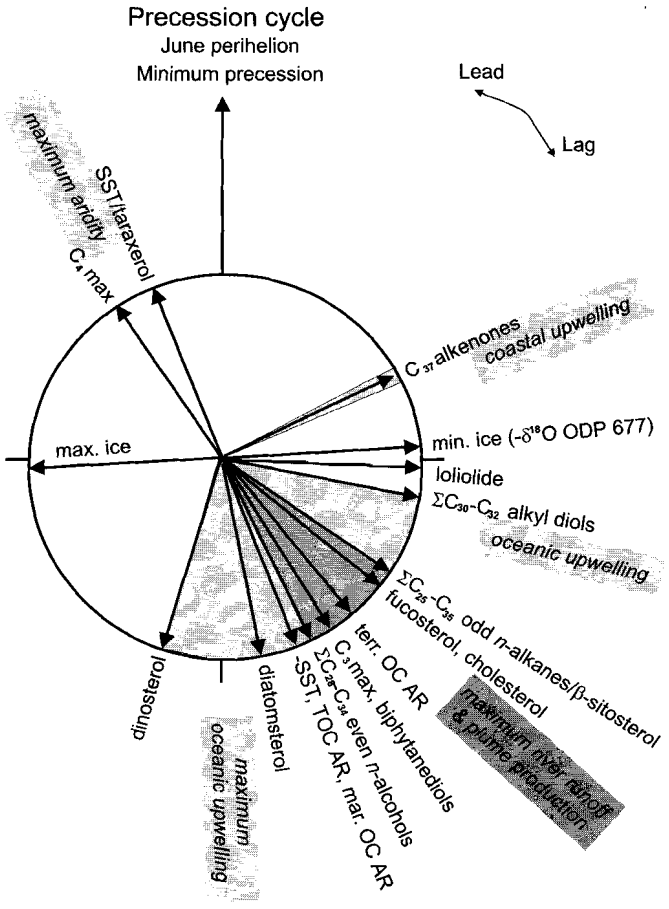

Figure 7.15: 23-kyr phase wheel showing phasing of lipid accumulation records in the precession band over the entire period from 1300 to 450 kyr BP. See text of Figure 7.13 for more explanation. Note that the record of the $\delta^{13}C_{org}$ values is not coherent in this cycle.

The parameters from PCA factor 2, maximum SST and taraxerol AR and the highest C_4 percentage, occur distinctly grouped in the 23-kyr cycle. Assuming a correct phase of the precessional variations of ODP Site 1077 versus ETP, the lead of the maximum SST and taraxerol AR over the precessional minimum might indicate an immediate response of the equatorial Atlantic on the northward-

deflected trade-wind vector associated with the maximum development of the northern African monsoon (Prell and Kutzbach, 1987). The meridional winds could have led to maximum SST due to decreased upwelling conditions and, thus, to highest SST and the maximum extension of mangroves along the coast. From investigations of Late Quaternary SST off the Congo and the Angolan coast (Schneider et al., 1995; 1996), however, it was shown, that maximum SST follows minimum precession by about 88° and 95°, respectively. We suggest that the differences between these phases and the results from our study indicate a phase error of about 110 to 120° (i.e., 7.7 kyrs) in the precessional variations of the age model of ODP Site 1077, which therefore limit our paleoceanographic implications.

The relation of the C_4 percentage with the SST is contrary to that detected in the longer cycles (Schefuß et al., submitted-a). While in those cycles lowest SST correlate to highest C_4 percentage, this is opposite in the precessional cycle. This is explained by the precessional influence on the low-latitude insolation. The highest SST occurs during maximum development of the northern African monsoon, i.e., during weakest upwelling. Subtropical southern Africa, the source region of the plant waxes, however, receives its main precipitation during the maximum development of the southern African monsoon, occurring half a precessional cycle later, coinciding with maximum upwelling. The monsoonal moisture transport apparently overrules the SST control on the tropical evaporation-precipitation balance. In the longer orbital cycles, 100-kyr (Fig. 7.13) and 41-kyr (Fig. 7.14), and in the long-term development (Fig. 7.5b, 7.5n), on the other hand, no such monsoon effect occurs, since low-latitude insolation changes do contain neither an obliquity nor an eccentricity component (Berger and Loutre, 1991).

The maximum accumulation of long-chain C_{37} alkenones is lagging the maximum SST by a quarter of a precession cycle. The C_{37} alkenones have been identified in the surface sediments of the Angola Basin as constituents produced in the coastal upwelling cells (Schefuß et al., submitted-c). The maximum AR of the C_{37} alkenones indicates that the mean annual wind blows parallel to the coast, causing strong coastal upwelling, but do not fertilise the surface waters with dissolved silicate. The strongest coastal upwelling thus occurs between the maximum development of the northern African monsoon, indicated by the highest SST, and the strongest oceanic upwelling offshore the Congo, driven by zonal winds. This relation is independent from a potential phase error.

In the quarter precession cycle, which is situated approximately opposite to the maximum SST, i.e., from 101 to 197° relative to -P, we detect maximum ARs of all remaining compounds and parameters having a high coherency in the 23-kyr cycle. Maximum ARs of terrigenous components, like the plant-wax *n*-alcohols, *n*-alkanes and terrestrial OC, occur during the same 6.1 kyr-period as the maximum production of diatom lipids, as β-sitosterol and fucosterol, and the maximum non-siliceous marine production, leading to maximum ARs of loliolide, cholesterol, biphytanediols, marine OC, TOC, long-chain alkyl diols, diatomsterol and dinosterol. Interestingly, the parameters indicating maximum river runoff, as the terrigenous bulk C_3 plant material, the maximum C_3 percentage of the plant-wax *n*-alkanes and possibly the plant-wax AR itself, and those indicating a substantial silicate enrichment by the river outflow, like β-sitosterol and fucosterol, occur in an even shorter period of 2 kyrs, i.e., within 31°. Maximum monsoonal conditions in southern Africa, leading to high precipitation in the Congo catchment during the austral summer, are thus, apparently, restricted to the 2000 years, which occur about half a precession cycle later than the weakest upwelling, causing highest SST. In our

case, the inferred maximum monsoonal conditions lead over the precession maximum, the maximum of southern African insolation. There might, as concluded above, be an error of about 120° in the phase, which would easily turn this lead into a lag.

The accumulation maxima of compounds, indicating highest river outflow show a broad co-occurrence with lipids that are produced during wind-driven oceanic upwelling and are not indicative for surface-water enrichment with dissolved silicate supplied by the Congo River (Schefuß et al., submitted-c). This is because oceanic upwelling during austral winter is strongest, when also the southern African monsoon during austral summer is strongest, i.e., when the northern African monsoon is weakest. It is, therefore, in the precessional cycle not possible to distinguish between a wind- and a river transport of the plant-wax compounds. Furthermore, maximum marine productivity due to strong upwelling occurs almost simultaneously with the maximum outflow of the Congo River in the precessional cycle, only separated by season. It is, therefore, not possible to separate fluvial silicate supply and oceanic upwelling in the precessional cycle by calculation of an 'excess siliceous productivity' (Schneider et al., 1997). The latter conclusion is independent from the potential phase error of the precessional variations at ODP Site 1077.

7.4.6. Tropical environmental response on the MPT

In the mid-Pleistocene, two major forcing regimes can be distinguished:

Before the growth of the additional global ice mass, a precessional cyclicity was prevalent. The dominance of low-latitude forcing was associated with a periodic enlarged river runoff, transporting dissolved silicate and C_3 plant terrigenous organic matter into the Angola Basin. The availability of silicate led to diatom production, as indicated by β-sitosterol, fucosterol and diatomsterol, off the Congo River mouth. Maximum monsoonal river outflow occurred in austral summer and strongest oceanic upwelling during austral winter, causing a coinciding high production of marine organic matter by river outflow and wind-driven upwelling in the precessional cycle.

After the onset of the MPT, the increasing global ice volume and the growing amplitude of the eccentricity cycle influenced the tropical environment. The enlarged ice volume increased the strength and zonality of the trade winds. Since the onset of the 100-kyr cycle (Fig. 7.9), the wind transport of plant-wax lipids and the wind-driven upwelling strongly increased. Enhanced oceanic upwelling led to higher eustigmatophyte productivity, but also coastal upwelling was increased, associated with higher haptophyte productivity.

The absolute level of marine productivity, however, was unaltered across the MPT. In the precessional cycle, highest marine organic matter production occurred during maximum oceanic upwelling and maximum river outflow, while in the eccentricity and obliquity cycle, maximum marine production took place during coastal upwelling, driven by strong coast-parallel winds. Maximum marine organic matter accumulation was always associated with the highest ARs of biphytanediols and loliolide due to a less severe oxic degradation at the sea floor (Schefuß et al., submitted-c).

There were, however, differences between the two ice-volume cycles, i.e., the 41- and 100-kyr cycle, regarding the marine phytoplankton response. The ice-volume growth in the 100-kyr cycle occurred in a sawtooth-like manner (Imbrie et

al., 1993) which presumably led to a relatively slow rotation and intensification of the mean annual trade-wind vector. In contrast, in the 41-kyr cycle, the growth of ice volume was more directly related to orbital forcing and led to a relative rapid increase in strength and zonality of the trade winds. It was, therefore, possible that silicate enrichment of the surface waters by river runoff occurred during ice-volume growth with strong winds in the 100-kyr cycle, causing a river-induced productivity maximum. On the other hand, significant surface-water fertilisation by river outflow and associated river-induced productivity was suppressed in the 41-kyr cycle.

In both ice-volume cycles, the highest accumulation of bulk terrigenous organic material occurred around maximum interglacial conditions, i.e., minimum ice volume, while in the precessional cycle it related to largest monsoonal river runoff, and also the maximum contribution of plant-wax lipids. These carry a predominant C_3 plant, i.e., rainforest, isotopic signature. In the longer orbital cycles, i.e., the 41- and 100-kyr cycles, however, the maximum plant-wax AR occurred during the growth of the ice volume, but significantly before the maximum of continental aridity, reflected by the maximum C_4 percentage of the plant-wax *n*-alkanes. The enhanced eolian transport of the plant waxes preceding maximum aridity indicates the de-stabilisation of the vegetation during increasing aridity and wind strength (Pokras, 1987).

The continental aridity is strongly coupled to the SST in the long-term, the longer orbital cycles and also in the 80-kyr cycle (Schefuß et al., submitted-a). The SST in the tropical Atlantic primarily controlled the atmospheric evaporation-precipitation balance (Ganopolski et al., 1998). The distinct 80-kyr cycle in the SST record likely was driven by the transitional 76-kyr ice-volume changes during the MPT (Mudelsee and Schulz, 1997), probably a re-adjustment of the enlarged ice sheets to their lower resonance frequency (Schefuß et al., submitted-b). The long-term SST development was linked to the severe breakdown of Atlantic deep ventilation during the MPT causing a long-term tropical warming by decreased northward heat export (Raymo et al., 1997; Schefuß et al., submitted-b). SST was also the dominant factor controlling the accumulation of mangrove lipids, indicating that the extent of mangrove vegetation was largely independent of sea-level changes in the mid-Pleistocene.

The general effects of the MPT on the ecosystem in the Angola Basin were thus a relatively decreasing importance of diatom productivity due to a lower availability of dissolved silicate and a higher relative importance of wind-driven upwelling and eolian transport of terrigenous biomarkers. These effects were exactly opposite to those in the classic upwelling areas of the eastern boundary currents, e.g., the Benguela system. There, the stronger trade winds since the MPT increased the diatom productivity due to the elevated silicate availability during coastal upwelling (Marlow et al., 2000).

7.5. Conclusions

- We investigated the environmental changes in the tropical Atlantic as response on the enlarged global ice volume and its changing frequency behaviour at the MPT using lipid biomarkers. Five distinct groups of the lipid accumulation rates and bulk geochemical parameters have been distinguished by principal component analysis, explaining a cumulative 82 % of the total lipid variance. Cross-spectral analyses reveal their phasing in orbital cycles.
- The contributions of eolian-transported biomarkers, i.e., the terrigenous plant-wax lipids, and of the lipids produced during strong wind-driven upwelling, like the long-chain alkenones and alkyl diols, were strongly increased with the onset of the 100-kyr cycle in trade-wind strength and zonality. The highest accumulation of the plant waxes in the longer orbital cycles preceded the maximum of continental aridity and indicates a de-stabilised vegetation by increasing wind strength and aridity. In contrast, their largest contribution in the precessional cycle related to maximum monsoonal Congo River runoff.
- The continental aridity, reflected by the C_4 percentage of the plant-wax lipids, and the accumulation of mangrove lipids were strongly coupled to the SST of the tropical Atlantic. SST controlled the atmospheric moisture balance in the longer orbital cycles and the long-term development. In the precessional cycle, the monsoon overruled the SST control of continental aridity. Sea-level changes did not influence the extent of mangrove vegetation in the mid-Pleistocene.
- The major sterol compounds represent either a diatom contribution induced by riverine supply of dissolved silicate, like β-sitosterol, fucosterol, and diatomsterol, or are produced during oceanic upwelling driven by strong zonal winds, like dinosterol and cholesterol. Therefore, these lipids mainly relate to precessional variations of river outflow and trade-wind zonality. In the precessional cycle, maximum trade-wind zonality coincided with maximum river runoff, occurring in austral winter and austral summer, respectively. Before the growth of global ice volume at the MPT, i.e., before 900 kyr BP, precessional forcing of river-induced and total marine productivity was predominant. Afterwards, the major sterols were only produced during the slow, sawtooth-like growth of the enlarged ice volume in the 100-kyr cycles. In the 41-kyr cycle, with its more linear response to orbital forcing, a large river runoff and surface-water fertilisation with dissolved silicate was not coinciding with the strengthened trade winds.
- The absolute level of bulk marine productivity was unaltered across the MPT. In the precessional cycle, highest marine organic matter production occurred during maximum oceanic upwelling and highest river runoff, while in the longer orbital cycles, maximum marine production took place during strong wind-driven coastal upwelling associated with haptophyte productivity. Maximum marine organic matter accumulation was always associated with the highest accumulations of biphytanediols and loliolide due to a less severe oxic degradation at the sea floor.
- The contribution of C_3 plant-derived, i.e., rainforest, terrigenous organic matter occurred during maximum interglacial conditions in the 100- and 41-kyr cycle, and during maximum monsoonal river outflow in the precessional cycle.
- Generally, the increased ice volume at the MPT suppressed the precessional variability in trade-wind zonality and monsoonal river runoff and thus decreased the periodic availability of dissolved silicate for a river-induced diatom

production. In turn, the increased trade-wind strength since the onset of the 100-kyr ice-volume variations led to a higher production of non-silicate marine organisms during wind-driven upwelling and elevated eolian transport of terrigenous biomarkers.

Acknowledgements

We gratefully thank the Ocean Drilling Program (ODP) for the supply of samples. We thank Marlèn Dekker, Wim Pool, Patty Slootweg, Elda Panoto, and Michiel Kienhuis for help with the GC-MS analyses. Gijs Nobbe (University of Utrecht) is thanked for providing the possibility for total organic carbon analyses. Stefan Schouten, Rich Pancost and Joe Werne are thanked for support during GC-irm-MS analyses. Johan van Bennekom is thanked for discussions on the recent hydrography of the Angola Basin.

References

Barrett S. M., Volkman J. K., and Dunstan G. A. (1995) Sterols of 14 species of marine diatoms (Bacillariophyta). *Journal of Phycology* **31**, 360-369.

Barth H. (1982) The biogeography of mangroves. In *Contributions to the ecology of halophytes* (ed. D. N. Sen and K. S. Rajpurohit), pp. 35-60.

Beastall G. H., Tyndall A. M., Rees H. H., and Goodwin T. W. (1974) Sterols in *Porphyridium* series. 4α-Methylcholesta-8,22-dien-3β-ol and 4α,24E–dimethyl-5α-cholesta-5,22-dien-3β-ol: two novel sterols from *Porphyridium cruentum*. *European Journal of Biochemistry* **41**, 301-309.

Beaton J. M., Spring F. S., Stevenson R., and Stewart J. L. (1955) Triterpenoids. Part XXXVII. The constitution of taraxerol. *Journal of Chemical Society*, 2131-2137.

Belt S. T., Cooke A. T., Robert J.-M., and Rowland D. (1996) Structural characterisation of widespread polyunsaturated isoprenoid biomarkers: a C_{25} triene, tetraene and panaene from the diatom *Haslea ostrearia* Simonsen. *Tetrahedron Letters* **27**, 4755-4758.

Berger A. and Loutre M. F. (1991) Insolation values for the climate of the last 10 million years. *Quaternary Science Reviews* **10**, 297-317.

Berger W. H. (1989) Global maps of ocean productivity. In *Productivity of the Ocean: Present and Past* (ed. W. H. Berger, V. S. Smetacek, and G. Wefer), pp. 429-455. Wiley-Interscience.

Berger W. H. and Jansen E. (1994) Mid-Pleistocene climate shift - the Nansen connection. *Geophysical Monographs* **84**, 295-311.

Berger W. H. and Wefer G. (1996) Central themes of South Atlantic circulation. In *The South Atlantic: Present and Past Circulation* (ed. G. Wefer, W. H. Berger, G. Siedler, and D. J. Webb), pp. 1-11. Springer.

Berger W. H., Wefer G., Richter C., and Shipboard Scientific Party (1998) Color cycles in Quaternary sediments from the Congo fan region (Site 1075): A statistical analysis. In *Proceedings of the Ocean Drilling Program, Initial Reports, Vol. 175*, Vol. 175 (ed. G. Wefer, W. H. Berger, C. Richter, et al.), pp. 561-567. Ocean Drilling Program.

Bird M. I., Summons R. E., Gagan M. K., Roksandic Z., Dowling L., Head J., Fifield L. K., Cresswell R. G., and Johnson D. P. (1995) Terrestrial vegetation change inferred from *n*-alkane $\delta^{13}C$ analyses in the marine environment. *Geochimica et Cosmochimica Acta* **59**, 2853-2857.

Biscaye P. E., Chesselet R., and Prospero J. M. (1974) Rb-Sr, $^{87}Sr/^{86}Sr$ isotope system as an index of provenance of continental dusts in the open Atlantic Ocean. *J. Researches Atmos.* **8**, 819-829.

Bolton E. W., Maasch K. A., and Lilly J. M. (1995) A wavelet analysis of Plio-Pleistocene climate indicators: a new view of periodicity evolution. *Geophysical Research Letters* **22**, 2753-2756.

Boon J. J. (1978) Molecular biogeochemistry of lipids in four natural environments. Ph.D. thesis, Delft University.

Boon J. J. and de Leeuw J. W. (1979) The analysis of wax esters, very long mid-chain ketones and sterol ethers isolated from Walvis Ridge diatomaceous ooze. *Marine Chemistry* **7**, 117-132.

Boon J. J., Rijpstra W. I. C., de Lange F., de Leeuw J. W., Yoshioka M., and Shimizu Y. (1979) Black Sea sterol - a molecular fossil for dinoflagellate blooms. *Nature* **277**, 125-127.

Borges Del Castillo J., Brooks C. J. W., Cambie R. C., Eglinton G., Hamilton R. J., and Pellitt P. (1967) The taxonomic distribution of some hydrocarbons in gymnosperms. *Phytochemistry* **6**, 391-398.

Brassell S. C. (1993) Applications of biomarkers for delineating marine paleoclimatic fluctuations during the Pleistocene. In *Organic Geochemistry* (ed. M. H. Engel and S. A. Macko), pp. 699-738. Plenum Press.

Brassell S. C. and Eglinton G. (1983) Steroids and triterpenoids in deep-sea sediments as environmental and diagenetic indicators. In *Advances in Organic Geochemistry, 1981*, pp. 684-697. J. Wiley & Sons.

Brassell S. C., Eglinton G., Marlowe I. T., Pflaumann U., and Sarnthein M. (1986a) Molecular stratigraphy: a new tool for climatic assessment. *Nature* **320**, 129-133.

Brassell S. C., Lewis C. A., de Leeuw J. W., de Lange F., and Sinninghe Damsté J. S. (1986b) Isoprenoid thiophenes: novel products of sediment diagenesis. *Nature* **320**, 160-162.

Brathauer U. and Abelmann A. (1999) Late Quaternary variations in sea surface temperatures and their relationship to orbital forcing recorded in the Southern Ocean (Atlantic sector). *Paleoceanography* **14**, 135-148.

Breteler F. J. (1969) The Atlantic species of *Rhizophora*. *Acta Botanica Neerlandica* **18**, 434-441.

Broecker W. S. (1991) The Great Ocean Conveyor. *Oceanography* **4**, 79-89.

Brown P. C., Painting S. J., and Cochrane K. L. (1991) Estimates of phytoplankton and bacterial biomass and production in the northern and southern Benguela ecosystem. *South African Journal of Marine Sciences* **11**, 537-564.

Cadée G. C. (1978) Primary production and chlorophyll in the Zaire River, estuary and plume. *Netherlands Journal of Sea Research* **12**, 368-381.

Cadée G. C. (1984) Particulate and dissolved organic carbon and chlorophyll a in the Zaire river, estuary and plume. *Netherlands Journal of Sea Research* **17**, 426-440.

Calvert S. E. and Pedersen T. F. (1992) Organic carbon accumulation and preservation in marine sediments: how important is anoxia. In *Productivity, Accumulation and Preservation of Organic Matter in Recent and Ancient Sediments* (ed. J. K. Whelan and J. W. Farrington), pp. 231-263. Columbia University Press.

Canfield D. E. (1989) Sulfate reduction and oxic respiration in marine sediments: implications for organic carbon preservation in euxinic environments. *Deep-Sea Research* **36**, 121-138.

Canfield D. E. (1994) Factors influencing organic carbon preservation in marine sediments. *Chemical Geology* **114**, 315-329.

Carlson T. N. and Prospero J. M. (1972) The large-scale movement of Saharan air outbreaks over the equatorial North Atlantic. *Journal of Applied Meteorology* **11**, 283-297.

Cerling T. E., Harris J. M., MacFadden B. J., Leakey M. G., Quade J., Eisenmann V., and Ehleringer J. R. (1997) Global vegetation change through the Miocene/Pliocene boundary. *Nature* **389**, 153-158.

Cerling T. E., Wang Y., and Quade J. (1993) Expansion of C_4 ecosystems as an indicator of global ecological change in the late Miocene. *Nature* **361**, 344-345.

Chen J., Farrell J. W., Murray D. W., and Prell W. L. (1995) Timescale and paleoceanographic implications of a 3.6 m.y. oxygen isotope record from the northeast Indian Ocean (Ocean Drilling Program Site 758). *Paleoceanography* **10**, 21-47.

Chester R., Elderfield H., Griffin J. J., Johnson L. R., and Padgham R. C. (1972) Eolian dust along the eastern margins of the Atlantic Ocean. *Marine Geology* **12**, 91-105.

Chester R. and Johnson L. R. (1971) Atmospheric dusts collected off the West African coast. *Nature* **229**, 105-107.

Chiapello I., Bergametti G., Chatenet B., Bousquet P., Dulac F., and Santos Soares E. (1997) Origins of African dust transported over the northeastern tropical Atlantic. *Journal of Geophysical Research* **102**, 13701-13709.

Chyong N. A. (1971) Atlantic Ocean phytoplankton south of the Gulf of Guinea on profiles along 11 and 14°S. *Oceanology* **11**, 896-901.

CLIMAP Members. (1981) Seasonal reconstructions of the Earth's surface at the last glacial maximum. *Geological Society of America Map and Chart Series* **MC-36**.

Collatz G. J., Berry J. A., and Clark J. S. (1998) Effects of climate and atmospheric CO_2 partial pressure on the global distribution of C_4 grasses: present, past and future. *Oecologia* **114**, 441-454.

Collister J. W., Rieley G., Stern B., Eglinton G., and Fry B. (1994) Compound-specific $\delta^{13}C$ analyses of leaf lipids from plants with differing carbon dioxide metabolism. *Organic Geochemistry* **21**, 619-627.

Conte M. H., Eglinton G., and Madureira L. A. S. (1995) Origin and fate of organic biomarker compounds in the water column and sediments of the eastern North Atlantic. *Philosophical Transactions of the Royal Society of London B* **348**, 169-178.

Cowie G. H. and Hedges J. I. (1994) Biochemical indicators of diagenetic alteration in natural organic matter mixtures. *Nature* **369**, 304-307.

Cox R. E., Mazurek M. A., and Simoneit B. R. T. (1982) Lipids in Harmattan aerosols of Nigeria. *Nature* **296**, 848-849.

Cranwell P. A. (1973) Chain-length distribution of *n*-alkanes from lake sediments in relation to post-glacial environmental change. *Freshwater Biology* **3**, 259-265.

Crowley T. J. (1992) North Atlantic deep water cools the Southern Hemisphere. *Paleoceanography* **7**, 489-497.

Darwin C. (1846) An account on the fine dust which falls on vessels in the Atlantic Ocean. *Quarterly Journal of the Geological Society London* **2**, 26-30.

de Leeuw J. W. and Baas M. (1986) Early stage diagenesis of steroids. In *Biological Markers on the Sedimentary Record* (ed. R. B. Johns), pp. 101-123. Elsevier.

de Leeuw J. W., Frewin N. L., van Bergen P. F., Sinninghe Damsté J. S., and Collinson M. E. (1995) Organic carbon as palaeoenvironmental indicator in the marine realm. In *Marine*

Palaeoenvironmental Analysis from Fossils, Vol. 83 (ed. D. W. Bosence and P. A. Allison), pp. 43-71. Geological Society Special Publication.

de Leeuw J. W. and Largeau C. (1993) A review of macromolecular organic compounds that comprise living organisms and their role in kerogen, coal and petroleum formation. In *Organic Geochemistry* (ed. M. H. Engel and S. A. Macko), pp. 23-72. Plenum Press.

de Leeuw J. W., Rijpstra W. I. C., and Schenck P. A. (1981) The occurrence and identification of C_{30}, C_{31} and C_{32} alkan-1,15-diols and alkan-15-one-1-ols in Unit I and Unit II Black Sea sediments. *Geochimica et Cosmochimica Acta* **45**, 2281-2285.

de Leeuw J. W., van der Meer F. W., Rijpstra W. I. C., and Schenck P. A. (1980) On the occurrence and structural identification of long-chain unsaturated ketones and hydrocarbons in sediments. In *Advances in Organic Geochemistry 1979* (ed. A. G. Douglas and J. R. Maxwell), pp. 211-217. Pergamon Press.

de Menocal P., Ortiz J., Guilderson T., Adkins J., Sarnthein M., Baker L., and Yarusinsky M. (2000) Abrupt onset and termination of the African Humid Period: rapid climate responses to gradual insolation forcing. *Quaternary Science Reviews* **19**, 347-361.

de Menocal P. B. (1995) Plio-Pleistocene African climate. *Science* **270**, 53-59.

de Menocal P. B. and Rind D. (1993) Sensitivity of Asian and African climate to variations in seasonal insolation, glacial ice cover, sea surface temperature, and Asian orography. *Journal of Geophysical Research* **98**, 7265-7287.

de Menocal P. B., Ruddiman W. F., and Pokras E. M. (1993) Influences of high- and low-latitude processes on African terrestrial climate: Pleistocene eolian records from equatorial Atlantic Ocean Drilling Program Site 663. *Paleoceanography* **8**, 209-242.

Deutsch C. V. and Journel A. G. (1992) *GSLIB: Geostatistical Software Library and User's Guide*. Oxford University Press.

Druyan L. (1989) Advances in the study of sub-Saharan drought. *International Journal of Climatology* **9**, 77-90.

Dupont L. M., Donner B., Schneider R. R., and Wefer G. (2001) Mid-Pleistocene environmental change in tropical Africa began as early as 1.05 Ma. *Geology* **29**, 195-198.

Eglinton G., Gonzales A. G., Hamilton R. J., and Raphael R. A. (1962) Hydrocarbon constituents of the wax coatings of plant leaves, a taxonomic survey. *Phytochemistry* **1**, 89-102.

Eglinton G. and Hamilton R. J. (1963) The distribution of *n*-alkanes. In *Chemical Plant Taxonomy* (ed. T. Swain), pp. 187-217. Academic Press.

Eglinton G. and Hamilton R. J. (1967) Leaf epicuticular waxes. *Science* **156**, 1322-1335.

Eglinton T. I., Benitez-Nelson B. C., Pearson A., McNichol A. P., Bauer J. E., and Druffel E. R. M. (1997) Variability in radiocarbon ages of individual organic compounds from marine sediments. *Science* **277**, 796-799.

Ehleringer J. R., Cerling T. E., and Helliker B. R. (1997) C_4 photosynthesis, atmospheric CO_2, and climate. *Oecologia* **112**, 285-299.

Eichmann R., Neuling P., Ketseridis G., Hahn J., Jaenicke R., and Junge C. (1979) *n*-Alkane studies in the troposhere-I. Gas and particulate concentrations in North Atlantic air. *Atmospheric Environment* **13**, 587-599.

Eisma D., Kalf J., and van der Gaast S. J. (1978) Suspended matter in the Zaire estuary and adjacent Atlantic Ocean. *Netherlands Journal of Sea Research* **12**, 382-406.

Eisma D. and van Bennekom A. J. (1978) The Zaire river and estuary and the Zaire outflow in the Atlantic Ocean. *Netherlands Journal of Sea Research* **12**, 255-272.

Eliassen A. (1976) *The trajectory model: a technical description*. Norwegian Institute of Air Research.

Ensminger A., van Dosselaer A., Spyckerelle C., Albrecht P., and Ourisson G. (1974) Pentacyclic triterpanes of the hopane type as ubiquitous geochemical markers: origin and significance. In *Advances in Organic Geochemistry 1973* (ed. B. Tissot and F. Bienner), pp. 245-260. Editions Technip.

Falkowski P. G., Barber R. T., and Smetacek V. (1998) Biogeochemical controls and feedbacks on ocean primary production. *Science* **281**, 200-206.

Farquhar G. D., Ehleringer J. R., and Hubick K. T. (1989) Carbon isotope discrimination and photosynthesis. *Annual Reviews of Plant Physiology and Plant Molecular Biology* **40**, 503-537.

Fischer G., Müller P. J., and Wefer G. (1998) Latitudinal $\delta^{13}C_{org}$ variations in sinking matter and sediments from the South Atlantic: Effects from anthropogenic CO_2 and implications for palaeo-pCO_2 reconstructions. *Journal of Marine Sciences* **17**, 471-495.

Freeman K. H., Hayes J. M., Trendel J.-M., and Albrecht P. (1990) Evidence from carbon isotope measurements for diverse origins of sedimentary hydrocarbons. *Nature* **343**(254-256).

Frewin N. L., Killops S. D., van Bergen P. F., de Leeuw J. W., and Collinson M. E. (1993) Preservation potential of biomacromolecules of higher plant cuticules in Florida Bay. In *Organic Geochemistry: Poster sessions from the 16th International Meeting on Organic Geochemistry, Stavanger* (ed. K. Øygard), pp. 566-569. Falch Hurtigtrykk.

Gagosian R. B. and Farrington J. W. (1978) Sterenes in surface sediments from the southwest African shelf and slope. *Geochimica et Cosmochimica Acta* **42**, 1091-1101.

Gagosian R. B. and Peltzer E. T. (1986) The importance of atmospheric input of terrestrial organic material to deep-sea sediments. *Organic Geochemistry* **10**, 661-669.

Gagosian R. B., Peltzer E. T., and Merill J. T. (1987) Long-range transport of terrestrially derived lipids in aerosols from the South Pacific. *Nature* **325**, 800-803.

Gagosian R. B., Peltzer E. T., and Zafiriou O. C. (1981) Atmospheric transport of continentally derived lipids to the tropical North Pacific. *Nature* **291**, 312-314.

Gagosian R. B., Volkman J. K., and Nigrelli G. E. (1983) The use of sediment traps to determine sterol sources in coastal sediments off Peru. In *Advances in Organic Geochemistry 1981* (ed. M. Bjorøy et al.), pp. 369-379. Wiley.

Ganopolski A., Rahmstorf S., Petoukhov V., and Claussen M. (1998) Simulation of modern and glacial climates with a coupled global model of intermediate complexity. *Nature* **391**, 351-356.

Gasse F., Stabell B., Fourtanier E., and van Iperen Y. (1989) Freshwater diatom influx in intertropical Atlantic: relationships with continental records from Africa. *Quaternary Research* **32**, 229-243.

Gelin F., Volkman J. K., de Leeuw J. W., and Sinninghe Damsté J. S. (1997) Mid-chain hydroxy long-chain fatty acids in microalgae from the genus *Nannochloropsis*. *Phytochemistry* **45**, 641-646.

Ghosh A., Misra S., Dutta A. K., and Choudhury A. (1985) Pentacyclic triterpenoids and sterols from seven species of mangrove. *Phytochemistry* **24**, 1725-1727.

Goad L. J. and Goodwin T. W. (1972) The biosynthesis of plant sterols. *Progress in Phytochemistry* **3**, 113-198.

Goad L. J. and Whithers N. (1982) Identification of 27-nor-(24R)-24-methylcholesta-5,22-dien-3β-ol and brassicasterol as the major sterols of the marine diatom *Gymnodinium simplex*. *Lipids* **17**, 853-858.

Goñi M. A., Ruttenberg K. C. R., and Eglinton T. I. (1998) A reassessment of the sources and importance of land-derived organic matter in surface sediments from the Gulf of Mexico. *Organic Geochemistry* **62**, 3055-3075.

Grice K., Klein Breteler W. M., Schouten S., Grossi V., de Leeuw J. W., and Sinninghe Damsté J. S. (1998) Effects of zooplankton herbivory on biomarker proxy records. *Paleoceanography* **13**, 686-693.

Hall D. M. and Jones R. L. (1961) Physiological significance of surface wax on leaves. *Nature* **191**, 95-96.

Hartnett H. E., Keil R. G., Hedges J. I., and Devol A. H. (1998) Influence of oxygen exposure time on organic carbon preservation in continental margin sediments. *Nature* **391**, 572-574.

Harvey R. H., Tuttle J. H., and Bell T. (1995) Kinetics of phytoplankton decay during simulated sedimentation: Changes in biochemical composition and microbial activity under oxic and anoxic conditions. *Geochimica et Cosmochimica Acta* **59**, 3367-3377.

Hastenrath S. (1982) On meridional heat transports in the world ocean. *Journal of Physical Oceanography* **12**, 922-927.

Hayes J. M. (1993) Factors controlling ^{13}C contents of sedimentary organic compounds: Principles and evidence. *Marine Geology* **113**, 111-125.

Hayes J. M., Freeman K. H., Popp B. N., and Hoham C. H. (1990) Compound-specific isotopic analysis: a novel tool for reconstruction of ancient biogeochemical processes. *Organic Geochemistry* **16**, 1115-1128.

Hedges J. I. and Prahl F. G. (1993) Early Diagenesis: Consequences for Applications of Molecular Biomarkers. In *Organic Geochemistry* (ed. M. H. Engel and S. A. Macko), pp. 237-253. Plenum Press.

Hinrichs K.-U., Schneider R. R., Müller P. J., and Rullkötter J. (1999) A biomarker perspective on paleoproductivity variations in two Late Quaternary sediment sections from the Southeast Atlantic Ocean. *Organic Geochemistry* **30**, 341-366.

Hoefs M. J. L., Rijpstra W. I. C., and Sinninghe Damsté J. S. (2002) The influence of oxic degradation on the sedimentary biomarker record I: Evidence from Madeira Abyssal Plain turbidites. *Geochimica et Cosmochimica Acta* **66**, 2719-2735.

Hoefs M. J. L., Schouten S., de Leeuw J. W., King L. L., Wakeham S. G., and Sinninghe Damsté J. S. (1997) Ether lipids of planktonic archaea in the marine water column. *Applied and Environmental Microbiology* **63**, 3090-3095.

Holtvoeth J., Wagner T., Horsfield B., Schubert C. J., and Wand U. (2001) Late-Quaternary supply of terrigenous organic matter to the Congo deep-sea fan (ODP Site 1075): implications for equatorial African paleoclimate. *Geo-Marine Letters* **21**, 23-33.

Hooghiemstra H., Melice J. L., Berger A., and Shackleton N. J. (1993) Frequency spectra and paleoclimatic variability of the high-resolution 30-1450 ka Funza pollen record (eastern Cordillera, Colombia). *Quaternary Science Reviews* **12**, 141-156.

Hopmans E. C., Schouten S., Pancost R. D., van der Meer M. T. J., and Sinninghe Damsté J. S. (2000) Analysis of intact tetraether lipids in archaeal cell material and sediments by High Performance Liquid Chromatography/Atmospheric Pressure Chemical Ion Mass Spectrometry. *Rapid Communications in Mass Spectrometry* **14**, 585-589.

Howard W. R. and Prell W. L. (1992) Late Quaternary surface circulation of the Southern Indian Ocean and its relationship to orbital variations. *Paleoceanography* **7**, 79-118.

Hsü C.-P. F. and Wallace J. M. (1976) The global distribution of the annual and semiannual cycles in precipitation. *Monthly Weather Review* **104**, 1093-1101.

Huang W.-Y. and Meinschen W. G. (1976) Sterols as source indicators of organic materials in sediments. *Geochimica et Cosmochimica Acta* **40**, 323-330.

Huang Y., Dupont L., Sarnthein M., Hayes J. M., and Eglinton G. (2000) Mapping of C_4 plant input from North West Africa into North East Atlantic sediments. *Geochimica et Cosmochimica Acta* **64**, 3505-3513.

Huang Y., Street-Perrott F. A., Metcalfe S. E., Brenner M., Moreland M., and Freeman K. H. (2001) Climate change as the dominant control on glacial-interglacial variations in C_3 and C_4 plant abundance. *Science* **293**, 1647-1651.

Imbrie J., Berger A., Boyle E. A., Clemens S. C., Duffy A., Howard W. R., Kukla G., Kutzbach J., Martinson D. G., McIntyre A., Mix A. C., Molfino B., Morley J. J., Peterson L. C., Pisias N. G., Prell W. L., Raymo M. E., Shackleton N. J., and Toggweiler J. R. (1993) On the structure and origin of major glaciation cycles 2. the 100,000-year cycle. *Paleoceanography* **8**, 699-735.

Imbrie J., Hays J. D., Martinson D. G., McIntyre A., Mix A. C., Morley J. J., Pisias N. G., Prell W. L., and Shackleton N. J. (1984) The orbital theory of Pleistocene climate: support from a revised chronology of the marine $\delta^{18}O$ record. In *Milankovitch and Climate, understanding the response to astronomical forcing*, Vol. 26 part 1 (ed. A. Berger, J. Imbrie, J. Hays, G. Kukla, and B. Saltzman), pp. 510. D. Reidel Publishing Company.

Imbrie J., McIntyre A., and Mix A. (1989) Oceanic response to orbital forcing in the late Quaternary: Observational and experimental strategies. In *Climate and Geo-sciences*, Vol. 285 (ed. A. Berger, S. Schneider, and J. C. Duplessy), pp. 121-164. Kluwer Acad. Pub.

Jansen J. H. F. (1985) Middle and Late Quaternary carbonate production and dissolution, and paleoceanography of the eastern Angola Basin, South Atlantic Ocean. In *South Atlantic Paleoceanography* (ed. K. J. Hsü and H. J. Weissert), pp. 25-46. Cambridge University Press.

Jansen J. H. F. (1990) Glacial-interglacial oceanography of the southeastern Atlantic Ocean and the paleoclimate of west central Africa. In *Paysages Quaternaires de L'Afrique centrale Atlantique* (ed. R. Lanfranchi and D. Schwartz), pp. 110-123. Institut Francais de Recherche Scientifique pour le Developpement en Cooperation.

Jansen J. H. F., Alderliesten C., Houston C. M., de Jong A. F. M., van der Borg K., and van Iperen J. M. (1989) Aridity in equatorial Africa during the last 225,000 years: a record of opal phytoliths/freshwater diatoms from the Zaire (Congo) deep-sea fan (NE Angola Basin). *Radiocarbon* **31**, 557-569.

Jansen J. H. F., de Lange G. J., van Bennekom A. J., et al. (1990) (Pale)oceanography and geochemistry of the Angola Basin (South Atlantic Ocean); Cruise Report R.V.Tyro, 30 September - 19 November 1989. *Netherlands Institute for Sea Research Report* **1990**, 1-65.

Jansen J. H. F. and Dupont L. M. (2001) A revised composite depth record for Site 1077 based on magnetic susceptibility and XRF core scanner (CORTEX) data. In *Proceedings of the Ocean Drilling Program, Scientific Results, Vol. 175*, Vol. 175 (ed. G. Wefer, W. H. Berger, C. Richter, et al.), pp. 1-10 [Online at: http://www-odp.tamu.edu/publications/175_SR/chap_20/chap_20.htm]. Ocean Drilling Program.

Jansen J. H. F., Ufkes E., and Schneider R. R. (1996) Late Quaternary Movements of the Angola-Benguela Front, SE Atlantic, and Implications for Advection in the Equatorial Ocean. In *The South Atlantic* (ed. G. Wefer, W. H. Berger, G. Siedler, and D. J. Webb), pp. 553-575. Springer-Verlag.

Jansen J. H. F., van der Gaast S. J., Koster B., and Vaars A. J. (1998) CORTEX, a shipboard XRF-scanner for element analyses in split sediment cores. *Marine Geology* **151**, 143-153.

Jansen J. H. F. and van Iperen J. M. (1991) A 220,000-year climatic record for the east equatorial Atlantic Ocean and equatorial Africa: evidence from diatoms and opal phytoliths in the Zaire (Congo) deep-sea fan. *Paleoceanography* **6**, 573-591.

Jansen J. H. F., van Weering T. C. E., Gieles R., and van Iperen J. (1984) Middle and Late Quaternary oceanography and climatology of the Zaire-Congo fan and adjacent eastern Angola Basin. *Netherlands Journal of Sea Research* **17**, 201-249.

Joussaume S. and 35 co-authors (1999) Monsoon changes for 6000 years ago: results of 18 simulations from the Paleoclimate Modeling Intercomparison Project (PMIP). *Geophysical Research Letters* **26**, 859-862.

Kalu A. E. (1979) The African dust plume: Its characteristics and propagation across West Africa in winter. *SCOPE* **14**, 95-118.

Katz E. J. and Garzoli S. L. (1982) Response of the western equatorial Atlantic Ocean to an annual wind cycle. *Journal of Marine Research* **40**, 307-327.

Killops S. D. and Frewin N. L. (1994) Triterpenoid diagenesis and cuticular preservation. *Organic Geochemistry* **21**, 1193-1209.

Klok J., Baas M., Cox H. C., de Leeuw J. W., and Schenck P. A. (1984) Loliolides and dihydroactinidiolide in a recent marine sediment probably indicate a major transformation pathway of carotenoids. *Tetrahedron Letters* **25**, 5577-5580.

Kohnen M. E. L., Sinninghe Damsté J. S., Kock-van Dalen A. C., ten Haven H. L., Rullkötter J., and de Leeuw J. W. (1990) Origin and diagenetic transformations of C_{25} and C_{30} highly branched isoprenoid sulphur compounds: Further evidence for the formation of organically bound sulphur during early diagenesis. *Geochimica et Cosmochimica Acta* **54**, 3053-3063.

Kolattukudy P. E. (1976) *The Chemistry and Biochemistry of Natural Waxes*. Elsevier.

Kolattukudy P. E. (1980) Cutin, Suberin and Waxes. In *The Biochemistry of Plants*, Vol. 4 (ed. P. K. Stumpf), pp. 571-641. Academic Press.

Krige D. G. (1951) A statistical approach to some basic mine valuation problems on the Witwatersrand. *Journal of the Chemical, Metallurgical and Mineral Society of South Africa* **52**, 119-139.

Kroopnick P. M. (1985) The distribution of ^{13}C of CO_2 in the world oceans. *Deep-Sea Research* **32**, 57-84.

Kuypers M. M. M., Pancost R. D., and Sinninghe Damsté J. S. (1999) A large and abrupt fall in atmospheric CO_2 concentration during Cretaceous times. *Nature* **399**, 342-345.

Laskar J. (1990) The chaotic motion of the solar system: A numerical estimate of the chaotic zones. *Icarus* **88**, 266-291.

Lau K.-M. and Weng H. (1995) Climate signal detection using wavelet transform: How to make a time series sing. *Bulletin of the American Meteorological Society* **76**, 2391-2402.

Leemans R. and Cramer W. P. (1991) *The IIASA database for mean monthly values of temperature, precipitation and cloudiness on a global terrestrial grid*. International Institute for Applied Systems Analysis.

Lepple F. K. and Brine C. J. (1976) Organic constituents in eolian dust and surface sediments from Northwest Africa. *Journal of Geophysical Research* **81**, 1141-1147.

Levitus S. and Boyer T. P. (1994) *World Ocean Atlas 1994, Volume 4: Temperature, NOAA Atlas NESDIS 4*. U.S. Department of Commerce.

Lichtfouse E., Derenne S., Mariotti A., and Largeau C. (1994) Possible algal origin of long chain odd *n*-alkanes in immature sediments as revealed by distributions and carbon isotope ratios. *Organic Geochemistry* **22**, 1023-1027.

Lorenz S., Grieger P., Helbig P., and Herterich K. (1996) Investigating the sensitivity of the Atmospheric General Circulation Model ECHAM 3 to paleoclimate boundary conditions. *Geologische Rundschau* **85**, 512-523.

Louda J. W. and Baker E. W. (1984) Perylene occurrence and possible sources in deep-ocean sediments. *Geochimica et Cosmochimica Acta* **48**, 1043-1058.

Lough J. (1986) Tropical Atlantic sea surface temperatures and rainfall variations in sub-Saharan Africa. *Monthly Weather Review* **114**, 561-570.

Lutjeharms J. R. E. and Stokton P. L. (1987) Kinematics of the upwelling front off southern Africa. *South African Journal of Marine Sciences* **5**, 35-49.

Lutjeharms J. R. E. and van Ballegooyen R. C. (1988) The retroflection of the Agulhas Current. *Journal of Physical Oceanography* **18**, 1570-1583.

Lyle M. (1988) Climatically forced organic carbon burial in equatorial Atlantic and Pacific Oceans. *Nature* **335**, 529-532.

Maasch K. A. (1988) Statistical detection of the mid-Pleistocene transition. *Climate Dynamics* **2**, 133-143.

Manabe S. and Broccoli A. J. (1985) The influence of continental ice sheets on the climate of an ice age. *Journal of Geophysical Research* **90**, 2167-2190.

Manabe S. and Stouffer R. J. (1988) Two Stable Equilibria of a Coupled Ocean-Atmosphere Model. *Journal of Climate* **1**, 841-866.

Mariotti A., Gadel. F., Giresse P., and Kinga-Mouzeo. (1991) Carbon isotope composition and geochemistry of particulate organic matter in the Congo River (Central Africa): Application to the study of Quaternary sediments off the mouth of the river. *Chemical Geology* **86**, 345-357.

Marlow J. R., Lange C. B., Wefer G., and Rosell-Melé A. (2000) Upwelling intensification as a part of the Pliocene-Pleistocene climate transition. *Science* **290**, 2288-2291.

Marlowe I. T., Brassell S. C., Eglinton G., and Green J. C. (1984) Long chain unsaturated ketones and esters in living algae and marine sediments. *Organic Geochemistry* **6**, 135-141.

Mazurek M. A. and Simoneit B. R. T. (1984) Characterization of biogenic and petroleum-derived organic matter in aerosols over remote, rural and urban areas. In *Identification and Analysis of Organic Pollutants in Air* (ed. L. H. Keith), pp. 353-370. Ann Arbor Science, Butterworth Publishers.

McIntyre A., Ruddiman W. F., Karlin K., and Mix A. C. (1989) Surface water response of the equatorial Atlantic Ocean to orbital forcing. *Paleoceanography* **4**, 19-55.

Meeuwis J. M. and Lutjeharms J. R. E. (1990) Surface thermal characteristics of the Angola-Benguela Front. *South African Journal of Marine Science* **9**, 261-279.

Merrit D. A., Brand W. A., and Hayes J. M. (1994) Isotope-ratio monitoring gas chromatography: methods for isotopic calibration. *Organic Geochemistry* **21**, 573-584.

Milankovitch M. (1930) *Mathematische Klimalehre und astronomische Theorie der Klimaschwankungen*. Gebrüder Borntraeger.

Miller J. R. and Russell G. L. (1989) Ocean heat transport during the Last Glacial Maximum. *Paleoceanography* **4**, 141-155.

Miller K., Fairbanks R. G., and Mountain G. S. (1987) Tertiary oxygen isotope synthesis, sea level history, and continental margin erosion. *Paleoceanography* **2**, 1-19.

Mix A. C., Ruddiman W. F., and McIntyre A. (1986) Late Quaternary paleoceanography of the tropical Atlantic, 1: Spatial variability of annual sea surface temperatures, 0-20,000 years B.P. *Paleoceanography* **1**, 43-66.

Moguedet G. (1980) Le milieu de mangrove au Congo. In *Mangroves d'afrique et asie*, Vol. 39 (ed. F. Blasco, C. Caratini, A. Fredou, P. Giresse, G. Moguedet, C. Tissot, and H. Weiss), pp. 5-19. Centre National de la Recherche Scientifique.

Mudelsee M. (2001) The phase relations among atmospheric CO_2 content, temperature and global ice volume over the past 420 ka. *Quaternary Science Reviews* **20**, 583-589.

Mudelsee M. and Schulz M. (1997) The Mid-Pleistocene climate transition: onset of 100 ka cycle lags ice volume build-up by 280 ka. *Earth and Planetary Science Letters* **151**, 117-123.

Mulitza S. and Rühlemann C. (2000) African monsoonal precipitation modulated by interhemispheric temperature gradients. *Quaternary Research* **53**, 270-274.

Müller P. J., Cepek M., Ruhland G., and Schneider R. R. (1997) Alkenone and coccolithophorid species changes in late Quaternary sediments from the Walvis Ridge: implications for the alkenone paleotemperature method. *Paleogeography, Paleoclimatology, Paleoecology* **135**, 71-96.

Müller P. J., Kirst G., Ruhland G., von Storch I., and Rosell-Mele A. (1998) Calibration of the alkenone paleotemperature index U^{K}_{37}' based on core-tops from the eastern South Atlantic and the global ocean (60°N-60°S). *Geochimica et Cosmochimica Acta* **62**, 1757-1772.

Müller P. J., Schneider R., and Ruhland G. (1994) Late Quaternary pCO_2 variations in the Angola Current: evidence from organic carbon $\delta^{13}C$ and alkenone temperatures. In *Carbon cycling in the glacial ocean: Constraints on the ocean's role in global change*, Vol. 117 (ed. R. Zahn et al.), pp. 343-366. Springer-Verlag.

Nes W. R. and McKean M. L. (1977) *Biochemistry of Steroids and other Isopentenoids*. University Park Press.

Nichols P. D., Jones G. J., and de Leeuw J. W. (1984) The fatty acid and sterol composition of two marine dinoflagellates. *Phytochemistry* **23**, 1043-1047.

O'Leary M. H. (1981) Carbon isotope fractionation in plants. *Phytochemistry* **20**, 553-568.

Pagani M., Freeman K. H., and Arthur M. A. (1999) Late Miocene atmospheric CO_2 concentrations and the expansion of C_4 grasses. *Science* **285**, 876-879.

Park J. and Maasch K. A. (1993) Plio-Pleistocene time evolution of the 100-kyr cycle in marine paleoclimate records. *Journal of Geophysical Research* **98**, 447-461.

Patterson G. W. (1987) Sterol synthesis and distribution in algal phylogeny. In *The Metabolism, Structure and Function of Plant Lipids*, Vol. 631-636 (ed. W. K. Stumpf, J. B. Mudd, and W. D. Nes). Plenum Press.

Patterson G. W. (1991) Sterols of algae. In *Physiology and Biochemistry of Sterols* (ed. G. W. Patterson and W. D. Nes), pp. 118-157. American Oil Chemist Society.

Peltzer E. T. and Gagosian R. B. (1987) Sampling and quantitation of lipids in aerosols from the remote atmosphere. *Analytica Chimica Acta* **198**, 125-144.

Peterson R. G. and Stramma L. (1991) Upper-level circulation in the South Atlantic Ocean. *Progress in Oceanography* **26**, 1-73.

Petit J. R., Jouzel J., Raynaud D., Barkov N. I., Barnola J.-M., Basile I., Bender M., Chappellaz J., Davis M., Delaygue G., Delmotte M., Kotlyakov V. M., Legrad M., Lipenkov V. Y., Lorius C., Pepin L., Ritz C., Saltzman E., and Stievenard M. (1999) Climate and atmospheric history of the past 420,000 years from the Vostok ice core, Antarctica. *Nature* **399**, 429-436.

Petit-Marie N. (1991) *Paleoenvironments du Sahara*. CNRS.

Petterssen S. (1956) *Weather Analysis and Forecasting*. McGraw-Hill.

Philander S. G. H. and Pacanowski R. C. (1986) A model of the seasonal cycle in the tropical Atlantic Ocean. *Journal of Geophysical Research* **91**, 14192-14206.

Pisias N. G. and Moore T. C., Jr. (1981) The evolution of Pleistocene climate: A time series approach. *Earth and Planetary Science Letters* **52**, 450-458.

Pokras E. M. (1987) Diatom record of late Quaternary climatic change in the eastern equatorial Atlantic and tropical Africa. *Paleoceanography* **2**, 273-286 .

Pokras E. M. and Mix A. C. (1985) Eolian Evidence for Spatial Variability of Late Quaternary Climates in Tropical Africa. *Quaternary Research* **24**, 137-149.

Poynter J. G., Farrimond P., Brassell S. C., and Eglinton G. (1989) Aeolian-derived higher plant lipids in the marine sedimentary record: Links with paleoclimate. In *Palaeoclimatology and palaeometeorology: modern and past patterns of global atmosphere transport* (ed. M. Leinen and M. Sarnthein), pp. 435-462. Kluwer.

Prahl F. G., de Lange G. J., Lyle M., and Sparrow M. A. (1989) Post-depositional stability of long-chain alkenones under contrasting redox conditions. *Nature* **341**, 434-437.

Prahl F. G., Dymond J., and Sparrow M. (2000) Annual biomarker record for export production in the central Arabian Sea. *Deep-Sea Research* **47**, 1581-1604.

Prahl F. G., Muehlhausen L. A., and Zahnle D. L. (1988) Further evaluation of long-chain alkenons as indicators of paleoceanographic conditions. *Geochimica et Cosmochimica Acta* **52**, 2303-2310.

Prahl F. G. and Wakeham S. G. (1987) Calibration of unsaturation patterns in long-chain ketone compositions for palaeotemperature assessment. *Nature* **330**, 367-369.

Prell W. L. (1982) Oxygen and carbon isotope stratigraphy for the Quaternary of Hole 502B: evidence for two modes of isotopic variability. In *Proceedings of the Deep-Sea Drilling Program, Initial Report*, Vol. 68 (ed. W. L. Prell and J. V. Gardner), pp. 455-464. U.S. Govt. Printing Office.

Prell W. L. and Kutzbach J. E. (1987) Monsoon variability over the past 150,000 years. *Journal of Geophysical Research* **92**, 8411-8425.

Prospero J. M. and Carlson T. N. (1972) Vertical and areal distribution of Saharan dust over the western equatorial North Atlantic Ocean. *Journal of Geophysical Research* **77**, 5255-5265.

Pye K. (1987) *Aeolian Dust and Dust Deposits*. Academic Press.

Radczewski O. E. (1939) Eolian deposits in marine sediments. In *Recent Marine Sediments (Symposium)* (ed. P. Trask), pp. 496-502. American Association of Petroleum Geologists.

Ratmeyer V., Balzer W., Bergametti G., Chiapello I., Fischer G., and Wyputta U. (1999) Seasonal impact of mineral dust on deep-ocean particle flux in the eastern subtropical Atlantic Ocean. *Marine Geology* **159**, 241-252.

Raymo M. E., Oppo D. W., and Curry W. (1997) The mid-Pleistocene climate transition: A deep sea carbon isotopic perspective. *Paleoceanography* **12**, 546-559.

Raymo M. E. and Ruddiman W. F. (1992) Tectonic forcing of late Cenozoic climate. *Nature* **359**, 117-122.

Raymo M. E., Ruddiman W. F., Shackleton N. J., and Oppo D. W. (1990) Evolution of Atlantic-Pacific $\delta^{13}C$ gradients over the last 2.5 m.y. *Earth and Planetary Science Letters* **97**, 353-368.

Repeta D. J. (1989) Carotenoid diagenesis in recent marine sediments: II. Degradation of fucoxanthin to loliolide. *Geochimica et Cosmochimica Acta* **53**, 699-707.

Riehl H. (1979) *Climate and Weather in the Tropics*. Academic Press.

Rieley G., Collister J. W., Stern B., and Eglinton G. (1993) Gas chromatography/Isotope ratio mass spectrometry of leaf wax *n*-alkanes from plants with differing carbon dioxide metabolisms. *Rapid Communications in Mass Spectrometry* **7**, 488-491.

Robinson N., Eglinton G., Brassell S. C., and Cranwell P. A. (1984) Dinoflagellate origin for sedimentary 4a-methylsteroids and 5a(H)-stanols. *Nature* **308**, 439-442.

Rohmer M., Boivier-Nave P., and Ourisson G. (1989) Distribution of hopanoid triterpenes in prokaryotes. *Journal of Genetic Microbiology* **130**, 1137-1150.

Rospondek M. J., Köster J., and Sinninghe Damsté J. S. (1997) Novel C_{26} highly branched isoprenoid thiophenes and alkane from the Menilite Formation, Outer Carpathians, SE Poland. *Organic Geochemistry* **26**, 295-304.

Ruddiman W. F. and Janecek T. (1989) Pliocene-Pleistocene biogenic and terrigenous fluxes at equatorial Atlantic Sites 662, 663, and 664. In *Proceedings of the Ocean Drilling Program, Scientific Results*, Vol. 108 (ed. W. F. Ruddiman, M. Sarnthein et al.), pp. 211-240. Ocean Drilling Program.

Ruddiman W. F., Raymo M. E., Martinson D. G., Clement B. M., and Backman J. (1989a) Pleistocene evolution: Northern Hemisphere ice sheets and North Atlantic Ocean. *Paleoceanography* **4**, 353-412.

Ruddiman W. F., Sarnthein M., Baldauf J., Backman J., Curry W., Dupont L. M., Janecek T., Pokras E. M., Raymo M. E., Stabell B., Stein R., and Tiedemann R. (1989b) Late Miocene to Pleistocene evolution of climate in Africa and the low-latitude Atlantic: Overview of Leg 108 results. In *Proceedings of the Ocean Drilling Program, Scientific Results*, Vol. 108 (ed. W. Ruddiman, M. Sarnthein et al.), pp. 463-484. Ocean Drilling Program.

Rühlemann C., Mulitza S., Müller P.J., Wefer G., and Zahn R. (1999) Warming of the tropical Atlantic Ocean and slowdown of thermohaline circulation during the last deglaciation. *Nature* **402**, 511-514.

Sackett W. M. (1989) Stable carbon isotope studies on organic matter in the marine environment. In *Handbook of Environmental Isotope Geochemistry* (ed. P. Fritz and J. C. Fontes), pp. 139-169. Elsevier.

Sargent J. R., Lee R. F., and Nevenzel J. C. (1976) Marine waxes. In *Chemistry and biochemistry of natural waxes* (ed. P. E. Kollattukudy), pp. 49-92. Elsevier.

Sarnthein M., Duplessy J. C., and Fontugne M. R. (1988) Global variations of surface ocean productivity in low and mid latitudes: Influence on CO_2 reservoirs of the deep ocean and atmosphere during the last 21,000 years. *Paleoceanography* **3**, 361-399.

Sarnthein M., Pflaumann U., Ross R., Tiedemann R., and Winn K. (1992) Transfer functions to reconstruct ocean paleoproductivity: a comparison. In *Upwelling Systems: Evolution Since the Early Miocene*, Vol. 64 (ed. C. P. Summerhayes, W. L. Prell, and K. C. Emeis), pp. 411-427. Geological Society Special Publication.

Sarnthein M., Tetzlaff G., Koopmann B., Wolter K., and Pflaumann U. (1981) Glacial and interglacial wind regimes over the eastern subtropical Atlantic and North-West Africa. *Nature* **293**, 193-196.

Sarnthein M., Winn K., Jund S. J. A., Duplessy J.-C., Labeyrie L., Erlenkeuser H., and Ganssen G. (1994) Changes in east Atlantic deepwater circulation over the last 30,000 years: Eight time slice reconstructions. *Paleoceanography* **9**, 209-268.

Sarnthein M., Winn K., and Zahn R. (1987) Paleoproductivity of oceanic upwelling and the effect on atmospheric CO_2 and climatic change during deglaciation times. In *Abrupt Climatic Change* (ed. W. H. Berger and L. D. Labeyrie), pp. 311-337. D. Reidel Publishing Company.

Schefuß E., Ratmeyer V., Jansen J. H. F., and Sinninghe Damsté J. S. (re-submitted) Carbon isotope analysis of *n*-alkanes in dust from the lower atmosphere over the central eastern Atlantic. *Geochimica et Cosmochimica Acta*.

Schefuß E., Schouten S., Jansen J. H. F., and Sinninghe Damsté J. S. (submitted-a) Aridity controls African C_4 plant abundance. *Nature*.

Schefuß E., Sinninghe Damsté J. S., and Jansen J. H. F. (submitted-b) Forcing of tropical Atlantic sea-surface temperatures during the Mid-Pleistocene transition. *Paleoceanography*.

Schefuß E., Versteegh G. J. M., Jansen J. H. F., and Sinninghe Damsté J. S. (2001) Marine and terrigenous lipids in South-East Atlantic sediments (ODP Leg 175) as paleo-environmental indicators: initial results. In *Proceedings ODP, Scientific Results*, Vol. 175 (ed. G. Wefer, W. H.

Berger, and C. Richter), pp. 1-34 [Online at: http://www-odp.tamu.edu/publications/175_SR/chap_10/chap_10.htm]. Ocean Drilling Program.

Schefuß E., Versteegh G. J. M., Jansen J. H. F., and Sinninghe Damsté J. S. (submitted-c) Lipid biomarkers as major source and preservation indicators in SE Atlantic surface sediments. *Deep-Sea Research, Part I.*

Schmieder F., von Dobeneck T., and Bleil U. (2000) The Mid-Pleistocene climate transition as documented in the deep South Atlantic: initiation, interim state and terminal event. *Earth and Planetary Science Letters* **179**, 539-549.

Schmitz W. J. (1995) On the interbasin-scale thermohaline circulation. *Reviews in Geophysics* **33**, 151-173.

Schneider R. R., Müller P. J., and Acheson R. (1999) Atlantic alkenone sea surface temperature records: Low versus mid latitudes and differences between hemispheres. In *Reconstructing Ocean History - a window into the future* (ed. F. Abrantes and A. C. Mix), pp. 33-56. Kluwer Academic / Plenum Publishers.

Schneider R. R., Müller P. J., and Ruhland G. (1995) Late Quaternary surface circulation in the east equatorial South Atlantic: Evidence from alkenone sea surface temperatures. *Paleoceanography* **10**, 197-219.

Schneider R. R., Müller P. J., Ruhland G., Meinecke G., Schmidt H., and Wefer G. (1996) Late Quaternary surface temperatures and productivity in the east-equatorial South Atlantic: Response to changes in trade/monsoon wind forcing and surface water advection. In *The South Atlantic: Present and past circulation* (ed. G. Wefer, W. H. Berger, G. Siedler, and D. J. Webb), pp. 527-551. Springer.

Schneider R. R., Müller P. J., and Wefer G. (1994) Late Quaternary paleoproductivity changes off the Congo deduced from stable carbon isotopes of planktonic foraminifera. *Palaeogeography, Palaeoclimatology, Palaeoecology* **110**, 255-274.

Schneider R. R., Price B., Mueller P. J., and Alexander I. (1997) Monsoon related variations in Zaire (Congo) sediment load and influence of fluvial silicate supply on marine productivity in the east equatorial Atlantic during the last 200,000 years. *Paleoceanography* **12**, 463-481.

Schoell M., Schouten S., Sinninghe Damsté J. S., and de Leeuw J. W. (1994) A molecular isotope record of Miocene climate changes. *Science* **263**, 1122-1125.

Schouten S., Hoefs M. J. L., Koopmans M. P., Bosch H.-J., and Sinninghe Damsté J. S. (1998) Structural characterization, occurrence and fate of archaeal ether-bound acyclic and cyclic biphytanes and corresponding diols in sediments. *Organic Geochemistry* **29**, 1305-1319.

Schouten S., Hoefs M. J. L., and Sinninghe Damsté J. S. (2000a) A molecular and stable isotopic study of lipids in Late Quaternary sediments from the Arabian Sea. *Organic Geochemistry* **31**, 509-521.

Schouten S., Hopmans E. C., Pancost R. D., and Sinninghe Damsté J. S. (2000b) Widespread occurrence of structurally diverse tetraether membrane lipids: Evidence for the ubiquitous presence of low-temperature relatives of hyperthermophiles. *Proceedings of the National Academy of Sciences* **97**, 14421-14426.

Schubert C. J., Villanueva J., Calvert S. E., Cowie G. L., von Rad U., Schulz H., Berner U., and Erlenkeuser H. (1998) Stable phytoplankton community structure in the Arabian Sea over the past 200,000 years. *Nature* **394**, 563-566.

Schulz H. D., Adegbie A., Boehme S., Brune A., Däumler K., Dehning K., de Vries U., Diekamp V., Enneking K., Ferdelman T., Funk J., Hell J., Hilgenfeldt C., Hinrichs S., Joppich C., Kasten S., Klump J., Lavik G., Meyer A., Ochsenhirt W.-T., Schewe F., Schneider R., Siemer S., Strotmann B., Stuut J.-B., von Lom-Keil H., Wagner T., Wenzhöfer F., and Zabel M. (1998) *Report and preliminary results of Meteor cruise M41/1 Malaga - Libreville, 13.2. - 15.3.1998.* Universität Bremen.

Schulz H. D., Dahmke A., Schinzel U., Wallmann K., and Zabel M. (1994) Early diagenetic processes, fluxes and reaction rates in sediments of the South Atlantic. *Geochimica et Cosmochimica Acta* **58**, 2041-2060.

Schulz M. and Statteger K. (1997) Spectrum: spectral analysis of unevenly spaced paleoclimatic time series. *Computers and Geosciences* **23**, 929-945.

Schütz L. (1980) Long range transport of desert dust with special emphasis on the Sahara. *Annals of the N. Y. Academy of Science* **338**, 515-532.

Seidov D. and Haupt B. J. (1997) Global ocean thermohaline conveyor at present and in the late Quaternary. *Geophysical Research Letters* **24**, 2817-2820.

Servain J., Picaut J., and Merle J. (1982) Evidence for remote forcing in the Equatorial Atlantic Ocean. *Journal of Physical Oceanography* **12**, 457-463.

Shackleton N. J. (1987) Oxygen isotopes, ice volume and sea level. *Quaternary Science Reviews* **6**, 183-190.

Shackleton N. J., Berger A., and Peltier W. R. (1990) An alternative astronomical calibration of the lower Pleistocene timescale based on ODP Site 677. *Transactions of the Royal Society of Edinburgh: Earth Sciences* **81**, 251-261.

Shackleton N. J. and Opdyke N. O. (1976) Oxygen-isotope and Paleomagnetic stratigraphy of Pacific core V28-239 late Pliocene to latest Pleistocene. *Geological Society of America* **145**, 449-464.

Shannon L. V. (1985) The Benguela ecosystem, Part I: Evolution of the Benguela, physical features and processes. *Annual Reviews in Oceanography and Marine Biology* **23**, 105-182.

Shannon L. V., Agenbag J. J., and Buys M. E. L. (1987) Large- and mesoscale features of the Angola-Benguela front. *South African Journal of Marine Science* **65**, 11-34.

Shannon L. V. and Pillar S. C. (1986) The Benguela Ecosystem Part III: Plankton. *Annual Reviews in Oceanography and Marine Biology* **24**, 65-170.

Silliman J. E., Meyers P. A., and Eadie B. J. (1999) Perylene: an indicator of alteration processes or precursor materials. *Organic Geochemistry* **29**, 1737-1744.

Simoneit B. R. T. (1977) Organic matter in eolian dusts over the Atlantic Ocean. *Marine Chemistry* **5**, 443-464.

Simoneit B. R. T. (1984) Organic matter of the troposphere-III. Characterization and sources of petroleum and pyrogenic residues in aerosols over the western United States. *Atmospheric Environment* **18**, 51-67.

Simoneit B. R. T. (1985) Application of molecular marker analysis to vehicular exhaust for source reconciliations. *International Journal of Environmental Analytical Chemistry* **22**, 203-233.

Simoneit B. R. T. (1997) Compound-specific carbon isotope analyses of individual long-chain alkanes and alkanoic acids in Harmattan aerosols. *Atmospheric Environment* **31**, 2225-2233.

Simoneit B. R. T., Cardoso J. N., and Robinson N. (1991) An assessment of terrestrial higher molecular weight lipid compounds in aerosol particulate matter over the South Atlantic from about 30-70°S. *Chemosphere* **23**, 447-465.

Simoneit B. R. T., Chester R., and Eglinton G. (1977) Biogenic lipids in particulates from the lower atmosphere over the eastern Atlantic. *Nature* **267**, 682-685.

Simoneit B. R. T., Cox R. E., and Standley L. J. (1988) Organic matter of the troposhere-IV. Lipids in Harmattan aerosols of Nigeria. *Atmospheric Environment* **22**, 983-1004.

Simoneit B. R. T. and Mazurek M. A. (1982) Organic matter of the troposphere-II. Natural background of biogenic lipid matter in aerosols over the rural western United States. *Atmospheric Environment* **16**, 2139-2159.

Sinninghe Damsté J. S. and de Leeuw J. W. (1990) Analysis, structure and geochemical significance of organically-bound sulphur in the geosphere: State of the art and future research. *Organic Geochemistry* **16**, 1077-1101.

Sinninghe Damsté J. S., Hoefs M. J. L., Rijpstra W. I. C., Schefuß E., de Lange G. J., and de Leeuw J. W. (1997) Bias of the sedimentary biomarker record through oxic degradation at different rates. *International Meeting on Organic Geochemistry*, Abstract.

Sinninghe Damsté J. S., Rampen S., Rijpstra W. I. C., Abbas B., Muyzer G., and Schouten S. (in press) A diatomaceous origin of long-chain diols and mid-chain hydroxy methyl alkenoates widely occurring in Quaternary marine sediments: Indicators for upwelling conditions. *Geochimica et Cosmochimica Acta*.

Sinninghe Damsté J. S., Rijpstra W. I. C., de Leeuw J. W., and Schenk P. A. (1988) Origin of organic sulphur compounds and sulphur containing high molecular weight substances in sediments and immature oils. In *Advances in Organic Geochemistry 1987*, Vol. 13 (ed. L. Matavelli and L. Novelli), pp. 593-606. Organic Geochemistry.

Sinninghe Damsté J. S., Rijpstra W. I. C., Hopmans E. C., Prahl F. G., and Schouten S. (2002a) Distribution of membrane lipids of planktonic crenarchaeota in the Arabian Sea. *Applied and Environmental Microbiology* **68**, 2997-3002.

Sinninghe Damsté J. S., Rijpstra W. I. C., and Reichart G.-J. (2002b) The influence of oxic degradation on the sedimentary biomarker record II: Evidence from Arabian Sea sediments. *Geochimica et Cosmochimica Acta* **66**, 2737-2754.

Sinninghe Damsté J. S., Rijpstra W. I. C., Schouten S., Peletier H., van der Maarel M. J. E. L., and Gieskes W. W. C. (1999) A C_{25} highly branched isoprenoid alkene and C_{25} and C_{27} *n*-polyenes in marine diatom *Rhizosolenia setigera*. *Organic Geochemistry* **30**, 95-100.

Skipski V. P., Smolowne A. F., Sullivan R. C., and Barclay M. (1965) Separation of lipid classes by thin-layer chromatography. *Biochimica et Biophysica Acta* **106**, 386-396.

Spicer R. A. (1989) Physiological characteristics of land plants in relation to environment through time. *Transactions of the Royal Society of Edinburgh: Earth Sciences* **80**, 321-329.

Standley L. J. and Simoneit B. R. T. (1987) Composition of extractable organic matter in smoke particles from prescribed burns. *Environmental Science and Technology* **21**, 163-169.

Summons R. E., Jahnke L. L., Hope J. M., and Logan G. A. (1999) 2-Methylhopanoids as biomarkers for cyanobacterial oxygenic photosynthesis. *Nature* **400**, 554-557.

Sun M.-Y. and Wakeham S. G. (1994) Molecular evidence for degradation and preservation of organic matter in the anoxic Black Sea Basin. *Geochimica et Cosmochimica Acta* **58**, 3395-3406.

Talbot H. M., Head R. N., Harris R. P., and Maxwell J. R. (1999) Stery esters of pyrophaeophobide b: a sedimentary sink for chlorophyll b. *Organic Geochemistry* **30**, 1403-1410.

Teece M. A., Maxwell J. R., Briggs D. E. G., Getliff J. M., Parkes J. R., and Leftley J. W. (1994) Laboratory degradation of lipids of the marine prymnesiophyte *Emiliania huxleyi* and significance for sediment studies. In *Lyell Meeting Volume*, Vol. Spec. Publ. *94/1*, pp. 5-8. NERC Earth Science Directorate.

ten Haven H. L., Baas M., de Leeuw J. W., and Schenck P. A. (1987a) Late Quaternary Mediterranean sapropels. I: On the origin of organic matter in sapropel S7. *Marine Geology* **75**, 137-156.

ten Haven H. L., Baas M., de Leeuw J. W., Schenck P. A., and Brinkhuis H. (1987b) Late Quaternary Mediterranean sapropels. II: Organic Geochemistry and Palynology of S1 Sapropels and Associated Sediments. *Chemical Geology* **64**, 149-167.

ten Haven H. L. and Rullkötter J. (1988) The diagenetic fate of taraxer-14-ene and oleanene isomers. *Geochimica et Cosmochimica Acta* **52**, 2543-2548.

ten Haven H. L. and Rullkötter J. (1991) Preliminary lipid analysis of sediments recovered during Leg 117. *Proceedings ODP, Scientific Results* **117**, 561-569.

ten Haven H. L., Rullkötter J., Sinninghe Damsté J. S., and de Leeuw J. W. (1990) Distribution of Organic Sulfur Compounds in Mesozoic and Cenozoic Sediments from the Atlantic and Pacific Oceans and the Gulf of California. In *Geochemistry of sulfur in Fossil Fuels*, Vol. 429 (ed. W. L. Orr and C. M. White), pp. 613-632. ACS Symposium Series.

Teshima S. I., Kanazawa A., and Tago A. (1980) Sterols of the dinoflagellate *Noctiluca milialis*. *Mem. Fac. Fisher. Kagoshima Univ.* **29**, 319-326.

Tetzlaff G. and Wolter W. (1980) Meteorological patterns and the transport of mineral dust from the north African continent. *Paleoecology of Africa* **12**, 31-42.

Tiedemann R., Sarnthein M., and Shackleton N. J. (1994) Astronomic timescale for the Pliocene Atlantic $\delta^{18}O$ and dust flux records of Ocean Drilling Program Site 659. *Paleoceanography* **9**, 619-638.

Tissot B. P. and Welte D. H. (1984) *Petroleum formation and occurrence*. Springer.

Tomlinson P. B. (1986) *The botany of mangroves*. Cambridge University Press.

Tulloch A. P. (1976) Chemistry of waxes of higher plants. In *Chemistry and Biochemistry of Natural Waxes* (ed. P. E. Kolattukudy), pp. 236-252. Elsevier.

Tulloch A. P. (1984) Epicuticular waxes of four Eragrostoid grasses. *Phytochemistry* **23**, 1619-1623.

Tyson R. V. (1995) *Sedimentary OM: Organic facies and palynofacies*. Chapman and Hall.

Ufkes E., Jansen J. H. F., and Brummer G.-J. A. (1998) Living planktonic foraminifera in the eastern South Atlantic during spring: indicators of water masses, upwelling and the Zaire (Congo) River Plume. *Marine Micropaleontology* **33**, 27-53.

Uliana E., Lange C. B., Donner B., and Wefer G. (2001) Siliceous phytoplankton productivity fluctuations in the Congo Basin over the past 460,000 years: Marine vs. riverine influence, ODP Site 1077. In *Proceedings ODP, Scientific Results*, Vol. 175 (ed. G. Wefer, W. H. Berger, and C. Richter), pp. 1-32 [Online at: http://www-odp.tamu.edu/publications/175_SR/chap_11/chap_11.htm]. Ocean Drilling Program.

van Bennekom A. J. and Berger G. W. (1984) Hydrography and silica budget of the Angola Basin. *Netherlands Journal of Sea Research* **17**, 149-200.

van Bennekom A. J., Berger G. W., Helder W., and de Vries R. T. P. (1978) Nutrient distribution in the Zaire estuary and river plume. *Netherlands Journal of Sea Research* **12**, 296-323.

van der Gaast S. and Jansen J. H. F. (1984) Mineralogy, opal, and manganese of middle and late Quaternary sediments of the Zaire (Congo) deep-sea fan: origin and climatic variation. *Netherlands Journal of Sea Research* **17**, 313-341.

van Iperen J. M., van Weering T. C. E., Jansen J. H. F., and van Bennekom A. J. (1987) Diatoms in surface sediments of the Zaire deep-sea fan (SE Atlantic Ocean) and their relation to overlying water masses. *Netherlands Journal of Sea Research* **21**, 203-217.

Venkatesan M. I. (1988) Occurrence and possible sources of perylene in marine sediments: a review. *Marine Chemistry* **25**, 1-27.

Versteegh G. J. M., Bosch H.-J., and de Leeuw J. W. (1997) Potential palaeoenvironmental information of C_{24} to C_{36} mid-chain diols, keto-ols and mid-chain hydroxy fatty acids; a critical review. *Organic Geochemistry* **27**, 1-13.

Versteegh G. J. M., Jansen J. H. F., de Leeuw J. W., and Schneider R. R. (2000) Mid-chain diols and keto-ols in SE Atlantic sediments. A new tool for tracing past sea surface water masses? *Geochimica et Cosmochimica Acta* **64**, 1879-1892.

Villanueva J., Grimalt J. O., Labeyrie L. D., Cortijo E., Vidal L., and Turon J.-L. (1998) Precessional forcing of productivity in the North Atlantic Ocean. *Paleoceanography* **13**, 561-571.

Voituriez B. and Herbland A. (1982) Comparaison des systemes productifs de l'Atlantique Tropical Est: Domes thermiques, upwellings cotiers et upwelling equatorial. *Rapp. P.V. Reun. Cons. Int. Explor. Mer.* **180**, 114-130.

Volkman J. K. (1986) A review of sterol markers for marine and terrigenous organic matter. *Organic Geochemistry* **9**, 83-99.

Volkman J. K., Barrett S. M., and Blackburn S. I. (1999) Eustigmatophyte microalgae are potential sources of C_{29} sterols, C_{22}-C_{28} *n*-alcohols and C_{28}-C_{32} *n*-alkyl diols in freshwater environments. *Organic Geochemistry* **30**, 307-318.

Volkman J. K., Barrett S. M., Blackburn S. I., Mansour M. P., Sikes E. L., and Gelin F. (1998) Microalgal biomarkers: A review of recent research developments. *Organic Geochemistry* **29**, 1163-1179.

Volkman J. K., Barrett S. M., Blackburn S. I., and Sikes S. L. (1995) Alkenones in *Gephyrocapsa oceanica*: implications for studies of paleoclimate. *Geochimica et Cosmochimica Acta* **59**, 513-520.

Volkman J. K., Barrett S. M., and Dunstan G. A. (1994) C_{25} and C_{30} highly isoprenoid alkenes in laboratory cultures of two marine diatoms. *Organic Geochemistry* **21**, 407-413.

Volkman J. K., Barrett S. M., Dunstan G. A., and Jeffrey S. W. (1992) C_{30}-C_{32} alkyl diols and unsaturated alcohols in microalgae of the class *Eustigmatophyceae*. *Organic Geochemistry* **18**, 131-138.

Volkman J. K., Barrett S. M., Dunstan G. A., and Jeffrey S. W. (1993) Geochemical significance of the occurrence of dinosterol and other 4-methyl sterols in a marine diatom. *Organic Geochemistry* **20**, 7-16.

Volkman J. K., Eglinton G., Corner E. D. S., and Forsberg T. E. V. (1980) Long-chain alkenes and alkenones in the marine coccolithophorid Emiliana huxleyi. *Phytochemistry* **19**, 2619-2622.

Volkman J. K., Farrington J. W., and Gagosian R. B. (1987) Marine and terrigenous lipids in coastal sediments from the Peru upwelling region at 15°S: Sterols and triterpene alcohols. *Organic Geochemistry* **11**, 463-477.

Wagner T. (2000) Control of organic carbon accumulation in the late Quaternary equatorial Atlantic (Ocean Drilling Program Sites 664 and 663): Productivity versus terrigenous supply. *Paleoceanography* **15**, 181-199.

Wakeham S. G., Hedges J. I., Lee C., Peterson M. L., and Hernes P. J. (1998) Composition and transport of lipid biomarkers through the water column and surficial sediments of the equatorial Pacific Ocean. *Deep-Sea Research, Part II* **44**, 2131-2162.

Wakeham S. G., Lee C., Hedges J. I., Hernes P. J., and Peterson M. L. (1997) Molecular indicator of diagenetic status in marine organic matter. *Geochimica et Cosmochimica Acta* **61**, 5363-5369.

Wakeham S. G., Peterson M. L., Hedges J. I., and Lee C. (2002) Lipid biomarker fluxes in the Arabian Sea: with a comparison to the Equatorial Pacific Ocean. *Deep-Sea Research Part II* **49**, 2265-2301.

Wakeham S. G., Schaffner C., Giger W., Boon J. J., and de Leeuw J. W. (1979) Perylene in sediments from the Namibian Shelf. *Geochimica et Cosmochimica Acta* **43**, 1141-1144.

Wara M. W., Ravelo A. C., and Revenough J. S. (2000) The pacemaker always rings twice. *Paleoceanography* **15**, 616-624.

Wefer G., Berger W. H., Richter C., and Shipboard Scientific Party (1998) *Proceedings of the Ocean Drilling Program, Initial Reports, Volume 175*. Ocean Drilling Program.

Werne J. P., Hollander D. J., Behrens A., Schaeffer P., Albrecht P., and Sinninghe Damsté J. S. (2000) Timing of early diagenetic sulfurization of organic matter: A precursor-product relationship in Holocene sediments of the anoxic Cariaco Basin, Venezuela. *Geochimica et Cosmochimica Acta* **64**, 1741-1751.

Westerhausen L., Poynter J., Eglinton G., Erlenkeuser H., and Sarnthein M. (1993) Marine and terrigenous origin of organic matter in modern sediments of the equatorial East Atlantic: the $\delta^{13}C$ and molecular record. *Deep-Sea Research* **40**, 1087-1121.

White F. (1983) *The Vegetation of Africa*. UNESCO.

Wilkinson L. (1988) *SYSTAT, the system for statistics*. SYSTAT.

Winter K. and Smith J. A. C. (1996) *Crassulacean Acid Metabolism: biochemistry, ecophysiology and evolution*. Springer.

Woodroffe C. D. and Grindrod J. (1991) Mangrove biogeography: the role of Quaternary environmental and sea-level change. *Journal of Biogeography* **18**, 479-492.

Yamamoto M., Ficken K., Baas M., Bosch H. J., and de Leeuw J. W. (1996) Molecular paleontology of the earliest Danian at Geulhemmerberg (the Netherlands). *Geologie en Mijnbouw* **75**, 255-267.

Summary

This thesis describes the environmental changes in the eastern tropical Atlantic and equatorial Africa during the Mid-Pleistocene Transition (MPT) as revealed by analyses of lipid biomarkers and their stable carbon isotope compositions. The MPT was the start of the Late Pleistocene ice ages, with an enlarged mean global ice volume varying in a predominant 100-kyr cyclicity. Before the MPT, global ice volume was, on average, smaller and had a prevalent 41-kyr cyclicity. The increase in mean global ice mass around 920 kyr BP significantly preceded the establishment of the 100-kyr cycle at 640 kyr BP. A pronounced effect of the MPT was the temporary severe decrease of the Atlantic deepwater ventilation, caused by the strongest reductions of North Atlantic Deep-Water formation in the last 2.5 million years.

The mid-Pleistocene time series of the eastern South Atlantic are based on investigations of the Ocean Drilling Program (ODP) sediment core 1077 from the lower Congo deep-sea fan in the Angola Basin. The Angola Basin is part of the tropical Atlantic and characterised by strong seasonal changes of the atmospheric circulation. During austral winter (June to August) strong Southern Hemisphere trade winds blow over the Angola Basin transporting vast amounts of atmospheric dust from dry areas in southern Africa. Wind-driven surface-water mixing causes elevated surface-water productivity by oceanic upwelling, i.e., by supply of nutrients to the photic zone from below a shallow nutricline, which is the result of the cyclonic gyre circulation in the Angola Basin. During austral summer (December to February) maximum monsoonal conditions are associated with high precipitation in southern equatorial Africa, leading to maximum discharge of river waters and maximum extension of the Congo River plume. A maximum of primary productivity is found in a narrow meridional zone about 150 to 200 km offshore, where the silicate-rich river waters mix with marine nutrients. Diatoms dominate phytoplankton productivity in the inner Congo River plume. Coastal upwelling in the Angola Basin is restricted to two small cells north and south of the Congo River mouth. The shallow coastal upwelling activity, however, causes no silicate enrichment in the surface waters.

Lipid biomarkers were used to reconstruct the past environmental conditions. Some classes of biota produce specific biochemicals, which can provide insights in the environmental conditions, when it is possible to relate these compounds to a class of organisms or even to specific organisms. A wide range of lipids was investigated on their biomarker values and their (paleo)environmental significance. The ^{13}C content of lipid biomarkers depends on their biosynthetic pathways and can thus provide insights into environmental conditions under which carbon-fixation occurred. The $\delta^{13}C$ values of leaf-wax lipids of different terrestrial vegetation types depend on the carbon-fixation mechanism (C_3, C_4 or CAM) utilised during photosynthesis.

Organic geochemical investigations of ODP Leg 175 shipboard samples provided an overview of the lipid biomarkers in the eastern South Atlantic sediments and their environmental implications. Based on these initial findings (Chapter 2) it was decided to pursue the examinations with sediments from the lower Congo fan. For a proper interpretation of lipid biomarker variations in the past and an accurate understanding of their significance, a calibration of lipid parameters was conducted using atmospheric dust samples and surface sediments from the research area. The main lipids in the aerosol samples are derived from the

epicuticular wax coating of terrestrial higher plant leaves (Chapter 3). Their stable carbon isotopic compositions mainly reflect the contemporary vegetation type on the adjacent continent. Wind abrasion of wax particles from leaf surfaces is apparently the primary process supplying terrestrial lipids to dust. The spatial distributions of the molecular and bulk organic geochemical parameters of the surface sediments of the eastern South Atlantic reflect the main production, transport and preservation processes (Chapter 4): wind-driven deep upwelling, shallow coastal upwelling, river transport of terrigenous material, eolian transport of plant waxes from dry continental areas, and productivity off the Congo, either river-induced or by oceanic upwelling.

To study the coupling between the high-latitude ice-volume changes of the MPT and the low-latitude climate, the mid-Pleistocene record of ODP Site 1077 was investigated in great detail. The temporal evolution of the sea-surface temperature (SST) in the Angola Basin was compared with the orbital insolation, global ice-volume and Atlantic deepwater ventilation changes (Chapter 5). The tropical SST development followed the changing frequency behaviour of the high-latitude ice volume, however, it responded significantly earlier on insolation changes in the main orbital cycles. This indicates an early response of wind-driven upwelling and heat advection in the tropical Atlantic on the changing thermal gradient in the South Atlantic. The long-term evolution of the tropical SST was, however, mainly influenced by the Atlantic deepwater ventilation, being strongly reduced during the MPT. The decreased surface-water export to the higher latitudes caused the long-term heat accumulation in the tropical Atlantic Ocean. The growth of the ice sheets during the MPT thus led to a long-term deviation of the tropical climate from the global cooling development. The accumulation of plant waxes was significantly increased after the growth of the additional global ice volume (Chapter 6). The compression of the atmospheric circulation cells caused an elevated eolian dust transport by stronger and more zonal trade winds. Large-scale vegetation changes in southern Africa, recorded as C_3/C_4 plant variations, did, however, not correlate with the global ice-volume and the, presumed parallel, pCO_2 changes. The vegetation changes were in phase with the tropical SST changes. In the obliquity and eccentricity cycle and the long-term development, low-latitude SST apparently directly controls African aridity via the tropical precipitation-evaporation balance and thus determines the large-scale vegetation in southern Africa. In the precessional cycle, in contrast, the monsoon causes simultaneous SST and C_4 plant minima due to the coincidence of maximum monsoon with maximum upwelling in this cycle. Accumulation rates of lipid biomarkers from various marine plankton classes were used to examine the response of the marine ecosystem in the Angola Basin on the MPT (Chapter 7). Precessional forcing of river-induced production and oceanic upwelling was dominant before the MPT. The growth of the ice volume suppressed the low-latitude forcing of marine productivity. Instead, production of lipids by wind-driven upwelling and eolian transport of plant waxes was strongly enhanced after the growth of the global ice volume and responded to the 100-kyr variability in trade-wind strength and zonality. The MPT thus led to important environmental changes in the tropical Atlantic and equatorial Africa by suppressing the low-latitude forcing via a reduced monsoonal influence and by increasing the ice-volume forcing via the stronger trade winds.

This thesis demonstrates the potential of lipid biomarkers to assess (paleo)-oceanographic and -climatic environmental changes in the marine and terrestrial

ecosystems in high temporal resolution and thus provides new insights in the linkage of the low- with the high-latitude climate.

Zusammenfassung

Diese Arbeit beschreibt die Umweltveränderungen im östlichen tropischen Atlantik und im äquatorialen Afrika während des Mittel-Pleistozänen Klimawechsels (Mid-Pleistocene Transition, MPT) mithilfe von Analysen von Lipid-Biomarkern und deren stabilen Kohlenstoff-Isotopien. Die MPT war der Anfang der Spät-Pleistozänen Eiszeiten, mit ihrem im Durchschnitt großen Eisvolumen und dessen überwiegenden 100.000-Jahre Variationen. Das globale Eisvolumen vor der MPT war im Durchschnitt kleiner und variierte vorwiegend in einem 41.000-Jahre Zyklus. Das Anwachsen der Eisschilde fand etwa 920 tausend Jahre vor heute (kiloyears before present, kyr BP) statt, deutlich vor dem Einsetzen des 100.000-Jahres Zyklus bei 640 kyr BP. Ein besonderer Effekt der MPT war die zeitweilige starke Abnahme der Atlantischen Tiefenwasser-Ventilation, verursacht durch die stärkste Reduktion der Bildung von Nord-Atlantischem Tiefenwasser in den letzten 2,5 Millionen Jahre.

Die Mittel-Pleistozänen Zeitserien aus dem östlichen Südatlantik basieren auf Untersuchungen an dem Ocean Drilling Program (ODP) Bohrkern 1077 vom Tiefseefächer des Kongo im Angola Becken. Das Angola Becken ist Teil des tropischen Atlantiks und durch einen starken saisonalen Wechsel in der atmosphärischen Zirkulation gekennzeichnet. Während des Südwinters (Juni bis August) weht ein starker Südpassat über das Angola Becken und transportiert große Mengen an Staub aus den trockenen Gebieten des südlichen Afrika. Die starke Durchmischung des Oberflächenwassers durch den Wind bewirkt eine erhöhte marine Produktivität durch Zufuhr von nährstoffreichem Tiefenwasser in die photische Zone. Die zyklonale Zirkulation des Oberflächenwassers ist der Grund für die flache Nutrikline im Angola Becken. Während des Südsommers (Dezember bis Februar), während des Monsuns, fällt der meiste Regen im südlichen äquatorialen Afrika, wodurch der Frischwasserausfluß des Kongo und die Ausdehnung der Flußwasserfahne maximal werden. In einer schmalen, Nord-Süd-gerichteten Zone, etwa 150 und 200 km vor der Küste, ist die marine primäre Produktivität durch die Mischung von silikat-reichem Flußwasser mit den marinen Nährstoffen am höchsten. Die Phytoplankton-Produktivität im inneren Bereich der Frischwasserfahne des Kongo wird von Diatomeen dominiert. Küstenauftrieb im Angola Becken ist auf zwei kleine Zellen, nördlich und südlich von der Kongomündung, beschränkt. Die flache Auftriebstätigkeit führt jedoch nicht zu einer Anreicherung des Oberflächenwassers mit Silikat.

Zur Rekonstruktion von früheren Umweltbedingungen wurden Lipid-Biomarker verwendet. Viele Organismen produzieren spezifische biochemische Verbindungen, welche Einblicke in die Umweltbedingungen verschaffen können, falls sich diese Verbindungen einer bestimmten Gruppe von Organismen oder sogar spezifischen Organismen zuordnen lassen. Eine Vielfalt von Lipiden wurde auf ihren Wert als Biomarker und auf ihre Bedeutung als (Paläo-) Umweltindikatoren hin untersucht. Die ^{13}C-Gehalte von Lipid-Biomarkern hängen von deren Biosynthese ab und ermöglichen so die Rekonstruktion der Umweltbedingungen zu Zeiten der Kohlenstoffixierung. Die $\delta^{13}C$ Werte von Pflanzenwachsen verschiedener Vegetationstypen sind daher abhängig vom Mechanismus der Kohlenstoffixierung (C_3, C_4, CAM) während der Photosynthese.

Organisch-geochemische Untersuchungen an, auf dem Bohrschiff entnommenen, Proben der ODP Fahrt 175 gaben einen ersten Überblick über die Lipid-Biomarker in den Sedimenten des östlichen Südatlantiks und ihrer Interpretation als

Umweltindikatoren. Ausgehend von diesen ersten Befunden (Kapitel 2) wurde beschlossen, die Untersuchungen an Sedimenten des Tiefseefächers des Kongo fortzusetzen. Zur korrekten Interpretation der Lipid Biomarker Variationen in der Vergangenheit und zum genauen Verständnis ihrer Bedeutung wurden die Lipid Parameter mithilfe von atmosphärischen Staubproben und Oberflächensedimenten aus dem Untersuchungsgebiet kalibriert. In den Aerosolen befinden sich überwiegend Lipide der Wachsschicht, welche auf den Blättern von terrestrischen höheren Pflanzen vorkommt (Kapitel 3). Ihre stabilen Kohlenstoffisotopen-Verhältnisse spiegeln hauptsächlich die Vegetation auf dem benachbarten Kontinent wider. Die terrigenen Lipide im Staub werden offenbar vorwiegend mit den Wachs-Partikeln von der Blattoberfläche abgeweht. Die Verteilungen der molekularen und sedimentären organisch-geochemischen Parameter in den Oberflächensedimenten des östlichen Südatlantik zeigen die wesentlichen Produktions-, Transport- und Erhaltungsprozesse (Kapitel 4): wind-abhängige tiefe Auftriebsaktivität, flacher Küstenauftrieb, Flußeintrag von terrestrischem Material, Windtransport der Pflanzenwachse aus trockenen Kontinentalgebieten, und marine Produktivität vor der Kongomündung, entweder verursacht durch den Ausstrom von Flußwasser oder durch ozeanischen Auftrieb.

Um die Kopplungen zwischen den Veränderungen des Eisvolumens während der MPT und des Klimas der niedrigen Breiten zu untersuchen, wurden die Mittel-Pleistozänen Zeitserien des ODP Kernes 1077 detailliert studiert. Die zeitliche Entwicklung der Oberflächenwassertemperaturen (SST) im Angola Becken wurde mit den Veränderungen in der orbitalen Insolation, in dem globalen Eisvolumen und in der Atlantischen Tiefenwasserzirkulation verglichen (Kapitel 5). Die Entwicklung der tropischen SST folgte dem sich änderndem Frequenzverhalten des Eisvolumens in den hohen Breiten, reagierte jedoch deutlich früher auf die Insolationswechsel in den Haupt-Orbitalzyklen. Diese Befunde belegen die schnelle Reaktion der wind-abhängigen Auftriebsaktivität und der Warmwasser-Advektion im tropischen Atlantiks auf die Veränderungen im Temperaturgradienten des Südatlantiks. Die langfristige Entwicklung der tropischen SST wurde jedoch hauptsächlich durch die Bildung des Atlantischen Tiefenwassers beeinflusst, die während der MPT stark reduziert war. Der verminderte nordwärtige Export von warmem Oberflächenwasser bewirkte die langfristige Erwärmung des tropischen Atlantiks. Das Anwachsen der Eisschilde während der MPT führte so also zu einer zeitweisen Abweichung des tropischen Klimas von dem langfristigen globalen Abkühlungstrend. Die Akkumulation der Pflanzenwachse verstärkte sich deutlich nach dem Anwachsen des globalen Eisvolumens (Kapitel 6). Die Kompression der atmosphärischen Zirkulationszellen erhöhte den Staubtransport durch den stärkeren und mehr zonal-gerichteten Passatwind. Großflächige Vegetationswechsel im südlichen Afrika, gemessen als Veränderungen im Verhältnis von C_3 zu C_4 Pflanzen, korrelierten jedoch nicht mit der Entwicklung des globalen Eisvolumens und den, vermutlich parallel verlaufenden, pCO_2 Variationen. Die Vegetation veränderte sich in Phase mit den tropischen SST Variationen. In den Obliquitäts- und Exzentrizitätszyklen, sowie in der langfristigen Entwicklung, ist die tropische SST der wichtigste klimatische Faktor, welcher offensichtlich direkt, über Verdunstung und Regenfall, die Trockenheit und somit die großflächige Vegetation im südlichen Afrika bestimmt. Im Präzessionszyklus jedoch bewirkt der Monsun zeitgleiche Minima in SST und der Verbreitung von C_4 Pflanzen durch das Zusammenfallen von Maxima in Monsun und Auftrieb in diesem Zyklus. Um die Reaktion des marinen Ökosystem im Angola Becken auf die MPT zu beschreiben,

wurden die Akkumulationsraten von Lipid-Biomarkern verschiedener Gruppen des marinen Planktons untersucht (Kapitel 7). Vor der MPT herrschte eine Präzessionsteuerung der marinen Produktivität vor, entweder induziert durch den Ausstrom von Flußwasser oder durch ozeanischen Auftrieb. Das Wachstum des Eisvolumens unterdrückte diesen Einfluß der niedrigen Breiten auf die marine Produktion. Stattdessen nahm sowohl die Produktion von Lipiden im windabhängigen Auftriebsgeschehen, als auch der Windtransport von Pflanzenwachsen stark zu und reagierten auf die 100.000-Jahre-Schwankungen in Stärke und Zonalität des Passatwinds. Die MPT führte somit zu tiefgreifenden Umweltveränderungen im tropischen Atlantik und im äquatorialen Afrika. Der Einfluss der niedrigen Breiten verringerte sich durch den schwächeren Effekt des Monsuns, während der Einfluss des Eisvolumens durch den stärkeren Passatwind zunahm.

Diese Arbeit belegt das Potential von Lipid-Biomarkern um (paläo)-ozeanographische und -klimatische Umweltveränderungen in marinen und terrestrischen Ökosystemen in hoher zeitlicher Auflösung zu beschreiben und verschafft somit neue Einsichten in die klimatischen Verbindungen zwischen niedrigen und hohen Breiten.

Samenvatting

Dit proefschrift beschrijft de milieuveranderingen in het oostelijke deel van de tropische Atlantische Oceaan en in equatoriaal Afrika tijdens de Midden-Pleistocene klimaatsovergang (Mid-Pleistocene Transition, MPT) aan de hand van analyses van lipide biomarkers en hun stabiele koolstofisotopen-samenstellingen. De MPT markeerde het begin van de Laat-Pleistocene ijstijden, die werden gekenmerkt door een groot globaal ijsvolume, dat varieerde met een dominante 100.000 jaar cycliciteit. Vòòr de MPT was het globale ijsvolume, gemiddeld gezien, kleiner en liet een preferente 41.000 jaar cycliciteit zien. De groei van de ijskappen vond 920 duizend jaar geleden (kiloyears before present, kyr BP) plaats, duidelijk vooroplopend op de komst van de 100.000 cyclus bij 640 kyr BP. Een uitgesproken effect van de MPT was de tijdelijke sterke vermindering van de Atlantische diepwater ventilatie, iets wat veroorzaakt werd door de sterkste afname van de formatie van Noord Atlantisch Diep-Water in de laatste 2.5 miljoen jaar.

De Midden-Pleistocene tijdseries van de oostelijke Zuid Atlantische Oceaan zijn gebaseerd op onderzoek van de Ocean Drilling Program (ODP) kern 1077, gelegen op diepzee-afzettingen van de Kongo in het Angolabekken. Het Angolabekken maakt deel uit van de tropische Atlantische Oceaan en wordt vandaag de dag gekarakteriseerd door sterke seizoensveranderingen in de atmosferische circulatie. Tijdens de winter op het zuidelijk halfrond (juni tot augustus) waait een sterke zuidoostelijke passaatwind over het Angolabekken, die grote hoeveelheden atmosferisch stof transporteert vanuit droge gebieden in zuidelijk Afrika. De sterke doormenging van oppervlaktewater door de wind zorgt voor een verhoogde mariene productiviteit door toevoer van nutriëntenrijk diepwater naar de fotische zone. De cyclonale circulatie van oppervlaktewater zorgt voor de ondiepe nutricline in het Angolabekken. Tijdens de zomer op het zuidelijk halfrond (december tot februari) heerst de moesson en valt de meeste neerslag in zuidelijk Afrika. Dit leidt tot een maximale afvoer van rivierwater en een maximale uitbreiding van de pluim van de Kongo. In een smalle noord-zuid gerichte zone, ongeveer 150 tot 200 km uit de kust, is de primaire productiviteit het hoogst door de vermenging van silicaatrijk rivierwater met mariene nutriënten. De productiviteit van plantaardig plankton binnenin de pluim van de Kongo wordt gedomineerd door diatomeeën. De opwelling langs de kust van het Angolabekken beperkt zich tot twee kleine cellen, ten noorden en ten zuiden van de monding van de Kongo. Deze ondiepe opwelling zorgt echter niet voor silicaatverrijking in het oppervlaktewater.

Om de milieuomstandigheden in het verleden te reconstrueren, is gebruik gemaakt van lipide biomarkers. Verscheidene klassen van organismen produceren specifieke biochemische verbindingen die inzicht kunnen geven in de milieuomstandigheden. Dit kan alleen als het mogelijk is om de biochemische component te relateren aan een klasse van organismen of zelfs tot hele specifieke typen van organismen. Er is een veelvoud aan lipiden onderzocht op hun waarden als biomarker en hun betekenis als indicator voor het (paleo)-milieu. De ^{13}C gehaltes in lipide biomarkers hangen af van hun biosynthese en stellen onderzoekers zo in staat om de milieuomstandigheden ten tijde van de koolstoffixatie te reconstrueren. De $\delta^{13}C$ waarden van plantenwassen van verschillende terrestrische vegetatietypen zijn afhankelijk van het koolstoffixatie mechanisme (C_3, C_4 of CAM) tijdens de fotosynthese.

Organisch-geochemisch onderzoek aan monsters van ODP tocht 175 heeft een eerste overzicht gegeven van de lipide biomarkers in sedimenten uit het oostelijke

deel van de Zuid Atlantische Oceaan en van hun interpretaties voor het milieu. Gebaseerd op deze eerste bevindingen (Hoofdstuk 2) is besloten door te gaan met onderzoek naar de sedimenten van de diepzee-afzettingen van de Kongo. Voor een juiste interpretatie van de variaties in lipide biomarkers in het verleden en een nauwkeurig begrip van hun betekenis, zijn de lipide parameters met behulp van stofmonsters en oppervlaktesedimenten uit het onderzoeksgebied gecalibreerd. Het overgrote deel van de lipiden in de stofmonsters blijkt afkomstig te zijn van de waslaag op de bladeren van terrestrische hogere planten (Hoofdstuk 3). Hun stabiele koolstofisotopen-samenstellingen weerspiegelen hoofdzakelijk het vegetatietype op het aangrenzende continent. Het afslijten van wasdeeltjes van het bladoppervlak door de wind, is het belangrijkste proces dat terrestrische lipiden aan stof toevoegt. De ruimtelijke verdelingen van de moleculaire en bulk organisch-geochemische parameters van de oppervlaktesedimenten uit het oostelijke deel van de Zuid Atlantische Oceaan weerspiegelen de productie-, transport- en preservatieprocessen (Hoofdstuk 4). Deze processen zijn: windgestuurde diepe opwelling, ondiepe opwelling langs de kust, transport van terrestrisch materiaal door de rivier, eolisch transport van plantenwassen vanuit droge continentale gebieden, en mariene productiviteit voor de monding van de Kongo, veroorzaakt door de uitstroom van rivierwater of door oceanische opwelling.

Om de klimatologische koppeling tussen de veranderingen in ijsvolume op hoge breedte ten tijde van de MPT en het klimaat op lage breedte te bestuderen, zijn in groot detail de Midden-Pleistocene tijdseries van ODP kern 1077 onderzocht. De ontwikkeling van de zeeoppervlakte temperatuur (sea-surface temperature, SST) in het Angolabekken door de tijd is vergeleken met veranderingen in de orbitale insolatie, het globaal ijsvolume en de Atlantisch diepwater ventilatie (Hoofdstuk 5). De ontwikkeling van de tropische SST blijkt het frequentiepatroon van het ijsvolume op hoge breedte te volgen, maar reageert significant eerder op insolatieveranderingen in de belangrijkste orbitale cycli. Dit wijst op een snelle reactie van de windgestuurde opwelling en het warmtetransport in de tropen op de temperatuurgradiënt in de Zuid Atlantische Oceaan. De evolutie van de tropische SST op lange termijn wordt echter in belangrijke mate beïnvloed door de Atlantische diepwater ventilatie, die tijdens de MPT sterk afnam. De afname in het transport van warm oppervlaktewater naar hogere breedtes veroorzaakte een langdurige ophoping van warmte in de tropische Atlantische Oceaan. De groei van de ijskappen tijdens de MPT leidde dus tot een langdurige tijdelijke afwijking van de tropische omstandigheden ten opzichte van de globale afkoeling. De accumulatie van plantenwassen bleek duidelijk te zijn toegenomen na de groei van het globale ijsvolume (Hoofdstuk 6). De gecomprimeerde atmosferische circulatiecellen leidden tot een verhoogd transport van eolisch stof door een sterkere en meer zonaal gerichte passaatwind. Grootschalige vegetatieveranderingen in zuidelijk Afrika, gemeten als C_3/C_4 plantenvariaties, correleren echter niet met het globale ijsvolume en de veranderingen in pCO_2 die -naar men vermoedt- parallel plaatsvonden. De vegetatieveranderingen bleken juist in fase te zijn met de veranderingen in de tropische SST. In de obliquiteit- en excentriciteitcycli en de lange-termijn ontwikkeling is de tropische SST de meest belangrijke klimaatsfactor, die ogenschijnlijk direct via de neerslag en verdamping, de droogte en dus de grootschalige vegetatie in zuidelijk Afrika bepaalt. In de precessiecyclus daarentegen, veroorzaakt de moesson gelijktijdige SST en C_4 planten minima als gevolg van het samenvallen van maximale moesson- en opwellingscondities in deze cyclus. Om de reaktie van het mariene ecosysteem in het Angolabekken op de MPT

te onderzoeken, zijn accumulatiesnelheden van lipide biomarkers van verschillende mariene planktonklassen gebruikt (Hoofdstuk 7). Vòòr de MPT werd de door de rivier veroorzaakte productie en de door de wind gestuurde opwelling gedomineerd door de precessiecyclus. De groei van het ijsvolume zorgde voor een afname in de invloed van de lage breedtes op de marine productiviteit. In plaats daarvan nam, na de groei van het globale ijsvolume, de productie van lipiden door windgestuurde opwelling en het eolisch transport van plantenwassen toe en reageerde op de 100.000 jaar variabiliteit in windsterkte en -zonaliteit. De MPT leidde dus tot belangrijke milieuveranderingen in de tropische Atlantische Oceaan en equatoriaal Afrika. De invloed van de lage breedtes beperkte zich door een afname in het effect van de moesson, terwijl de invloed van het ijsvolume door de sterkere passaatwind toenam.

Dit proefschrift toont het potentieel van lipide biomarkers om in hoge tijd-resolutie de (paleo)-oceanografische en klimaatsveranderingen in het verleden in zowel het mariene en als het terrestrische milieu te bepalen, en levert zo nieuwe inzichten in de verbinding tussen het klimaat op lage en hoge breedtes en hun effecten op mariene en terrestrische ecosystemen.

Dankwoord

I thank the co-authors, the persons named in the acknowledgments and all the people who supplied positive contributions to this thesis.

I am grateful to my promotor, Jan W. de Leeuw, for having offered me this fascinating Ph.D.-project and his sustained support.

The co-promotores, Jaap S. Sinninghe Damsté and J. H. Fred Jansen did the supervision of the scientific progress. I strongly appreciate their effort, also in our long and detailed discussions, which often made me feel like a bridge between two worlds.

I highly enjoyed the conversations with Stefan Schouten, Rich Pancost, Gerard Versteegh and Arnoud Boom about stable isotopes and their link with climate and vegetation.

The discussions with Johan van Bennekom about the oceanography of the Angola Basin and with Hanno Kinkel about South-Atlantic paleoceanography were surely of great help for the understanding of the research area.

Special thanks go to Marianne Baas and Michiel Kienhuis for always being ready to answer any question about methods and technics.

Gijs Nobbe and Gert de Lange are thanked for their support in the laboratory of the University of Utrecht.

I thank Gerald Ganssen from the VU Amsterdam for giving me the possibility to participate in the SUPO research cruise.

All the people from the MBT and MCG departments, i.e., Margot Bik, Peter Blokker, Jerome Bonnin, Yvonne van Breugel, Geert-Jan Brummer, Marco Coolen, Marlèn Dekker, Bart van Dongen, Eric Epping, Astrid Forster, Marie-Aude Haeberle, Wim Helder, Ellen Hopmans, Erica Koning, Marcel Kuijpers, Neven Loncaric, Marcel van der Meer, Jort Ossebaar, Elda Panoto, Frank Peeters, Wim Pool, Sebastiaan Rampen, Irene Rijpstra, Patty Slootweg, Rienk Smittenberg, Alina Stadnitskaia, Jan-Berend Stuut, Tjeerd van Weering, Joe Werne, Bas West, Cornelia Wuchter, Claar van der Zee, are acknowledged for the creation of the stimulating working atmosphere at the Royal NIOZ.

I am very grateful to Claudia for her enduring patience and support.

Curriculum Vitae

Enno Schefuß was born on the 27th of July 1971 in Brühl/Germany. After successful completion of the Gymnasium in Erftstadt-Lechenich in 1991, he fulfilled civil service in the Marienhospital Frauenthal. In 1992 he started to study Geology/Paleontology at the University of Cologne. After working for 2 months during summer 1994 at the Alfred-Wegener Institute for Polar and Marine Research in Bremerhaven, he continued to study Marine Geology at the Christian-Albrechts-University in Kiel. In 1996 he participated in the European student exchange program ERASMUS and studied at the University of Utrecht/The Netherlands for 6 months. In 1998 he achieved his Diploma in Marine Geology from the CAU Kiel. In the same year he started as Ph.D. student ('onderzoeker in opleiding') at the Netherlands Institute for Sea Research (NIOZ), which later became the Royal NIOZ, employed by the Netherlands Organisation for Scientific Research (NWO). Since November 2002 he works as postdoctoral scientist in the Marine Geology department of the University Bremen.